UNIVERSITY OF OKLAHOMA

GRADUATE COLLEGE

MICROBIAL MEDIATED CARBON AND NITROGEN FEEDBACKS TO ELEVATED CO_2 AND SWITCHGRASS ESTABLISHMENT IN GRASSLAND ECOSYSTEMS

A Dissertation submitted to the graduate faculty in partial fulfillment

of the requirements for the degree of

DOCTOR OF PHILOSOPHY

in

MICROBIOLOGY

by

Colin Thomas Bates

Norman, Oklahoma

2021

MICROBIAL MEDIATED CARBON AND NITROGEN FEEDBACKS TO ELEVATED CO_2 AND SWITCHGRASS ESTABLISHMENT IN GRASSLAND ECOSYSTEMS

A DISSERTATION APPROVED FOR THE DEPARTMENT OF MICROBIOLOGY AND PLANT BIOLOGY

BY THE COMMITTEE COSISTING OF

Dr. Jizhong Zhou, Chair

Dr. John P. Masly

Dr. Lee R. Krumholz

Dr. Paul A. Lawson

Dr. Bradley S. Stevenson

© Copyright by Colin Thomas Bates 2021

All Rights Reserved

ACKNOWELDGMENTS

"Somewhere, something incredible is waiting to be known." -Carl Sagan

The pursuit of knowledge has been a quintessential driving force in my life for as long as I can remember. My journey to earn a doctoral degree has been filled with both challenges and rewards that have enriched my life in a myriad of ways. This work would not have been possible without the kind helping hands of those that pushed me along on my own path of discovery. Firstly, I would like to thank my principal mentor and advisor, Dr. Jizhong Zhou. Dr. Zhou invested in me by giving me the encouragement, guidance, tools, and financial support throughout my Ph.D. program for my research to succeed. Thank you for providing me with a working environment that fostered free thinking, for always pushing me to be better, and for your brilliant expertise in addressing numerous scientific questions related to my work. I also cherish the opportunities you provided me to collaborate and learn from other world renown researchers. I aim to carry all the lessons you have taught me for the entirety of my career.

My dissertation committee members, I would like to thank you each for your generous support, your difficult questions, and for leading me towards doing the best science I can achieve. I would like to thank my outside committee member Dr. Masly specifically for teaching me the foundations for programming in R, without that base of knowledge, I never would have the skills to visualize or perform analyses on my data and for always being my advocate. I thank Dr. Lawson, for his wonderful course and for inspiring me to be a better communicator and instructor to future students. I deeply appreciate Dr. Krumholz for guiding me in developing my scientific reasoning skills and for the insightful discussions we had over results and method selection when I ran into issues with my research. Last but not least, I would like to thank Dr. Stevenson for always asking

the challenging questions and for his leadership on formulating meaningful hypotheses for my work.

Next, I would like to sincerely thank my fellow collaborators at the Institute of Environmental Genomics, who taught me proper laboratory safety and techniques, experimental design, data analysis, manuscript crafting, DNA sequencing, sample collection and field work. Specifically, I want to thank Dr. Escalas for the monumental support and guidance he has given me over the years. From collecting samples with him every month, to monthly zoom meetings going over data analysis questions, he has been instrumental in the growth of my research abilities. He has also helped me develop as a scientific writer immensely. I also must thank Dr. Kuang for all the incredible support and guidance he has offered me over the years. From the many different theoretical ecological discussions to helping me improve my data analysis capabilities and most importantly his help in organizing ideas for manuscripts and his brilliant theory crafting. Ying Fu I would like to thank for her incredible help in sequencing and Geochip analysis. I would like to thank Dr. Xuanyu Tao for the years of support and assistance he has provided me with. We came into the department and the lab together as fellow students and his intelligence, insight into experimental design, kindness, and friendship I will always deeply cherish. I would also like to thank Dr. Daliang Ning, Dr. Linwei Wu, Dr. Liyou Wu, Dr. Gangsheng Wang, and Dr. Joy Van Nostrand for each of their guidance on statistical, data analysis, sequencing, modeling, or lab management support they provided me over the years. I also want to thank Dr. Lauren Hale for her always incredible comments during manuscript crafting. She has a brilliant way of thinking and always helped improve my writing and hone my scientific questions for broad appeal to the

scientific community. Without the amazing team of researchers both past and present from IEG I this work would not have been possible.

I would also like to thank all the collaborators I have been fortunate enough to have had the chance to work with over the years whose efforts have made this work possible. Work related to the switchgrass project I would like to thank Dr. Mary Firestone (UC Berkeley) for her incredible leadership as the head PI, Dr. Jennifer Pett-Ridge (LLNL) for her extraordinary feedback during manuscript crafting and providing data on the deep pit samples, the Oklahoma Mesonet environmental monitoring network, and particularly Bradley Ilston, for the use of their weather monitoring stations to provide data for our trace gas flux calculations, and the Noble Research Institute and specifically Dr. Yuan Wang, Dr. Kelly Craven, Dr. Malay Saha, and all the auxiliary staff who added in establishing, maintaining, and helped in sampling the two field plots in southern Oklahoma.

I would also like to thank my family and friends for their words of encouragement and motivation. Specifically, my mother Dr. Cheryl Bates for always inspiring me to do my best, my father Don Bates for fostering my interests in science as a kid, my grandparents Don and Ann Bates for supporting my education goals and for their love, Frank Gill for always believing in me and being the best teaching mentor a new teacher could ask for, Cameron Forbus, Ethan Grabau, John McConnel, Jordan Matthews, Kyle Traughber, Madison Niederhauser, and Richard Schmidt for their years of friendship and support. I also need to thank my love Tanya Ball for her unending support, love, guidance, and companionship over the years. She always motivates me to become the best version of myself I can be. Without her, this work would not have been possible.

The switchgrass research is supported by the U.S. Department of Energy Office of Science, Office of Biological and Environmental Research Genomic Science program under the award

number DE-SC0014079 to the UC Berkeley, Nobel Research Institute, University of Oklahoma, the Lawrence Livermore National Laboratory (LLNL), and the Lawrence Berkeley National Laboratory. Work at LLNL was conducted under the auspices of DOE Contract DE-AC52-07NA27344 and Genomic Science Program award SCW1555.

ABSTRACT OF THE DISSERTATION

Microbial mediated carbon and nitrogen feedbacks to elevated CO_2 and switchgrass establishment in grassland ecosystems

by

Colin Thomas Bates

Doctor of Philosophy, Department of Microbiology and Plant Biology
University of Oklahoma, Norman, September 2021
Dr. Jizhong Zhou, Chair

Anthropogenic climate change is the greatest scientific and political challenge of the twenty-first century. Since the industrial revolution, global climate change has elevated greenhouse gas concentrations in the atmosphere, increased the global mean surface temperatures of the Earth, caused a rise in sea levels, enhanced the frequency of extreme weather events, and is having severe effects on the biosphere. Climate change has also accelerated in recent decades, and many uncertainties remain about the lasting effects on ecosystems and human welfare. Additionally, nitrogen deposition has increased dramatically and may alter terrestrial ecosystem functionality. Therefore, nitrogen deposition combined with climate change may accelerate soil carbon loss, creating more 'marginal lands' of low nutrient availability. To address these concerns, it is vital to understand the response of soil microbes to aspects of climate change, nitrogen additions, and changes in land usage. Microorganisms are essential in biogeochemical cycling and regulating carbon feedbacks between the biosphere, soil, and atmosphere. However, their

responses to elevated CO_2, N deposition, and changes in land usage (*e.g.*, bioenergy crop production) are difficult to predict, limited by a lack of mechanistic understanding due to the complexities of microbial communities, their considerable ecosystem functionalities, and intricate interactions between plants and other microbes. Advancements in high throughput metagenomic sequencing and environmental microbiology have allowed for a deeper understanding of the critical role microbial diversity and functions have in maintaining ecosystem functionality. This dissertation focuses on grassland soil microbial communities and their responses to elevated CO_2, nitrogen deposition, and bioenergy crop establishment. It goes on to further address more theoretical questions associated with fundamental microbial ecology as they relate to species-time-area relationships and seeks to quantify the effects the microbial community has on soil carbon stocks in marginal lands.

The first research chapter focuses on answering questions related to how free-living diazotrophic microorganisms respond to elevated CO_2 and nitrogen deposition treatment, both in terms of their functionality and diversity. Soils were collected from the Cedar Creek Ecosystem Science Reserve in Minnesota. Heavy $^{15}N_2$ gas soil incubations were utilized to assess the nitrogen fixation rates and functionality of the diazotrophic community, while high-throughput amplicon sequencing of the bacterial, fungal, and diazotrophic communities allowed for quantification of the diversity changes due to treatment effects. Elevated CO_2 and nitrogen deposition significantly stimulated nitrogen fixation rates, while the combined treatment reduced rates back down to ambient levels. The treatments had no significant effect on diazotrophic richness, but the community dissimilarity between treatments was significant, revealing an effect on the beta diversity of diazotrophs. Fungal communities under nitrogen deposition were marked by a drop in the relative abundance of fungi in the *Glomeromycota* class, containing arbuscular mycorrhizal

fungi. The functional potential of the bacterial community assessed by GeoChip DNA microarray revealed a reduction in signal intensity for many nitrate reductase-related genes (*i.e., narG, nirK,* and *nirS*) under nitrogen addition. Additionally, recalcitrant carbon cycling genes (*i.e., vanA* and *ligninase*) functional potential was elevated under the combined treatment. This study reveals the implications that elevated CO_2 and nitrogen deposition combined may reduce free-living diazotrophic functionality and could alter soil nutrient cycling, which may lead to a depletion of native carbon stocks in the soil.

Next, switchgrass establishment was investigated and its ecological impacts on soil chemistry, soil biota, and trace greenhouse gas emissions in highly eroded marginal lands of low soil nutrient quality. We performed a comparative analysis using seasonal soil chemical profiling, high-throughput amplicon sequencing of the bacterial community, and *in situ* field measurements of trace gas fluxes over a seventeen-month timeline to monitor changes between two contrasting soil types with different plant cover (*i.e.*, switchgrass or fallow with annual weeds/grasses). Our results revealed carbon accumulation in the topsoil at our sandy loam site with switchgrass but not at the clay loam site with switchgrass. Significantly elevated CO_2 emissions were observed from the clay loam switchgrass plot, along with reductions in microbial diversity (both alpha and beta). Surprisingly, methane consumption was significantly reduced by an estimated 39 and 47% at the clay loam and sandy loam switchgrass plots. Together, the results of this study suggest that differences in soil carbon stocks and greenhouse gas fluxes are different at highly degraded sites with switchgrass.

Then, the temporal and spatial microbial diversity was assessed to ask how switchgrass establishment alters prokaryotic species-time-area relationships in nutrient-poor soil and what biotic or abiotic factors regulate the changes in diversity over space and time. By using paired plots

at each site, with and without switchgrass, and tracking the soil physicochemical properties and bacterial biodiversity using 16S rRNA high-throughput sequencing, it was found that taxa turnover was higher over time than with increasing area. Soil heterogeneity was also found to be higher at the clay loam site, and that this heterogeneity was related to and helped in explaining the species-time-area relationships observed from each of the plots. Seasonal turnover of soil phosphorus concentrations was positively related to the species-area relationship, perhaps reflecting the linkage changes in phosphorus have with plant growth and thus the effect plants have on the overall bacterial diversity. This study links the importance of soil nutrient condition and heterogeneity to regulating the soil bacterial biodiversity for different spatial scales and over time.

Finally, the potential impact on deep soil carbon stocks is evaluated under deep-rooted switchgrass to establish if the long-term accumulation of root biomass in the deep soil layers influences heterotrophic respiration rates of microorganisms and has consequences on the soil carbon balance. We examine this using soil taken along a depth profile of cores from paired plots in two contrasting soil types that either have or do not have switchgrass growing for at least ten years prior to sampling. A heavy isotopic ^{13}C priming soil incubation experiment was conducted in the lab to determine heterotrophic respiration rates along with a BioLog functional degradation assays, PLFA microbial biomass estimates, and high-throughput sequencing of the bacterial communities of the native soil, and both before and after isotopic priming. A differential response to plant residual carbon inputs was found between long-term selected microbial communities from different sites depending on the root system. The results suggest that soil type and microbial community structure play important roles in regulating the deep carbon pool and the potential for increasing the soil carbon sink capacity with deep-rooted plants in nutrient-poor soils.

Overall, the work presented in this dissertation provides evidence of prokaryotic communities' response to elevated CO_2 and nitrogen deposition altering community functionality, reveals the ecological impacts of switchgrass establishment and consequences on microbial diversity at scale and over time, and evaluates the priming effect of the subsurface soils under deep-rooted switchgrass. The findings presented here represent novel insights into understanding microbial-mediated carbon and nitrogen cycling in grassland ecosystems and assess the sustainability of switchgrass cultivation from a microbial perspective on marginal lands.

Keywords: climate change, soil microbial community, nitrogen deposition, heterotrophic respiration, metagenomics, alpha and beta diversity, species-time-area relationship, ecosystem function, priming effect, microarray, GeoChip, high-throughput sequencing

Table of Contents

LIST OF FIGURES

CHAPTER FOUR

CHAPTER FIVE

LIST OF TABLES

ABBREVIATIONS

GHG	Greenhouse gas
SG	Switchgrass
FL	Fallow field treatment
SL	Sandy-loam
CL	Clay-loam
EPS	Extra cellular polymetric substance
SOC	Soil Organic Carbon
SOM	Soil Organic Matter
MAOM	Mineral Associated Soil Organic Matter
OM	Organic Matter
AM	Arbuscular mycorrhizal fungi
ECM	Ectomycorrhizal fungi
BNF	Biological Nitrogen Fixation
eCO_2	Elevated carbon dioxide treatment
SAR	Species Area Relationship
STR	Species Time Relationship
STAR	Species-Time-Area Relationship
ANOVA	Analysis of Variance
ANOSIM	Analysis of Similarities
NMDS	Non-metric Multidimensional Scaling
SEM	Structural Equation Modeling
CCA	Canonical Correspondence Analysis

CHAPTER ONE

INTRODUCTION

Section 1.1 EFFECTS OF ANTHROPROGENIC CLIMATE CHANGE AND NITROGEN DEPOSITION

1.1.1 Overview of the global climate change crisis

Humans have undoubtedly increased global greenhouse gas (GHG) concentrations through industrial, agricultural, and energy production activities. Since 2011, GHG concentrations have continued to rise and are reaching annual averages of 332 ppb for nitrous oxide (N_2O), 1866 ppb for methane (CH_4), and 410 ppm (higher levels than at any time in 2 million years) for carbon dioxide (CO_2) in 2019 (IPCC, 2021). These GHGs alter Earth's climate via absorbing and then re-emitting thermal energy back into the atmosphere, thereby warming the planet causing the Greenhouse effect. Due to the continuous anthropogenic release of various GHGs (CO_2 being the major contributor), each of the last four decades has continued to become excessively warmer than any decade that preceded it since 1850 (Figure 1.1 IPCC, 2021).

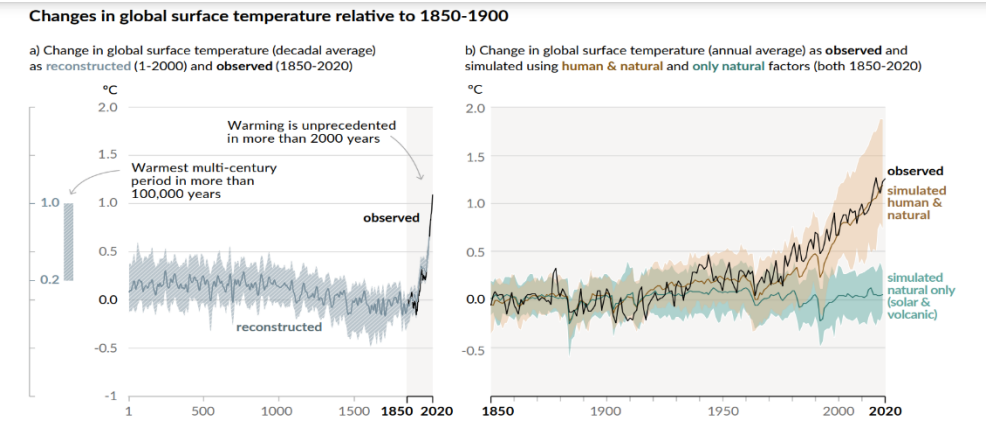

Figure 1.1 History of global temperature changes and causes of recent warming for: a) changes in global surface temperatures reconstructed from paleoclimate archives and from direct observations and **b)** changes in global surface temperature over the past 170 years.

Global warming has increased the global average surface temperatures by over 1° C since 1880 (NOAA, 2021). This warming effect has shifted global precipitation patterns, increased the global mean sea level, caused the retreat of Arctic Sea ice and glaciers, and will increase the frequency of extreme weather events like droughts, heatwaves, and flooding events. Such changes spurred on by GHGs heating the atmosphere and altering the hydrosphere will have consequences for Earth's biosphere.

1.1.2 Climate change effects on Earth's biosphere

With the rise of these GHGs emitted from anthropogenic causes and the continued increases in average global temperatures, a key question for ecology is how Earth's life systems are coping under global climate change. However, first, it is essential to point out that the variable effects of climate change are differential depending on the spatial scale of biospheric levels (Figure 1.2; Penuelas *et al.*, 2013).

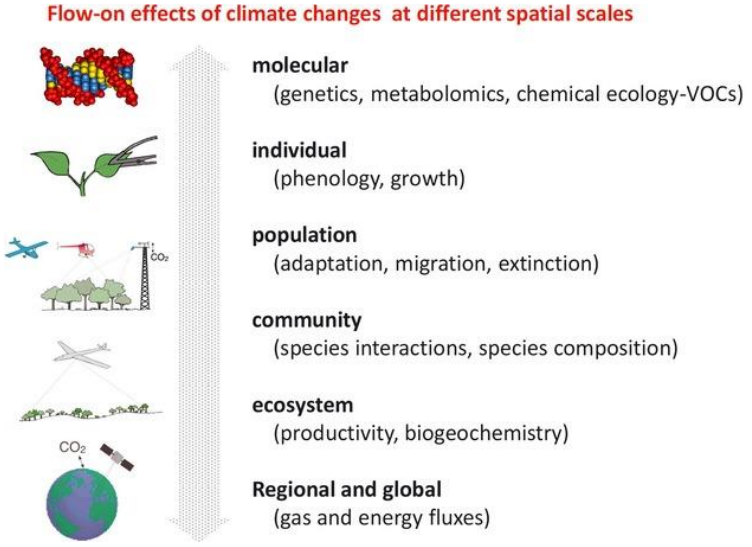

Figure 1.2 Impacts of climate change on life at different spatial scales from the molecular to the biospheric levels.

For the proposes of this dissertation, the focus will be on the effects climate change has on various soil microbial and plant systems. For example, many studies examine the phenotypic responses of organisms to drought and warming at the molecular level. Some plants (*i.e., Erica multiflora*) subjected to drought have exhibited increased concentrations of antioxidant compounds, lower concentrations of sugars, amino acids, and P (Rivas-Ubach *et al.,* 2012) relative to control individuals, revealing a strong relationship between the metabolome and elemental stoichiometry. To cope with drought, soil microbes have been shown to accumulate organic molecules (Schimel, 2018) to reduce their total solute osmotic potential (Csonka, 1989; Killham & Firestone, 1984; Wood, 2015); these molecules include proline, glycine betaine, trehalose, and glutamate. According to a recent meta-analysis (Chen *et al.,* 2020), soil microbes that experience elevated warming for prolonged periods may have increased lignin and cellulose degradation activity, which may reduce the recalcitrant C pools, possibly further exacerbating climate-C feedbacks. Microbes can also improve the local environment via the production of extracellular polymeric substances (EPS); these are primarily polysaccharides, proteins, DNA, and other materials released by live or dying cells (More *et al.,* 2014) to act as a sponge and delay drying. However, these are just a few examples of the myriad of ways organisms at the molecular level are adapting to various climate change conditions.

On an individual level, some microbes, like those belonging to several *Firmicutes* groups (Filippidou *et al.,* 2016), can go dormmate when conditions are not suitable for growth (Jones & Lennon 2010), forming Endospores. Other microbes can undergo different forms of dormancy, but this remains a poorly understood area of soil biology. Bacteria may also regulate their individual response to warming and temperature stress through the production of heat shock

proteins, which act as chaperon proteins to help stabilize and ensure correct protein folding of newly synthesized proteins in the cell. However, the molecular mechanisms each microorganism has adopted for heat shock protein regulation are finely controlled and can be positive, negative, and even using two opposite coexisting strategies for regulation of these complex gene networks (Roncarati & Scarlato, 2017). Plants can also alter their physiology and morphology to adapt at an individual level to climate stress. For example, plants can change the allocation of resources within their bodies, decrease their photosynthetic rate, increase their water use efficiency, and decrease their growth and reproductive outputs. Plants and microbes can also influence each other in response to climate stress via plant-microbe interactions, which will be discussed later in this dissertation.

At the population and community levels, genotypic adaptations or microevolutionary shifts in populations and communities via changes in allele frequencies in response to both temperature and drought have been observed for various plant communities (Franks *et al.,* 2007; Jump *et al.,* 2008; Eveno *et al.,* 2008) altering phenology and population dynamics. For soil microbes, climate change can also alter climate variability (*e.g.,* severe drought or rainstorms), which can have direct effects on microbial community dissimilarity and assembly and may even lead to a reduction in rare taxa important for specific ecosystem functionality and resiliency (Kuang *et al.,* 2021).

Finally, at the ecosystems and global scales, plant communities can lengthen the period of time plants are active and increase the uptake of atmospheric CO_2 through changes in phenology. However, drought and access to important growth factors like N or P can limit total CO_2 fixation (Angert *et al.,* 2005; Ciais *et al.,* 2005; Zhao & Running, 2010). Soil microbes at this level regulate the organic C stored in soils and its release back to the atmosphere; under climate

warming in high latitude regions, heterotrophic respiration can be enhanced (*i.e.,* depending on the microbial community composition), causing a loss of C from these organic-rich soils (Johnston & Sibly, 2018). Severe C feedbacks resulting from enhanced microbial respiration in the soil can result in further increases in GHG emissions and potentially enhanced climate warming over time. Such increases in the concentration of CO_2 in the atmosphere have variable effects on plants and soil C stocks globally.

1.1.3 Effects of elevated CO_2 on plants and soil C stocks

Terrestrial ecosystems have the potential to remove up to 30 percent of the CO_2 emitted by human activities annually (Friedlingstein *et al.,* 2020); however, the duration of this C stock in the soil depends on how plant biomass, microbial degradation activities, and soil organic carbon (SOC) respond to future increases in atmospheric CO_2 levels (Schimel *et al.,* 2015; Torbert *et al.,* 2000; Keenan *et al.,* 2016). In experimental settings, plant biomass often increases in elevated CO_2 (eCO_2) experiments (Baig *et al.,* 2015; Drake *et al.,* 2011; Norby *et al.,* 2005), yet SOC has been observed to increase, decrease or remain unchanged (Groenigen *et al.,* 2014). Mechanisms that drive these differences in SOC response to eCO_2 are poorly understood and create many uncertainties in future climate projections (Friedlingstein *et al.,* 2014; Todd-Brown *et al.,* 2014). A recent meta-analysis of over one hundred eCO_2 experiments (Terrer *et al.,* 2021) found that the effect on SOC stocks is attributed to a negative relationship with plant biomass, in that, when biomass is highly stimulated by eCO_2 treatment, SOC storage declines; conversely when biomass is weakly stimulated, SOC storage increases. The authors of the meta-analysis assert that this trade-off in biomass to SOC stocks appears to relate to plant nutrient acquisition, in which plants increase their biomass by mining the soil for nutrients, which decreases SOC storage. A positive relationship formalized by first-order kinetics (Olson, 1963) is postulated between inputs and SOC

storage when eCO_2 stimulated plant biomass increases carbon inputs (litter) into the soil. However, this hypothesis ignores SOC losses associated with accelerated SOM decomposition sometimes observed under eCO_2 (Kuzyakov *et al.*, 2019). Thus, through the economics of plant resource acquisition, plants invest in belowground root growth, exudates, and symbiotic bacteria and fungi, which can accelerate the decomposition of SOM via the priming effect to enable further plant nutrient uptake.

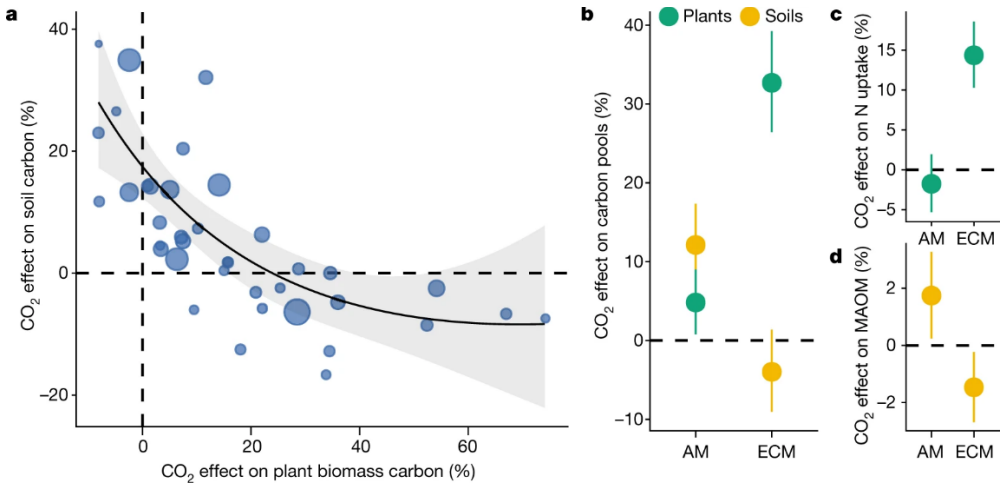

Figure 1.3 the inverse relationship (**a**) can be explained by different efficiencies in plant nutrient uptake (**c**) between AM and ECM nutrient acquisition strategies driving opposite effects on plant biomass and SOC pools (**b**), including MAOM stocks (**d**). The regression line in **a** is based on a quadratic mixed-effect meta-regression model and 95% confidence interval (R^2=0.67, P<0.001, n=38). Dots in **a** represent the individual experiments in the meta-analysis, with dot sizes proportional to model weights. Dots in **b-d** represent overall effect sizes from meta-analysis and 95% confidence intervals.

The authors of the meta-analysis go on to further stress that the difference between symbiotic associations between plants and fungi (*i.e.*, arbuscular mycorrhizae (AM) and ectomycorrhizal (ECM)) lead to differential responses on SOM stocks and plant biomass gains (Figure 1.3, Terrer *et al.*, 2021). ECM--associated plants tend to have better N efficiency and uptake under eCO2, thus enhance plant biomass; however, this depletes SOC stocks as fungal partners mine for N in the SOM. AM associated plants under eCO_2 (*e.g.*, grasses), N uptake is not significantly enhanced, and the plants allocate more biomass to increasing root production and rhizodeposition (Nie *et al.*,

2013; Treseder, 2004; Jastrow *et al.,* 2005), which limits overall plant biomass gains, but decreases soil C losses (Carrillo *et al.,* 2016). It has also been demonstrated that the mineral-associated soil organic matter (MAOM) is increased under eCO_2 strongly in AM-dominated systems than in ECM systems (Cotrufo *et al.,* 2019; Craig *et al.,* 2018). Increased MAOM may allow for greater future C storage in these soil systems like those of grassland systems, where AM-associated plants dominate. However, the effects of N deposition in addition to eCO_2 remain understudied in grassland ecosystems.

1.1.4 Anthropogenic nitrogen deposition

Anthropogenic N deposition is rapidly becoming a compounding issue as it threatens the functionality of many terrestrial ecosystems (Waldorp *et al.,* 2004). The global N cycle has doubled over the last century (Fowler *et al.,* 2013) as a result of increased N deposition from various sources. In the past, the reactive-N deposition for the terrestrial ecosystem in the 1860s was around 15.88 Tg per year, while by the beginning of the 1990s, it was estimated at 63.5 Tg per year (Galloway *et al.,* 2004). This four-fold change in N deposition is expected to continue to increase and may reach up to 125 Tg per year by 2050 (Galloway *et al.,* 2000). Terrestrial ecosystems (*i.e.,* grassland) productivity are widely accepted to be nutrient-limited (Chapin *et al.,* 2011). With the advent of the Haber-Bosch process, in which atmospheric N_2 is converted to ammonia (NH_3) by a metal-catalyzed reaction with H_2 under high temperatures and pressure, N deposition via industrial-scale fertilizer application has revolutionized agricultural productivity worldwide. Although N deposition can lead to increased plant growth, the effects of such wide use fertilization treatments caused many unforeseen negative impacts to natural ecological systems. For example, N deposition can lead to soil acidification, reduced plant diversity, increased invasive

species occurrence, and increased N leaching into bodies of water which can lead to eutrophication events. Additionally, N deposition can impact climate change through increased GHG nitrous oxide (N_2O) emissions from agricultural soils via microbial activity, and these emissions are projected to increase in the future (Yang *et al.,* 2021). Therefore, it is critical to model and understand microbial and plant feedbacks to N deposition to better understand its effects on grassland ecosystems.

Section 1.2 DEEP ROOTED PERENNIALS AND CARBON STORAGE

1.2.1 Benefits of deep-rooted perennials in grasslands

Deep-rooted perennial bioenergy grasses such as switchgrass (*Panicum virgatum*), miscanthus (*miscanthus x giganteus*), and species in the *Sorghum* genus have been broadly associated with increases in topsoil carbon levels at many sites when compared to shallow-rooted annual grassland ecosystems (Kantola *et al.,* 2017; Govindasamy *et al.,* 2021). This is mainly due to increases in root biomass, litter, and exudates from perennial crop systems, which have been shown to improve soil carbon stability and aggregate formation (Tiemman & Grandy, 2015). For the purposes of this dissertation, switchgrass will be the primary focus and its impacts on marginal lands in southern Oklahoma.

Switchgrass (SG; *Panicum virgatum* L.) is a tall perennial grass native to the central North American Plains and has been identified as an auspicious bioenergy crop suitable for future large-scale cultivation in the U.S. (Mclaughlin & Kszos, 2005). This enthusiasm for SG stems from it having the ability to exhibit high biomass despite being grown on low-quality soils unfit

for traditional agricultural practices (Tilman *et al.,* 2006). Furthermore, this crop has been shown to improve soil productivity over long-term cultivation (Gelfand *et al.,* 2013) through the net input of soil carbon (Ma *et al.,* 2000). Thus, SG may substantially enhance GHG reductions associated with the substitution of fossil fuels for renewable energy (Anderson-Teixeira *et al.,* 2009). SG is also highly drought tolerant (Barney *et al.,* 2009) and acts to prevent topsoil erosion, two problems common for farming in the American Southwest (OK, TX, and NM). Hence, SG has the potential for ecosystem restoration on nutrient-poor soils and climate change mitigation while serving as a viable renewable energy source.

The US Department of Energy plans to replace 30% of transportation fossil fuels with biofuel by 2030 (Bouton, 2007). To carry out such an aggressive agenda, it will require substantial increases in the current land usage to shift towards bioenergy crop cultivation. An estimated 15 million hectares (Bouton, 2008) of arable land would need to be converted into SG fields to even approach the goals set by the Department of Energy. Fortunately, SG is a native North American perennial grass, with a broad range (Elbersen *et al.,* 2013), low nutritional input requirements, thus, allowing it to be considered a good candidate for growth on marginal lands seen as unsuitable for common agronomic crop growth (Sanderson *et al.,* 1996). The continental U.S. has an estimated 11% of its mainland considered 'marginal lands' (Milbrandt *et al.,* 2014), which currently represent an underutilized resource that may be well-suited for SG cultivation. This is particularly true in Oklahoma, as SG could be used to prevent soil erosion while improving the soil organic carbon content via SG's deep-rooted architecture providing carbon deposition to the soil. Chapter 3 will investigate the ecological effects of switchgrass establishment in marginal lands.

1.2.2 Carbon storage potential

Human land usage for agricultural purposes has altered the terrestrial soil C balance; it has been estimated that globally a 133 Pg C debt has been incurred for the top 2 meters of soil (Sanderman *et al.,* 2017) as a direct result of agricultural practices. In the USA, states like Iowa alone have experienced a loss of as much as 200 gigatons of SOC in roughly 112 years (Donigian *et al.,* 1994). The loss of C from the soil can be associated with turnover in other OM nutrients like N and P, which can reduce soil fertility of sites after the introduction of agricultural practices (Tiessen *et al.,* 1994). In Oklahoma, severe drought and poor farming practices caused the ecological disaster known as "The Great American Dust Bowl" in the 1930s. Wind erosion would then remove much of the nutrient-rich topsoil creating marginal lands of low soil nutrient quality. The implementation of deep-rooted perennial grasses like SG in many of these sites still affected may improve soil C stocks and prevent wind erosion. However, potential C accrual occurring by the additional root inputs may be offset by higher heterotrophic respiration rates, stimulated by microbial C mineralization as a product of the 'rhizosphere priming' effect (Cheng *et al.,* 2014). Thus, the total amount of SOC and its storage is dependent and regulated by the mineral composition of the soil (Torn *et al.,* 1997), nutrient content (Shahzad *et al.,* 2018), and activity/composition of microorganisms' present (Poeplau *et al.,* 2019). Therefore, the types of belowground plant-microbe interactions and their consequences on soil C stocks are vital to this question of C sequestration rates of deep-rooted perennial grasses. Chapter 5 of this dissertation addresses the priming effect of long-term switchgrass cultivation along a soil depth profile.

1.2.3 Plant-microbe interactions

Microbes and plants have coevolved for millions of years. Understanding the biochemical and genomic basis between plant-microbe interactions is a grand challenge in agriculture, microbial ecology, and plant biology. By focusing on these links between plants and microbes during SG cultivation, improvements in agricultural practices could lead to enhanced soil nutrient acquisition and recycling. A deeper understanding of the microbial ecology of SG-influenced systems can also lead to more mechanistic explanations of how SG may enhance ecosystem services like C sequestration (McLaughlin & Kszos, 2005) and soil fertility. Early in SG establishment, the plant invests heavily in its belowground biomass (Collins *et al.,* 2010). This functional trait has allowed SG to survive in prairie soils that are low in nutrient availability. As SG establishes a healthy and large root system early in its growth, another priority for the plant may be to excrete root exudate profiles to establish microbial symbiosis with the host plant. These plant-microbe linkages can provide vast nutrition and survival benefits to the plant (Ghimire & Craven, 2011; Kim *et al.,* 2012; Ghimire *et al.,* 2009). Some of the best-studied plant-microbe symbiotic associations are from root-nodulating bacteria and root-associated arbuscular mycorrhizal fungi (AMF) (Bauer *et al.*, 2012). AMF are known for their ability to infect root cells then extend out through the soil medium to act as extensions to the plant root system. This ancient (Remy *et al.,* 1994) symbiotic relationship allows the plant to have an enhanced acquisition of P from both organic and inorganic P containing compounds along with other micronutrients and water in exchange for plant-derived carbon substrates (Barea *et al.,* 2008). Beneficial bacterial partners can also aid in P acquisition for their plant hosts. For example, bacterial P04 solubilizers (*e.g., Pseudomonas* and *Burkholderia*) can contribute to Pi absorption in plants (Rodriguez &

Fraga, 1999). Although mineralized P levels may decrease, the plant available P may increase under SG cultivation.

Nitrogen limitation is often a major factor determining plant growth in tallgrass prairie ecosystems (Risser & Parton, 1982). Although directly interacting nitrogen-fixing bacteria, like those belonging to the *Rhizobiaceae*, are found closely associated with members of the plant family *Leguminaceae*; other free-living diazotrophic nitrogen-fixing bacteria may play a vital role in nitrogen acquisition in SG influenced soils. Specific root exudates can target these free-living diazotrophic bacteria to aid in meeting the plants' nitrogen demands. The greatest impact SG can have on low-quality soils is the large input of C. This new influx of C may increase microbial richness and diversity while promoting higher activity in the soil biota provide higher overall ecosystem functionality.

Section 1.3 MICROBIAL MEDIATED BIOGEONUTRIENT CYCLING

1.3.1 Diazotrophic nitrogen fixers and microbial nitrogen cycling

Most N enters the biosphere through the conversion of atmospheric N_2 into ammonia, known as biological nitrogen fixation (BNF; diazotrophy) (Welsh, 2000). BNF is carried out only by prokaryotic organisms (*i.e.,* bacteria and archaea) (Raymond *et al.*, 2004) and is vital for providing N to other biosynthetic pathways for all N-containing compounds. As previously mentioned, some nitrogen-fixing bacteria are associated with eukaryotic hosts and form root nodule symbiosis with legumes (Pawlowski *et al.,* 1996). Others are known as free-living diazotrophs and can fix nitrogen for their growth along with contributing to environmental N levels in the soil, often through directed plant-microbe interactions (Figure 1.4, Smercia *et al.,* 2019).

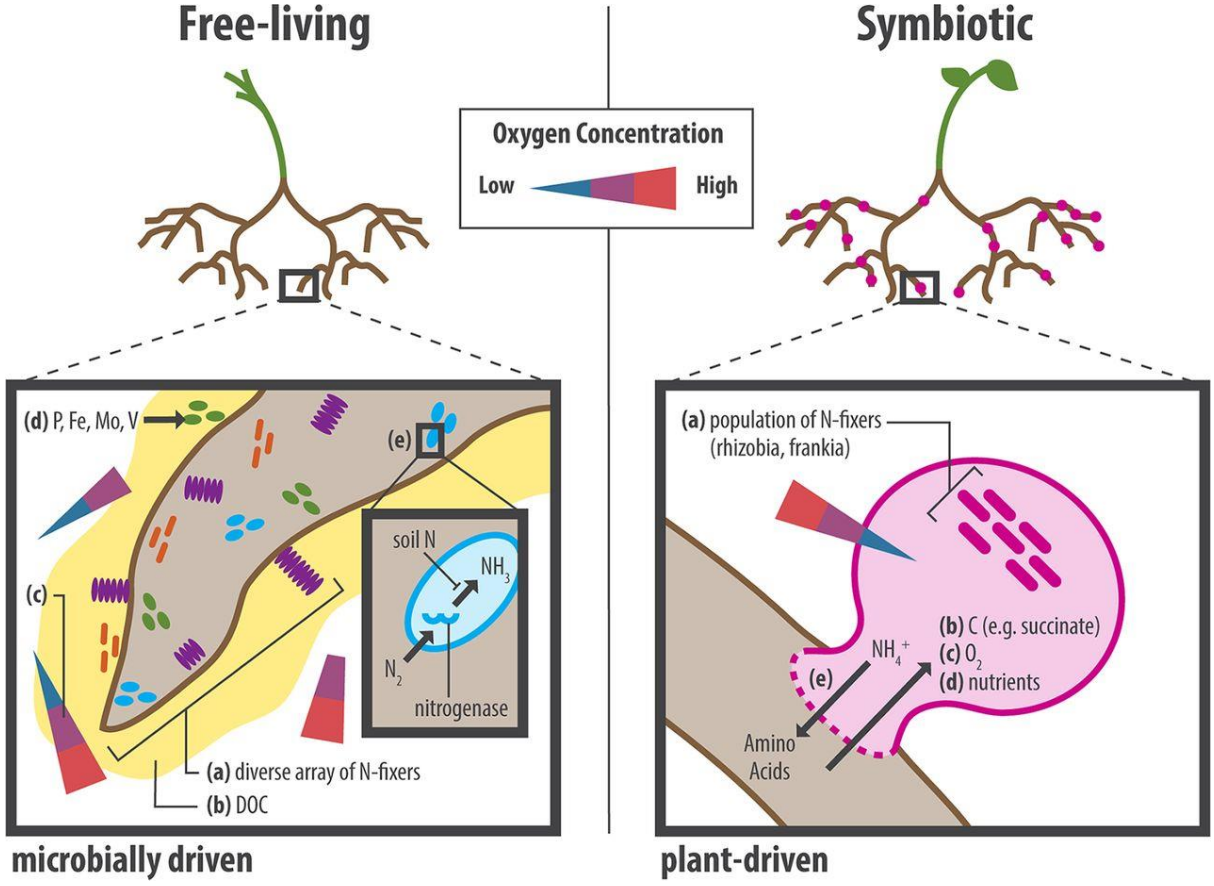

Figure 1.4 Contrasting habitats of free-living and symbiotic nitrogen fixation. (a) NF carried out by a diverse array of N fixers living in a community, while symbiotic N fixation is performed only by a few bacteria (e.g., rhizobia) living in a population. (b) NF is supported by dissolved organic carbon in the soil, while symbiotic N fixers receive a constant supply of simple C compounds directly from the host plant. (c) oxygen concentrations in the rhizosphere are variable and driven by soil structure, texture, root and microbial respiration. Symbiotic N fixers are supplied oxygen at low concentrations by their host plant. (d) nutrients necessary are acquired by the diazotroph while they are delivered by the host plant for symbiotic N fixers. (e) Diazotrophs in the rhizosphere can access N from the soil and from fixation while all symbiotically fixed N is delivered to the plant.

Free-living diazotrophs have a wide range of oxygen tolerance and can be anaerobic (*e.g.*, *Clostridium desulfovibrio* and Archean methanogens like *Methanococcus*), facultative anaerobes (*e.g.*, *Klebsiella pneumoniae*, *Paenibacillus polymyxa*, *Bacillus macerans*, and *Escherichia intermedia*), aerobes (*e.g.*, *Azotobacter vinelandii*), and oxygenic/anoxygenic photosynthetic

bacteria (*e.g.*, *Anabaena cylindrica* and *Rhodobacterr sphaeroides*). At the community level, it has been demonstrated that community shifts in free-living diazotrophic microbes can relate to ecosystem function (Hu & Buckley, 2009). They can also be important in C cycling, degrading organic matter, and root exudates to support their N fixation rates. Chapter 2 will focus on these free-living diazotrophs in grassland ecosystems and how they are affected by elevated CO_2 and N deposition treatments in terms of functionality and diversity.

Microbes are also responsible for the decrease of nitrogen compounds like ammonia in the soil that are oxidized to nitrite and nitrate through a process known as nitrification. This is usually a two-step process where ammonia is first oxidized to nitrite by ammonia-oxidizing bacteria and/or archaea, then subsequently to nitrate by nitrite-oxidizing bacteria and was first described in 1890 by Russian microbiologist Sergei Winogradsky (Wonogradsky, 1890). Nitrifiers are ecologically important since they mediate oxidative pathways in the nitrogen cycle. Ammonium oxidizing bacteria (AOB) catalyze the first step of the nitrification reaction and are members of *Betaproteobacteria*, *Gammaproteobacteria*, and ammonia-oxidizing Archaea groups (Konneke *et al.,* 2005). The second reaction of nitrate to nitrite is conducted by members of the *Nitrospinae*, *Nitrospirae*, *Proteobacteria*, and *Chloroflexi* phyla (Ward, 1996).

Finally, microbes can drive the process of reducing nitrate and nitrite back to gaseous forms of N, principally nitrous oxide and molecular nitrogen gas (N_2), via denitrification. These steps complete the nitrogen cycle releasing nitrogen back into the atmosphere. Denitrifying microorganisms are widely distributed in nature and are found in soils, freshwater, marine systems, sediments, waste treatment systems, and even in the gastrointestinal tracts of animals (Tiedje, 1988). The broad distribution has resulted in a great diversity of denitrifying bacteria (Zumft, 1997) with over 50 genera known, and it is estimated to represent 10-15% of bacteria populations

in water, soil, and sediment (Eldor, 2015). N can often be the limiting nutrient in agricultural systems, making denitrification important as it can result in a loss of fertilizer depending on a range of conditions. The release of N_2O is also problematic as it is a GHG with a global warming potential 265-298 times that of CO_2 for a 100-year timescale. Thus, understanding what affects denitrifying bacteria is key to prevent fertilizer loss and limit GHG emissions from agricultural settings.

1.3.2 Soil carbon cycling, heterotrophic respiration, and the priming effect

The carbon cycle is the biogeochemical cycle where C is exchanged among the geosphere, hydrosphere, biosphere, pedosphere, and atmosphere of the Earth. In terrestrial ecosystems, plants are critical to fixing carbon from the atmosphere via photosynthesis into the biosphere. C can then be deposited in the soil as decaying plant biomass (*e.g.,* leaf and root litter) or directly secreted (*i.e.,* root exudates) into the soil to recruit microbial symbiotes. The fate of this C is then up to soil microbial decomposition and the chemical recalcitrance of the compounds. Soils, therefore, are important sinks in the C cycle as up to 80% of the global terrestrial C pool (IPCC, 2000, 2007) is found in soil systems in some form. The total decomposition and release of this C via respiration is large and has been estimated to be an order of magnitude larger than anthropogenic CO_2 emissions (Raich & Potter, 1995). This soil respiration can be broken down into constitute sources, with heterotrophic respiration by soil biota accounting for roughly half, while the remainder is from plant roots and associated fungi (Hogberg *et al.,* 2001; Cisneros-Dozal *et al.,* 2006; Subke *et al.,* 2006; Bardgett *et al.,* 2008). Although abiotic factors such as temperature and moisture have considerable effects on decomposition rates, soil organisms are directly responsible for a vast majority of OM decomposition. This is mainly due to the fact that soil microbes can produce specific enzymes capable of degrading even the most recalcitrant of plant-

derived compounds such as lignin (Romani *et al.,* 2006; Masai *et al.,* 2007; Paul, 2007). Besides climate (*e.g.,* temperature and moisture) and soil variables (*e.g.,* pH and SOC content), biotic factors including litterfall, vegetation type, plant productivity, and soil biota diversity can influence heterotrophic respiration rates (Yan *et al.,* 2015; Xialou *et al.,* 2020; Nielsen *et al.,* 2011). Additionally, evidence indicates that the plant rhizosphere, or area of soil adjacent to the plant roots in which the chemistry and microbiology are influenced by the plant's growth and nutrient exchange, plays a critical role in C cycling (Finzi *et al.,* 2015; Hou *et al.,* 2017) and heterotrophic respiration. Live roots have been shown to suppress SOM decomposition rates by 50% or stimulate it by 380% when compared to soil incubated without plants (Cheng *et al.,* 2014). This effect plant roots have on soil decomposition rates is known as the rhizosphere priming effect, while the general priming effect is defined as a change in SOM decomposition rates due to substrate additions (Lohins, 1926; Bingemann *et al.,* 1953). Both are useful in understanding microbially regulated decomposition and heterotrophic respiration rates in soils.

Section 1.4 SOIL MICROBIAL SPECIES-TIME-AREA RELATIONSHIPS

1.4.1 Microbial temporal and area scaling

A fundamental grand challenge in ecology is to try and understand the forces that both shape and maintain biodiversity at various spatial scales over time. Central to our understanding the spatial scaling of biodiversity on Earth is whether macroscopic organisms differ from microscopic organism with diversity scaling. Currently, we know microbes tend to have greater rarity, less evenness, and greater richness than those of macroorganisms (Locey & Lennon, 2016). Traditional views have established the concept of microbial cosmopolitanism, which reasons that

due to the high abundance and small size, microbes are at dispersal levels in which dispersal limitation is practically nonexistent (Green & Bohannan, 2006). This results in 'cosmopolitan' distributions where 'everything is everywhere' -the environment just selects the specific community based on abiotic conditions (Bass-Becking, 1934). Given the small size and high abundance of microbes, it would then follow that microbes have reached levels where dispersal limitation is practically nonexistent, creating these 'cosmopolitan' distributions (Fenchel & Finlay, 2004; Finlay, 2002). However, studies have revealed evidence of microbial population isolation, weakening these traditional viewpoints, as the primary argument for low speciation rates is the lack of dispersal barriers for microbes (Papke & Ward, 2004). Additionally, global studies of microbial strains from specific environments (Whitaker *et al.*, 2003) and regional-scale analysis of lake bacterial assemblages (Reche *et al.*, 2005) have shown a distance decay relationship independent of environmental heterogeneity, contradicting the hypothesis of microbial cosmopolitanism. The relationship between species richness and sampled area (species-area relationship; SAR) is one of the most widely studied patterns in ecology. Taxonomic groups (S) or spatial scales (A) generally follow a power-law where $S \propto A^z$ is commonly assumed. Recently, SAR of microbial diversity has garnered substantial attention (Zhou *et al.*, 2008; Horner-Devine *et al.*, 2004; Shade *et al.*, 2013), and various studies have demonstrated SAR appears to be a universal law in ecology (van der Gast *et al.*, 2008; Deng *et al.*, 2018) even for microbes.

Similar to SAR, species-time relationships (STR) are believed to be fundamental patterns in ecology (Rosenzweig, 1995). This stems from the enduring hypothesis that the number of species observed in a fixed area increases with the length of time (Preston, 1960). The increase in species richness is centered on ecological processes (*e.g.*, climatic variability, successional changes, stochastic processes, or metapopulation dynamics) shaping and changing species richness

over time (Adler & Lauenroth, 2003; White *et al.,* 2006). Thus far in microbial ecology, STR has had little attention, mainly from the scarcity of long-term data sets. However, recent studies are beginning to address STR in microbial ecology (Guo *et al.,* 2019; Rivett *et al.,* 2021). Chapter 4 in this dissertation will investigate the species-time-area relationship of the soil microbial community during switchgrass establishment.

Section 1.5 GOALS AND OBJECTIVES

This dissertation aims to address how grassland soil microbial communities respond to elevated CO_2 and N deposition treatments and to understand ecosystem-level responses of plant-microbe interactions on soil respiration rates, microbial community dynamics, and feedback on soil C stocks when under the influence of the deep-rooted perennial bioenergy crop switchgrass. Samples from field experiments in Minnesota and Southern Oklahoma were collected to utilize high-throughput genomic technologies, functional assays, and intensive sampling designs to characterize the microbial taxonomy, community dynamics, species diversity scaling, specific functionality, functional potential, and interactions between these factors to address specific questions and test hypothesis relating to plant-microbe interactions, address soil nutrient and C cycling, and basic ecological impacts at these sites. Grassland ecosystem soils were assessed in these studies presented, with variation in sites for soil nutrient conditions, soil erosion rates, and soil texture. The following summarizes the focus for each of the research chapters presented in this dissertation.

Chapter 2 presents a study that examines the interactions between elevated CO_2 and N deposition treatments on the functionality and community structure of free-living diazotrophic N

fixing organisms. Field samples were collected from the Cedar Creek Ecoscience Reserve in central Minnesota, USA, where plots in a randomized block design experiment which experienced eighteen years of elevated CO_2 and N deposition treatments prior to sample collection. Soil samples were utilized in a heavy $^{15}N_2$ soil incubation to assess the nitrogen fixation rate of the diazotrophic community. DNA was also extracted from soils for amplicon sequence library construction of the *nifH* gene, 16S bacterial rRNA gene for community analysis, ITS for the sequencing of fungal community members, and assessing the microbial functional potential using the GeoChip 5.0, a comprehensive functional gene microarray. Focusing on the impacts these treatments have on the diazotrophic community and its functionality, we address the following questions: 1) does elevated CO_2 stimulate N fixation rates? 2) will N deposition reduce the relative abundance of N fixers in the soil and therefore influence N fixation rates? Overall, this study is targeted to provide a detailed look at how microbial communities, functional genes, and N input functionality are influenced by the treatments presented, leading towards a mechanistic understanding of the future of N/C cycling in grassland soils under elevated CO_2 and with anthropogenic N additions.

Chapter 3 introduces a study on the ecosystem-level effects of switchgrass cultivation in marginal lands of low soil nutrient availability (N/P) on microbial communities and trace soil GHG fluxes. The core aim of this study is to show the effects of switchgrass establishment in two common but contrasting marginal soils and the soil geochemistry/microbial impacts of such establishment. The experiment was carried out over seventeen months at two sites in Southern Oklahoma. Soil chemistry, trace gas fluxes, and microbial community diversity/structure were assessed continuously every month for the duration of the experiment. We hypothesized that relative to fallow control plots, switchgrass plots would increase in soil C over time, have increased

heterotrophic soil respiration rates (while N_2O and CH_4 fluxes would remain relatively constant between plant cover types) and that the bacterial richness and beta diversity would decrease over time under switchgrass establishment. High-throughput amplicon sequencing was used to assess the changes in the microbial community dynamics along with direct real-time *in situ* measurement of soil trace gas fluxes and time series soil chemistry profiling of each of the sites. This study seeks to quantify the ecological impacts of switchgrass establishment in marginal soils by assessing the microbial community dynamics, soil trace gas fluxes, and impacts on soil chemistry over time.

Chapter 4 utilizes the same dataset introduced in the previous chapter to address fundamental theoretical questions on bacterial diversity scaling both over time and across space. This experiment utilized a nested grid of increasing areas of samples across the field sites expanding from an origin spot in the middle of the field and extending in each of the four cardinal directions to draw area squares of various magnitudes. This sampling continued for seventeen months continuously across all areas sampled to show the change in microbial alpha diversity over time. We hypothesized that microbial diversity turnover will accumulate faster over time when compared to greater spatial scales and that soil heterogeneity of the sites is related to the microbial species-time-area relationship. High throughput 16S rRNA amplicon sequencing was used to address these questions related to microbial alpha diversity scaling. Together with soil chemistry, this study aims to further explore ecological scaling laws and the relationship to microbial diversity scaling and environmental heterogeneity at local scales in these marginal lands with switchgrass.

Chapter 5 is a study on the effects of long-term cultivation of switchgrass on the subsurface deep C pool and how the microbial community influences the soil priming effect. The core aim of this study is to address the impact that accumulated root biomass has on microbial heterotrophic respiration rates and, consequently, the soil carbon balance at depth in the subsurface layers of

marginal lands. This experiment was conducted by deep soil coring at two sites that have experienced roughly ten years of switchgrass influence and comparing fallow plots where short-rooted annual grasses dominated. Deep soil cores were processed, the soil was taken for DNA extraction followed by 16S rRNA sequencing for microbial community analysis, and some fresh soil was kept in the lab for a ^{13}C labeled C priming experiment to establish the differences in heterotrophic respiration between plant root type by depth. We hypothesized that soil type, the microbial community composition, and the root type will influence the amount of heterotrophic respiration. Additionally, deep-rooted perennial grass systems (*e.g.,* switchgrass) will preferentially influence the microbial community to degrade more labile carbon sources allowing the accumulation of more recalcitrant C sources leading to a build of the carbon stocks.

The summary chapter reviews the major results and conclusions from each study presented, highlights their significance in contributing to filling our current knowledge gaps, and evaluates the implications of these studies on future research. Overall, this dissertation provides field evidence and seeks to test hypotheses related to microbial functionality and community dynamics on grassland ecosystems related to carbon and nitrogen cycling and to improve models of future climate change scenarios, SOC pools, and modifications in sustainable land usage for marginal lands.

CHAPTER TWO

ADDITIVE EFFECTS OF ELEVATED CO_2 AND NITROGEN DEPOSITION SUPPRESS NITROGEN FIXATION RATES IN A DIVERSE GRASSLAND

ABSTRACT

Diazotrophic or nitrogen fixing bacteria are critical to providing organic nitrogen (N) to plants in many terrestrial ecosystems. Currently, concern is rising for the overall effect global climate change (spurred on by increasing levels of CO_2 in the atmosphere), and the increased reliance on N deposition may have on N limited grassland ecosystems. Therefore, it is imperative that the effects of increasing levels of CO_2 and N deposition be tested on native free-living diazotrophic bacterial communities to understand how these factors affect both diversity and functionality. Here, we report a well-replicated study (n = 48) of the effect elevated CO_2, N deposition, and their combined treatment has on N fixation rates, diazotrophic community dynamics, plant biomass, and other microbial/environmental parameters. Our results reveal that individually, elevated CO_2 and N deposition both increase N fixation rates; however, the combination of these two factors knocks down N fixation rates back to ambient levels, suggesting an antagonistic effect when both are present. The diazotrophic community (assessed by *nifH* sequencing) did not show significant differences in alpha diversity metrics between treatments but did show a significant difference between groups for beta diversity and overall community dispersion. Functional potential (using DNA microarray Geochip 5.0) of N cycling genes revealed a general trend of a reduction in signal intensity for the N deposition treatment, while C cycling genes varied in probe intensity depending on the treatment. Our structural equation model showed strong direct effects of N deposition on many aspects of soil chemistry, plant biomass, and microbial features. Together, our results suggest that elevated CO_2 and N deposition treatments may reduce the functionality of the diazotrophic community and may have consequences for N/C cycling and stocks in these soils.

2.1 INTRODUCTION

The influx of carbon (C) into our atmosphere via anthropogenic activities is considered the largest disturbance of our biosphere and has shaped a majority of climate research in the 21st century. Increases in global C levels in the atmosphere have begun to radically change how it traps heat and is altering Earth's climate with growing concern (IPCC 2014). Since the 1880s, Earth's surface temperatures have increased by over 1 °C (IPCC, 2021) and are projected to increase another 1.9 to 6.4 °C by 2100 (IPCC, 2021). As a result of this global warming, Earth's terrestrial ecosystems will have severe alterations in their ecosystem functions, likely leading to reductions in various ecosystem services, which will have severe and variable consequences on biological organization levels. Additionally, N deposition has become another major concern that threatens the functionality of many terrestrial ecosystems (Waldrop et al., 2004). Currently, it is suggested that the global N cycle has doubled over the last century (Fowler et al., 2013) as a result of an increase in various N deposition sources (*i.e.*, N-fertilizer use, fossil fuel combustion, burning of biomass, and changes in land usage) to the environment. Specifically, it has been suggested that the reactive-N deposition for terrestrial ecosystems in the 1860s was 15.88 Tg year^{-1} while at the beginning of the 1990s, it was estimated to be 63.5 Tg year^{-1}, a four-fold change in N deposition (Galloway et al., 2004). Additionally, N deposition is expected to continue to increase and may reach up to 125 Tg year^{-1} by 2050 (Galloway, 2000). Thus, understanding the interplay between elevated atmospheric C levels and increased N deposition is essential to understanding, mitigating, and modeling these anthropogenic disturbances and their effects on terrestrial ecosystem functionality.

Grasslands account for up to 31-43% of the total land area on Earth (FAO, 2014) and provide a wide range of ecosystem services, such as providing carbon storage, erosion control, climate mitigation, pollination, and can regulate water supply and help flow regulation (Bengtsson et al., 2019). Additionally, a majority of agriculture takes place in grassland ecosystems, making them vital in food production and for the livelihood of many people across the globe. Thus, it is critically important to understand how elevated CO_2 and increased N deposition may impact grassland ecosystems. Elevated CO_2 has been shown to stimulate photosynthesis (Ainsworth and Long, 2005) and can increase plant biomass (Craine *et al.,* 2003), but this is often limited by other factors, such as water limitations, plant species, and nitrogen or other nutrient availability. Furthermore, N deposition may also increase plant biomass; however, little is known on the effects of these factors on the free-living diazotrophic microorganisms living in the soil who are essential for supplying N to these environments in the absence of N deposition by fertilization.

Biological nitrogen fixation (BNF; diazotrophy) is the conversion of molecular nitrogen (N_2) into ammonia (Welsh, 2000) and is exclusively carried out by prokaryotic organisms (Raymond *et al.,* 2004). Thus, diazotrophy provides the basis for biosynthetic pathways of nitrogen-containing compounds such as proteins and nucleic acids. Some prokaryotic nitrogen fixers are associated with eukaryotic hosts such as *Rhizobium* and *Bradyrhizobium* genera that form root nodule symbiosis with legumes (Pawlowski *et al.,* 1996). However, many nitrogen fixers in the soil are free-living diazotrophic organisms that can fix nitrogen for themselves and contribute to environmental N levels. Free-living diazotrophic organisms also play a key role in soil organic matter cycling (Kaschuk & Hungria, 2017), vital to C cycling and providing N inputs to soil ecosystems. Overall, BNF contributes up to 96% of the N input derived from natural processes and is the second major contributor to life after photosynthesis (Ormeno-Orrillo *et al.,*

2013). It is estimated that BNF has an annual global input at approximately 55 Tg of N (Crews & Peoples, 2005). Preserving diazotrophic diversity is useful in contributing ecosystem services that BNF provides, like increased soil fertility and mitigation of greenhouse gas emissions (Kaschuk & Hungria, 2017). However, it is currently unknown whether these benefits are conferred by the greater abundance of a few species or by more diverse communities that ensure functional redundancy. Additionally, the effects of elevated CO_2 and N deposition need to be addressed for how they affect free-living diazotrophic bacterial diversity.

In this study, we report the results from a well-replicated long-term (17 years at the time of sampling for continuous treatment) elevated CO_2, N deposition, and combination of these treatments in the diverse (16 species) plant community plots from the BioCON (Biodiversity, CO_2, N deposition) experiment in Minnesota. We measured the nitrogen fixation rates and *nifH* abundance/alpha diversity of free-living nitrogen fixers in the ambient CO_2 (Control) or elevated CO_2 (eCO_2) with N deposition ($eNeCO_2$ and eN). Additionally, we sequenced 16S bacterial and 18S ITS fungal sequences to explore the diversity changes due to these treatments. Geochip 5.0 DNA hybridization microarray technology was used to probe the functional potential differences in C/N cycling genes between the treatments. We hypothesized that elevated CO_2 would increase nitrogen fixation rates via increased plant-microbe interactions in the rhizosphere to meet their N demand as they increase their biomass and lead to: (i) higher *nifH* richness, and (ii) N deposition will act to suppress N fixation rates due to the plants decreasing their reliance on diazotrophic N sources for growth. We further explore the impacts these treatments have on functional potentials of C/N cycling genes and the community dissimilarity between treatments for all microbial communities assessed (bacterial 16S and ITS fungal), as well as determine the interplay between environmental soil parameters and other variables.

2.2 MATERIALS AND METHODS

2.2.1 Study area, sample collection, and elevated CO_2 and nitrogen deposition treatments

Samples were collected from the BioCON FACE experiment which is in the Long-Term Ecological Research site at Cedar Creek Ecosystem Science Reserve in Minnesota, USA (Latitude: 45^o N, Longitude: 93^o W). Details on the site are described in Adair *et al.*, 2011 (Adair *et al.*, 2011). Briefly, BioCON soils are sandy (93% sand) and generally considered poor in soil organic matter (SOM) with relatively low total N content. The BioCON experiment consists of 354 plots evenly distributed among six 20 m diameter circular areas and was established in 1997. For this experiment, only the diverse 16 species plots (12 plots for each treatment; n = 48) were used which contain four functional plant groups (C3 and C4 perennial grasses, forbs, and legumes). Beginning in 1998, the CO_2 concentrations in three of the rings have been elevated by 180 ppm CO_2 above the ambient concentrations during each day of each subsequent growing season. For the nitrogen deposition treatment, half of the plots received 4 g N m^2 yr^{-1} applied as 34% ammonium nitrate pellets (regular lawn or agricultural fertilizer) 3 times per growing season (May, June, and July), which is a deposition rate similar to heavily industrialized areas and represents roughly doubling the N availability in the plots. The plots that receive N amendments receive an addition ^{15}N enrichment at the time of fertilization of 0.1058g of 5 atom % ^{15}N (as $^{15}NH_4{}^{15}NO_3$) per application. The BioCON experiment follows a split-plot arrangement of the treatments in a randomized design with the elevated CO_2 treatment split as a whole-plot factor and subplot treatments for plant diversity and N deposition randomly distributed within the rings. Soil samples were collected from the top 10-15 cm of soil in September of 2015. Soil samples were then place on ice and shipped to the IEG lab at the University of Oklahoma in Norman where the soil DNA extractions, sequencing, and heavy $^{15}N_2$ soil incubations were carried out.

2.2.2 Soil chemistry, plant above and belowground biomass estimates

All soil chemical and plant measures were obtained from the Cedar Creek Ecosystem Science Reserve Complete Dataset (https://www.cedarcreek.umn.edu/research/data) for the BioCON (Biodiversity, elevated CO_2, and N enrichment experiment) sixteen plant species plots. Soil moisture for each plot was taken in the summer of 2015 via tube access and expressed in proportion soil moisture for soil depths 0-17 cm. Five soil cores were taken per plot at various depths. In this study, the 0-10 cm soil samples were used for further analysis. After the soil samples were dried, it was sieved to remove roots and other plant material. Percent total C and N was measured with a C-N Analyzer (NA15000, Carlo-Erba Instruments or ECS 4010, COSTECH Analytical Technologies Inc.) in 2012 for each of the plots used in this study at the 0-10 cm soil depth. Soil pH was data used in this study was collected in 2014 and pH was taken from samples taken for nitrogen mineralization. Soil samples were taken and transferred into a solution of 1M KCl, which was used to extract available nitrogen (ammonium, nitrate, nitrite). The supernatant was then pipetted off the soil/KCl mixture into vials. This solution was then analyzed for nitrogen content. The samples were then frozen until measured for pH and this was used to approximate soil pH values using a pH probe. Nitrate and ammonium levels from 2002 were used as they were the most recent measures available that included all diverse plant community plots. Above ground and below plant biomass was recorded by weight in grams per meter squared via harvesting in the late summer of 2015, just prior to our soil sampling for active nitrogen fixation rates. Plants were clipped approximately 1 cm above the soil level, sorted and dried to estimate aboveground biomass. Three root cores for each plot at 0-20 cm were used for biomass estimates. Root samples were then placed on a soil screen and sprayed with water to separate roots from the soil. Roots were then sorted by crowns, coarse roots, and fine roots and placed into separate bags then dried

and weighed for biomass estimates. Total root biomass (addition of each sorted root type) was used in this study for further analysis.

2.2.3 Microbial community DNA isolation and purification

A freeze grinding method outlined in Zhou, J., Bruns. M. A., & Tiedjie, J. M., 1996 was used for crude DNA extractions in combination with the MBio Powersoil DNA extraction kit for all soil samples in this study. This method yielded both high quality and quantity of DNA extracted from the soil. DNA quality was verified evaluating the absorbance at wavelengths of 230 nm, 260 nm, and 280 nm detected by a NanoDrop ND-1000 spectrophotometer (Thermo Fisher Scientific, Waltham, MA, USA). The 260/280 nm absorbance ratios were > 1.8 and > 1.7 for 260/230 nm ratios used for further analysis. DNA amounts were quantified using PicoGreen and a FLUOstar OPTIMA fluorescence plate reader (BMG LABTECH INC., Cary, NC, USA) and used for gene array labeling and sequencing library preparation. All purified DNA samples were stored at -80 ^{o}C.

2.2.4 Bacterial 16S*, nifH*, and ITS community sequencing

For microbial community profiling, a two-step PCR method (Wu *et al.*, 2015) was used for amplification of the V4 region of the bacterial 16S gene using the 515F and 806R primers. Amplification of the *nifH* gene amplicons was conducted using the PoIF (TGCGAYCCSAARGCBGACTC) and PoIR (ATSGCCATCATYTCRCCGGA) primers (Feng *et al.*, 2019). ITS amplification was carried out using the ITS7F (5′-GTGARTCATCGARTCTTTG-3′) and ITS4R (5′-TCCTCCGCTTATTGATATGC-3′) primers (Feng *et al.*, 2020). The forward PCR primer for each amplicon library contained an Illumina adapter sequence, followed by a forward primer pad, a forward primer link and then the either the

515-forward primer, PoIF, or ITS7F; in addition to these, the reverse primer sequences also contained a sample-unique barcode sequence inserted between the reverse Illumina adapter and the reverse primer pad sequences for parallel sequencing of a set of samples for each of the amplicon libraries constructed. After amplification and the products were quantified using PicoGreen on a FLUOstar Optima Fluorescence plate reader. One hundred ng PCR products from each sample were then combined into one tube and run on a 1% agarose gel at 100V for 45 min and purified through QIquick Gel Extraction Kit (Quiagen) column. The purified sample was then quantified again using PicoGreen in triplicate, to ensure the accuracy of each library concentration. Each pooled sample was then diluted to 2 nM; 10 µL of 0.1 N NaOH was then added into 10 µL of sample DNA for denaturation. This DNA was diluted to 6 pM and mixed with an equal volume of 6 pM Phi X library in order to increase sequence diversity. Finally, the mixture (600 µL) was loaded into a reagent cartridge and sequenced on a MiSeq (Illumina, Inc., San Diego, CA, USA) platform and following the manufacturer's instructions. Raw sequencing was processed as described in Guo, *et al,*. 2018 using the website (http://zhoulab5.rccc.ou.edu:8080/) on the Galaxy pipeline (Giardine *et al.*, 2005).

2.2.5 Heavy isotopic nitrogen soil incubations

Prior to the soil incubations with heavy isotopic $^{15}N_2$ gas, all soil samples were sieved with a 4 mm sieve to remove plant roots, rocks, and unwanted material. Soil samples were stored at 5 °C then allowed to activate at room temperature for 24 hours prior to isotopic incubation. For each of the three technical replicates used in the isotopic incubations, 5 g dry weight of soil was weighted and placed into 15 mL glass vials and sealed with a rubber plug. A total of 288 samples (48 samples, a control N_2 and heavy isotopic $^{15}N_2$ group, and 3 technical replicates) were used in the soil incubation experiment. The heavy isotopic group was treated with 99.8% atom-enriched

$^{15}N_2$ gas. Soil samples were taken from the initial time point and 10 days after sealing. Before gas injection the headspace was evacuated and flushed three times with an inert gas (100% He), then for the control group 15 mL of a gas mixture (80% N_2 and 20% O_2) of synthetic air was added to the head space of each sample. In the heavy isotopic group, after headspace evacuation and flushing, an 80% $^{15}N_2$ and 20% O_2 mixture was added in the same amount to each vial's headspace using gas tight syringes. The gas mixture was created in airtight gas bags to simulate the atmospheric concentrations of N_2 and O_2. During the 10-day incubation period, soils were kept at room temperature and in the dark with aluminum foil covering the vials. All soil samples taken were dried in an oven for > 24 hours to remove moisture before packaging in Tn capsules to be sent to The Stable Isotope Facility located at The University of California in Davis for heavy isotopic mass-spec analysis. Soil samples were first combusted at 1080 °C in a reactor packed with chromium oxide and silvered copper oxide. After combustion, the oxides are removed in a reduction reactor with reduced copper at 650 °C. Helium was used as the carrier gas that flows through a water trap and samples are passed through a Micro Cube elemental analyzer (Elementar Analysenysteme GmbH, Hanau, Germany) then passed through a PDZ Europa 20-20 isotope ratio mass spectrometer (Sercon Ltd., Cheshire, UK).

2.2.6 Nitrogen fixation rates

The final delta values for $\delta^{15}N$ used for the calculation of the nitrogen fixation rate were calculated using the following equation:

$$\delta 15N(‰) = [\ (R_{sample}\ /\ (R_{Air}) - 1]\ x\ 1000$$

where R_{sample} and R_{Air} represent the isotopic ratio of $\delta^{15}N$ in the sample relative to the air as a standard. The percent ^{15}N accumulation in the soil was calculated using the following formula:

$$N_s\% = \frac{[\delta_t - \delta_c]}{[\delta_s - \delta_c]} x\ 100$$

Where $N_s\%$ is the proportion of heavy ^{15}N isotope that is accumulating in the soil from the synthetic air mixture injected into the headspace of the vials, δ_t is the $\delta^{15}N$ ratio found in the heavy isotopic treatment soils, δ_c is the $\delta^{15}N$ ratio found in the control soils, and δ_s is the $\delta^{15}N$ in the isotopic gas mixture. Thus, the N fixed by the free living diazotrophs in the soil over the course of the soil incubation experiment was calculated as:

$$N(\mu g \cdot kg^{-1} soil\ \cdot day^{-1})$$

$$= N_s(\%)\ x\ total\ soil\ N\ (\mu g \cdot kg^{-1} soil\ \cdot day^{-1})\ /100$$

Where the total soil N was adjusted to be in terms of micrograms of N per kg of soil per day, yielding the nitrogen fixation rates for each of the treatment groups. It should be recognized the calculated potential rates shown in this experiment can differ from the *in situ* rates due to various bottle effects, but such rates are commonly used for assessing the relative differences in the activities of microbial communities.

2.2.7 Geochip 5.0 DNA microarray

GeoChip 5.0 was used in this study to investigate the microbial functional structure. GeoChip 5.0 is a comprehensive gene array containing 167,044 probes designed for covering

395,894 coding sequences from ~1500 functional gene families involved in microbial C, N, S, and P cycling, energy metabolism, stress response, metal homeostasis, viruses, and virulence. For each sample, 1 µg DNA was diluted (to a volume of 25 µL) and mixed with 20 µL of random primers (Invitrogen by Life Technologies, Grand Island, NY, USA), then denatured for 5 min at 99.9 ^{o}C and immediately chilled on ice. 1 µL of florescent dye Cy-3 dUTP (GE Healthcare UK Limited, Bukinghamshire, UK), 2.5 µL of dNTPs (5 mM Dagc-tp, 2.5 mM dTTP), and 80 U of the large Klenow fragment (Imer Inc. CA, USA) were added to the denatured DNA. This mixture was then incubated for 6 hours at 37 ^{o}C, followed by a heating treatment at 95 ^{o}C for 3 min. Labeled DNA was purified using the QIAquick PCR purification kit (Qiagen, Valencia, CA, USA) according to the manufacturer's instructions. Cy-3 dye concentration was measured on a NanoDrop ND-1000 spectrophotometer (NanoDrop Products). Labeled DNA was then dried in a Savant SPD1010 SpeedVac concentrator system (Thermo Fisher Scientific, Waltham, MA, USA) at 45 ^{o}C for 45 mins. Labeled DNA was resuspended in 10 µL hybridization solution containing 2.68 µL of sample tracking control (Roche NimbleGen, Inc., Madison, WI, USA), 40% formamide, 25% SSC, 1% SDS, 1.6% Cy3-labeld alignment oligo, 1.5% Cy5-labled alignment oligo, and 2% Cy5-labled common oligonucleotide reference standard target (Roche NimbleGen, Inc., Madison, WI, USA). After a denaturing step at 95 ^{o}C for 5 min, the mixtures were spun down and kept at 42 ^{o}C to before being dispensed onto the glass microarray slide. Each array was preheated to 42 ^{o}C in the 12-Bay MAUI Hybridization system (BioMicro Systems, inc., Salt Lake City, UT, USA) for at least 5 min prior to sample loading. Hybridizations were performed on the MAUI Hybridization system at 42 ^{o}C in the presence of 40% formamide for roughly 16 hours with mixing. Mixers were then removed from the slides while soaking in buffer I. Each slide was manually washed in buffer I for an additional 120 seconds, then placed in buffer II for 60 seconds and in buffer III for 15 seconds and

spun dry in a NimbleGen slide spinner. All washing buffers were proved by NimbleGen. Dried microarrays were then scanned with a laser power of 100% and a photomultiplier (PMT) gain of 100% by a MS 200 Microarray Scanner (NimbleGen) at 532 nm and 635 nm. NimbleScan software version 2.5 (NimbleGen) was used to grid the images. After gridding, every spot (containing one unique probe) on the GeoChip array was fixed into a 7 x 7 pixel square and was adjacent to four blank equal-sized squares (void spaces). The probe signal was then calculated as the average intensity of the center 5 x 5 pixels for each spot, and the background noise signal was an average of the void intensity for each spot. The signal and background intensity report was generated via the NimbleScan software. Raw data from the NimbleSan was then submitted to the Microarray Data Manager on our website (http:///ieg.ou.edu/microarray/) and analyzed using the data analysis pipeline with the following major steps: (i) Raw signal intensities (Cy3 channel) on each array were multiplied by a normalization weight I, which is the ratio of the maximum average universal standard intensity (Cy5 channel) among all the samples divided by the average universal standard intensity of each array; (ii) signal intensities on each array were then multiplied by a normalization weight II, which is the ratio of the maximum total raw intensity (Cy3 channel) among all the samples divided by the total raw intensity of each array; (iii) spots with SNR (signal to noise ration) ≥2 were considered as positive. Otherwise they were treated as negative spots with 0 value (iv) and spots with signal intensity lower than 1000 were not considered as positive and were removed from subsequent analysis; (v) if a probe appeared in only one-fourth or fewer of the samples in one treatment group (three out of twelve samples), it was removed from that group before any further analyses; (vi) signal intensities were transformed to their natural logarithm; (vii) the mean ratio in each sample was then calculated by dividing the transformed signal intensity of each probe by the average transformed signal intensity for all detected probes in each sample; (viii) because

we have functional data to support *nifH* function, *nifH* probes underwent a further selection criteria with selection of probes that correlated probe intensities with the functional outputs measured by the heavy nitrogen fixation assay.

2.2.8 Statistics

All analyses were conducted using the R statistical software (R Core Team, 2014) (3.4.4) and figures were generated using the package ggplot2 (Wickham, 2009). Data normality was tested utilizing the Shapiro test and the homogeneity of variance by the Bartlett test. Differences between groups tested using the Student's T-test when statistical assumptions were met. Differences between groups for nitrogen fixation rates were determined by ANOVA and TukeyHSD with Cohen's d providing a measure of the effect size between treatments. Dispersion and dissimilarity between groups in the microbial communities for bacterial 16S, fungal ITS, and *nifH* communities tested using PCoA, ANOSIM, Adonis test, and MRPP. NMDS was used to visualize the differences in community structure for microbial communities. A CCA plot was used to link soil characteristics, plant biomass estimates, and nitrogen fixation rates to the free living diazotrophic community.

Structural equation modeling (SEM) was used to explore the direct and indirect relationships among environmental variables, plant biomass estimates, and microbial variables. Based on a correlation analysis among all variables, we first considered a full model that included all reasonable pathways, then eliminated nonsignificant pathways until we obtained a final model. We used a χ^2 test and the root mean square error (RMSE) to evaluate the fit of our model (n = 48). The SEM-related analysis was performed using the lavaan R package (Rossel, 2012).

2.3 RESULTS

2.3.1 Impacts of treatments on soil characteristics

Nitrogen deposition treatment significantly lowered ($p < 0.01$; by Student's T-test) the soil pH levels (**Table 2.1**) at each plot (eN and eNeC treatments) when compared to control or elevated CO_2 treatments.

Table 2.1: Differences in soil properties for each treatment. Values are mean ± SD values.

Variable	Control	elevated CO_2	elevated N	elevated CO_2 elevated N
	Mean ± SD	Mean ± SD	Mean ± SD	Mean ± SD
pH	6.24 ± 0.25	6.38 ± 0.24	5.89 ± 0.25	6.02 ± 0.28
Proportion Soil Moisture	0.05 ± 0.021	0.077 ± 0.02	0.036 ± 0.025	0.075 ± 0.01
Total soil C (%)	1.1 ± 0.26	1.3 ± 0.26	1.29 ± 0.27	1.31 ± 0.26
Total soil N (%)	0.0934 ± 0.018	0.1034 ± 0.018	0.1023 ± 0.019	0.1033 ± 0.018
C/N Ratio	11.7 ± 0.74	12.3 ± 1.1	12.6 ± 0.6	12.7 ± 0.99
Nitrate (mg/kg)	0.0254 ± 0.021	0.0226 ± 0.024	0.0273 ± 0.022	0.071 ± 0.023
Ammonium (mg/kg)	0.37 ± 0.28	0.26 ± 0.33	0.39 ± 0.32	0.17 ± 0.33

There were no differences between the control and elevated CO_2 treatments or between nitrogen treatment plots. Proportional soil moisture (**Table 2.1**) was significantly lower ($p < 0.05$; by Student's T-test) for elevated N only when compared to elevated CO_2 or the combined treatment but was not significantly different from the control treatment plots. Percent total soil C was significantly lower ($p < 0.05$; by Student's T-test) between the control plots and the combined treatment plots only. No statistical differences were observed between treatments for percent total N in the soil. Both nitrogen treatments had a significantly higher C/N ratio when compared to the control treatment but no difference between each other or the elevated CO_2 treatment. Nitrate levels were significantly higher ($p < 0.05$; Wilcoxon rank sum test) for the combined treatment (eNeC) when compared to the other groups. The combined treatment also showed a significantly reduced

level ($p < 0.05$; Wilcoxon rank sum test) of ammonium present in the soil when compared to the control group.

2.3.2 Impacts of treatments on nitrogen fixation rates, *nifH* alpha diversity, and community dissimilarity

Analysis of N-fixation rates in the soil revealed (**Figure 2.1**) there was a significant ($p < 0.001$; by ANOVA and Tukey HSD) stimulation in rates for both the elevated CO_2 (Large effect size by Cohen's d = 2.57, **Table S2.1**) and the N deposition treatments (Large effect size by Cohen's d = 2.46) when compared to the control group plots.

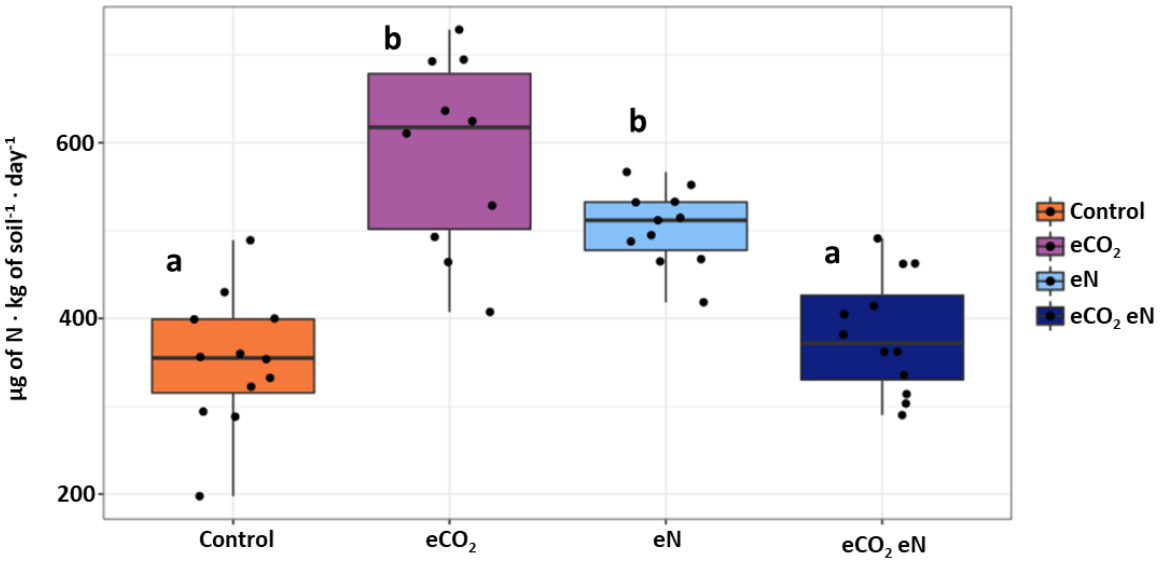

Figure 2.1 Isotopic derived mean nitrogen fixation rates at the BioCON site for the plots with sixteen plant species by treatment. Letters indicate significance by ANOVA and TukeyHSD ($p < 0.001$). Each plot consisted of 12 biological replicates and 3 technical replicates. Rates were from ^{15}N accumulation after 10 days of $^{15}N_2$ incubation (methods).

However, most surprising was a suppression of the rates back to ambient control levels with the combined treatment (no statistically significant difference between these groups). In terms of the total *nifH* observed species for each group (**Table S2.2**), the combined treatment had the highest

at 1229 while similar numbers were observed for the eCO_2 and N deposition treatments (1184 and 1145, respectively) with the Control plots having the lowest *nifH* species richness at 1077. There was no significant difference between the average observed species means, Chao1 index, Shannon index, or when using the Simpson index (**Table S2.2**) between the groups. Although, all treatment groups tended to have higher values for all the alpha diversity metrics when compared to the Control plots. A non-metric multidimensional scaling (NMDS) (**Figure 2.2a**) of the *nifH* community shows tight clustering of the N deposition treatments, while the control and elevated CO_2 have more dissimilarity from the other treatments.

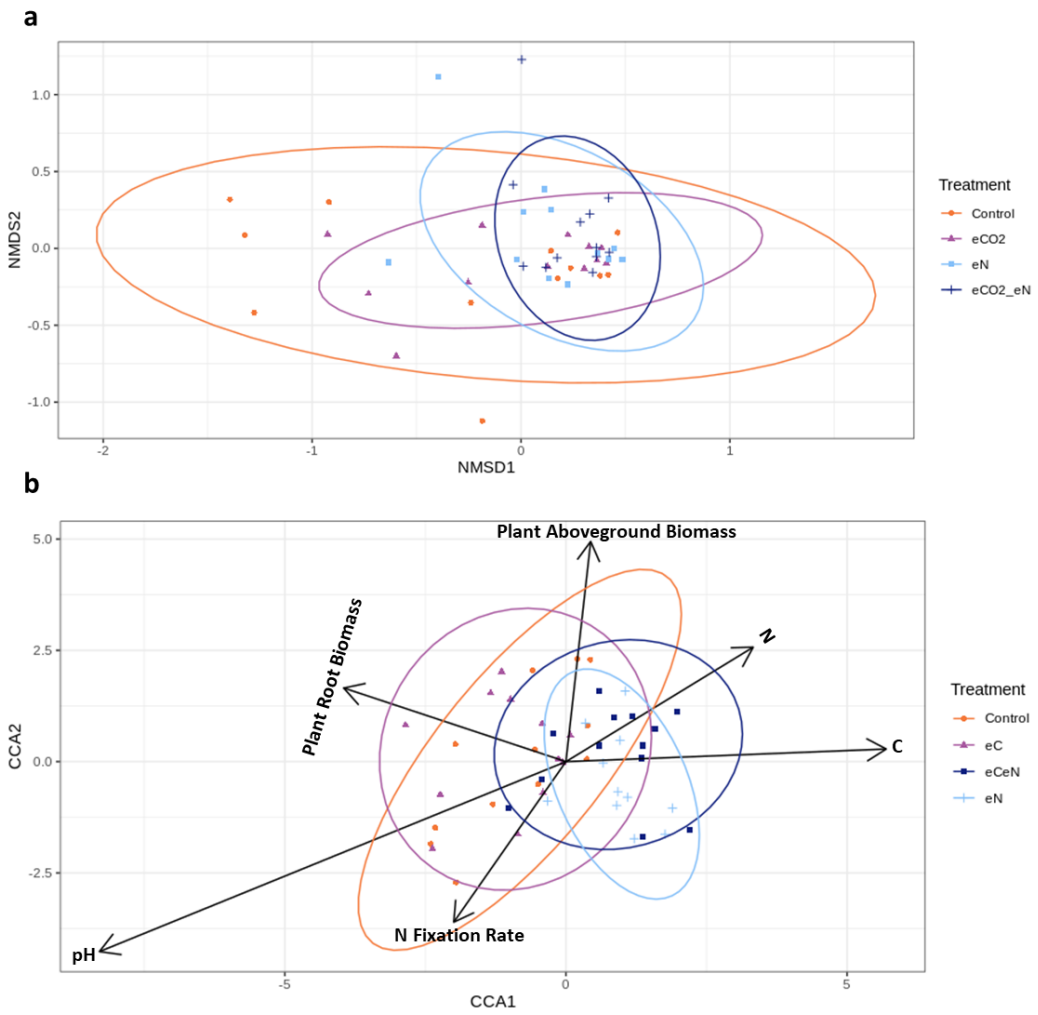

Figure 2.2 NMDS and CCA of the *nifH* gene community by treatment for: **a**, NMDS using Bray-Curtis distance; **b**, Canonical correspondence analysis (CCA) of the samples (circle, triangles, squares, and plus signs) and major environmental and functional factors. The overall CCA was significant ($p < 0.05$).

A dispersion plot using a principal coordinates analysis (PCoA) (**Figure S2.1a**) reveals a similar pattern to the NMDS, as the N treatments cluster away from the control and elevated CO_2 plots. ANOSIM was then used to establish a statistically significant difference in each treatment groups dispersion compared to the control treatment (**Figure S2.1b**, $p < 0.05$). A canonical correspondence analysis (**Figure 2.2b**, $p < 0.05$) revealed the *nifH* community composition was shaped by the influence of plant root biomass in the elevated CO_2 plots while total N/C percent

was a major factor in shaping the free-living diazotrophic community in both N deposition treatments.

2.3.3 Impacts of treatment on microbial community dynamics

The bacterial 16S microbial relative abundance of phyla between groups (**Figure 2.3a**) showed a few significant differences ($p < 0.05$ by Student's T-test) between the elevated CO_2 and N deposition treatments but not between any of the other treatments.

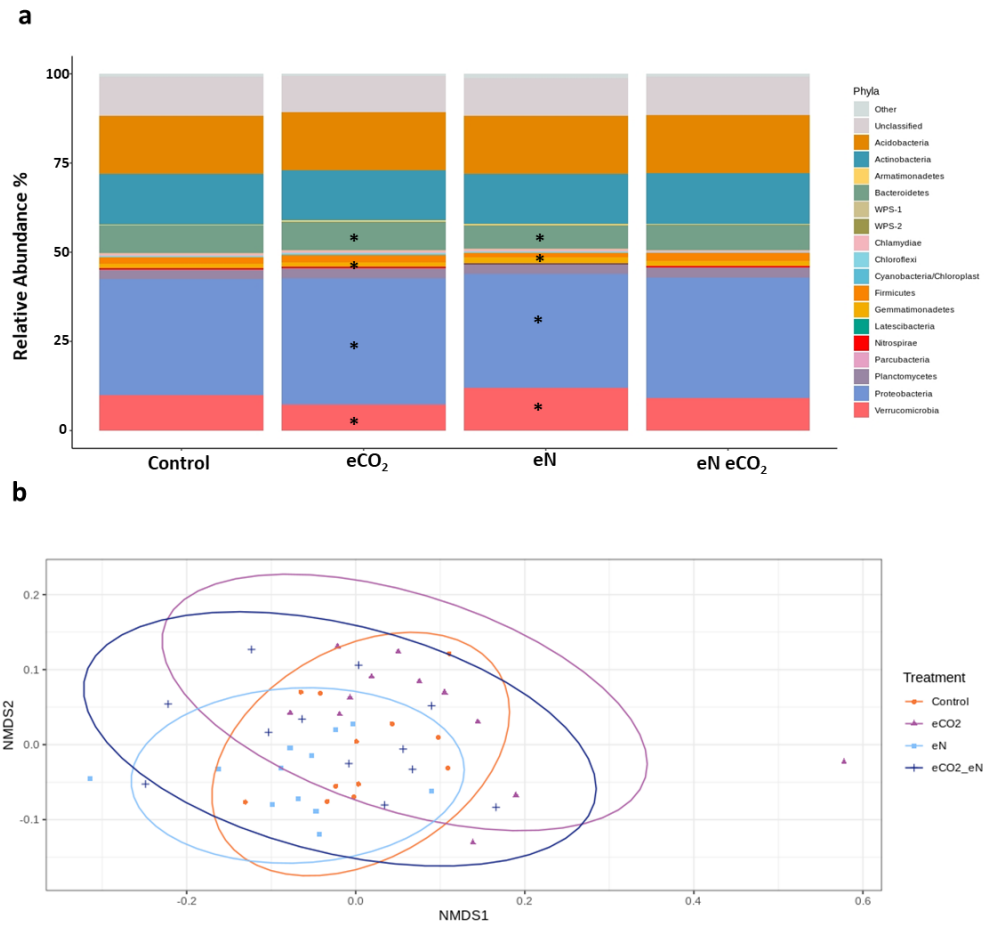

Figure 2.3 Differences in bacterial community between treatments for: **a**, Relative abundance breakdown of the 16S bacterial phyla for the BioCon site by treatment; **b**, NMDS using Bray-Curtis distance of the 16S community at the OTU level by treatment. Asterisks denote significant difference ($p < 0.05$ by Student's T-test) between the relative abundance of phyla when compared to the control group.

We observed a significantly higher relative abundance of *Verrumicrobia* and *Gemmatimonadetes* phyla in the N deposition treatment while the eCO_2 treatment had significantly more *Proteobacteria* and *Bacteroidetes* phyla present. The NMDS of the bacterial community (**Figure 2.3b**) reveals little dissimilarity between the communities based on treatment. Alpha diversity in terms of number of OTUs and Shannon index (**Figure S2.2ab**, $p < 0.05$) was reduced for the N deposition treatment only. There were no statistical differences between groups for phylogenetic

diversity (**Figure S2.2c**). The 16S microbial community did not show any significant dispersion differences by group in the PCoA or tested by ANOSIM (**Figure S2.3ab**).

For the ITS fungal microbial community (**Figure 2.4a**), relative abundance shifts in various fungal classes were mainly observed in the elevated CO_2 treatment.

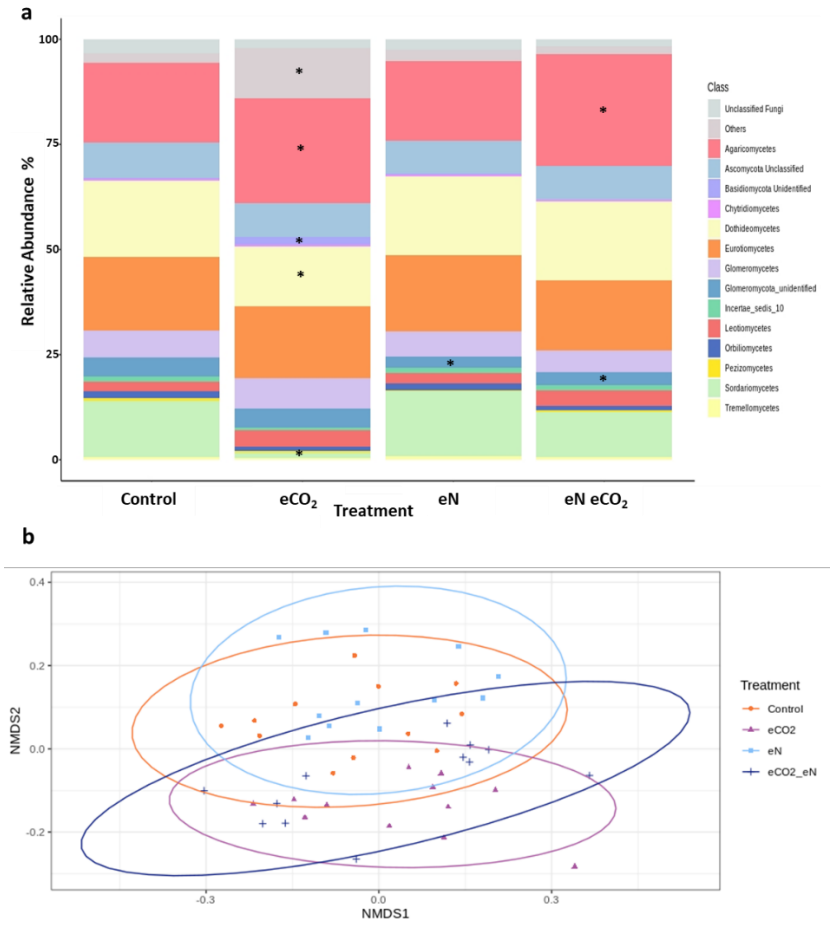

Figure 2.4 Differences in fungal community between treatments for: **a**, Relative abundance of different fungal classes for the BioCon site by treatment; **b**, NMDS of the ITS fungal community using Bray-Curtis distance by treatment. Asterisks denote significant difference ($p < 0.05$ by Student's T-test) between the relative abundance of phyla when compared to the control group.

Specifically, the *Sordariomycetes* and *Dothideomycetes* were significantly ($p < 0.05$ by Student's T-test) lower than any of the other treatments for the elevated CO_2 treatment, while the

Basidiomycota and others category were significantly elevated. Both treatments that had elevated CO_2 showed and increased relative abundance in *Agaricomycetes* relative to the control or N deposition treatment, while in both N addition treatments unidentified *Glomeromycota* were significantly reduced compared to the control or elevated CO_2 treatments. The NMDS for the fungal community between treatments (**Figure 2.4b**) revealed more clustering for the control and N deposition treatment with both elevated CO_2 and the combined treatment overlapping. The dispersion of the community tested with PCoA and ANOSIM (**Figure S2.4ab**) showed a significant difference ($p < 0.001$) between each group and again confirmed a tighter overlapping of elevated CO_2 and the combined treatment.

2.3.4 Geochip 5.0 functional potential of N/C cycling genes

Geochip microarray functional potentials (**Figure 2.5a**) for the *nifH* gene log normalized signal intensity aligned with our measures of nitrogen fixation rates for the different treatments with both elevated CO_2 and N deposition treatments having significantly higher ($p < 0.05$ by Student's T-test) signal intensity than either the control or combined treatment groups.

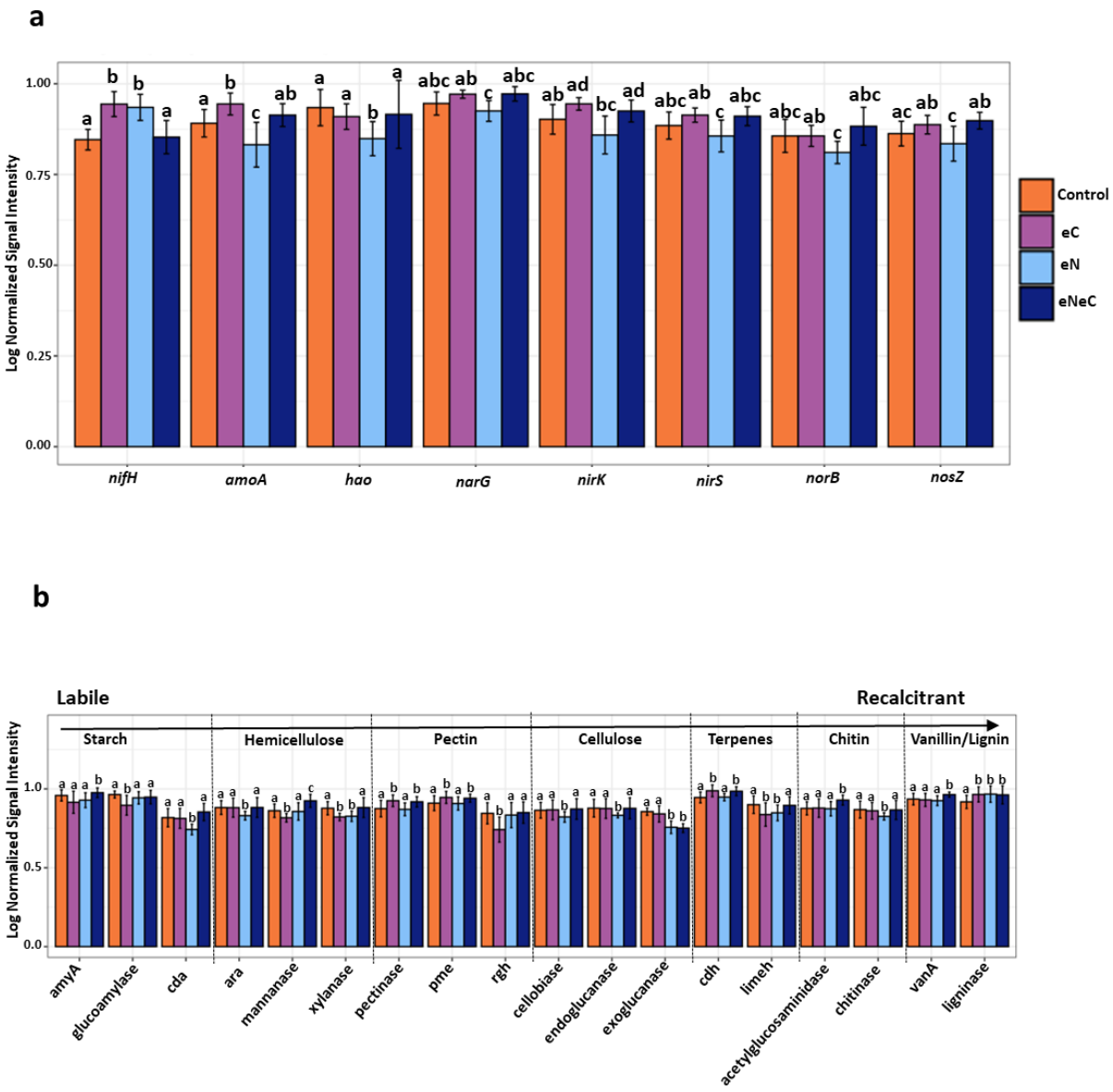

Figure 2.5 Geochip normalized signal intensity for: **a**, Nitrogen cycling genes from the BioCon plots by treatment group and **b**, carbon cycling genes by treatment ordered from labile to recalcitrant carbon source. All values are mean ± standard deviation. Significance established by letters using t-test with p values less than 0.05.

The ammonia monooxygenase gene *amoa* (important for aerobic ammonia oxidizing organisms) showed significantly higher signal intensity for the elevated CO_2 treatment and significantly lower intensity for the N deposition treatment when compared to the control group. The gene encoding

hydroxylamine oxidoreductase *hao* revealed a significant decrease in signal intensity in only the N deposition treatment. The *narG, nirK,* and *nirS* genes involved in nitrite reduction had a significant decrease in signal intensity for the N deposition treatment when compared to the elevated CO_2 treatment. The nitric oxide reductase subunit B gene *norB* also showed a lower signal intensity in the N deposition treatment when compared to the elevated CO_2 treatment only. The *nosZ* gene which encodes nitrous-oxide reductase had significantly higher signal intensity for both elevated CO_2 and the combined treatment when compared to the N deposition treatment. Overall, many nitrogen cycling genes showed a reduction in signal intensity for the N deposition treatment, especially when compared to the elevated CO_2 treatment.

For carbon cycling genes (**Figure 2.5b**), the gene *amyA* which encodes the enzyme amylase (important for hydrolysis of starch into simple sugars) had a significantly higher signal intensity for the combined treatment group when compared to the other groups. Glucoamylase (saccharification of starch/dextrin to glucose) signal intensity revealed a significant decrease for the elevated CO_2 treatment when compared to the other treatments. The *cda* gene signal intensity significantly dropped for the N deposition treatment only when compared to the other treatments. The *ara* gene encoding L-arabinose operon for the breakdown of five carbon L-arabinose showed a significant decrease in the N deposition treatment. The mannanase gene signal intensity revealed a significant decrease for elevated CO_2 treatment with an elevated signal with the combined treatment when comparing the control and N deposition groups. Signal intensity for the xylanase gene showed a reduction for both elevated CO_2 and N deposition treatments when compared to the control; however, the combined treatment rescued signal intensity back to comparable levels to the control group. For pectin cycling genes, like pectinase and the *pme* gene, elevated CO_2 and the combined treatment significantly increased signal intensity when compared to the control or N

deposition groups. The *rgh* gene showed significant reduced signal intensity in only the elevated CO_2 treatment. Cellulose cycling genes (cellobiase, endoglucanase, and exoglucanase) all exhibited a similar significant decrease in signal intensity for N deposition treatments with exoglucanse also showing a decrease for the combined treatment when compared to the control and elevated CO_2 groups. For genes related to terpene cycling *cdh* and *limeh*, the former (*cdh*) saw an increase in signal intensity with elevated CO_2 and the combine treatment, while the latter (*limeh*) had a decrease in signal intensity for elevated CO_2 and N deposition when compared to the control and combined treatment groups. The acetylglucosaminidase signal intensity showed an increase only in the combined treatment. For chitinase, a decrease in signal intensity was observed in only the N deposition treatment group. The gene *vanA* which encodes vanillate O-demethylase revealed a signal increase when under the combined treatment, while lignin degradation gene ligninase showed a significant increase in all treatment groups relative to the control group.

2.3.5 Structural equation model links microbial features to plant biomass estimates and soil conditions

Structural equation modeling (SEM) was used for an in-depth analysis of the direct and indirect effects of elevated CO_2 and N deposition (**Figure 2.6**) on microbial features (*i.e.*, Microbial alpha diversity, *nifH* abundance, and phylogenetic diversity), plant biomass estimates (*i.e.*, root and aboveground), and soil conditions (*i.e.*, soil pH and C/N %).

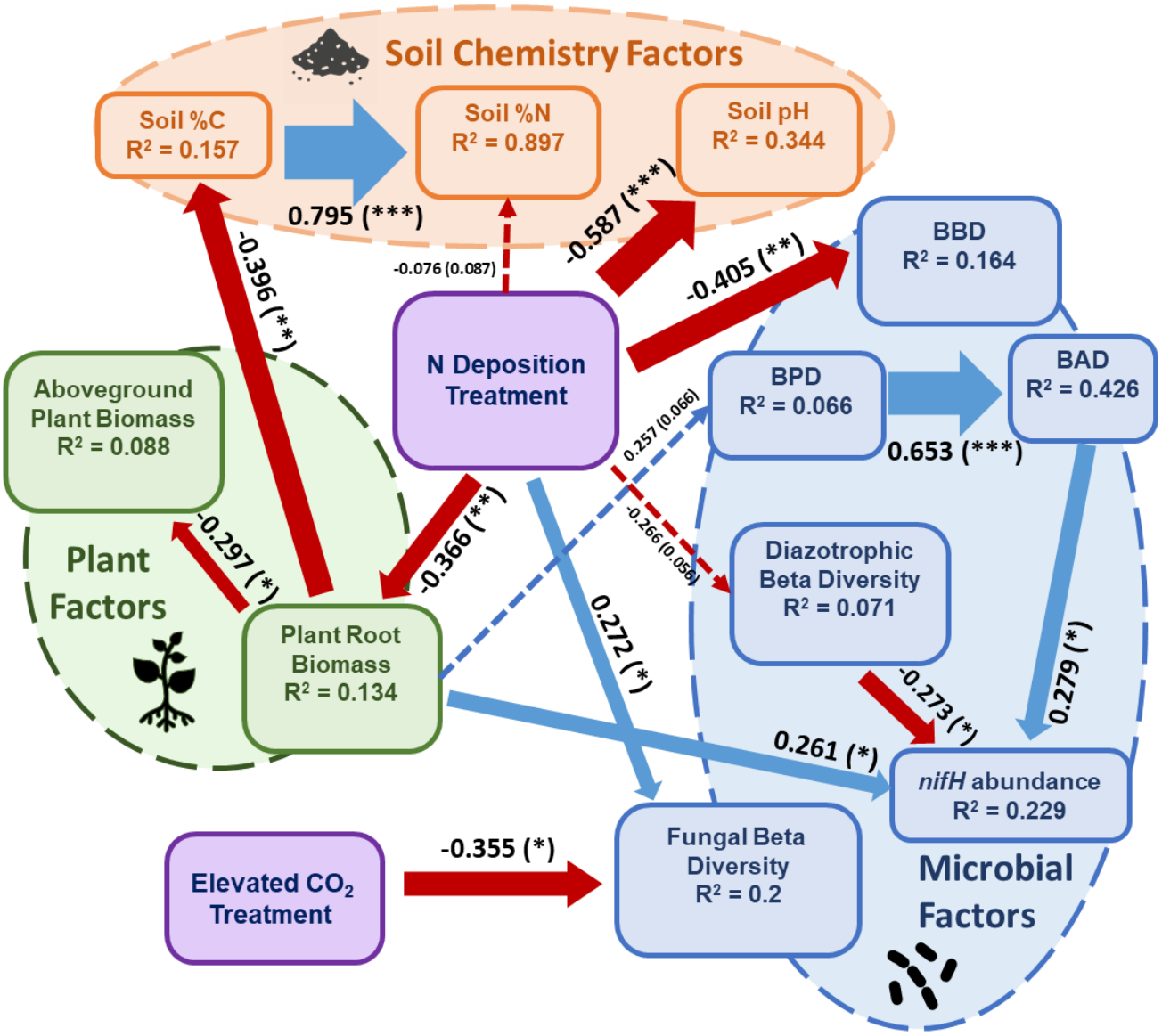

Figure 2.6 Structural equation modeling showing the relationships among environmental variables and *nifH* abundance. Model for *nifH* abundance at the BioCON site ($\chi 2 = 56.608$, d.f. = 46, P = 0.136, n = 48). Blue and red arrows represent significant ($p < 0.05$) positive and negative pathways, respectively. Numbers near the pathway arrows indicate the standard path coefficients (β). Width of the arrows are proportional to the strength of the relationship. Dashed lines represent marginally significant correlations accounted for in the model. N deposition = elevated nitrogen deposition treatment; Plant Root Biomass = total belowground root biomass estimated from 3 cores taken from 0-20 cm; Plant Above Biomass = total weight of aboveground plant biomass clipped 1 cm and above the ground; BBD = Bacterial Beta Diversity; the Bray Curtis distance based PCoA1 axis for the community; BPD = Bacterial Phylogenetic Diversity; the phylogenetic diversity of 16S sequences; *nifH* abundance = abundance of nifH sequences for each plot; Diazotrophic Beta Diversity = *nifH* sequences Bray Curtis distance based PCoA axis 1 beta diversity; BAD = Bacterial Alpha Diversity; number of observed bacterial species per sample; Fungal Beta Diversity = ITS sequences using Bray Curtits distance based PCoA axis 1 for beta diversity; Soil %C = total soil C by percent in the soil; Soil %N = total soil N by percent in the soil; and pH = soil pH.

By starting with a complete model including all factors and eliminating non-significant factors, our final SEM contained only one significant link of elevated CO_2 to fungal beta diversity ($\beta = -0.355$, $p < 0.05$). N deposition had significant negative direct effects on soil pH ($\beta = -0.587$, $p <$

0.001), root biomass (β = -0.366, $p < 0.01$) and bacterial beta diversity (β = -0.405, $p < 0.01$) and a positive effect on fungal beta diversity (β = 0.272, $p < 0.05$). The percent total soil C had a strong positive direct effect on soil N levels (β = 0.795, $p < 0.001$). Aboveground plant biomass (β = -0.297, $p < 0.05$) was negatively related to root biomass, perhaps indicating a difference in biomass allocation for the plants depending on N deposition treatment as N deposition had a negative effect on the root biomass (β = -0.366, $p < 0.01$). Root biomass (β = 0.261, $p < 0.05$) had a positive influence on *nifH* abundance, highlighting an indirect effect of N deposition on *nifH* abundance. Microbial phylogenetic diversity (β = 0.653, $p < 0.001$) had a positive strong direct effect on microbial alpha diversity (β = 0.279, $p < 0.05$) which in turn had a positive effect on *nifH* abundance. N deposition also showed a negative relationship to bacterial beta diversity (β = -0.405, $p < 0.01$). Overall, the model demonstrated the regulation N deposition had on the system in altering various soil chemical, plant biomass, and microbial features in these plots with elevated CO_2 having the greatest effect on fungal beta diversity.

2.4 DISCUSSION

In this study, the effects of elevated CO_2 and N deposition were assessed on free-living diazotrophic microbes' community dynamics and functionality, as well as the effects on soil bacterial and fungal communities and their functional potential for N/C cycling. As hypothesized, elevated CO_2 did enhance nitrogen fixation rates. Surprisingly, N deposition also increased nitrogen fixation levels, contrary to our original hypothesis. Additionally, the combined treatment suppressed N fixation rates back down to ambient levels. The *nifH* alpha diversity was not affected by the treatments, but the beta diversity and community dispersion were significantly different from each other by treatment group, and the N deposition treatments were more clustered than the control or elevated CO_2 treatment. Soil microbial communities have been known to show

sensitivity to various nutrient inputs. Previously, N fertilization has been shown to reduce microbial biomass and respiration rates (Ramirez *et al.,* 2012; Janssens *et al.,* 2010; Treseder *et al.,* 2008), with specific functional groups of microbes (*i.e.,* ammonia oxidizers or mycorrhizal fungi) showing strong responses to N additions (Wessen *et al.,* 2010; Egerton-Warburton *et al.,* 2007; Treseder, 2004). A global grassland study investigating elevated N and P inputs revealed consistent microbial community shifts corresponding to various ecological attributes of the community members (Leff *et al.,* 2015). This may imply that regardless of microbial community composition, changes in nutrient availability elicits changes in community composition in consistent ways through the selection of specific microbial groups based on functional traits. Consistent with this conclusion, elevated N did significantly reduce the fungal class members of *Glomeromycota*, which exclusively contains arbuscular mycorrhizal fungi, and reduce the functional potential of *amoa* genes which may reflect a reduction in ammonium oxidizing bacteria.

2.4.1 N deposition, elevated CO_2 and N fixation

Nutrient availability has been well established as a critical driver of BNF (Reed *et al.,* 2011). A recent global meta-analysis of terrestrial BNF under N addition revealed an overall inhibition of BNF (by up to 19%) while P additions had an inconsistent effect (*i.e.,* inhibiting free-living N fixers and stimulating symbiotic N fixation) (Zheng *et al.,* 2019). However, N inputs have been shown not to inhibit BNF if the ecosystem continues to be N-limited (Reed *et al.,* 2007) or if the N inputs are unable to exceed the total N demand (Rousk *et al.,* 2014). This may explain why the N deposition treatment stimulated N fixation, as our study site is considered N-limited, and the amount of N input may not meet or exceed the total N demand. Nevertheless, further research is required to elucidate the precise mechanics of the observed response in N fixation rates to N addition.

The combined treatment (eCO_2 x eN) suppressing the N fixation rates may reflect differences in plant-soil interactions and the cost/benefit of different N acquisition strategies (Terrer *et al.,* 2018). For instance, one hypothesis predicts N-limitation for plant response to elevated CO_2 levels is determined by the type of N-acquisition strategy, which in turn, depends on the symbiotic plant-microbe interaction. While both treatments may stimulate N fixation rates independently, the C allocation to microbial symbionts associated with the plant roots may be altered in response to the combined treatments as plant-available N is provided via direct N deposition to meet enhanced CO_2 fertilization rates. Studies conducted in chemostats have revealed the availability of N sources (i.e., NH_4^+ or NO_3^-) in the environment may trigger organisms to stop N_2 fixation activity (Cejudo & Paneque, 1988). Thus, the combination of higher N sources in the soil and less belowground C from the plants may downregulate the activity of free-living diazotrophs in the soil as the plants reduce exudate production in favor of increasing their biomass. A meta-analysis (Terrer *et al.,* 2016) found that the type of microbial symbiont and N availability were critical factors in explaining plant biomass across eCO_2 experiments, with a significant and strong interaction between the two factors. Additionally, plants that associate with arbuscular mycorrhizal fungi have been shown to have a low response to eCO_2 under limited N availability unless associated with N fixers. By contrast, plants associated with ectomycorrhizal fungi showed biomass enhancements by elevated CO_2 despite growing in N limiting environments. Therefore, a cost-benefit for C allocation may be occurring in the plants, which may have consequences for the amount of N fixed by free-living diazotrophic microbes dependent on root exudates for the functionally expensive process to fix N_2. However, our study only represents a snapshot of N fixation rates, and therefore, additional experimentation with more timepoints and environments will need to be conducted to generalize our findings.

2.4.2 Impacts on C/N cycling

The effects of eCO_2 on soil C cycling under N deposition did not show a clear pattern and was variable depending on the C degradation gene category in our Geochip 5.0 dataset (**Figure 2.5b**). Meta-analysis (Zhou *et al.*, 2016) shows that N fertilization may increase soil respiration under elevated CO_2. Generally, our results showed the combination treatment had an enhanced functional potential for genes involved in the degradation of more recalcitrant C compounds (terpenes, chitin, vanillin, and lignin), while N deposition alone tended to reduce the degradation potential of these molecules. This may reflect the effects eCO_2 has on priming and could lead to increased degradation of these stable soil organic matter (SOM) constitutes by microbial degradation, thereby decreasing the soil C storage and increasing heterotrophic respiration rates.

2.4.3 Conclusion

Overall, nitrogen fixation rates were increased by 61 and 38% for elevated CO_2 and N deposition, respectively. The alpha diversity of the diazotrophic community remained unchanged by treatment levels; however, microbial diazotrophic beta diversity and community dispersion were significantly different between treatments. Together, our findings leave a troubling implication that further N deposition as CO_2 levels rise may lead to a reduction in microbial free-living diazotrophic functionality. This potentially may alter soil N/C levels and could lead to the depletion of native N/C socks in the soil, creating a lasting impact on future grassland N/C cycling processes.

CHAPTER THREE

CONVERSION OF MARGINAL LAND INTO SWITCHGRASS CONDITIONALLY ACCRUES SOIL CARBON BUT REDUCES METHANE CONSUMPTION

ABSTRACT

Switchgrass is a deep-rooted perennial native to the US prairies and an attractive feedstock for bioenergy production; when cultivated on marginal soils it can provide a potential mechanism to sequester and accumulate soil carbon (C). However, the impacts of switchgrass establishment on soil biotic/abiotic properties are poorly understood. Additionally, few studies have reported the effects of switchgrass cultivation on marginal lands that have low soil nutrient quality (N/P) or in areas that have experienced high rates of soil erosion. Here, we report a comparative analyses of soil greenhouse gases (GHG), soil chemistry, and microbial communities in two contrasting soil types (with or without switchgrass) over 17 months (1,428 soil samples). These soils are highly-eroded, 'Dust Bowl' remnant field sites in southern Oklahoma, USA. Our results revealed that soil C significantly increased at the sandy-loam (SL) site, but not at the clay-loam (CL) site. Significantly higher CO_2 flux was observed from the CL switchgrass site, along with reduced microbial diversity (both alpha and beta). Strikingly, methane (CH_4) consumption was significantly reduced by an estimated 39% and 47% at the SL and CL switchgrass sites, respectively. Together, our results suggest that soil C stocks and GHG fluxes are distinctly different at highly degraded sites when switchgrass has been cultivated, implying that carbon balance considerations should be accounted for to fully evaluate the sustainability of deep-rooted perennial grass cultivation in marginal lands.

3.1 INTRODUCTION

Taking place over three waves during the 1930s, the American 'Dust Bowl' was a catastrophic ecological disaster that brought severe drought and dust storms to the central prairies of the US and affected roughly 40 million hectares of land (Schubert *et al.,* 2004; Worster 1982; Baumhardt 2003). These climatic events, combined with many years of poor land management and soil cultivation, exacerbated topsoil erosion, creating many 'marginal' lands of low soil nutrient quality, notably across Oklahoma and the Southwestern USA (Texas, Kansas, Colorado, and New Mexico). Since then, many of these sites have remained suboptimal for agricultural development. It has been suggested that widespread cultivation of deep-rooted perennial grasses may aid in soil restoration at these sites, while also offering further economic benefits to farmers in the form of cellulosic feedstocks for bioenergy production (Gelfand *et al.,* 2007). It is estimated that 15 million hectares of arable land would need to be converted into biofuel crops to meet the US Department of Energy's plan to replace 30% of transportation fossil fuels with biofuels by 2030 (Bouton *et al.,* 2007; Bouton *et al.,* 2008). An estimated 11% of the contiguous USA is considered nutrient-poor or 'marginal' land (Milbrandt *et al.,* 2014) and currently represents an under-utilized resource that may be well suited for cultivation of switchgrass or other deep-rooted perennials (Stoof *et al.,* 2015).

Switchgrass (*Panicum virgatum* L.), a tall perennial deep-rooted grass native to the Central North American Plains, is a well-studied bioenergy crop, and thought to be suitable for large-scale

cultivation in the USA (McLaughlin and Kszos 2005). Switchgrass may even be implemented more broadly as it has been projected to grow favorably in numerous regions globally, both with and without irrigation (Ditomaso *et al.,* 2013). This enthusiasm stems from switchgrass' high productivity even on low-quality soils unfit for traditional row-crop agriculture, with little to no additional inputs (Tillman *et al.,* 2006). Long-term cultivation experiments suggest that switchgrass can provide a net input of C into soil (Gelfand *et al.,* 2013; Ma *et al.,* 200; Slessarev *et al.,* 2020). Therefore, large-scale switchgrass cultivation may help to simultaneously offset GHG emissions and improve soil quality through C sequestration at nutrient-poor sites (Anderson-Teixeria *et al.,* 2009). Switchgrass is also known to be highly drought tolerant (Barney *et al.,* 2009) and can prevent topsoil erosion owing to its high root biomass, which increases the surface area for exudation, and can further improve soil C stability and aggregate formation (Tiemann *et al.,* 2015; Sher *et al.,* 2020). Like other perennial crops, switchgrass has been broadly associated with increases in soil C at many experimental sites across the central Great American Plains (Liebig *et al,* 2008; Zan *et al,* 2001; Frank *et al.,* 2004). However, only a few studies have evaluated switchgrass cultivation at sites with low soil N, C, or P contents or in marginal lands that have experienced high rates of topsoil erosion (Gelfand *et al.,* 2013; Dabney *et al.,* 2004). Thus, we currently have a very limited understanding of how switchgrass row-crop systems in nutrient-poor marginal lands can affect (i) soil geochemical composition, (ii) soil microbial diversity, and (iii) overall ecosystem functionality, specifically GHG fluxes.

Potential C accrual due to increased root inputs may be offset by higher soil CO_2 production arising from stimulated microbial C mineralization, the so-called 'rhizosphere priming' effect (Cheng *et al.,* 2014). Thus, while the total amount of soil organic carbon (SOC) may increase, the C input by switchgrass along a depth profile may also prime the degradation of preexisting SOC

by the indigenous soil microbial community (Ashiq *et al.,* 2017; Fontaine *et al.,* 2007). Regulation of this priming response depends on the mineral composition (Shahzad *et al.,* 2018), nutrient content (Torn *et al.,* 1997), and microorganisms present (Poeplau *et al.,* 2019). Therefore, to evaluate the carbon cycle benefits of deep-rooted perennials in marginal lands, it is essential to assess not only the balance of C-based GHG fluxes (CO_2 and CH_4) but also other GHG (such as N_2O) and changes in soil microbiomes.

Because soil microorganisms are critical drivers of soil nutrient cycling, understanding plant-microbe interactions during switchgrass cultivation could help shape land management strategies that promote soil nutrient acquisition (*e.g.,* nitrogen fixation) and recycling, while reducing GHG emissions. A recent review of switchgrass-associated microbiomes suggests that mycorrhizal fungi, associated N-fixing bacteria, and fungal endophytes play particularly key roles in increasing switchgrass biomass, providing a substantial portion of the plant's nitrogen demand, and improving drought tolerance (Hestrin *et al.,* 2020). By examining the microbial diversity and associated functional processes of switchgrass-influenced systems, prior research has revealed some of the mechanisms underlying the enhancement of ecosystem services such as C sequestration, soil fertility, and regulation of GHG emissions (Bouton *et al.,* 2007; Lange *et al.,* 2015; Ker *et al.,* 2014; Clark *et al.,* 2005; Bahulikar *et al.,* 2014; Ghimire *et al.,* 2009; Kim *et al.,* 2012). For instance, it has been shown that N fertilization, at least at some sites, did not increase soil-surface carbon dioxide (CO_2) emissions despite promoting above (Ghimire *et al.,* 2011; Mulkey *et al.,* 2006) and below-ground biomass (Lee *et al.,* 2007). However, the relative impact of methane (CH_4) emissions during switchgrass establishment at highly eroded sites is not yet fully understood (Monti *et al.,* 2012; Robertson *et al.,* 2004; Fritsche *et al.,* 2010). Additionally, the ecological consequences of land conversion, its impact on soil microbial diversity, and

functionality, as well as the overall sustainability of switchgrass cultivation in low-quality soils, remain to be demonstrated.

In grasslands and agricultural systems, above (*i.e.*, plant) and below (*i.e.*, microbial) ground biodiversity (Lange *et al.*, 2014) and biomass (Thakur *et al.*, 2015; Chen *et al.*, 2019) are related, and edaphic conditions can influence these relationships. A meta-analysis of temperate grasslands suggest a correlation between plant and bacterial beta diversity but not alpha diversity (Prober *et al.*, 2015). Previous studies of the microbiomes of monoculture agroecosystems have revealed differences in nitrogen-fixing bacterial communities (Mao *et al.*, 2013), seasonal dynamics (Liang *et al.*, 2019), and core microbiome members between different plant species (Jesus *et al.*, 2016). Therefore, in the transition from an annual plant species to a monoculture perennial crop, we expect a decrease of both alpha and beta microbial diversity.

In this study, we monitored the belowground microbiological and chemical impacts of switchgrass establishment and consequences for soil GHG emissions over two consecutive growing seasons (n = 17 months) in two nutrient-poor (N and P) field sites with low C content in southern Oklahoma (designated SL and CL for their sandy-loam soil and clay-loam soil texture, respectively). We compared soil belowground (root) productivity, chemistry (C, N, and P), soil GHG fluxes (CO_2, CH_4, and N_2O), and microbial community composition at each site with switchgrass or without switchgrass (natural fallow plots). We hypothesize that the following trends would be observed in the field plots with switchgrass: (i) increased topsoil C concentrations over time; (ii) CO_2 production increases, with CH_4 emission and N_2O fluxes remaining relatively stable; and (iii) the microbial community would be altered during establishment and both species richness and beta diversity would decrease over time.

3.2 MATERIALS AND METHODS

3.2.1 Field site, soil sampling, and root biomass estimation

Samples were collected from two sites in southern Oklahoma, a sandy-loam site (SL) near the Texas border (34.18691°N, -97.08487°W) and a clay-loam site (CL) in Ardmore (34.172100°N, -97.07953°W) (**Table S3.1**). Prior to our experiment, the SL field site experienced crop rotation between small grains (wheat, rye, oat, and triticale) in the winter season and soybeans in the summer. Soybean was terminated before seed set to prepare the land for small grain planting as a cover crop. At the CL site, Bermuda grass was the dominant plant cover for at least 20 years prior to our study. These sites were selected for their low soil nutrient content (N and P) and their history of topsoil erosion.

In the summer of 2016, two plots were established at each site, a switchgrass field plot (27 x 22 m) containing 500 genetically distinct individuals of the lowland Alamo variety with a 1 m spacing between plants and a corresponding fallow plot (27 x 22 m) (**Figure S3.2a,b**). All plots were tilled to 30 cm before the start of the experiment, and then planted with switchgrass seedlings with 1 m spacing. Switchgrass plots were sustainably managed, without any chemical fertilizers, herbicides, or watering. Fallow plots were allowed to undergo a natural succession of grasses and weeds over the time course of the experiment and served as controls to compare the dynamics in soil carbon, trace gas fluxes, and microbial community composition with the switchgrass treatment. In November of 2016, a survey was conducted to determine the vegetative cover of the two fallow plots. The SL fallow surface was mostly composed of bare soil (~52%); plant litter (~31%) and annual forbs (~17%) covered the rest of the plot. The CL fallow surface was dominated by annual grass species (~86%), annual forbs (~2%), and bare soil (~1%) covering the remaining

surface of the plot. Common plant genera at both fallow sites included the following: *Oxalis, Dichanthelium, Cynodon, Brassica, Lamium, Trifolium, Cyperus, Geranium, Erigeron, Conyza,* and *Digitaria.*

At each plot, to allow GHG measurements, 21 PVC collars (diameter 23.63 cm x 12.8 cm height) (**Figure S3.2c**) were embedded 8 cm into the soil and placed in a cross design across the field with five collars extending in each cardinal direction from a central origin collar at the plot center. After trace gas measurement from each collar, two soil cores (0 - 20 cm in depth) were taken from within a 20 cm radius of each collar (**Figure S3.2d**), thoroughly mixed, and separated into two aliquots, one for geochemical analyses and one for DNA extraction. Sampling flags were placed to prevent re-sampling the same location twice, and each core was filled by topsoil taken from outside the plot. All soil samples were immediately stored on dry ice, transported back to the lab in less than five hours, and stored at either 5 ℃ for geochemical analyses or -80 ℃ for DNA extraction.

In May 2017, the total belowground root biomass was estimated using a method accounting for differences in root density between the plants in each row (Frasier *et al.,* 2016). Briefly, six pairs of plants were selected, and a transect consisting of four 0-1 m cores was performed between each pair of plants (**Figure S3.3a**). The two cores at the end of the transect represent the root density 'with-in' rows, and the two middle cores represent the root density of the 'between-rows'. Each core was divided into five 20 cm 'slices' of soil. For each depth, roots were collected by sieving and soaking the soil in water, before being dried and weighted. For fallow plots, four randomly assigned 1 m^2 subplots were selected, in which a four 0-1 m soil cores transect was collected (**Figure S3.3b**). No roots were detected from fallow soil cores below 60 cm depth.

3.2.2 Soil geochemistry, pH, and moisture

Soil pH, moisture, total soil C and N, plant-available P, nitrate (NO_3), and ammonium (NH_4) pools were measured according to standard methods (Soil Sampling and Methods of Analysis, 2007). Briefly, 10 g of soil was placed into a 50 ml tube with distilled H_2O added to the 50 ml fill line. Tubes were gently shaken for 30 minutes and given an hour to settle before pH measurement using a pH probe (Acccumet excel XL15 pH meter, Fisher Scientific, Hampton NH, USA). Soil moisture was determined by a gravimetric drying protocol that dried > 5 g of soil for one week at > 60 ℃ before re-weighing to establish the percent of water lost. To determine other soil geochemical parameters, soil samples were dried in an oven at 60 ℃ for a week followed by sieving to remove unwanted material with a 4 mm sieve. Soil samples were then shipped seasonally to the Oklahoma State University (OSU) soil testing Lab where Mehlich III extractions (to quantify the plant available P in the soil), KCL extractions (to determine NH_4 and NO_3 concentrations) were performed and total soil C/N amounts were measured via dry combustion (LECO corporation, St. Joseph MI, USA). To establish initial conditions, 3 replicate 2 meter soil pits were dug at each site prior to switchgrass planting, and sampled every 2 cm (Table S1). Soil chemical analyses were conducted on air-dried soils at the Oregon State University Central Analytical Laboratory in Corvallis OR. Particle size analysis (sand/silt/clay) was conducted on 40 g of soil using the hydrometer method (Sheldrick and Wang, 1993). pH and electrical conductivity (EC) were determined in a 1:1 soil/water ratio (McLean, 1982). Total C and N were determined by combustion and a thermal conductivity detector (AOAC Official Method, 1997). Loss on ignition organic matter was measured after treatment in a muffle furnace (Nelson and Sommers, 1996). Total P content was determined by digestion with nitric acid; extracts were analyzed by Inductively Coupled Plasma Atomic Emission Spectrometry (ICP-AES) (Sah and Miller, 1996). Bioavailable

P was determined using the Bray and Olsen methods for acidic to neutral pH soils (Diamond, 1995; Olsen and Sommers, 1982; Prokopy, 1995). Organic P was measured on 2 g soil extracted with NaOH-EDTA (Bowman and Moir, 1993), amorphous P by ammonium-oxalate extraction (McKeague and Day, 1966), and crystalline P by citrate-dithionite extraction (Mehra and Jackson, 2013).

3.2.3 Environmental parameters

Daily environmental data for 21 different environmental variables (at 5 to 15-minute resolution) were obtained from two weather monitoring stations of the Oklahoma MESONET network (http://mesonet.org/) closest to the field sites (Ardmore and Burneyville, located 1.43 km and 2.3 km from CL and SL, respectively). Variables used included air temperature, bare soil temperature, covered soil temperature, atmospheric pressure, relative humidity, and precipitation (**Table S3.2** and **Table S3.3**).

3.2.4 Trace gas fluxes

CO_2, CH_4, and N_2O fluxes were measured monthly via cavity ring-down spectrometry using a Picarro G2508 analyzer (Picarro, Santa Clara, CA, U.S.A.). Measurements were taken continuously every 2 seconds from a total of 6 minutes per collar, to obtain gas concentrations in parts per million. Raw data from each gas were separated and then manually inspected to remove the beginning and the end of the measurements, which are often influenced by the pushing/pulling of the gas chamber (volume of the chamber + collar = 7,917 cm^3). Then three models (linear, quadratic, and exponential) were fitted for each sample and gas species to

characterize the variation of gas concentrations across time and the 'best model' was selected based on AIC scores. Flux estimations for each of the gases were then calculated using the following equation (Christiansen *et al.,* 2015):

$$F = \frac{dC}{dt} \cdot \frac{PV}{A \cdot R(273.15+T)} \times 3600$$

Where $\frac{dC}{dt}$ is the slope of the best fit model at t = 0, V is the chamber volume (L), A is the chamber area (m^2), R is the gas constant in L atm K^{-1} mol^{-1}, and T is the temperature in Celsius, when the chamber pressure is assumed to be equal to 1 atm. The 3600 factor is included to convert the flux to hourly values. For CO_2 fluxes, F was then divided by 1000 to obtain the units of millimoles per m^2 per hour.

3.2.5 Soil DNA extractions, microbial community sequencing and analysis

All molecular biology procedures and DNA sequencing were performed at the Institute for Environmental Genomics (IEG, University of Oklahoma, USA). A freeze grinding method (Zhou *et al.*, 1996) was combined with the Powersoil DNA extraction kit (Qiagen, Venlo, Netherlands) to extract DNA from a total of 1,428 soil samples, which yielded soil DNA of both high quantity and quality. For microbial community profiling, a two-step PCR method (Wu *et al.,* 2015) was used for amplification of the V4 region of the bacterial 16S rRNA gene using the 515F, 5'-GTGCCAGCMGCCGCGGTAA-3' and 806R, 5'-GGACTACHVGGGTWTCTAAT-3' primers. Sequencing of the 16S rRNA gene amplicons was conducted on the Illumina Mi-Seq DNA sequencing platform (Illumina Inc., San Diego, CA, U.S.A.). Amplicon sequence data were analyzed using an internal pipeline known as the Amplicon Sequencing Analysis Pipeline (Zhang

et al., 2014) (ASAP, version 1.4). MiSeq sequences were quality checked with FastQC (version 0.11.5), pair-end sequences were merged based on their 3' overlap using PEAR (version 0.9.10) with a quality score cutoff set to 20, and assembly length between 200-400 with the minimum overlap length set to 50 bp. The program *split_libraries_fastq.py* from the QIIME package (Kuczynski *et al.,* 2012) (version 1.9.1) was used to assign reads to each sample (demultiplexing) based on the barcodes for each individual sample with a maximum allowed barcode error of 0 and the trimming quality score set to 20. Primer sequences were then trimmed and removed. Sequences from multiple split libraries were merged. Dereplication was performed by USEARCH (Edgar, 2010) (version 9.2.64) using the command *fastx_uniques* (utilizing the size-out option for sequence abundance output). Operational Taxonomic Units (OTUs) were clustered using UPARSE, with the OTU identity threshold set to 0.97 and the singletons/chimeric sequences removed (Edgar, 2013). An OTU table was generated by the command -*usearch_global* in USEARCH. Each representative sequence for each OTU was classified with the RDP Classifier (Wang *et al.,* 2007) (16S: training set 16, June 2016) with the confidence cutoff set to 0.8. OTUs in the 16S sequence reads assigned to Chloroplast at the Order level were removed. Representative sequences for each OTU were used to construct a phylogenetic tree. Sequences were then aligned using MAFFT (Katoh *et al.,* 2002) (version 3.8.31) and alignments were filtered using Gblocks (Castresana *et al.,* 2000) (version 0.91b) with the options -t=d, -b4=3 and -b5=h. FastTree (Price *et al.,* 2009) was used for constructing the phylogenetic tree using the filtered alignments. The phylogenetic tree and OTU tables were used to calculate alpha diversity (phylogenetic based indexes) and beta diversity (UniFrac distance) using programs packaged in QIIME (Caporaso *et al.,* 2010) and R (R Core Team, 2014).

3.2.6 Statistical analyses

All analyses were conducted using R statistical software (R Core Team, 2014) (3.4.4) and figures were produced using the package ggplot2 (Wickham, 2009). Data normality was tested using the Shapiro test. We tested for differences in GHG flux and microbial alpha diversity between plots using linear mixed models to correct for repeated measurements (*i.e.*, collars within plots) and to analyze the data over time (R package *lme4*) (Bates *et al.*, 2015). Pairwise comparisons for soil trace gas production between treatments were conducted using Wilcoxon Rank Sum test and effect sizes were calculated using Mann-Whitney U Test. Differences in soil biogeochemical properties between treatment were tested using Kruskal-Wallis test and effect size was calculated using epsilon squared. Soil geochemical dissimilarity was calculated from scaled data using Euclidean distances (*vegan* R package). Then mean dissimilarity across GHG collars was used to construct linear mixed models to view changes in dissimilarity over time. Differences in microbial community structure across plot, site and time were tested using a PERMANOVA test based on Bray Curtis and weighted-UniFrac dissimilarity for taxonomic and phylogenetic diversity, respectively. We used PERMDISP (Anderson, 2006), a distance-based test for homogeneity of multivariate dispersion, to assess differences in beta diversity between treatments using the 'betadisper' function (*vegan* R package). Differences in relative abundance between groups and time points were calculated by multiple Student T-Tests; p-values were adjusted by conservative Bonferroni correction to compensate for increased Type 1 errors over multiple time points.

Structural equation modeling **(**SEM) was used to explore the direct and indirect relationships among environmental variables and GHG fluxes (CO_2 and CH_4) at both sites. Based on correlation analyses among all variables (**Figure S3.3**), we first considered a full model that included all reasonable pathways, then eliminated nonsignificant pathways until we obtained a

final model with only significant pathways. We used a χ^2 test and the root mean square error (RMSE) to evaluate the fit of our model. To correct for potential temporal autocorrelation, we used averaged microbial and environmental data for each trace-gas collar sampling location, averaged across time points within each plot. For the CO_2 model, all sampling locations were pooled in a single SEM model (n = 84). However, for CH_4, a consistent SG effect was found across the sites. Therefore, two models (n = 42) were created, one for the SG and one for FL plots to compare and identify differences in environmental factors that contribute to the CH_4 fluxes between the two treatments. The SEM-related analysis was performed using the lavaan R package (Rosseel, 2012).

3.3 RESULTS

3.3.1 Changes in root biomass and soil chemistry

We observed a large difference in the field-scale estimates of belowground root biomass (**Figure 3.1a**) between the switchgrass and fallow plots (17.8 and 64 times higher for SL and CL, respectively). Root biomass was estimated for each soil layer in kilograms per meter squared. The estimated total root biomass of all soil layers in the top 1 m added together for the switchgrass plots was 16.9 kg/m^2 for the SL site and 14.1 kg/m^2 for the CL site, while the fallow plots had 0.95 kg/m^2 of roots in the SL and 0.22 kg/m^2 in the CL site. Generally, root biomass decreased along the soil depth at both sites. The SL switchgrass site had higher root biomass estimates at lower depths (60-100 cm, p value < 0.05 by student's t-test) than the CL site, which contributed to a slightly higher total root biomass.

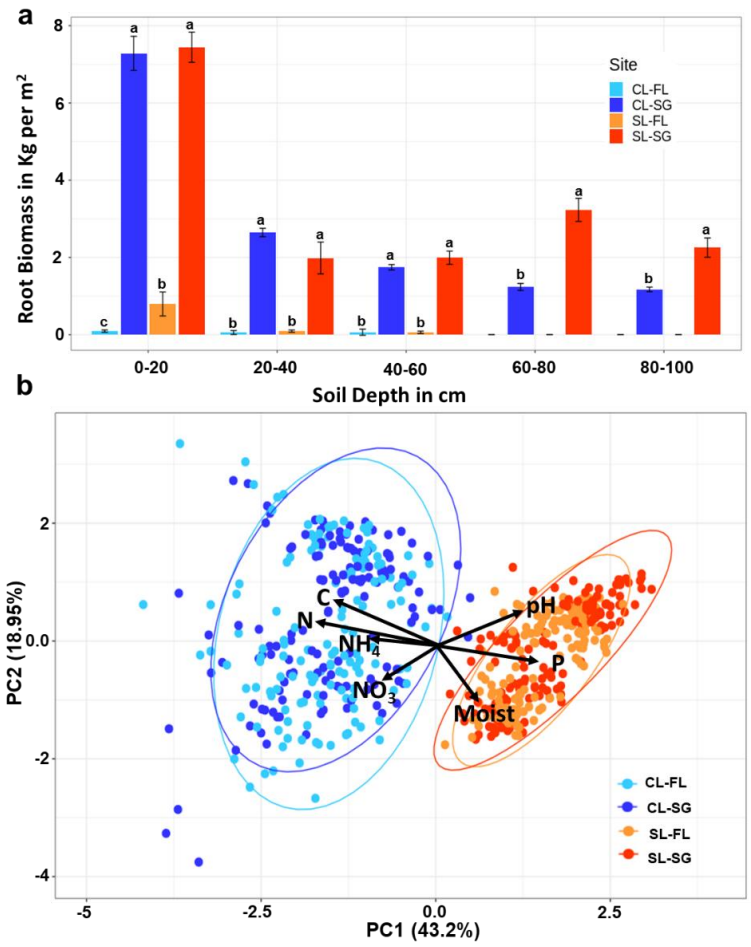

Figure 3.1 Differences in root biomass estimates and soil chemical properties between the two studied sites. a, difference between fallow and switchgrass plots for estimated root biomass by depths (n = 4), letters indicate significant difference between groups by student t-test; **b**, Principal component analysis of soil chemical properties by site and treatment (seasonal samples displayed, n = 588). Blue colors represent the CL site while red/orange colors signify the SL site. Dark colors represent the SG samples. Variation contained in each PC axis are displayed next to each axis.

A principal component analysis (PCA) of the soil chemistry data (Soil C, N, P, NO_3, NH_4, pH and soil moisture levels) revealed strong differences between the two sites (**Figure 3.1b**). Heterogeneity of the geochemical parameters was higher at the CL site with an average

dissimilarity of 2.96 ± 0.73 compared with 2.52 ± 0.24 for the SL site, and illustrated by the greater dispersion of samples from the CL site in **Figure 3.1b**.

The total soil surface C (0 – 20 cm) at the SL site increased over the 17-month period in the switchgrass plot (**Figure 3.2a**) ($r^2 = 0.12$, $p < 0.001$) and was significantly higher than in the fallow plot (**Table 3.1**, $p < 0.001$, large effect size = 0.4). Switchgrass also had a homogenizing effect for soil C, probably due to the increase in belowground root biomass, and reduced the overall dissimilarity between samples compared to the fallow plots which had patchy plant cover. These increases in soil C occurred evenly across the plot area (**Figure S3.4a**). In contrast, the total soil C content remained constant in the CL switchgrass plot (**Figure 3.2a**).

Table 3.1 Differences in physico-chemical soil properties for each site and treatment after 17-months. Values are mean ± SD values and significance was test by Kruskal-Wallis rank sum test.

Variable										
	Mean ± SD	Mean ± SD	Chi-squared	p	Effect Size	Mean ± SD	Mean ± SD	Chi-squared	p	Effect Size
pH	6.5 ± 0.67	6.7 ± 0.95	1.32	0.25	-	5.73 ± 0.44	5.85 ± 0.57	2.17	0.14	-
Soil Moisture (%)	7.1 ± 4.1	8.7 ± 6	3.27	0.07	-	10.4 ± 6.8	9.82 ± 5.5	0.75	0.39	-
Total soil C (%)	0.47 ± 0.09	0.61 ± 0.12	118	**< 0.0001*** **	0.40 Large	1.3 ± 0.42	1.3 ± 0.36	0.86	0.40	-
Total soil N (%)	0.06 ± 0.01	0.07 ± 0.01	55.4	**< 0.0001*** **	0.19 Medium	0.11 ± 0.02	0.11 ± 0.02	0.27	0.6	-
Phosphorus (ppm)	55.6 ± 13	73.7 ± 9.7	128	**< 0.0001 *** **	0.44 Large	22.6 ± 9.7	17.5 ± 6.5	27.7	**< 0.001****	0.095 Medium
Nitrate (ppm)	3.5 ± 3.7	2.2 ± 3	16.8	**< 0.001****	0.06 Small	8.3 ± 9.8	8.9 ± 15	2.37	0.12	-
Ammonium (ppm)	13.6 ± 11	14.5 ± 10	1.73	0.19	-	18.5 ± 11	17.9 ± 11.5	0.61	0.44	-

*Effect size shown by *epsilon* squared with small (0.01 - < 0.08), medium (0.08 - < 0.26), and large (≥ 0.26) ranges.

Total surface soil N was significantly higher in the SL switchgrass plot compared to the fallow plot (Table 1, $p < 0.0001$, medium effect size = 0.19) and these N levels significantly decreased over time ($r^2 = 0.05$, $p < 0.01$) (**Figure 3.2b**), coinciding with an increase in the soil N heterogeneity in the plot ($r^2 = 0.12$, $p < 0.0001$) (**Figure S3.4b**). In contrast, we measured a significant increase in the total soil N in the CL fallow plot ($r^2 = 0.12$, $p < 0.01$) (**Figure 3.2b**). Nitrate concentration were significantly reduced for the switchgrass treatment at the SL site (**Table**

3.1, $p < 0.001$, small effect size = 0.06). All sites and plots showed a significant reduction in NO_3 concentrations over time (Fig. S5a) along with increased homogeneity. No significant differences were observed in soil NH_4+ concentrations during the length of our study at either site (**Figure S3.5b**). Total plant available P levels decreased over time in the SL site ($r^2 = 0.05$, $p < 0.01$) (**Figure 3.2c**) and became more homogeneous across the plot despite the SL switchgrass treatment having significantly higher total plant available P content compared to the fallow (**Table 3.1**, $p < 0.0001$, large effect size = 0.44). In the CL site, plant available P also decreased in the switchgrass plot compared to the fallow (**Table 3.1**, $p < 0.001$, medium effect size = 0.095, and **Figure 3.2c**).

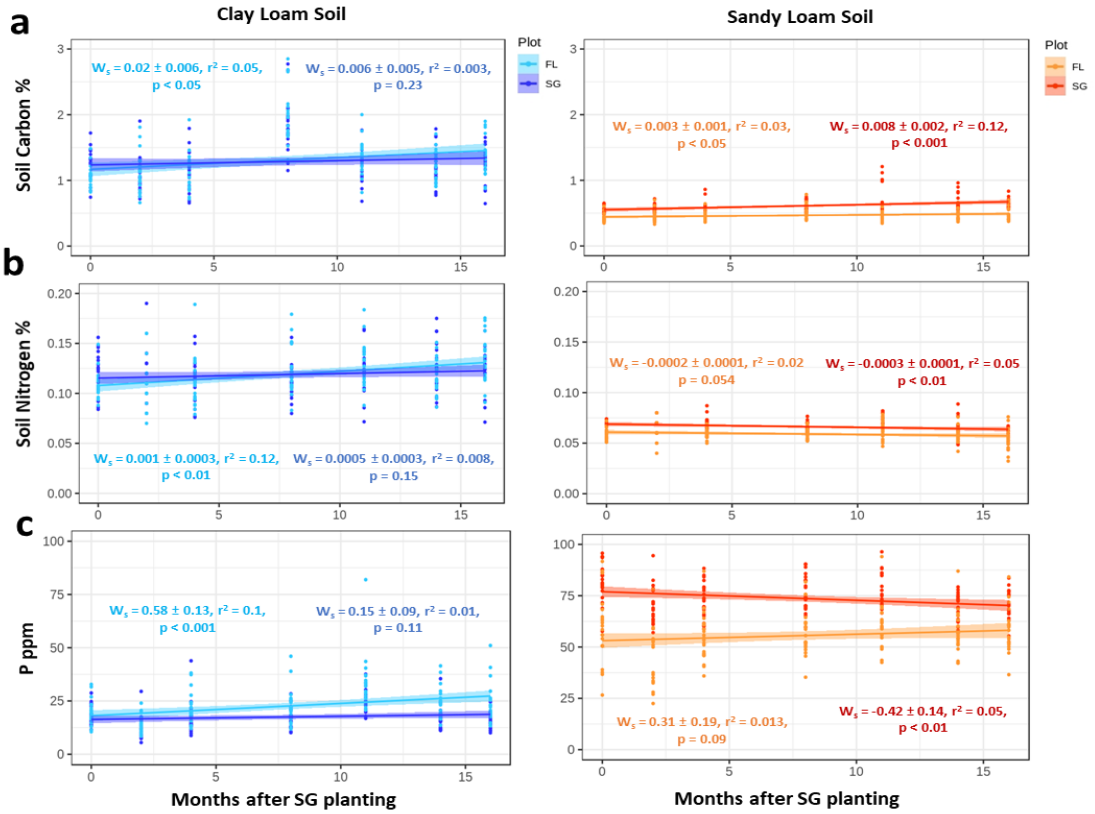

Figure 3.2. Changes in soil chemistry through two seasons of switchgrass establishment. a, Total soil carbon percentages; **b**, Total soil nitrogen percentages; **c**, Concentration of plant available phosphate content in parts per million. The best linear model describing the relationship is presented. W_s: estimated model slope and associated error. p-values represent the significance of each model. Each time point is comprised of twenty-one replicates per plot (n = 588, seasonal samples).

3.3.2 Greenhouse gas (GHG) fluxes at the soil-atmosphere interface

CO_2 flux exhibited a similar seasonal trend at both sites with the apex of emissions occurring during summer months and the minimum in late Fall/early Winter months (**Figure 3.3**). At the SL site, switchgrass treatment led to significantly higher total CO_2 flux for 29% of the months after switchgrass planting (Wilcoxon $p < 0.001$, **Figure 3.3a**) while the fallow was significantly higher for only 24% of the total months measured. The average CO_2 flux over the 17-months did not differ in the SL site between switchgrass (6.76 ± 5.23 millimoles$\cdot m^{2} \cdot hour^{-1}$) and the fallow plots ($6.87 \pm 5.87$ millimoles$\cdot m^{2} \cdot hour^{-1}$). At the CL site, there was a significant difference between plot treatments in the average CO_2 flux over the 17-month period ($p < 0.001$) with the switchgrass plot at 9.98 ± 6.04 millimoles$\cdot m^{2} \cdot hour^{-1}$ and the fallow at 9.22 ± 6.62 millimoles$\cdot m^{2} \cdot hour^{-1}$, although the effect size was small (0.13). When comparing the two sites, the CL site had significantly higher total soil CO_2 fluxes for both switchgrass and fallow plots than those measured at SL (Wilcoxon $p < 0.001$).

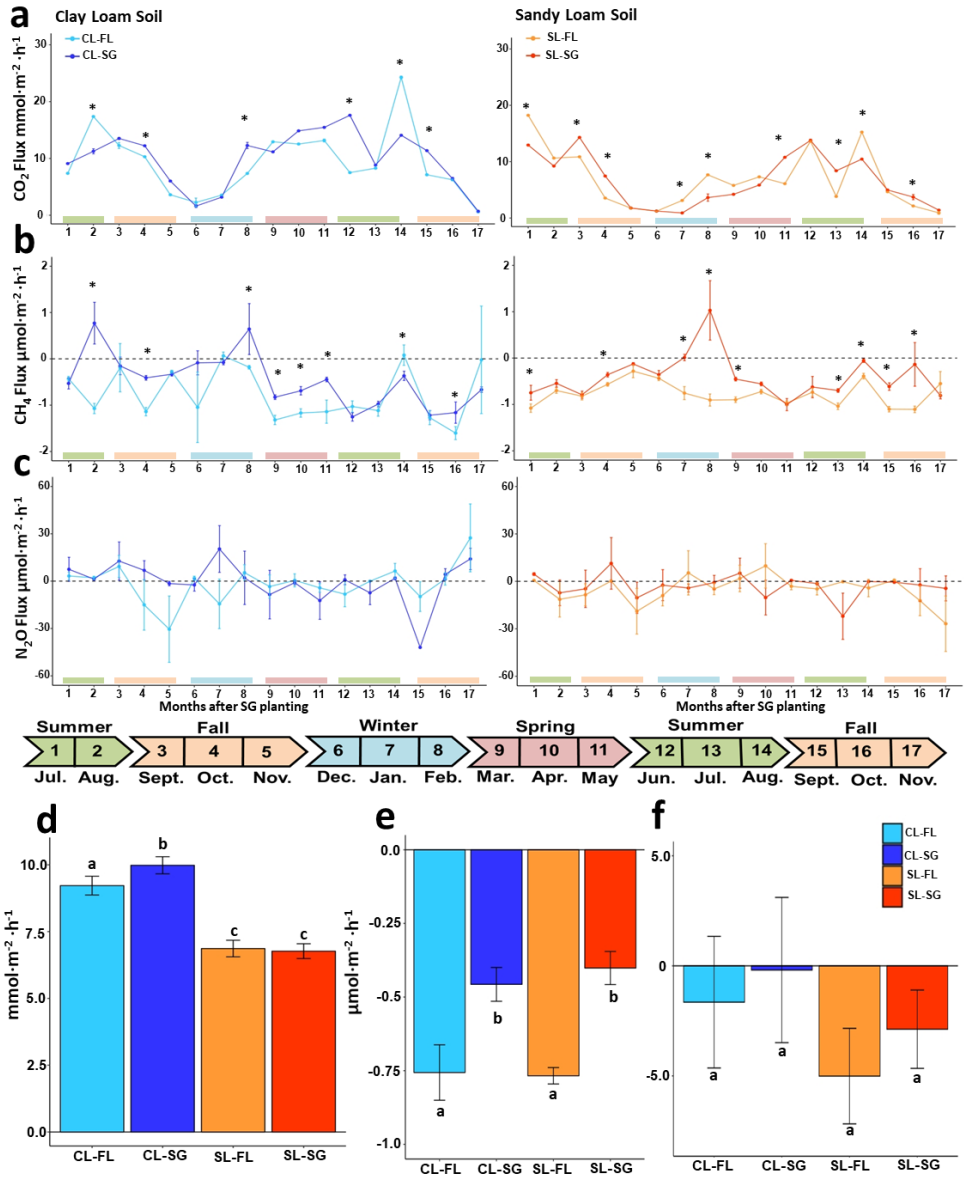

Figure 3.3. Greenhouse gas (GHG) fluxes during grassland conversion to switchgrass. **a**, **b**, **c**: GHG fluxes at each site over 17 months (mean and standard error estimated using 21 replicates for each time points, n = 1,428) for: **a**, carbon dioxide flux; **b**, methane flux; **c**, nitrous oxide. **d**, Average GHG fluxes over 17-months for: **d**, carbon dioxide; **e**, methane flux; **f**, nitrous oxide flux. Different letters and asterisk indicate significant difference between groups by Wilcox sign test with p-value < 0.01.

CH_4 fluxes (**Figure 3.3b**, **Table S3.4**) differed significantly between switchgrass and fallow (Wilcoxon $p < 0.001$, small effect size = 0.15), with a tendency toward higher CH_4

emissions or lower CH_4 consumption levels in the switchgrass plots for 41% of the months after switchgrass was planted (41% and 52% for CL and SL, respectively). CH_4 flux in the CL fallow was higher only at one time point (14^{th} month after switchgrass establishment). Overall, the 17-month average CH_4 consumption rate was -0.44 ± 1.07 micromoles·m^2·$hour^{-1}$ for switchgrass treatments (-0.46 ± 1.08 and -0.41 ± 1.06 micromoles·m^2·$hour^{-1}$ for CL and SL, respectively) and -0.77 ± 1.15 in the fallow (-0.76 ± 1.78 and -0.77 ± 0.53 and micromoles·m^2·$hour^{-1}$ for CL and SL, respectively) (**Figure 3.3e**, **Table S3.4**). Taken together, we observed a significant effect of switchgrass cultivation, with reduced CH_4 consumption rates at both sites ($p < 0.05$, a small effect size = 0.14).

We did not measure significant differences for N_2O fluxes between the switchgrass (-0.26 ± 2.55 micromoles·m^2·$hour^{-1}$ at CL and -2.88 ± 2.09 micromoles·m^2·$hour^{-1}$ at SL) and fallow plots (-1.65 ± 2.5 micromoles per m^2 per hour at CL and -5.01 ± 2.16 micromoles per m^2 per hour at SL) at either site over the 17-months of observations (**Figure 3.3f**).

3.3.3 Microbial community dynamics

Microbial alpha diversity, calculated as OTU richness, showed a site-specific response to switchgrass cultivation. In the SL site, OTU richness was significantly higher in the switchgrass plot (**Table S3.4**, $p < 0.0001$, Medium effect size = 0.38). OTU richness did not change over time in the SL switchgrass plot (**Figure 3.4a**) but increased in the fallow plot ($p < 0.001$), despite a decrease in phylogenetic diversity (PD) ($p < 0.05$, **Figure 3.4b**). At the CL site, microbial species richness decreased significantly over time in both switchgrass ($p < 0.01$) and fallow plots ($p < 0.001$). For PD, this decay was observed only in the switchgrass plot ($p < 0.01$). Chao1 and

Shannon indices showed similar trends per site over time (**Figure S3.6**). Switchgrass cultivation significantly (PERMDISP, $p < 0.05$) decreased the beta diversity at the CL (FL = 0.2323 and SG = 0.2179) and SL (FL = 0.2349 and SG = 0.2273) sites when compared to the paired fallow plots, with decreases in the average distance to the median for the homogeneity of multivariate dispersion.

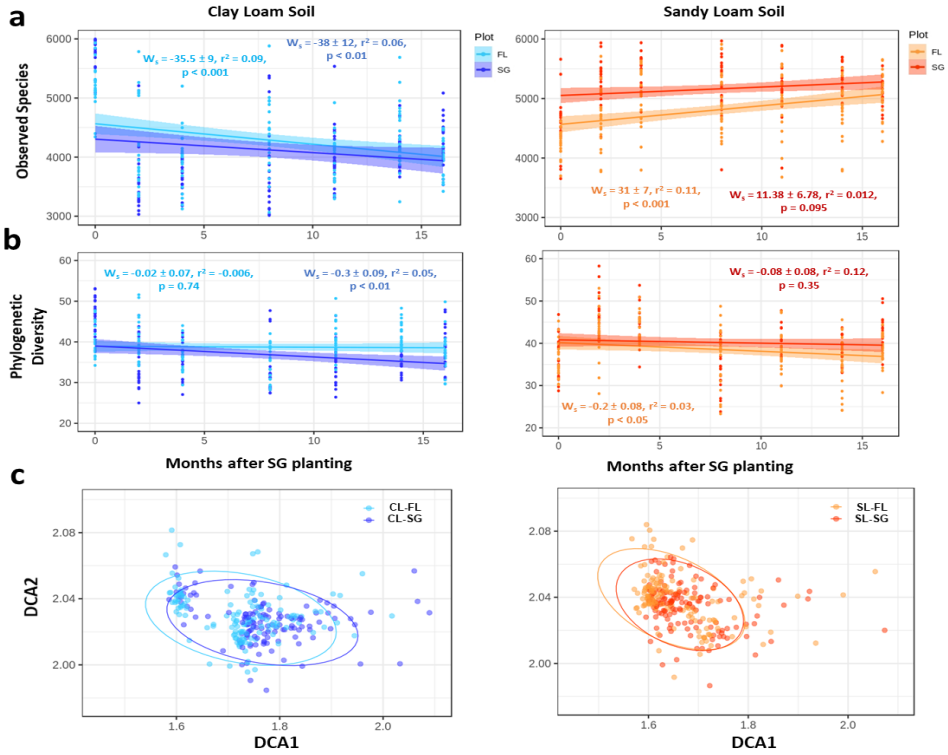

Figure 3.4. Changes in microbial diversity and structure in response to switchgrass planting. a, Number of observed species through time; **b**, Phylogenetic diversity. **c**, Detrended correspondence analysis of the 16S community separated by site for all time points and plots (n= 1,428). Significant differences were found between sites, plant cover types, and through time (PERMANOVA, $p < 0.01$). Dark colors represent the switchgrass samples.

We observed significant differences in the bacterial community structure (beta diversity) between sites, plant cover type, and over time (**Figure 3.4c**, PERMANOVA, $p < 0.01$, **Table S3.5**).

Relative abundance of major phyla showed large changes from the initial planting and two months after the experiment began (**Figure 3.5**). At all sites, at least five abundant phyla exhibited changes in relative abundance. The relative abundance of Firmicutes (0.6 – 0.14 %) changed over the course of the experiment in both fallow plots. The structure of microbial communities from the switchgrass plots appeared less variable than in the corresponding fallow plots. In the CL site, the strongest differences in dominant phyla relative abundance between plots (switchgrass vs fallow) were observed at eight and fourteen months after switchgrass planting (Feb. 2017 and Aug. 2017, **Table S3.6**). After eight months, seven phyla (*Actinobacteria, Bacteroidetes*, *Chloroflexi*, *Deinococcus-Thermus*, *Firmicutes*, *Planctomycete*s, and *Verrucomicrobia*) exhibited different abundance between treatment, while only four phyla (*Actinobacteria*, *Chloroflexi*, *Cyanobacteria*, and *Deinococcus-Thermus*) were different after fourteen months. For the SL site, the largest shifts in community composition occurred in the last two time points, *i.e*., fourteen and sixteen months after switchgrass establishment. After fourteen months, three phyla were significantly different between treatment (*Acidobacteria*, *Bacteroidetes* and *Deinococcus-Thermus*) and after sixteen months four groups were significantly different (*Acidobacteria*, *Bacteroidetes*, *Cyanobacteria*, and *Verrucomicrobia*).

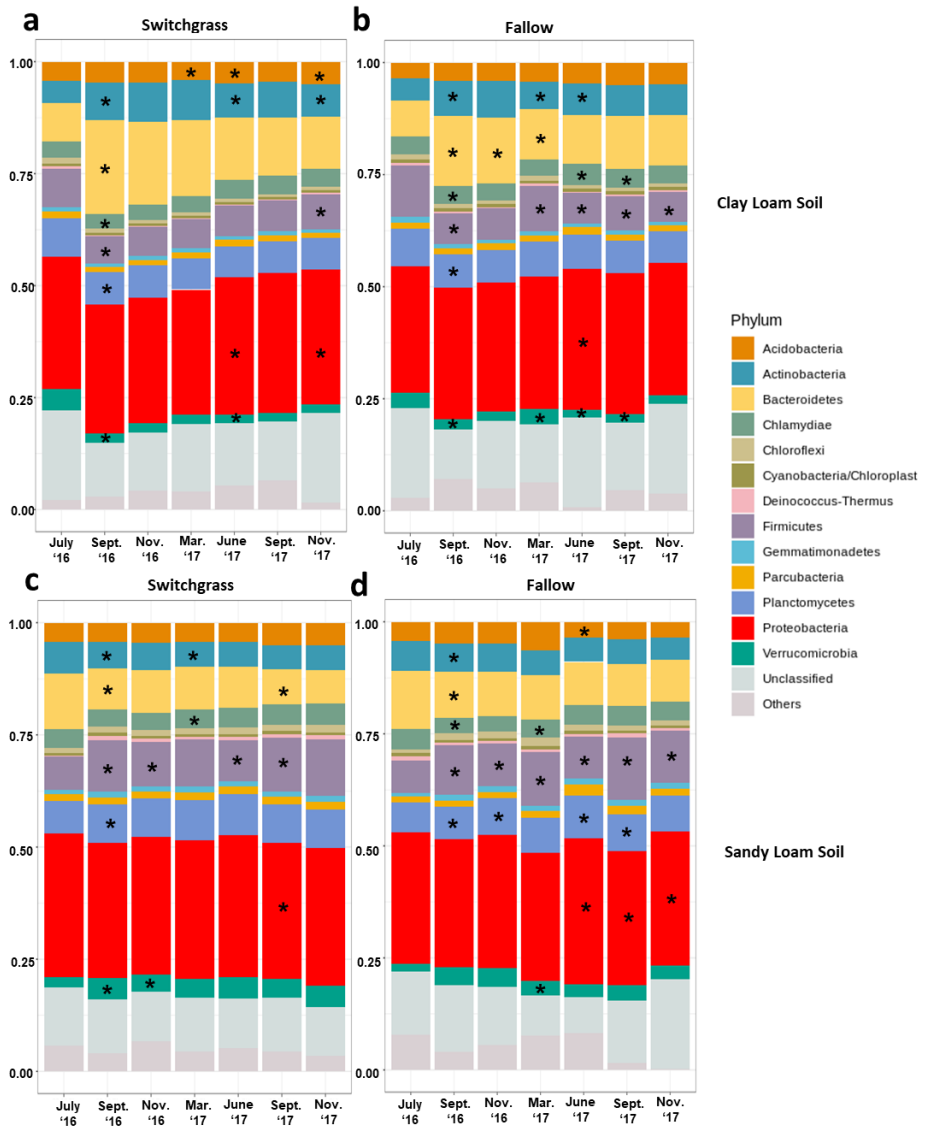

Figure 3.5. Changes of relative abundance for major phyla. Taxonomic identity was determined with the RDP classifier at 80% sequence match criteria. OTU table was trimmed by abundant OTUs (> 0.001%). Difference between time points within each plot for: **a**, Clay-loam switchgrass (CL-SG) plot; **b**, Clay-loam fallow (CL-FL) plot; Sandy-loam switchgrass (SL-SG) plot; Sandy-loam fallow (SL-FL) plot. Significant differences between the pervious time point for each group denoted by asterisk (*) symbols within each phyla bar.

We used canonical correspondence analysis (CCA) to link environmental variables to the microbial community (**Figure 3.6**). A clear separation between microbial communities from the

two sites was observed. Microbial communities from the SL site were correlated with plant available P and soil pH, while CL communities were associated with total soil N, NH_4, and NO_3. In addition, fallow communities from CL were far more dispersed, with switchgrass soil communities at this site clustered by N source or along a soil moisture gradient.

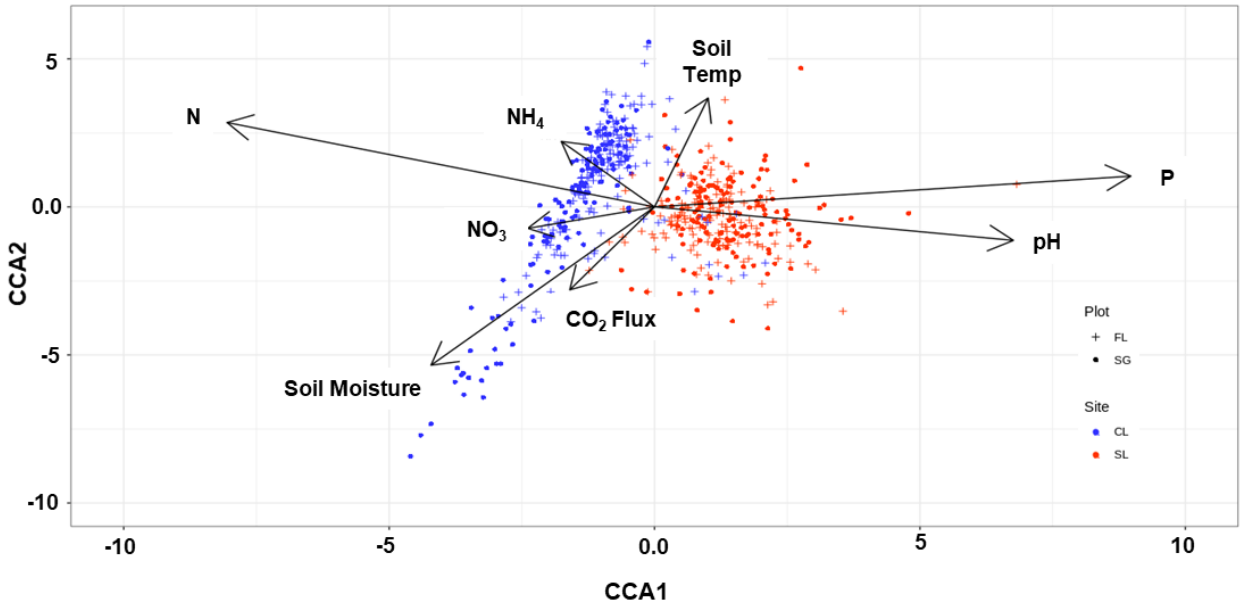

Figure 3.6. Relationships between environmental factors and microbial communities structure. Canonical correspondence analysis (CCA) linking microbial communities structure with environmental variables (n = 1,428). Samples are shown by plot and site type with significant environmental variables shown in black arrows.

3.3.4 Structural equation model links microbial features to soil properties and trace gas fluxes

Structural equation modeling (SEM) was used for an in-depth analysis of the direct and indirect effects of environmental drivers on CO_2 and CH_4 fluxes. For CO_2 fluxes (**Figure 3.7a**) the model confirmed the importance of the site effect on soil C and microbial communities, with

strong direct effects (based on standardized coefficient) being directed from the site and toward total C ($\beta = -0.48$, $p < 0.05$) and microbial alpha diversity ($\beta = 0.89$, $p < 0.05$). Plant available P strongly influenced the levels of C ($\beta = 0.59$, $p < 0.01$) and microbial biomass in the system ($\beta = -0.28$, $p < 0.05$). Important variables influencing CO_2 fluxes included soil temperature ($\beta = 0.33$, $p < 0.05$), microbial biomass ($\beta = 0.33$, $p < 0.05$) and plant cover ($\beta = 0.16$, $p < 0.05$). Microbial biomass appeared mostly dependent on N content ($\beta = 0.68$, $p < 0.001$) and to a lower extent on P content and the type of plant cover.

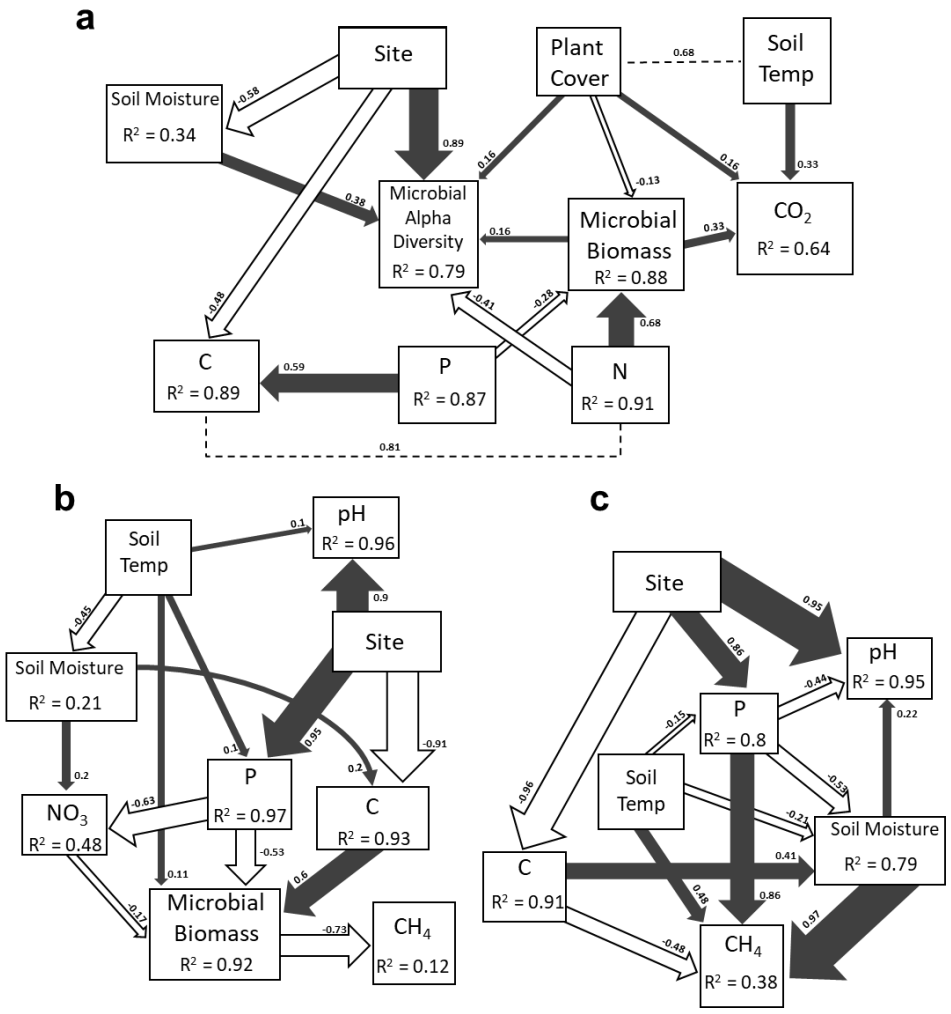

Figure 3.7. Structural equation modeling showing the relationships among environmental variables and GHG fluxes. a: Model for total carbon dioxide flux generated from the seasonal data (χ^2 = 13.355, d.f. = 9, P = 0.147, n = 84). **b**: Model for methane flux generated from seasonal data of switchgrass plots only (χ^2 = 18.02, d.f. = 17, P = 0.388, n = 42). **c**: Model for methane flux generated from seasonal data of fallow plots only (χ^2 = 7.131, d.f. = 6, P = 0.309, n = 42). Dark gray and white arrows represent significant ($p < 0.05$) positive and negative pathways, respectively. Numbers near the pathway arrows indicate the standard path coefficients (β). Width of the arrows are proportional to the strength of the relationship. Dashed lines represent residual correlations accounted for in the model. Plant Cover = Switchgrass (positive) or mixed annual grassland plant cover (negative) at the plot; Site = SL (positive) or CL (negative) soil site; CO_2 = total soil carbon dioxide flux; Soil Temp = soil temperature at a depth of 10 cm for bare soil in degrees Celsius; Soil Moisture = gravimetric per cent soil moisture; P = plant available phosphorus content; Microbial Alpha Diversity = number of observed bacterial species per sample; NO_3 = nitrate concentrations; CH_4 = methane flux; and pH = soil pH.

In the SEM model for CH_4 in switchgrass plots (**Figure 3.7b**), the site effect was pronounced and mostly directed toward P levels ($\beta = 0.95$, $p < 0.001$) and soil C levels ($\beta = -0.91$, $p < 0.001$). Soil temperature did not have an influence on CH_4 fluxes directly, it was important in this model via its direct effects on soil moisture ($\beta = 0.21$, $p < 0.01$), P ($\beta = 0.1$, $p < 0.01$), and microbial biomass ($\beta = 0.11$, $p < 0.05$). Microbial biomass was influenced by soil C ($\beta = 0.6$, $p < 0.001$), plant available P ($\beta = -0.53$, $p < 0.001$), nitrate level ($\beta = -0.17$, $p < 0.01$), and soil temperature ($\beta = 0.11$, $p < 0.05$). Overall, we found that CH_4 fluxes in the SG plots were directly depended on microbial biomass ($\beta = -0.73$, $p < 0.05$) suggesting a biological effect to the CH_4 fluxes. In contrast, the SEM model for CH_4 fluxes at the FL plots (**Figure 3.7c**) suggested more environmental regulation, as soil moisture ($\beta = 0.97$, $p < 0.001$), plant available P ($\beta = 0.86$, $p < 0.01$), soil temperature ($\beta = 0.48$, $p < 0.001$), and soil C ($\beta = -0.48$, $p < 0.05$) directly influenced CH_4 fluxes.

3.4 DISCUSSION

In this study, we examined the differences of soil chemistry, microbial community structure, and GHG fluxes in contrasting soil types with or without switchgrass. As hypothesized, increases in CO_2 production, and a reduction in alpha and beta microbial community diversity were observed in the CL switchgrass plot. In contrast, at the SL site, we observed an increase in microbial alpha diversity, while beta diversity was reduced; there was no differences in CO_2 production at this site. However, an increase in topsoil C levels was observed between plots with and without switchgrass for the SL site. Our most striking result is the observation of a systematic and significant reduction of CH_4 consumption rates, which altered the soil CH_4 sink capacity in

the switchgrass plots. Although the CH_4 emission rates in this relatively mesic landscape were far lower than those reported for systems with anaerobic, water-logged conditions like peatlands (Dise, 1993) and wetlands (Bartlett and Harriss, 1993), CH_4 emission effects may not be negligible during marginal land transitions to switchgrass row-cropping (Fritsche *et al.,* 2010) due to the severity of its global warming potential (28 to 34 times higher than CO_2). However, comprehensive GHG budgets along with spatially-explicit modeling of soil and plant C stocks, should be considered to fully evaluate the effect of large scale conversion at these prairie sites.

3.4.1 Soil type dictates the effects that switchgrass has on geochemistry

Our study revealed significant site-level differences in soil C accrual, total soil N levels and depletion of soil P content after switchgrass establishment. The CL site, with initially higher relative nutrient content, showed little change over time (17 months) for any of the soil geochemical parameters. Reported (Ma *et al.,* 2000) changes in soil geochemistry by switchgrass cultivation in clay-loam soils were only detected after longer periods of time (over a decade). It is likely that prolonged sampling at our CL site would provide improved assessments of switchgrass-induced soil C changes. We also noted that nitrate content (**Fig. S3.5a**) significantly declined with time, over switchgrass establishment, which may suggest assimilation by the plants, microbes, or an increased activity of denitrifying bacteria.

Surface soil C content significantly increased at the SL site (27% higher total C after two growing seasons) over the course of switchgrass establishment. This is consistent with other estimates showing switchgrass systems can increase soil C stocks in a relatively short amount of time (Abraha *et al.,* 2019; Slessarev *et al.,* 2020). However, we observed significant depletion in soil N and P contents at the SL site with switchgrass over time, though we note that these values were higher than in the fallow from the beginning of our experiment. One explanation for this

observation is that N and P have been taken up into the switchgrass tissue, which could explain the higher belowground root biomass observed in the SL site at lower soil depths. Indeed, the higher plant available P conditions at this site could allow switchgrass to extend deeper into the subsurface soils for water or micronutrient availability and thus support a greater investment of belowground root biomass.

Seasonal sampling of NH_4-N was not sufficient in explaining large seasonal variations observed over the time course of our experiment. For example, a spike in soil NH_4 levels (**Fig. S3.5b**) was detected during October of 2016 and June of 2017, which could be the signature of episodic N fixation events occurring in switchgrass during/before flowering as reported previously (Roley *et al.,* 2019). However, our temporal resolution for this geochemical parameter was not detailed enough to adequately explain these anomalies.

3.4.2 Microbial community shifts under switchgrass establishment

Microbial community diversity and composition at each site had differential responses to switchgrass establishment. Broadly, alpha diversity measures in the CL switchgrass plot decreased over time and revealed a higher amount of clustering and similarity in the overall community structure compared with the fallow. Analogous to secondary plant successional dynamics, the microbial community at the CL site may be more influenced by the change from short rooted annuals to the monoculture of deep-rooted perennial switchgrass, causing a loss in microbial diversity (Cline *et al.,* 2015), with a lower number of taxa and more homogeneous community composition. This follows our expectations (hypothesis iii) that switchgrass cultivation would lower microbial alpha and beta diversity. However, for SL, the Shannon index significantly

increased over time under switchgrass cultivation and the community composition was altered. This result may be indicative of switchgrass-induced improvements in soil quality (increased soil C concentrations), which led to changes in functionality (Leff *et al.,* 2015).

Microbial community structure was altered by switchgrass establishment (**Table S3.5**) and through time at each of the sites relative to the fallow soil communities. These changes in community structure may reflect different survival strategies that switchgrass may employ in the recruitment of specific taxa to its rhizosphere based on differences between the geochemistry of the two sites. Several previous studies provide evidence that switchgrass can recruit a beneficial microbiome, particularly mycorrhizal fungi, associative N-fixing bacteria, and fungal endophytes (Hestrin *et al.,* 2020). Future investigations into rhizosphere microbiome succession (Chen *et al.,* 2019; Prober *et al.,* 2015; Mao *et al.,* 2013) during establishment may provide insights into direct plant-microbe interactions that facilitate switchgrass establishment in these nutrient-poor soils.

3.4.3 Factors controlling soil GHG flux

Contrary to our hypothesis, CO_2 production was significantly enhanced by switchgrass establishment only at the CL site. Based on previous studies (Fontaine *et al.,* 2007; Shahzad *et al.,* 2018), we expected higher root respiration and the potential for deep C mineralization to enhance CO_2 production at both sites after switchgrass establishment. However, the CL site had an overall higher CO_2 emission rate during our field monitoring. This response may be mediated by the relatively higher preexisting C content found at this clay-loam site (Kang *et al.,* 2016), since root biomass levels were estimated to be similar at each site. Our SEM model revealed direct linkages between microbial biomass and CO_2 production, suggesting that the amount of microbes in the

soil play an important role in regulating CO_2 flux and has long been linked to land usage and environmental variables that influence CO_2 flux (Wagai *et al.,* 1998). Overall, our study suggests differential CO_2 production responses that depend on soil type when under the same land usage (*i.e.,* switchgrass cultivation). Based on our results and those measured for the entire active soil horizon in nearby sites (Slessarev *et al.,* 2020), sandy-loam marginal sites may provide more sustainable benefits in terms of increased C accrual during switchgrass establishment, as well as reductions in surface CO_2 fluxes.

With our methane flux monitoring, we showed a significant reduction in CH_4 consumptions at both sites with switchgrass cultivation. Although CH_4 emission rates were low and measured at only a few time points within the switchgrass plots, consistently lower CH_4 consumption rates were observed in the switchgrass plots relative to the fallow plots throughout the experiment. Total CH_4 consumption rates for switchgrass plots were 47% and 39% lower than in the corresponding fallows for CL and SL, respectively. During the period of 2008-2017, global emissions from both agriculture and waste sources were estimated to be 206 Tg CH_4 y^{-1}, which represents 56% of the total anthropogenic emissions (Saunois *et al.,* 2019). Recent estimates for 2018 and 2019 have shown an increase in atmospheric methane by 8.5 and 10.7 ppb (Jackson *et al.,* 2020), respectively, prompting the need for future mitigation, since CH_4 has 28 to 34 times the global warming potential (GWP) over a 100 year time horizon than CO_2 (Stocker *et al.,* 2013). Based on our results, CH_4 flux profiles of each site may be altered by an estimated 0.48 $kg \cdot ha^{-1} \cdot yr^{-1}$ when cultivated with switchgrass. Methane flux from our SEM models was also found to be correlated with microbial biomass, but only in the SG plots, suggesting a potential biological effect of switchgrass on the microbial community, which may have promoted the growth of key community members that can alter methane emissions (*i.e.,* methanogens or methanotrophs). However, our analyses of

community composition could not support further associations between CH_4 flux and microbial community members. In contrast to CO_2 and CH_4 fluxes, we did not observe any significant effect between soil type and plant cover type (switchgrass vs fallow) on N_2O fluxes in these marginal, sustainably managed (no fertilizer) soils.

Overall, total soil C levels increased by 27% following switchgrass planting and 17-months of monitoring in our sandy-loam site, but remained unchanged in our clay-loam site. Total CO_2 production was significantly affected under switchgrass at the clay-loam site but not at the sandy-loam site. The annual CH_4 consumption was reduced by 39 to 47% under switchgrass, implying that methane fluxes should be accounted for in C budgets to reach a sustainable cultivation of switchgrass. Switchgrass establishment had a significant influence on the microbial community composition over time and homogenized soil microbiota profiles at both sites. Considerations of soil type and nutrient conditions should be factors in the selection of future sites for sustainable large-scale bioenergy cultivation in order to meet objectives for terrestrial C sequestration and improved soil fertility.

CHAPTER FOUR

SOIL HETEROGENEITY REGULATES MICROBIAL SPECIES-TIME-AREA RELATIONSIHP UNDER SWITCHGRASS IN MARGINAL LANDS

ABSTRACT

A fundamental challenge in ecology is to understand the forces that both shape and maintain biodiversity at various spatial scales over time. Here, we aim to characterize the species-time-area relationship (STAR) over 17 months within prokaryotic communities (n = 1428) under bioenergy crop (switchgrass) establishment at two 'Dust Bowl' remnant field sites (designated SL-silt loam and CL-clay loam) in Oklahoma that are low in nitrogen (N) and phosphorus (P) nutrient availability. We hypothesize that nutrient availability, along with the activation of beneficial plant-microbe interactions, will regulate microbial biodiversity scaling and that temporal species accumulation will have a stronger effect on species number than area. Paired plots at each site, including a control fallow plot and a plot cultivated with switchgrass, were assessed by profiling (i) the spatial and temporal scaling of bacterial communities biodiversity using 16S rRNA high-throughput sequencing and (ii) tracking the topsoil physiochemical properties over two complete growing seasons. Soil nutrient heterogeneity was found to be higher at the CL site than at the SL site. Furthermore, the soil heterogeneity of the soil nutrient conditions across the different spatial scales was related to and helped in explaining the different patterns of STAR observed for each plot. At both sites, taxa accumulation was higher over time than with increasing area. Remarkably, the seasonal species-area relationship was positively related to the heterogeneity of soil P concentrations at both sites by multiple linear regression models. This linkage may reflect that the changes in P may influence the growth of the plants and thus mediate the soil nutrient conditions and plant-microbe interactions, which consequently will affect the overall bacterial diversity of the ecosystem. Together, our results stress the importance of nutrient conditions and heterogeneity in regulating soil bacterial biodiversity at different scales and over time.

4.1 INTRODUCTION

Ecology is predicated by the existence of general biodiversity scaling laws that are both some of the most predictively powerful relationships known in biology and have yet to fully explain the mechanisms regulating microbial diversity and turnover. For the purposes of this study, we define biodiversity scaling as the increase of diversity in a given area over time or the accumulation of diversity when sampling a larger area. We also will define the relationships between microbial taxa and area or time as species-area relationships (SAR) and species-time relationships (STR), respectively. Recent efforts have been able to use biodiversity scaling relationships to estimate Earth's total microbial diversity (Locey & Lennon, 2016). However, these laws are often tested at large scales for general trends (Zhou *et al.,* 2016; Deng *et al.,* 2018) that avoid quantifying local processes that may occur in specific ecosystems. As such, it is rare to find studies that look at these relationships at smaller scales (Meyer *et al.,* 2018), where such predictive power might be more practical in addressing the impacts of local environmental changes on microbial biodiversity. Furthermore, while spatial scaling has been studied intensively, scaling across time (Guo *et al.,* 2019) has been understudied in microbial ecology. Therefore, understanding the drivers and impacts of temporal scaling is key to advancing our understanding of microbial scaling laws, mainly due to the highly rapid and dynamic aspects of many natural microbial systems.

While studies on microbial SAR and STR have been primarily focused on natural ecosystems, the impacts of such relationships resulting from anthropogenic activities and changes in land usage have remained understudied. The predictive power that such scaling laws can generate would be of interest in the emerging field of ecosystem restoration efforts, especially to predict the trajectory of ecosystem response to various mitigation actions. Currently, climate

change threatens natural systems at a global scale as the most extensive anthropogenic disturbance to alter the environment, and thus it has profound consequences on the biosphere (Deutsch *et al.,* 2008; IPCC, 2014) that may require future ecosystem restoration efforts to minimize biodiversity losses. Since 1880, the Earth's surface temperatures have increased by 1 ^{o}C (IPCC, 2018) and are expected to continue to increase by another 1.1 to 6.4 ^{o}C (IPCC, 2014) by the end of the century. As a result of this global warming, precipitation patterns at both regional and global scales will continue to be altered, resulting in more extreme climatic events that have severe effects on ecosystem functions, likely leading to a reduction in various ecosystem services. Thus, climate change has severe and variable effects on biological organization levels from individuals to biomes (Dillon *et al.,* 2010).

Among these extreme climate changes includes prolonged drought events that may greatly affect grassland ecosystems, leading to increased soil desiccation and erosion rates that can cause a reduction in the nutrient content of topsoil layers creating 'marginal lands.' Current trends in extreme climate events are analogous to the historical ecological disaster of the 1930s, the American 'Dust Bowl' which brought about severe drought and dust storms to the central plains of the USA (Baumhardt, 2003; Schubert *et al.,* 2004). Since then, many sites across Oklahoma and the Southwestern USA have remained suboptimal for agricultural development due to excessive topsoil erosion. Therefore, legacy marginal lands that have remained highly weathered can serve as a valuable resource to study the effects of soil restoration and changes in land usage to improve soil quality. Therefore, the implementation of deep-rooted perennial grasses has been suggested to aid in various aspects of soil restoration and may offer economic relief for these sites by serving as cellulosic feedstock for bioenergy production (Gelfand *et al.,* 2013; Milbrandt *et al.,* 2014). Additionally, one aspect of soil restoration this study aims to focus on is the concept of soil

restoration altering the levels of biodiversity with the goal of bringing back the 'natural' levels of biodiversity after a shift in land usage. However, questions remain regarding how scale during soil restoration efforts will affect soil microbial diversity or under what time frame will it take to accumulate biodiversity given a change in land usage for soil restoration purposes?

Switchgrass (*Panicum virgatum L.*) is a native C4 perennial deep-rooted grass that is a well-studied bioenergy crop suitable for cultivation across the USA. Switchgrass can provide improvements in soil quality through C sequestration (Ma *et al.,* 2000; Anderson-Teixeria *et al.,* 2009; Slessarev *et al.,* 2020) is highly drought-tolerant (Barney *et al.,* 2009) and can prevent topsoil erosion due to its remarkably high root biomass that penetrates deep soil layers without the need for chemical fertilizer. However, few studies have reported the effects of switchgrass cultivation at marginal lands with low nutrient content or at sites that have experienced high rates of erosion (Gelfand *et al.,* 2013; Milbrandt *et al.,* 2014; Stoof *et al.,* 2015; Ashiq *et al.,* 2017; Bates *et al.,* 2021). Additionally, few studies have looked at the influence switchgrass can have on the belowground microbial community dynamics at either scale or over time (Bates *et al.,* 2021). The soil microbial community can serve as vital drivers of nutrient cycling, which is critically important for soil functionality and is facilitated by specific plant-microbe interactions. Thus, the establishment of switchgrass on marginal lands may influence the biodiversity scaling of the soil microbial community over both time and space. Therefore, assessing the restoration impacts on these legacy marginal lands can yield critical insights for understanding fundamental biodiversity scaling laws and informing climate change mitigation strategies to prevent future climate catastrophes like the Great American Dust Bowl of the 1930s.

Here our study quantifies the impact of the SAR, STR, and their combination (species-time-area relationship; STAR) in highly degraded 'Dust Bowl' remnant marginal lands with low

soil N and P content, in which switchgrass has been planted for both soil restoration and biofuel production purposes. We answered three key questions: (1) does switchgrass establishment change the way microbial diversity is accumulated through space and time when compared to a control fallow plot, (2) between time and area, which factor has a more significant influence on taxa turnover during ecosystem restoration with switchgrass planting, and (3) which underlying environmental parameters (*e.g.*, soil heterogeneity, nutrient content, etc.) or biological factors (*e.g.*, plant diversity) are driving these scaling relationships? Therefore, with these questions in mind, we hypothesized that microbial taxa turnover through time will be enhanced by higher taxa accumulation when compared to scale, regardless of soil type or cover crop (switchgrass or annual grasses/weeds), and that soil heterogeneity will be an important predictor of higher microbial diversity at larger scales.

4.2 MATERIALS AND METHODS

4.2.1 Field site and soil sampling

Samples were collected as described in Bates *et al.*, 2021; briefly, two field sites in southern Oklahoma were established in 2016, a sandy-loam (SL) site (33.881715°N, -97.275167°W) and a clay-loam (CL) site (34.172100°N, -97.07953°W). Site selection was predicated on their characteristic low soil nutrient content (N and P) as well as for their history of topsoil erosion. At each field site, two plots were established, a lowland Alamo variety switchgrass seedling dominated plot and a corresponding fallow plot. All plots were tilled and sustainably managed without the addition of water, chemical fertilizers, or herbicides. Soil cores (0 – 20 cm in depth) were taken across each plot in a cross design with increasing scaling area across the entire field in each cardinal direction centered around an origin at the center of each plot. All soil samples were

immediately stored on dry ice, transported back to the lab within five hours, and stored at -80 ℃ for DNA extraction and 5 ℃ before geochemical analysis.

4.2.2 Soil geochemistry

As described in Bates *et al.*, 2021; briefly, soil pH, moisture, total soil C and N, plant-available P, nitrate (NO_3), and ammonium (NH_4) pools were all measured following standard methods (Soil Sampling Methods of Analysis, 2007). Soil pH was determined using 10 g of soil with distilled H_2O added to the 50 ml fill line in a 50 ml tube, then tubes were gently shaken for 30 minutes and allowed to settle for one hour before pH measurement using a pH probe (Acccumet excel XL15 pH meter, Fisher Scientific, Hampton NH, USA). Soil moisture was determined via a gravimetric drying protocol where > 5 g of soil was dried for one week at > 60 ℃ before re-weighing to establish the percent of water lost during drying. All soil geochemical parameters were determined at the Oklahoma State University (OSU) soil testing Lab where Mehlich III extractions (to quantify the plant available P in the soil), total soil C/N amounts via dry combustion (LECO corporation, St. Joseph MI, USA), and KCL extractions (to determine NH_4 and NO_3 concentrations) were performed. Prior to shipping to the OSU soil testing Lab, all soil samples were dried in an oven at > 60 ℃ for a week followed by sieving the soil with a 4 mm sieve to remove roots, rocks, and other unwanted material from the samples.

4.2.3 Soil DNA extractions, microbial community sequencing and analysis

Molecular procedures and DNA sequencing were performed at the Institute for Environmental Genomics (IEG, University of Oklahoma, USA). Soil DNA extractions were carried out utilizing a freeze grinding method (Zhou *et al.,* 1996) combined with the Powersoil DNA extraction kit (Qiagen, Venlo, Netherlands) to extract DNA from a total of 1,428 soil

samples. For the microbial community profiling, a two-step PCR method (Wu *et al.,* 2015) was selected to amplify the V4 region of the bacterial 16S rRNA gene using the 806R, 5'-GGACTACHVGGGTWTCTAAT-3' and the 515F 5'-GTGCCAGCMGCCGCGGTAA-3', primers. An Illumina Mi-Seq DNA sequencing platform (Illumina Inc., San Diego, CA, U.S.A.) was used for all sequencing on the 16S rRNA gene amplicons. Amplicon sequencing data was analyzed as described in Bates et al., 2021 using the Amplicon Sequencing Analysis Pipeline (ASAP, version 1.4). Briefly, MiSeq sequencing quality checks were performed with FastQC (version 0.11.5), pair-end sequences were then merged using PEAR (Zhang *et al.,* 2014) (version 0.9.10) with a quality score cutoff set to 20, and the assembly length between 200-400 (minimum overlap length set to 50 bp). Demultiplexing based on barcodes of individual samples was carried out utilizing the *split_libraries_fastq.py* from the QIIME package (Kuczynski *et al.,* 2012) (version 1.9.1). Next primer sequences were trimmed and removed then sequences from multiple split libraries were merged. The *fastx_uniques* command from USEARCH (Edgar, 2010) (version 9.2.64) was used for dereplication. Clustering of Operational Taxonomic Units (OTUs) was carried out with UPARSE, with the OTU identity threshold set to 0.97 and chimeric/singleton sequences removed (Edgar, 2013). The OTU table was generated by the command *-usearch_global* in USEARCH. OTU classification was carried out on each representative sequence using the RDP Classifier (Wang *et al.,* 2007) with the confidence cutoff set to 0.8. Any OTUs in the sequence reads that were assigned to Chloroplast at the Order level were removed. A phylogenetic tree was constructed using the representative sequences for each OTU. All sequences were aligned using MAFFT (Katoh, 2002) and the alignments were filtered with Gblocks (Castresana, 2000). FastTree (Price *et al.,* 2009) was used for the construction of the phylogenetic tree using filtered alignments.

4.2.4 Calculation of species-time-area relationships

To calculate the species-area relationship the standard power law equation (Green & Bohannan, 2006) was used:

$$S = cA^z$$

Where S is the species number, c is a constant dependent on the units of A, A is area in m^2, and z is the slope of the species-area relationship in log-log space. Analogous to this is the species-time relationship power law equation:

$$S = cT^w$$

Where S remains the species number, c is a constant dependent on the units of T, T is the time in months, and w is the slope of the species-time relationship again in log-log space. We can then combine both equations to represent the species-time-area relationship using:

$$S = cA^zT^w$$

$$InS = z * InA + w * In\mathrm{T} + \mathrm{b}$$

Where all the variables remain the same as mentioned above and b is the intercept, simultaneously allowing us to show the changes in species richness across both area and over time.

4.2.5 Statistical analyses

All analyses were conducted using the R statistical software (R Core Team, 2014) (3.4.4) and figures were produced using the package ggplot2 (Wickham, 2009). Data normality was tested using the Shapiro test. Non-parametric pairwise Wilcoxon tests were utilized for establishing differences between treatments in soil heterogeneity as defined using the turnover in soil chemical variables (determined using the coefficient of variation or cv) over time. To correct for repeated measurements across our sampling time period, we used mixed linear models (R package *lme4*)

(Bates *et al.*, 2015) to analyze the data. We generated multiple linear regression models by using the mean and cv values at the largest level (Area 5) of P, N, and C, which were identified as the most important factors based on the PCA analysis. Next, we conducted a stepwise method for variable selection based on the AIC values, where P.cv was selected for the final model. We then related the z-values to the heterogeneity of phosphorus by fitting the linear and non-linear regression models (with the linear model based on AIC score).

4.3 RESULTS

4.3.1 Site level differences in soil heterogeneity

Soil heterogeneity between the two sites was strikingly different (**Figure S4.1ab**) with significantly higher heterogeneity found at the CL site ($P < 0.05$, determined by pairwise Wilcoxon test, **Figure S4.1c**) regardless of switchgrass cultivation. Soil heterogeneity (PC1 coefficient of variation) was then plotted by time (in months) and by area (in m^2) to establish trends in how the soil heterogeneity changed within plots given time and scale (**Figure 4.1**).

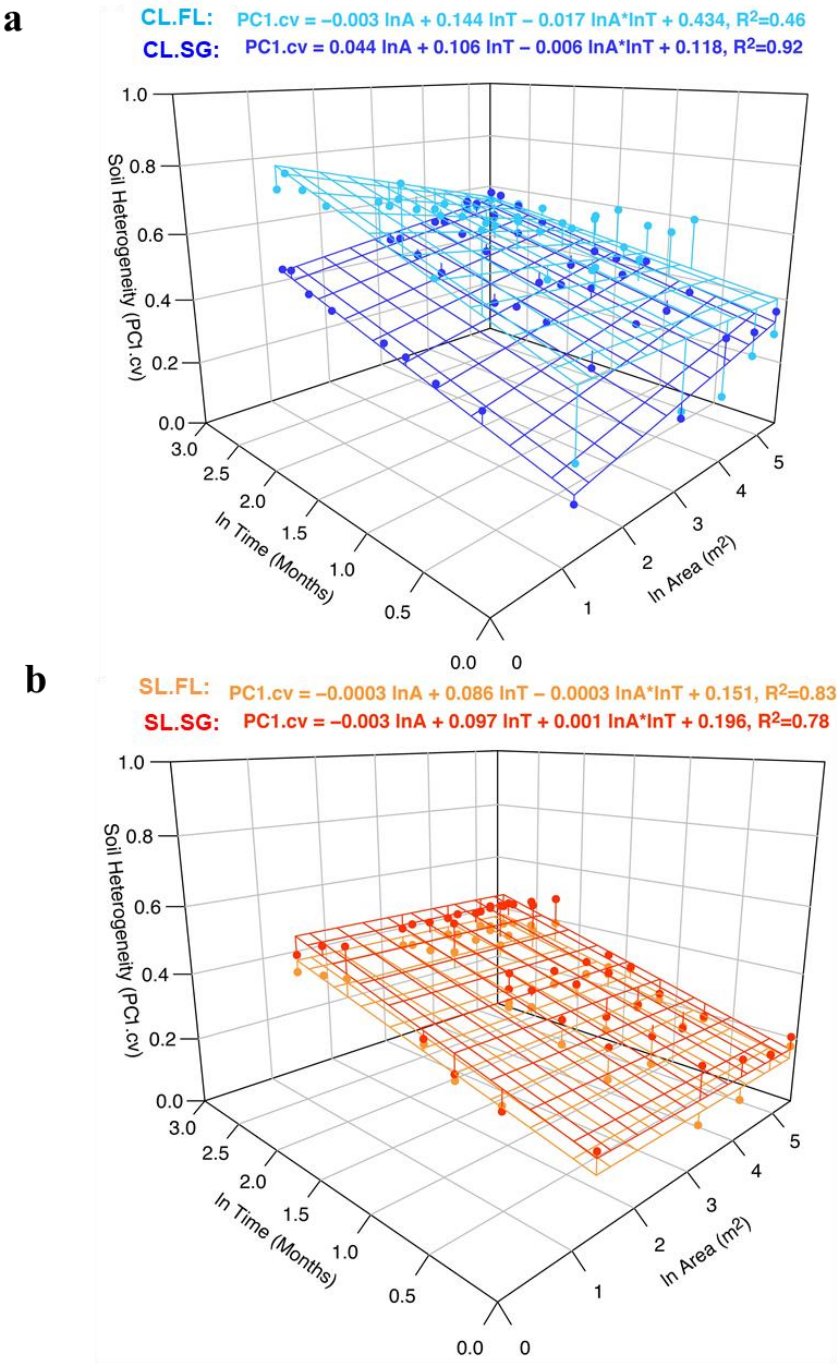

Figure 4.1 Soil heterogeneity by time and area for: a, the clay-loam site; **b**, the sandy-loam site. Equations for each plot and R^2 values displayed above each 3D plot in respective colors.

Interestingly, the surface represented by the fallow treatment in the CL soil (**Figure 4.1a**) intersected the switchgrass treatment as heterogeneity increased given greater time and area, resulting in the final months at the largest scale surpassing the heterogeneity of the fallow. Soil heterogeneity increased in both of these plots with time, although the fallow had an overall higher slope over time. In contrast, at the SL site, the plot with switchgrass had higher soil heterogeneity consistently over time and at scale (Figure 4.1b) allowing the two surfaces to remain parallel.

4.3.2 Species-time-area relationships (STAR)

Seasonal dynamics of accumulated species richness expressed by z-values (**Figure S4.2**) showed that both fallow treatments tended to have higher values at more time points than corresponding plots with switchgrass over the 17 months of observations. The CL site also tended to have the overall higher z-values when compared to the SL site over time. Next slopes were compared for both increasing area (z-values) and over time (w-values) (**Figure 4.2**).

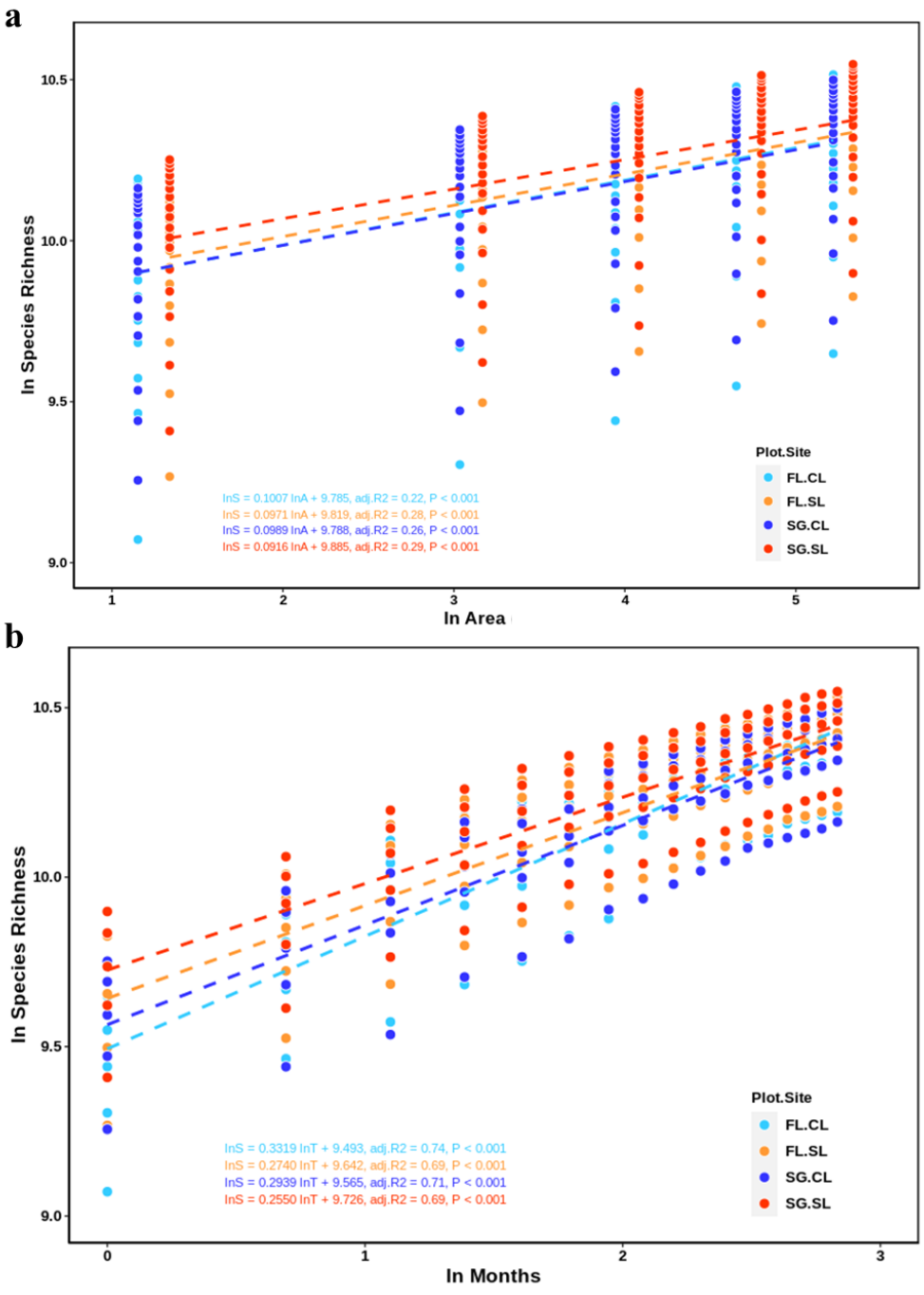

Figure 4.2 Bacterial species richness in each plot for: a, species-area relationship for increasing areas in m^2; **b**, species-time relationship for increasing time in months. Linear models for each plot shown in color below trend lines.

SL plots had higher species richness than the CL plots with the switchgrass treatment having the absolute highest number of species in the plot both over time and with increasing area. However, the slopes were higher for the CL site relative to the SL. Overall, we observed higher species accumulation over time than across area was observed, regardless of plot. Investigating the dynamics between w-values (species-time relationship) and area (**Figure 4.3a**)

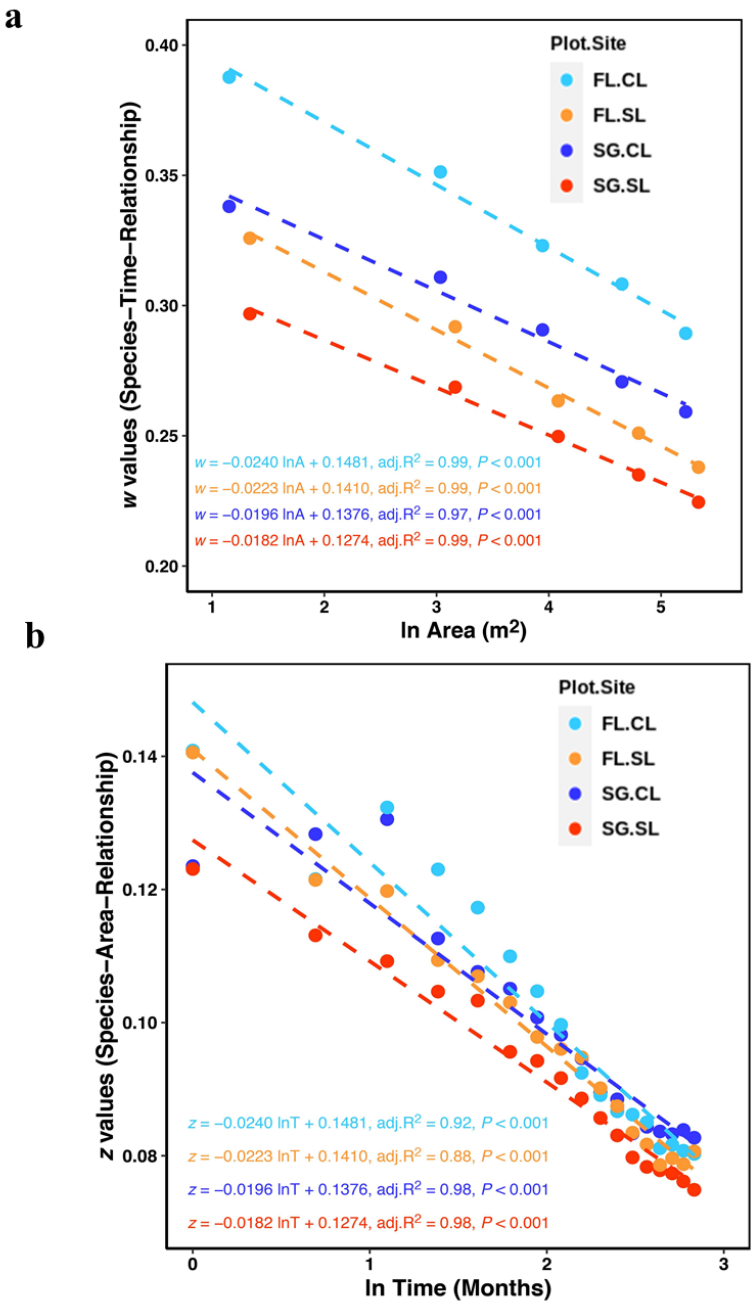

Figure 4.3 Linear correlations for: a, species-time relationship (w-values) with increasing areas by plot; **b**, species-area relationship (z-values) with increasing time in months by plot. Linear models for each plot shown in color below trend lines.

revealed that accumulation consistently decreased with increasing spatial scale, again emphasizing that the clay-loam site has a higher species accumulation when compared to the SL site, regardless

of scale. The relationship between z-values and increasing time (in months) (**Figure 4.3b**) showed that z-values decreased and became more similar over time.

The STAR between treatments and plots (**Figure 4.4**) confirmed higher species accumulation was occurring over time rather than across increasing areas in the plots. At the CL site (**Figure 4.4a),** surfaces intersect along the temporal axis, showing that although the fallow had lower species accumulation early in the experiment, by the end it had overtaken species accumulation occurring in switchgrass plot.

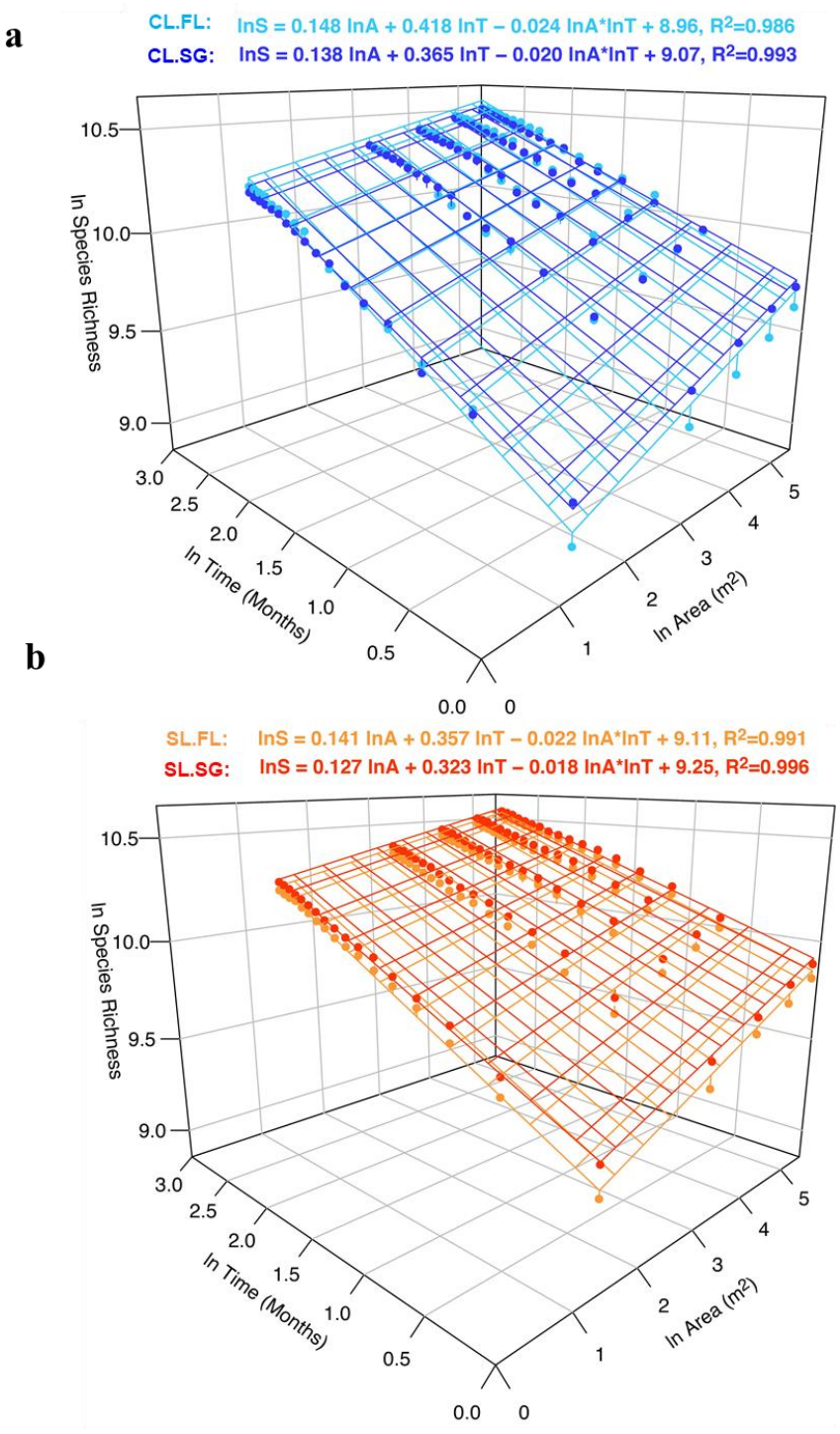

Figure 4.4 Bacterial species richness by time and area for: a, the clay-loam site between switchgrass and fallow treatments; **b**, the sandy-loam site between switchgrass and fallow treatments. Equations for each plot and R^2 values displayed above each 3D plot in respective colors.

This result may be linked to the successional dynamics occurring in the plant community in the fallow at this site. Although this trend was not observed at the SL site (**Figure 4.4b**), in which the switchgrass plot had higher species accumulation regardless of time or scale.

4.3.3 Linking soil heterogeneity to species turnover

Multiple linear regressions were used to link the species-area relationship with various soil chemical parameters (*i.e.*, soil carbon, nitrogen, or phosphorous content). After applying a stepwise method for variable selection based on AIC values for each regression, the turnover of phosphorous (using the coefficient of variation) showed a significant positive correlation with z-values for all plots (**Figure 4.5**).

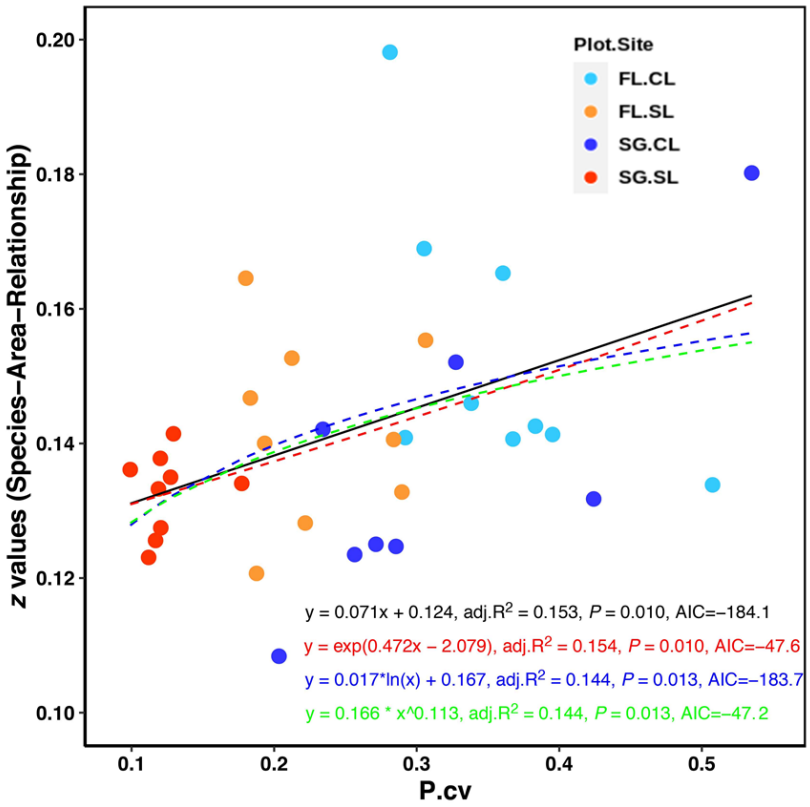

Figure 4.5 Multiple linear regression models between z values and phosphorous turnover for each plot. A stepwise method was used for variable selection based on AIC scores. All plots showed significant positive relationship between z values and phosphorous turnover.

Thereby, linking the turnover of soil phosphorus with the species accumulation across area and suggesting that as phosphorus turnover increases so does the soil bacterial species diversity across area at these marginal land sites.

4.4 DISCUSSION

In this study, we examined the rate of diversity accumulation over time and space in two contrasting marginal land sites that underwent soil restoration efforts with switchgrass cultivation. More precisely, we tested how edaphic conditions and plant cover impact the rate of diversity accumulation. As hypothesized, the accumulation of species richness over time (w = 0.289 ±

0.043) was much higher than that of the accumulation with increasing area (z = 0.097 ± 0.017), suggesting a stronger temporal effect on the overall species number. Our z values reported here were comparable to the range of z values for plants and animals which usually ranges from 0.1 to 0.3 (Rosenzweig, 1995). The z values reported here were also comparable to other microbiome scaling studies like those of forest soils across at temperature gradient (0.02 to 0.1; Deng *et al.,* 2018), human vaginal microbiomes (0.095 to 0.171; Li and Ma, 2019), and prokaryotic communities in lakes (0.104; Reche *et al.,* 2005). The temporal accumulation or w values reported here were higher than those of transplanted soils (0.04 to 0.12; Ling *et al.,* 2015), but lower than that of communities under direct stress treatments like long-term environmental warming (0.512; Guo *et al.,* 2019), perhaps indicating the natural taxa shifts going on due to the change in plant cover type at our sites. Additionally, the heterogeneity of the soil geochemistry and nutrient conditions across different spatial scales over time was related to and helped in explaining the different patterns of STAR for each plot. More specifically, the seasonal dynamics of SAR (z-values) were positively related to the heterogeneity of soil P concentrations. One of the underlying mechanisms that may explain this is that P changes may have a greater influence on the growth of the plants in each plot, which in turn, have a greater ability to meditate the soil nutrient conditions and thus coordinate various plant-microbe interactions, consequently affecting the overall bacterial diversity.

4.4.1 Soil heterogeneity and nutrient turnover

In our previous study, Bates *et al.,* 2021, it was observed that the percent soil C increased over time at the SL site with little changes observed for the CL site. However, further analysis shown here revealed a higher soil heterogeneity occurring at the CL site relative to either of the SL plots. Soil heterogeneity has been an issue for agriculture, especially when considering

precision crop protection (Patzold *et al.,* 2008) methods to ensure crop protection at the field scale. It has also been shown in grazing experiments (Pilar *et al.,* 2016) that soil food web response to grassland management depends on soil texture and organic matter content, implying ecosystem functionality sensitivity is highly depended on underlying soil characteristics like heterogeneity, especially when under new land usage regimes. Differences in soil heterogeneity have also been shown to impact the yield of plants (Cahill & Casper, 1999; Einsmann *et al.,* 1999; Wijesinghe *et al.,* 2000), and their allocation of biomass between their roots (Jackson, Manwaring and Caldwell, 1990; Jackson & Caldwell, 1996) and shoots (Robinson, 1994) as well as have consequences for the overall community structure (Hutchings *et al.,* 2003; Baer *et al.,* 2020). In our study, this may have impacts on individual switchgrass plants in our plots at the CL site in terms of higher variability in both above and belowground biomass yields than those plants growing at the SL site.

4.4.2 Linking soil heterogeneity to STAR in marginal lands

Pervious work has revealed that there is a positive relationship between bacterial diversity and soil heterogeneity (Curd *et al.,* 2018; Fiona *et al.,* 2020) and that at larger scales the accumulation rate of bacterial communities is strongly correlated with that of the turnover rate of soil habitats (Ranjard *et al.,* 2013). Our work confirms these findings with the higher soil heterogeneity plots at the CL site yielding an elevated species-time-area relationship (w-values and z-values) at increasing areas/time (**Figure 4.3ab**) when compared to the SL site. Indeed, the changes in species richness against both time and area (**Figure 4.4ab**) mirror those of soil heterogeneity (Figure 4.1ab) for each of the sites and treatments. This may reflect similarities in diversity scaling associated with micro- and macroorganisms being driven by similar processes (selection and dispersal). Our seasonal dynamics of changes in z-values (**Figure S4.2**) revealed microbial z-values that were comparable to that of macroorganism z-values which can range

between 0.1 and 0.3 (Finlay, 2002; Green & Bohannan *et al.,* 2006). Remarkably, our finding for a positive correlation between soil P heterogeneity and microbial spatial diversity scaling may reflect a top-down control of the plants meeting their P limitation through cooperation via variable plant-microbe interactions. Changes in P nutrient availability may affect the plants more as a consequence of differences between microbe and plant N/P nutrient limitations (Capek *et al.,* 2018). Thus, to meet their P demand for growth in these nutrient limited marginal soils, the plants may be recruiting various phosphate solubilizing bacteria (Richardson *et al.,* 2009; Liang *et al.,* 2020; Bononi *et al.,* 2020) to aid in the acquisition of P given the variability across the plots. This may be modifying the community structure at scale, as it has been shown that changes in rhizosphere exudate profiles can recruit specialized community members (Hu *et al.,* 2018; Murphy *et al.,* 2021) and may modify their abundance in the soil. Additionally, it has been recently demonstrated that even antagonistic bacterial strains can evolve into mutualistic rhizosphere companions rapidly (within 6 months) (Li *et al.,* 2021) further giving plants ways to modify the functional relationship between various bacterial strains in the soil. Therefore, the plants act as moderators of the soil microbial community and thus alter the overall bacterial diversity in the plots. Interestingly, regardless of site, we observed higher w/z values (**Figure 4.3**) in linear correlations with opposite factors (area/time) for fallow treatments suggesting a role higher plant diversity has in regulating the greater microbial diversity.

4.4.3 Conclusion

Overall, our results align with our hypothesis that microbial diversity accumulation over time was higher than that over greater spatial scale, and that soil heterogeneity was linked to spatial scaling and important in understanding microbial STAR. Microbial z-values were found to be comparable to macroorganism derived z-values from other studies. Soil P heterogeneity was

positively correlated with microbial diversity scaling and could reflect the control plants have on microbial diversity over increasing areas. Together, our results stress the importance of nutrient condition and heterogeneity in regulating soil bacterial biodiversity and that in these marginal lands, diversity accumulation over time is greater than with increasing scale over the establishment of switchgrass.

CHAPTER FIVE

SWITCHGRASS ALTERS SUBSURFACE MICROBIAL COMMUNITY WHICH INFLUENCES THE DEEP C PRIMING EFFECT IN MARGINAL LANDS

ABSTRACT

Deep-rooted prairie grasses have been shown to improve soil productivity over long-term cultivation through the net input of soil carbon, these perennial grasses have the global potential for greenhouse gas (GHG) mitigation of up to 1 Pg of carbon dioxide per year. However, we know little about how the accumulation of root biomass (*i.e.,* the continuous input of slow C via root litter) in deep soil layers influences the respiration of soil heterotrophic microorganism, which will consequently regulate the soil carbon balance. By investigating soil carbon priming we found a differential response (*i.e.,* the dynamics of their decomposition/respiration along a depth profile) to plant residual carbon inputs (slow C) between long-term selected microbial communities from two different sites with deep and shallow root systems. Specifically, a significantly lower ratio of primed to substrate-induced respiration was detected for the deeper (60cm -150cm) soil layers for the sandy-loam site, suggesting more respired CO_2 was originating from the added slow-C. Microbial enzyme decomposition modeling (MEND) of the soil carbon pools projected for 300 years showed a higher potential for C accumulation at the sandy-loam site and depletion of mineral associated C at the clay loam site. Depending on soil type, nutrient condition, and microbial community structure; switchgrass alters the deep soil carbon pool with absolute increases at the cost of depleting old mineral protected carbon. Our results suggest that soil type and therefore microbial community structure play vital roles in how switchgrass triggers changes in the deep carbon pool. This study highlights the potential for increasing the soil carbon sink capacity in marginal lands through the influence of deep rooting plants.

5.1 INTRODUCTION

It is currently estimated that within the first meter of soil (without considering permafrost regions) there is as much as 1,500 Gt of carbon (Hiederer & Kochy, 2011), of which, half is stored below the top 30 cm (Hiederer & Kochy, 2011; Jobbagy & Jackson 2000; Balesdent *et al.*, 2018). This deep soil organic carbon (SOC) pool may be vulnerable to microbial degradation due to increase carbon cycling (Hungate *et al.,* 1997) becoming a future carbon source further exacerbating climate change. However, specific deep soil ecosystems may act as potential carbon sinks helping to mitigate these negative soil-atmospheric carbon dynamics. Of interest are deep rooted perennial grassland systems which can have root biomass reach depths of up to 2 m or more. These deep-rooted systems provide excellent carbon sinks and are currently being evaluated as potential agronomic bioenergy crops. Yet, despite these benefits, and when considering grasslands account for roughly 31.5% of Earth's total land area (FAO, 2014), it is critical to understand the effect these plants have on deep carbon profiles due to the potential large-scale impact they may have if widely cultivated. Currently, little is understood about how and when deep SOC is being accumulated or mineralized in response to changes in land usage (Harper & Tibbett, 2013; Guo & Gifford, 2002).

Switchgrass cultivation -along with other perennial deep-rooted plants- has been broadly associated with increases in topsoil carbon levels at many different sites when compared to native shallow-rooted annual grassland ecosystems (Zan *et al.,* 2001; Frank *et al.,* 2004; Ferchaud *et al.,* 2016; Kantola *et al.,* 2017). This is due to the increases in root biomass, litter and exudates found from land use conversion to perennial crop systems and has been considered to improve soil carbon stability and aggregate formation (Tiemann & Grandy, 2015). However, while the total amount of SOC may increase, deep-rooted systems may also prime the stable deep SOC for degradation by the indigenous soil microbial community with the input of fresh plant-derived carbon (Fontaine *et al.,* 2007; Shahzad *et al.,* 2018) along the depth profile. Regulation of this priming response is then reliant on the soil mineral composition (Torn *et al.,* 1997), soil nutrient content (Poeplau *et al.,* 2019), and specific microbial community members (Lange *et al.,* 2015) present in deeper soil layers. Therefore, essential to understanding the sustainability of deep-rooted bioenergy crops is to assess the influence these crops have on deep carbon pools to inform better land management practices.

Nevertheless, directly testing these interacting effects at large landscape scales remains challenging, aside from theoretical thought experiments (Anderson-Teixeria *et al.,* 2012). Therefore, spatially-explicit ecosystem modeling combined with field data and laboratory soil incubations has the potential to help address questions on deep soil carbon stability for perennial bioenergy crop systems. Ecosystem modeling approaches have already been utilized to probe permafrost carbon-climate feedbacks (Koven *et al.,* 2015; Schuur *et al.,* 2015), estimate the impacts of conservation on ecosystem services (Ferraro *et al.,* 2015), and provide mechanistic ecosystem-level forecasting (Ye *et al.,* 2015) to improve land management practices. In this study, we utilized the MEND model (Wang *et al.,* 2013; Wang *et al.,* 2015), which incorporates microbial

physiology and community ecological dynamics to estimate changes in carbon cycling. The MEND model has been shown to improve predictions for changes in soil carbon stocks due to climate feedbacks at both field and global scales. Using both field site data and soil C priming incubation, we tested the effects of deep-rooted bioenergy crop in two marginal Oklahoma soils to identify SOC turnover dynamics with soil depth and when compared to a native annual grassland system.

Here we hypothesize that depending on soil type, deep-rooted perennial grass systems (*e.g.*, Switchgrass) can improve soil carbon stability in part, by the continual input of fresh plant-derived C compounds (e.g., root exudates) into the soil which stimulates the microbial community towards preferential labile carbon degradation allowing more recalcitrant C sources (*e.g.*, root litter) to accumulate over time. This shift in the microbial community activity levels allows for more C substrates to enrich the soil, ultimately become sequestered from the atmosphere. Conversely, short rooted annual grassland systems have an influence on only the top few centimeters of soil where C turnover is often much higher. This limits the influence of their root systems; therefore, they cannot easily retain C in the deep soil, and this may lead to decreased C sequestration rates. Deep-rooted systems by investing C resources into enhancing the microbially derived soil functioning (*e.g.*, nutrient cycling), ensure positive soil benefits that will last for their multi-year growth. However, if soils contain high mineral protected C aggregates, that is, small aggregates that are made up of microbial products and persist in the soil due to chemical bonding to minerals, deep-rooted systems may stimulate C priming through enhanced C mineralization. The removal of stable mineral protected C at these sites could leave SOC vulnerable to future losses due to climate change.

5.2 MATERIALS AND METHODS

5.2.1 Study sites

Field samples for this study were exclusively obtained at two research farm sites (PDF with a clay-loam soil texture and RR with a sandy-loam soil texture) managed by the Noble Research Institute. The PDF farm site is located just west of Ardmore, OK (34.219859 ^{o}, -97.210111^{o}) while the Red River Farm (RR) is located near Burneyville, OK (33.887778^{o}, -97.285278^{o}) and is considered low in soil organic matter (SOM) content and soil nitrate concentrations. SG has been growing at both sites for > 10 years before sampling. A shallow rooted mixed grassland fallow (FL) was maintained near the SG plots at each site.

5.2.2 Soil coring and sample processing

We utilized a #15-SCS / Model GSRPS Giddings hydraulic probe equipped with a 1.2 m tube and a sterile plastic liner to collect each soil core. At each of the two field sites (PDF and RR), Three replicate soil cores were taken per two treatment groups (SG and FL), for a total of six cores per site. Each soil core was divided into five soil depths (0-30cm, 30-60cm, 60-90cm, 90-120cm, and 120-150cm) at the PDF site and seven soil depths (0-30cm, 30-60cm, 60-90cm, 90-120cm, 120-150cm, 180-210cm, 210-240cm) at the RR site, respectively. After each core was taken out, hole depth and soil core length were measured to estimate the amount of soil compaction that occurred during coring. Once the soil core was retrieved, the inner plastic liner with the soil is taken out of the metal coring tube and cut into the various depth sections for each site outlined above. After the labeling of each section, a sterile metal core of smaller diameter was used to core the larger core, this was to avoid sampling the sides of the core to avoid contamination from the other soil layers during the coring process. The top and bottom 1-0.5 cm of each core

circumference was shaved off and discarded to avoid contamination. A section of this inner core was then collected using sterile technique and stored in 50 ml Falcon tubes and labeled for DNA extraction and PLFA extractions, respectively. Next, soil was be taken, stored, and sent for chemical analysis of the depth profile. The rest of the soil core was wrapped in aluminum foil, labeled in a Ziploc bag and put on wet ice for soil activity experiments, quantifying soil moisture, soil pH, and the remaining soil frozen at -80 ^{o}C to be retained as archive soil. In the lab, soil was mixed within each replicate for each depth defined. All plant roots were removed. The remaining soil was sieved with a 4 mm sieve to remove any rocks or unwanted debris. This soil was kept at 4 ^{o}C until their use in the active isotopic soil carbon incubation.

5.2.3 Soil chemical methods and analyses

Soil samples were dried in an oven at 60^{o}C for a week and sieved to remove unwanted material with a 4 mm sieve. Soil samples were then shipped to the OSU soil testing lab where they performed Mehlich III extractions for quantifying the plant-available phosphorous in the soil, KCL extractions for nitrate and ammonium concentrations, along with performing test to determine total N, C and OM percentages in the soil at each depth via dry combustion (LECO corporation, St. Joseph MI, USA). Soil pH was determined by suspending 10 g of soil for each depth and each replicate in a 50 ml Falcon tube and adding to a volume of 50 ml ddH_20, then shaking for 30 minutes followed by allowing the soil to settle for 1 hour before pH measurement is conducted using a standard pH probe (Acccumet excel XL15 pH meter, Fisher Scientific, Hampton NH, USA). Soil moisture was assessed by massing out 5 g of soil and recording the mass for a weight tin then allowing the soil sample to dry for 1 week before re-massing to establish % moisture from the loss of water after drying. Water holding capacity (WHC) using the ‘European’ maximum

water holding capacity method (Naeth *et al.,* 1991; Blažka & Fischer, 2014) was assessed in the lab by placing a section of each core in a cylinder and saturating the soil sample with water. Saturated soil samples were then placed on an absorbent membrane and allowed to reach equilibrium as the excess water was drained out by gravity. Water holding capacity was then calculated from the weight of the water contained in the sample vs. the oven dry weight of the soil core section. Soil C stability, examined through residence time of soil C pools, was estimated by the analysis of the radiometric decay of ^{14}C (Frank *et al.,* 2012), measured at the Center for Accelerated Mass Spectrometry (CAMS) facility at Lawrence Livermore National Laboratory. Overall C pools were measured via density fractionation with sodium polytungstate to examine differences in the accessible C, C enclosed in soil aggregates, and mineral-associated C (Sollins *et al.,* 2007).

5.2.4 Soil DNA extraction and 16S amplicon sequencing

A freeze grinding method outlined in Zhou, J., Bruns, M. A., & Tiedje, J. M. ,1996 was used for crude DNA extractions in combination with the MBio Powersoil DNA extraction kit for all depths. This was due to these methods in combination yielding both high quantity and a high quality of DNA extracted from the soil. For microbial community profiling, a two-step PCR method (Wu *et al.,* 2015) was used for amplifying the V4 region of the bacterial 16S rRNA gene using the 515F and 806R primers.16S amplicon sequencing was conducted on the Illumina Mi-Seq DNA sequencing platform routinely used for microbial ecological studies (Caporaso *et al.,* 2012).

5.2.5 Sequence processing

Amplicon sequence data was analyzed using an internal pipeline known as the Amplicon Sequencing Analysis Pipeline (ASAP, version 1.4). MiSeq sequences were subjected to a quality check with the FastQC (version 0.11.5). Pair-end sequences were then merged based on the 3' overlap using PEAR (Zhang *et al.*, 2014; version 0.9.10) with a quality score cutoff set to 20, an assembly length between 200-400 with the minimum overlap length set to 50 bp. The program split_libraries_fastq.py from the QIIME package (Kuczynski *et al.*, 2012) (version 1.9.1) was used to assign reads to each sample (demultiplexing) based on the barcodes with the maximum barcode error of 0 and the trimming quality score set to 20. Primer sequences for the forward and reverse primer sequence were trimmed and removed. Sequences from multiple split libraries were then merged. Dereplication was performed using USEARCH44 (Edgar, 2010) (version 9.2.64) under the command fastx_uniques (utilizing the -sizeout option for sequence abundance output). Operational Taxonomic Units (OTUs) were then clustered using UPARSE with the OTU identity threshold set to 0.97 and the singletons/chimeric sequences removed (Edgar, 2013). The OTU table was made using the command -usearch_global in USEARCH. Each representative sequence for each OTU was classified using the RDP Classifier (Wang *et al.*, 2007) (16S: training set 16; ITS: trainset fungalits_warcup) with the confidence cutoff set to 0.8. OTUs in the 16S sequence reads assigned to Chloroplast at the Order level were then removed. Representative sequences for each OTU were used to construct a phylogenetic tree. Sequences were aligned using MAFFT (Katoh, 2002)(version 3.8.31) and alignments were filtered using Gblocks (Castresana, 2000) (version 0.91b) with the options -t=d, -b4=3 and -b5=h. FastTree (Price *et al.*, 2009) was used in constructing each phylogenetic tree using the filtered alignments. The phylogenetic tree and OTU tables were used for the calculations of alpha diversity (phylogenetic based indexes) and beta

diversity (UniFrac distance) using programs packaged in QIIME (Caporaso *et al.*, 2010) and R (R Core Team, 2014).

5.2.6 PLFA soil extractions

Phospholipid fatty acid (PLFA) analysis was conducted utilizing a high throughput method (Buyer & Sasser, 2012) using 2.5 g of wet soil for each PLFA extraction at each depth. PLFA analysis was conducted on initial soil core soils and at the end of the soil ^{13}C incubation experiment. This was to quantify the microbial biomass in the soils in the field as well as after the incubation. Soil samples were dried *in vacuo* overnight at room temperature in a centrifugal evaporator then 2 g of dry weight soil is determined and placed in test tubes. Bligh-Dyer extractant containing internal standard was added and tubes were sonicated in an ultrasonic for three 10-minute cycles with a five second vortex step used in-between each sonication step. Tubes were centrifuged at 3500 rpm for 15 minutes then the supernatant is transferred into a clean glass test tube. Organic molecules were separated by adding water and chloroform then vertexing to mix. Tubes were centrifuged again for 15 minutes at 3500 rpm and the bottom chloroform layer is transferred to a clean glass test tube. Samples were dried for 1hr at room temperature by centrifugal evaporation using a SpeedVac. Lipid class organics were then further separated via a solid phase extraction (SPE) utilizing a 96-well plate outfitted with 50 mg of silica per well. Each well is preconditioned with three washes with methanol and chloroform, and samples were dissolved in 1ml of chloroform then transferred to each column in the 96-well plate and allowed to pass through the silica wells. Neutral lipids are further removed with an additional wash of 1ml of chloroform followed up by a removal of glycolipids via a 1ml wash with acetone. Samples were then eluted from each column with 5:5:1 methanol: chloroform: H_2O via a gravity drip. Samples are once again dried for 1hr at room temperature with the SpeedVac. Transesterification reagent (0.2 ml of

a 0.01 Molar Potassium Hydroxide 3:1 Methanol: Toluene solution) is added to each tube and incubated at 37^{o}C for 15min. Chloroform (0.4ml each) and acetic acid (0.075 M) are added, mixed, and allowed to sit until phase have completely separated. The bottom chloroform layer is then transferred to a GC vial and dried via a SpeedVac. Samples are resuspended in hexane and placed in a sample limited-volume insert inserted into each GC vial. Samples were run via an Agilent Technologies 6890 gas chromatograph (GC) with an autosampler, split-splitless inlet and flame ionization detector, under hydrogen carrier gas, controlled by the MIDI MIS Sherlock and Agilent ChemStation software. Fatty Acid Methyl Esters (FAMEs) were identified using the MIDI PLFAD1 calibration mix and naming table. FAME biomarkers used for each microbial category defined in **Table S5.1**.

5.2.7 BioLog community functional profiling

Biolog TM ECO plates containing 31 different C sources (Biolog Inc., Hayward, California, USA) were used to estimate community level carbon utilization at each soil depth for each site before and after ^{13}C soil incubations. 0.5 g of soil from each sample were diluted to obtain a cell density of approximately 1 × 10 8 cells/ml, and each plate was inoculated with 100 µl suspension fluid per well. The plates were then incubated at 25 ^{o}C in the dark and the subsequent color development was measured using an autosampler and a microplate reader every 12 hours for 5 days (592 nm).

5.2.8 Soil ^{13}C priming incubation

The carbon priming experiment was conducted in the laboratory post soil processing of the cores for each depth. 20 g of dry weight soil from each of the depths was massed out and placed into 25 ml flasks for each incubation. One set of each biological replicate at each depth was treated as a control group while another set had ^{13}C-labled *Avena fatua* (oat) shoot biomass (^{13}C atom 99%) grinded, then added to each flask at a mass ratio of 0.67% of the soil mass and mixed. The control group was also mixed to adjust for soil disturbance. Soil moisture was adjusted for both groups to be 60% of the water hold capacity of the soil by adding deionized water to each of the soil flask incubations then adjusting every 2 days to remain consistent. All incubations were kept at room temperature. Flasks were then be covered with aluminum foil and allowed exposure to open air to keep aerobic conditions. Gas sampling was conducted in a time series 0 days, 1 day, 3 days, 7 days, 14 days, 21 days, 35 days, 49 days and 60 days after the initial soil flask setup. At each sampling point, headspaces were sealed with an air-tight rubber stopper and initially sampled then sampled again after a 12 hour incubation has elapsed. Headspace gas were extracted by a gas-tight syringe from each flask and then injected into a 12-ml Exetainer evacuated vial (Labco International Inc., Houston, TX, USA) and diluted with N_2 gas. Carbon dioxide concentrations and δ^{13}C were quantified at the Stable Isotope Facility at the University of California in Davis.

5.2.9 δ^{13}C calculations

Carbon content from carbon dioxide was determined using the universal gas law at standard temperature and pressure and calculating µg C-CO_2.

$$n = \frac{PV}{RT} \quad (1)$$

Where *n* is the moles of air in each vessel with *V* volume at a *P* of 1 atm under *T* 298K and using the universal gas law constant *R* (82.05 ml atm/mol K). Then carbon content was adjusted for atmospheric concentrations and scaled for the volume of the incubation jar headspace per hour per gram of soil. The mineralization of the plant substrate was distinguished from the soil organic C mineralization based on the changes of stable isotopic composition ($\delta^{13}C$) derived from:

$$\delta 13C(‰) = [\ (R_{sample}\ /\ (R_{VPDB}) - 1]\ \ x\ 1000 \tag{2}$$

where R_{sample} is the mass ratio of ^{13}C to ^{12}C of the sample, and R_{VPDB} is the mass ratio of ^{13}C to ^{12}C of the international Peedee belemnite (PDB) standard. According to (Waldrop & Firestone, 2004) the percent carbon substrate emissions were calculated using the formula below:

$$C_s\% = \frac{[\delta_t - \delta_c]}{[\delta_s - \delta_c]} x\ 100 \tag{3}$$

Where C_s% is the proportion of evolved CO_2 from the labeled plant substrate, δ_t is the $\delta^{13}C$ (‰) of the evolved CO_2 in the treatment group, δ_c is the $\delta^{13}C$ (‰) of the control group, and δ_s is the $\delta^{13}C$ (‰) of the labeled plant substrate. Thus, the $C0_2$-C produced by the plant substrate during the incubation was calculated from:

$$CO_2 - 13C(\mu g g^{-1} soil) = C_s(\%)\ x\ total\ evolved\ CO_2 -$$

$$C(\mu g g^{-1} soil)/100$$

(4)

The absolute priming effect with the addition of the plant substrate was calculated from:

$$Primed\ soil\ CO_2 - C(\mu g\ C\ g^{-1} soil) =$$

$$CO_2 - C_{treatment} - CO_2 - C_{control}$$

(5)

Where CO_2-$C_{treatment}$ is the labelled CO_2-C evolved from the plant substrate amended soil, CO_2-$C_{control}$ is the CO_2-C evolved from the control soils. The priming effect of the soil organic C, expressed as the % increase compared to CO_2-C evolved from the control was calculated from:

$$Priming\ Effect(\%) = 100\ x\ [\frac{(C_{treatment}\ -\ C_{control})}{C_{control}}]$$

(6)

5.2.10 Aboveground plant and belowground root biomass estimates

Belowground estimates of total root biomass was estimated for the nearby long-term monitoring switchgrass plots via the Frasier agronomic row-crop root biomass estimation method (Frasier *et al.*, 2016). Briefly, four soil cores are taken within one meter of two adjacent switchgrass plants down to a meter in depth. Two of the cores are taken close to each switchgrass plant the other two cores are taken in the inter-row spaces. Then each core is separated by 20 cm segments and the roots are separated via 250 µm sieve and washing step. Roots are collected from each depth with tweezers and dried then massed. Total field root biomass is estimated by considering the

difference in root biomass for the inter-row and row positions per field hectare and summed for the total field biomass. Above ground plant biomass was estimated via annual plant biomass harvesting and massing for each field site.

5.2.11 CO_2 soil flux measurements

At two switchgrass field plots established in 2016, within 5km of our test plots, long term monitoring for soil trace gas flux was conducted on a monthly basis over a 3-year period. Each of these plots has 21 total trace gas collars set up in a cross design across each switchgrass field plot. Soil respiration rates (CO_2 flux) was measured via cavity ring-down spectrometry (Picaro G2508, Santa Clara, CA, U.S.A.) continuously for 6 minutes per collar. This allowed us to obtain gas concentrations in parts per million. Sampling primarily occurred between the hours of 8 am -12 pm to represent the daily average flux for each plot. Raw data was trimmed by manual inspection and ad hoc parameters; then model fitting (linear, quadratic, and exponential) is applied and the 'best model' is selected based on AUC scores. Flux estimations are then calculated using the following equation (Christiansen *et al.*, 2015):

$$F = \frac{dC}{dt} \cdot \frac{V}{AR(273.15+T)} \times 3600$$

Where $\frac{dC}{dt}$ is the slope of the carbon dioxide flux regression line at t = 0, V is the chamber volume in L, A is the chamber area in m^2, R is the gas constant in $LK^{-1}mol^{-1}$, T is the temperature in Celsius, when the chamber pressure is assumed to be equal to 1 atm. The 3600 factor is included to convert the flux to hourly values. F was then divided by 1000 to obtain the correct units.

5.2.12 Field site environmental parameters and measurements

Daily environmental data for 21 different variables (at 5 to 15-minute resolution) were obtained from two weather monitoring stations belonging to the Oklahoma MESONET network (http://mesonet.org/) near our field sites. Variables used included air temperature, bare soil temperature, covered soil temperature, atmospheric pressure, relative humidity, and precipitation. GPP values for each site were obtained via satellite images provided by the Earth Observation and Modeling Facility at the University of Oklahoma.

5.2.13 MEND-modeling

To better understand the subsurface microbially mediated soil carbon dynamics in our study systems, a microbially enabled decomposition model (MEND) (Wang *et al.,* 2012; Wang *et al.,* 2017) was used in this study. The MEND model is useful for sophisticated modeling of many parameters associated with soil carbon dynamics including representing microbial dormancy, resuscitation, and mortality within its parameters. More specifically, it can simulate soil organic matter (SOM) decomposition in response to various changes in the environmental conditions by explicitly modeling microbe-mediated oxidative and hydrolytic processes. Here, soil C pools were initialized by the measurements of soil organic C and microbial biomass C in both field sites (PDF and RR) and both treatment groups (Switchgrass and Fallow) at two soil depths (Topsoil layer is 0-30 cm and the subsoil layer 30-60 cm). To determine the microbial parameters in the soil samples, experimental data from the priming soil incubations (CO_2 respiration) was combined with field *in situ* CO_2 production fluxes to calibrate lab incubations with field measurements. The stochastic shuffled complex evolution (SCE) algorithm was used in order to determine the model parameters by achieving the highest goodness-of-fit between modeled and combined measured CO_2 fluxes. The microbial traits or parameters (*e.g.,* microbial growth, mortality, maintenance, active verse dormant fractions, and C use efficiency) used represent the microbial community

characteristics as they relate to soil C mineralization. The model was simulated with those various parameters and was run for 300 years to predict the long-term effects on SOM decomposition by deep-rooted switchgrass systems in both soil types (Clay-loam and Sandy-loam).

5.2.14 Statistical analyses

All analyses were conducted utilizing the R statistical platform (R Core Team, 2014) and plots were generated utilizing the package ggplot2 (Wickham, 2009). Data normality was assessed utilizing the Shapiro test in R. The difference between soil C/N was determined using the non-parametric Kruskal-Wallis test. The student t-test was utilized when comparing the accumulated respiration rates and the primed to substrate-induced respiration rates. The adonis test was used when establishing differences between site, depth, and treatment groups in the BioLog Ecoplates data. Hierarchical partitioning analysis was used to identify the most likely casual factors determining mean activity levels and carbon substrate richness in the BioLog community carbon substrate usage assay. Differences in microbial community structure for site, depth and treatment were tested using a PERMANOVA test based on Bray Curtis and weighted-UniFrac dissimilarity for taxonomic and phylogenetic diversity, respectively. To understand the differences between groups in our soil carbon simulation, a one-way ANOVA with a post-hoc Tukey HSD test was conducted.

5.3 RESULTS

5.3.1 Soil chemical differences with depth

To examine if the long-term establishment of deep-rooted perennials (*i.e.,* switchgrass) influenced the soil geochemistry, it was imperative that we compare the total C and N amounts between our switchgrass and fallow treatments (**Figure 5.1**).

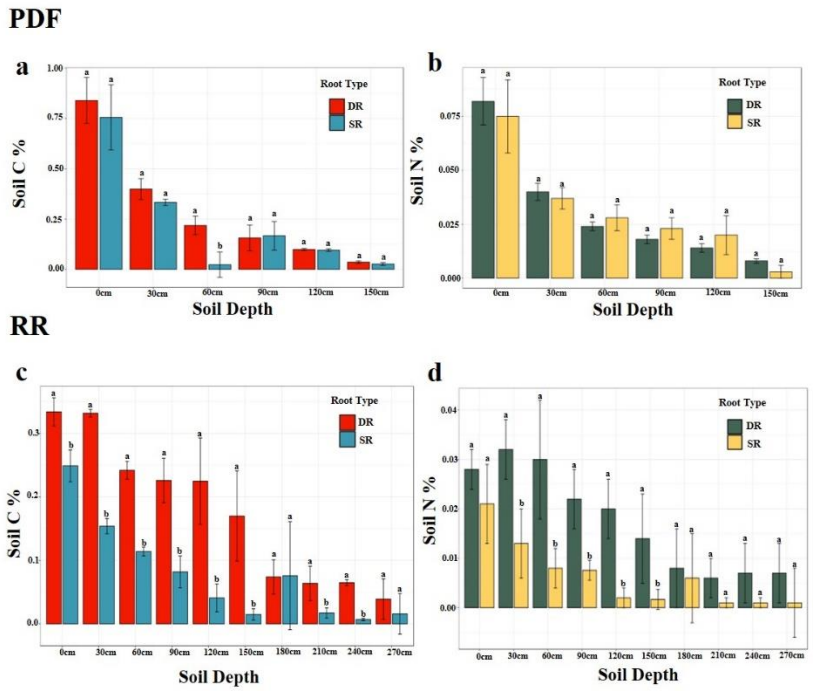

Figure 5.1 Differences (mean and standard error) in soil geochemical properties by site, root system type, and by depth for: a, soil carbon percentages at the PDF site from 0cm to 150cm depth between the deep rooted (DR) switchgrass plot and shallow rooted (SR) fallow; **b**, soil nitrogen percentages at the PDF site; **c**, soil carbon percentages at the RR site from 0cm to 270cm depth; **d**, soil nitrogen percentages at the RR site. Different letters signify significant difference between root type established by the Kruskal Wallis test with p values < 0.05.

At the PDF site, only one depth (60 cm) showed markedly lower amounts of C for the short-rooted annuals (established by the non-parametric Kruskal-Wallis test with $p < 0.05$) when compared to the deep-rooted perennials. There were no significant differences in the total N amounts between the two root systems for any depth in this clay-loam soil. In stark contrast, the RR site showed significant differences between the treatments, with the deep-rooted perennials having higher amounts of C and N (excluding the 0-30 cm layer for N) down to 180 cm in the soil column. C differences between the root systems then continued from 210-240 cm depths, illustrating the C building and even the potential C sequestration effect switchgrass had at depth in this sandy-loam soil.

5.3.2 Soil priming incubation and heterotrophic soil respiration rates

Daily respired CO_2-C amounts between the controls and the ^{13}C-labeled plant residue soil incubations (**Figure S5.1**) showed the expected higher respiration amounts by the ^{13}C-labeled incubations over the controls. The short-rooted and deep-rooted samples showed similar trends with higher daily respiration rates (excluding the 120-150 cm PDF site that had a peak rate after 14 days of incubation) early in the priming experiment tapered off by the end of the 60-day incubation period.

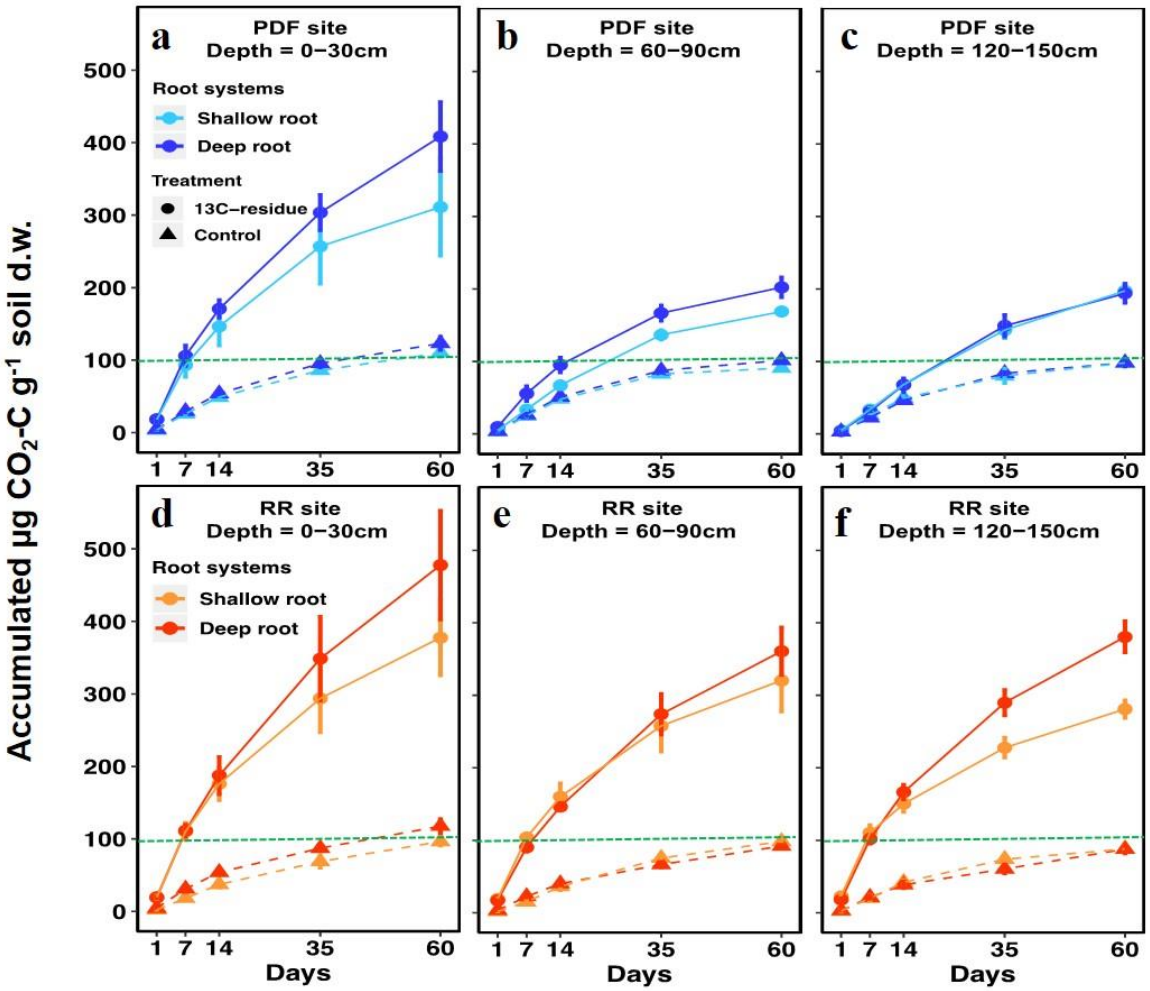

Figure 5.2 Accumulated soil respiration over the incubation time by dry weight per soil gram for: **a**, the PDF site from 0-30cm soil depth; **b**, the PDF site from 60-90cm; **c**, the PDF site from 120-150cm; **d**, the RR site from 0-30cm; **e**, the RR site from 60-30cm; **f**, the RR site from 120-150cm. All value represent mean ± standard error of the mean (n = 3).

The overall accumulated CO_2-C (corrected for dry-weight per gram of soil; **Figure 5.2**) showed similar profiles with significant differences between the controls and ^{13}C-labeled soil incubations. Topsoil (0-30 cm) showed the highest accumulation of CO_2-C over the course of the experiment, with the subsoil (120-150 cm) generally showing the lowest total accumulated levels.

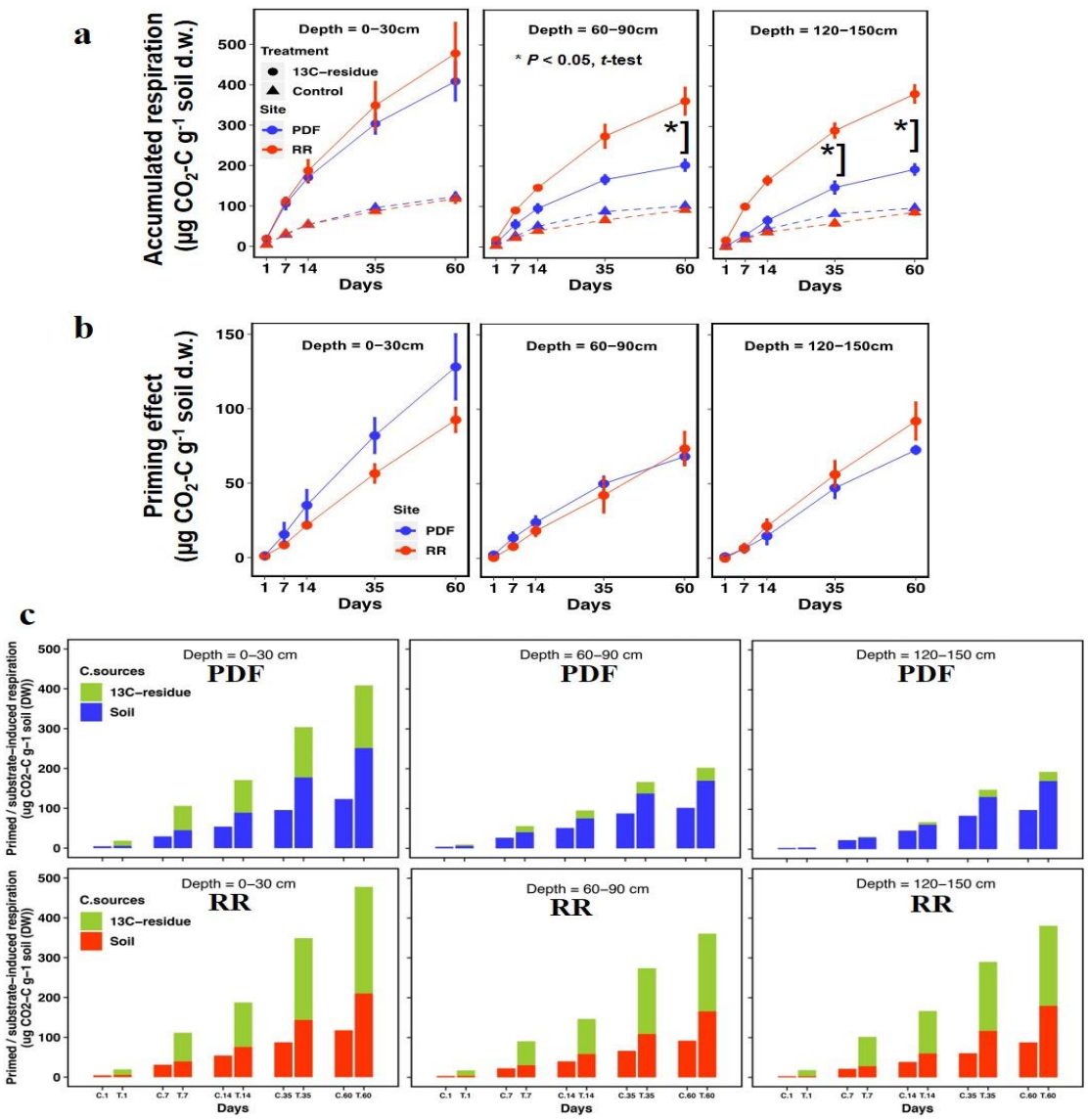

Figure 5.3 Effects of added ^{13}C-labeled plant residue on the deep-rooted SG for: a, accumulated soil heterotrophic respiration; **b**, the priming effect between the PDF and RR sites at different soil depths over the 60 days of soil incubation; **c**, primed over the substrate-induced accumulated CO_2-C between controls and ^{13}C-plant residue incubations for each site and soil type by time course. Results are expressed in accumulated values. All error bars presented are standard error (n = 3) and asterisks signify significant differences

No significant differences between the root systems were detected, but there was a difference between the deep-rooted SG systems depending on the soil type from the depths (60-90 cm and

120-150cm established by t-test with $p < 0.05$, **Figure 5.3a**). No significant difference in the calculated priming effect was observed between the root systems (**Figure S5.2**) or between soil types within the deep-rooted systems (**Figure 5.3b**). However, the primed to substrate-induced respiration was higher in the PDF deep-rooted system when compared to the RR site for all time points at both the 60-90 cm and 120-150 cm depths (**Figure S5.3**, established by t-test with $p < 0.05$). A breakdown of which source (the soil or ^{13}C-labeled plant material) produced the accumulated CO_2-C (**Figure 5.3c**) revealed that the proportion of respired CO_2-C from the soil was higher in the lower soil depths in the PDF deep-rooted incubations when compared to the RR site. This established a differential preference between the two soil types for what the microbes were responding to and actively degrading overtime during the soil incubations. At the RR site, more fresh input ^{13}C utilization was occurring in the soil while the clay-loam soil community responded to the priming differently by degrading a larger proportion of the soil-derived C than the fresh ^{13}C-labeled material at the lower soil depths.

5.3.3 Microbial biomass and carbon substrate usage profiles

Microbial biomass was enriched after the addition of ^{13}C-labeled plant residue during the soil incubations when compared to the original soils (**Figure S5.4a**). However, no significant differences were observed between either the soil types or treatments between sites before or after the soil incubations. When exploring the differences between phospholipid fatty acid methyl ester (FAME) microbial biomarkers, an enrichment in gram-negative bacteria was observed in the lower depths after ^{13}C-labeled plant residue was added (**Figure S5.4b**). We also observed an increase in the anaerobic microbial biomarkers in the original soils for the deeper soil samples. Biomarkers attributed to the *Actinomycetes* decreased in the deeper soil samples after ^{13}C soil incubations were carried out.

BioLog Ecoplates established a decrease in mean activity levels along the depth profile, and it was observed that there was similar C substrate richness between sites and treatments within each soil depth assayed (**Figure S5.5a,b**). Hierarchical partitioning analysis (**Figure S5.5c,d**) revealed that soil depth and treatment were the likely causal factors in determining the differences between mean activity levels and C substrate richness, respectively. Mean activity rates significantly increased after ^{13}C-plant substrate addition (**Figure S5.6**) with soil depth the likely causal factor regulating the response as mean activities decreased with increasing soil depth. Carbon substrate richness was then increased after ^{13}C-labeled plant material addition (**Figure S5.7**) and was less influenced by soil depth at both sites.

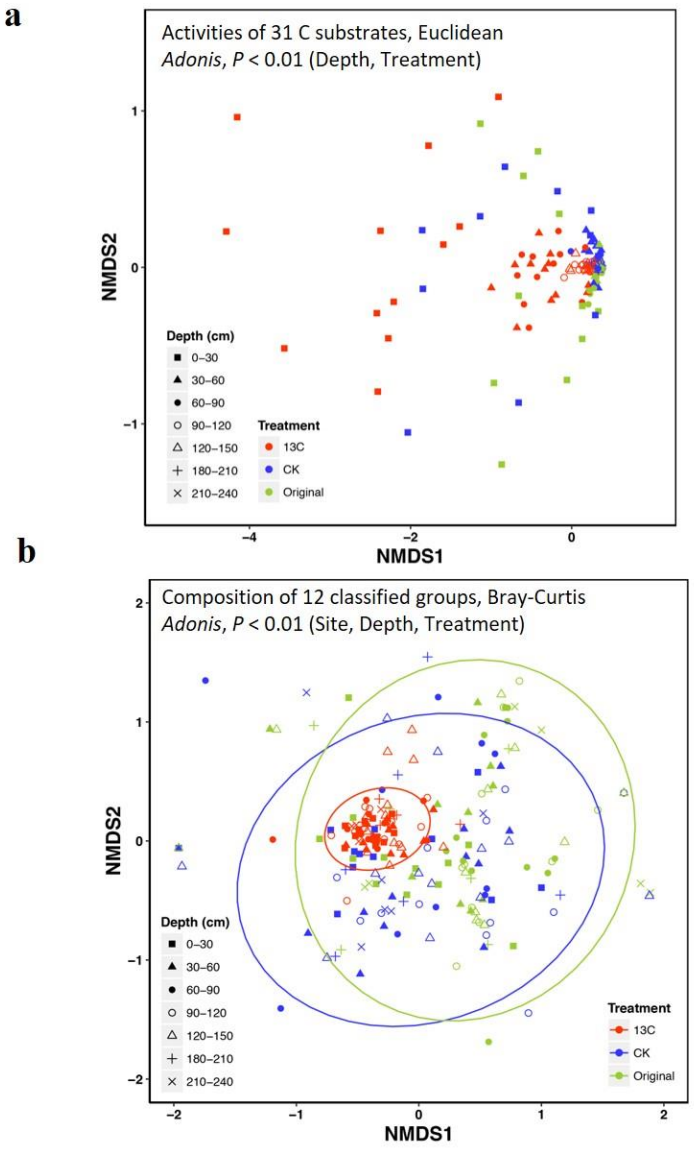

Figure 5.4 Non-metric multidimensional scaling of the BioLog Ecoplates for: a, the functional structure of carbon substrate usage between the original soils and the control and ^{13}C soil priming incubations groups by soil depth; **b**, the composition of 12 classified carbon groups by Bray-Curtis distance between original soils, control and ^{13}C priming soil incubations. All groups were found to have significant differences between each other by Adonis with p values < 0.01.

Using non-metric multidimensional scaling (**Figure 5.4**) of the BioLog activities and 12 different C composition groups, C substrate richness increased after ^{13}C incubation with the activity changing between soil depth and ^{13}C-labeled plant material treatment. In other words, the microbial communities tended to use more different types of labile C substrates after the ^{13}C treatment, but root type did not show differences in C substrate usage.

5.3.4 Microbial diversity and community dynamics

Alpha diversity (measured as species richness, **Figure S5.8**) and phylogenetic diversity (**Figure S5.9**) of the bacterial communities were not significantly different between root types by depth, although both metrics were higher in deep-root systems relative to the shallow-root systems for each of the topsoil layers at each site. The addition of the ^{13}C-labeled plant material caused a decrease in species richness and phylogenetic diversity (**Figure S5.8b,d** and **Figure S5.9b,d**). The most prevalent bacterial phyla present in the incubation samples (**Figure S5.10** and **Figure S5.11**) were *Actinobacteria*, *Proteobacteria*, *Acidobacteria*, and *Verrucomicrobia*. ^{13}C-labeled plant material tended to enrich *Proteobacteria* along the soil depth profile at both sites, while the control treatment enriched both *Actinobacteria* and *Acidobacteria* for each soil type.

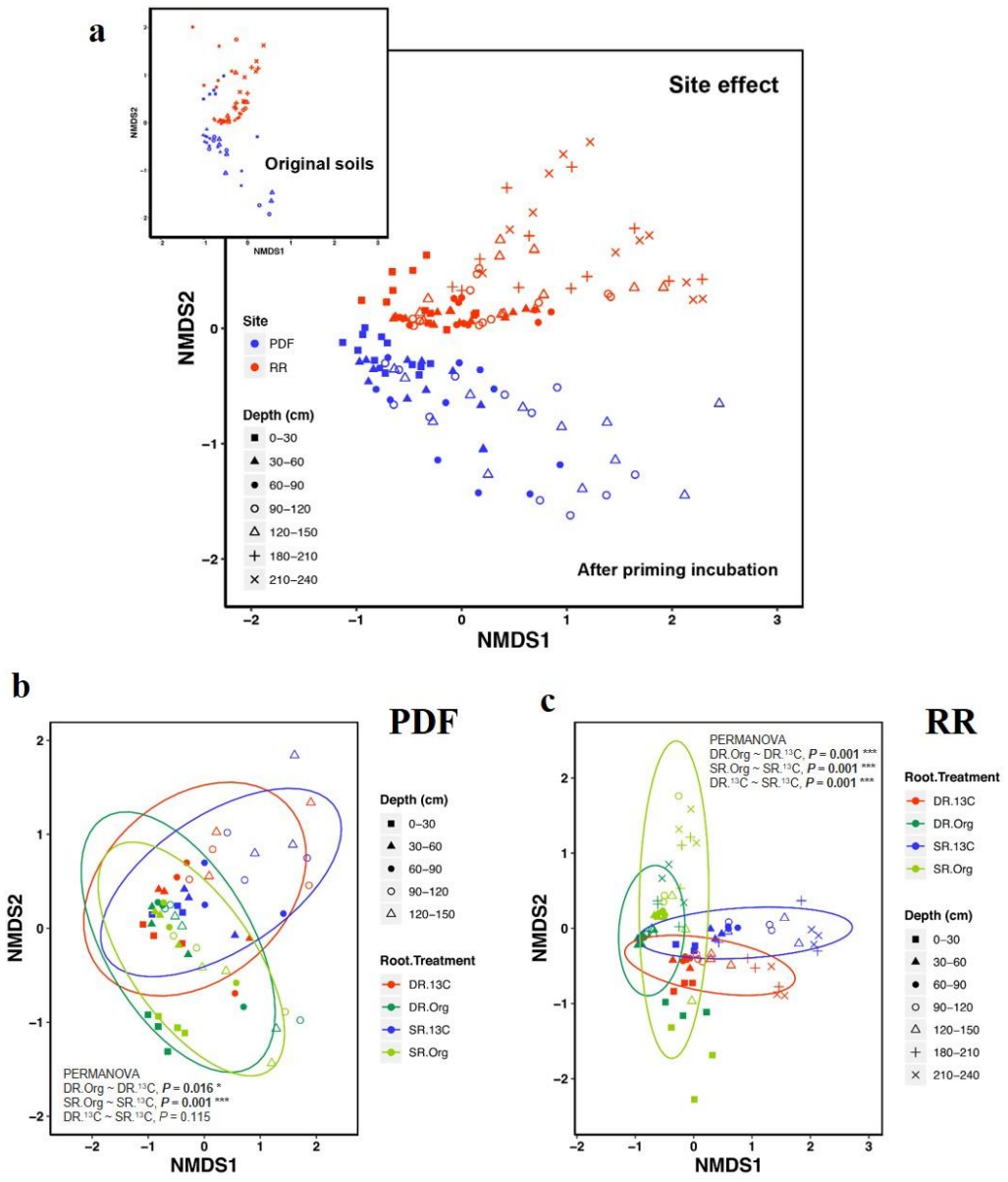

Figure 5.5 Non-metric multidimensional scaling of the bacterial community for: a, the site level effect both before and after priming soil incubations; **b**, the PDF site comparing the original soils and after the ^{13}C priming soil incubations separated by root type; **c**, the RR site comparing the original soils and after the ^{13}C priming soil incubations separated by root type. Significant differences in community structure determined by PERMANOVA.

When looking at the overall microbial community structure (**Figure 5.5**), no significant differences were observed between the root types for the PDF site (**Figure 5.5b**). However,

significant effects (PERMANOVA, $p < 0.001$) were observed between the root systems on the microbial community structure in the RR soil (**Figure 5.5c**). Both sites showed a significant treatment effect with the ^{13}C-labeled plant material addition (**Figure S5.12**) on the community structure.

5.3.5 Soil carbon modeling

To address the fundamental uncertainty regarding the effects and establishment of switchgrass on the deep soil C stocks and long-term C dynamics in marginal lands, we turned to modeling the soil carbon dynamics by integrating our lab-based models with field-based measurements to predict future C stocks more accurately under switchgrass. First, our lab-based model performance (**Figure S5.13a**) was assessed and found to have higher R^2 for the topsoil ($R^2 = 0.93$) relative to the subsoil ($R^2 = 0.72$) when comparing the simulated and observed accumulated CO_2-C. The field-based model (**Figure S5.13b**), which consisted of using *in situ* soil trace gas field measurements of CO_2 production over a 17-month time frame (Bates *et al.*, 2021), showed higher Rh for the perennials at each site (the clay-loam $R^2 = 0.5$ and sandy-loam $R^2 = 0.7$) over the shallow-rooted annuals (clay loam $R^2 = 0.32$ and sandy-loam $R^2 = 0.35$). The field-based model's validation of Rh was performed only using the switchgrass plots (**Figure S5.13c**), which yielded similar R^2 performance for each site (clay-loam $R^2 = 0.54$ and sandy-loam $R^2 = 0.50$). With these models validated and calibrated, we were able to combine the lab and field-based respiration data with the MEND model parameters, which account for microbial decomposition processes to model the long-term dynamics for various organic C pools at each of the sites depending on root system type (**Figure 5.6**).

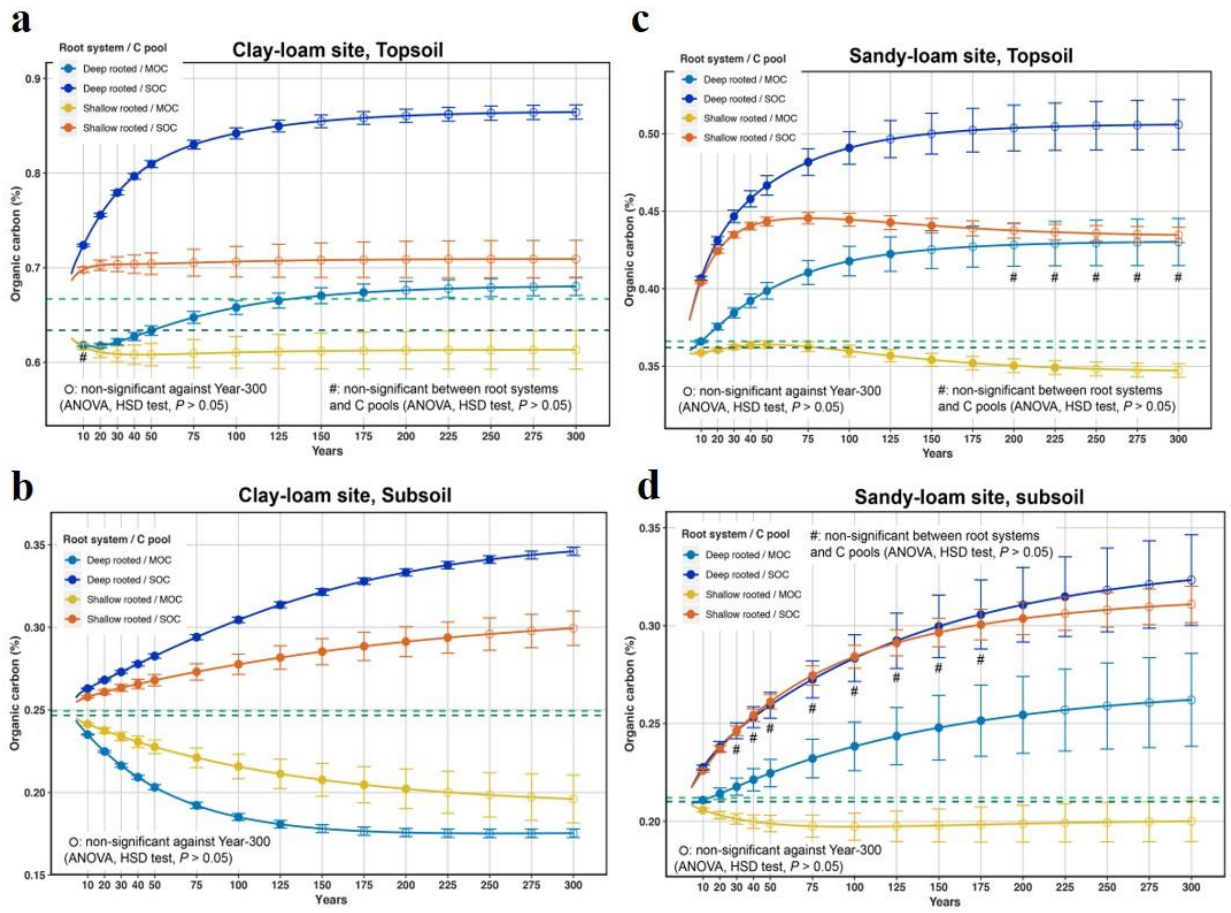

Figure 5.6 Long-term simulation of different organic carbon pools by root system types for: a, the clay-loam topsoil; **b**, the clay-loam subsoil; **c**, the sandy-loam topsoil; **d**, the sandy-loam subsoil. Significance established by ANOVA and HSD test with $p < 0.05$.

Our simulation revealed that all projected C pools reach a steady-state rapidly and many maintain their dynamics over the 300 years forecasted. One clear difference between the sites is that the deep-rooted system shows a depletion of mineral-associated carbon (MOC) in the clay-loam subsoil, while in the sandy-loam subsoil, MOC continues to slowly build over time. We then used a comparison of the ratio between the projected and original SOC to investigate the effect of the different root systems, soil types, and soil depths on the total C stocks.

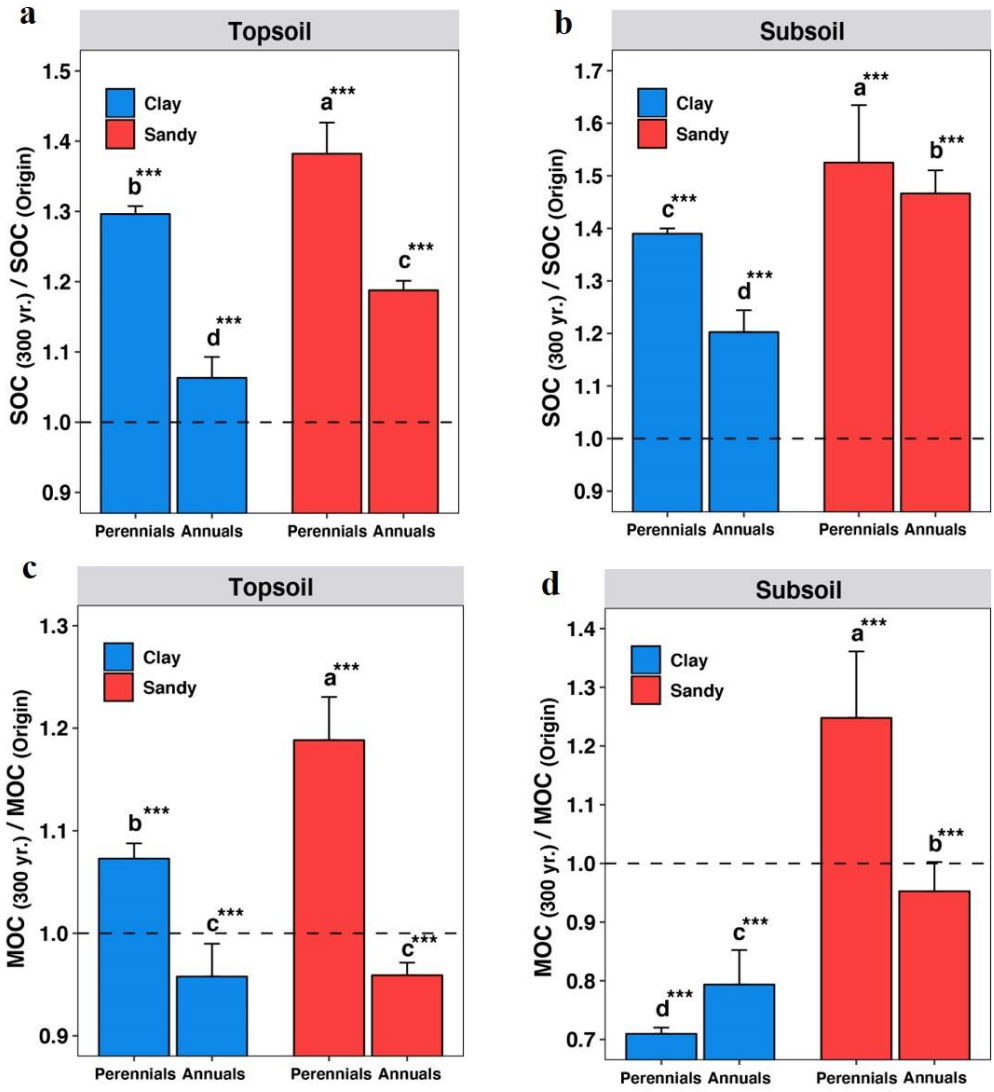

Figure 5.7 Ratio of C pools of 300 year projection over original soil between root type and soil texture for: a, topsoil in terms of soil organic matter (SOC); **b**, subsoil in terms of SOC; **c**, topsoil in terms of mineral associated carbon (MOC); **d**, subsoil in terms of MOC. One-way ANOVA with post-hoc Tukey HSD test to compare the ratios. Values with different letter signify differences at $p < 0.05$.

Based on these results (**Figure 5.7a,b**), the long-term cultivation of deep-rooted switchgrass may result in a significantly larger amount of SOC than under the shallow-rooted annuals. In addition, significantly higher SOC was projected to accumulate in the sandy-loam site rather than in the

clay-loam site. We also examined the comparison between the projected and original MOC (**Figure 5.7c,d**) and found that although the total C stock increased, the MOC significantly decreased. This decrease in MOC was especially pronounced in the fine-textured clay-loam site in the subsoil layer, while the only projected increase was for the sandy-loam soil with switchgrass for both the top and subsoil layers. Finally, to link the microbial community back to our projection on soil C stocks, we looked at the ratio between delta Rs and Rs in the control group during our soil priming incubation (**Figure S5.14a,b**). We observed no significant difference between the two ratios and the soil types/root types in the topsoil layer; however, this ratio was significantly higher in the sandy-loam subsoil layer, which may indicate that the community is more actively responding to the addition of the ^{13}C-labeled plant substrate than the clay-loam community. Similarly, we found no significant difference between the ratio between the delta ^{13}C-Rs and the delta total-Rs in the topsoil (Figure S14c). However, the ratio was significantly higher in the sandy-loam subsoil layer (**Figure S5.14d**), which may provide a punitive explanation about the simulated higher MOC formation as the microbes in the sandy-loam subsoil layer have a higher capacity to decompose and assimilate added plant substrate that is introduced to them.

5.4 DISCUSSION

In this study, we quantified the microbially induced priming effect in the subsurface soil and examined the effects of root system type (short/deep) on C stocks to better quantify the impacts of long-term switchgrass cultivation in marginal lands. As hypothesized, switchgrass increased the percent of total C for many of the soil layers, but only at the sandy-loam RR site when compared to the control fallow with short-rooted annuals. In contrast, the switchgrass influenced clay-loam soil of the PDF site did not see a significant increase in the percent of total C when compared to their corresponding fallow. Although the starting soil C amounts were overall higher at the PDF

site when compared to the RR site. No significant priming effect was observed in our soil priming laboratory incubations when comparing root type. However, when comparing the two switchgrass plots, the accumulated soil respiration revealed higher respiration rates occurring for the subsoil layers at the PDF site relative to the RR site. Our most striking result was the differences observed in the primed to substrate-induced respiration for the subsoil layers, revealing that the microbial community at the RR site preferentially degraded the added ^{13}C-labeled plant substrate while the PDF community had elevated rates of C mineralization after priming. Our integrated lab and field-based simulated carbon pool model further supported these findings by establishing the overall increase in SOC levels under switchgrass influence, while MOC levels were projected to increase in the subsoil of the sandy-loam RR soil only. Site selection for switchgrass cultivation of marginal lands with sandy-loam soil texture may afford more C sequestration benefits than those of clay-loam sites for future bioenergy programs. However, larger-scale studies with further replication are needed to ensure the generalizability of our findings in this study.

5.4.1 Edaphic factors regulating switchgrass C storage

Switchgrass has been broadly associated with increases in C accrual across many locations in the US (Ma *et al.,* 2000; Anderson-Teixeria *et al.,* 2009; Gelfand *et al.,* 2013) and has been observed to increase soil C stocks at a relatively rapid rate (Abraha *et al.,* 2019). However, relatively few studies have investigated its impacts on soil C stocks in nutrient-poor marginal lands (Dabney *et al.,* 2004; Gelfand *et al.,* 2013). Additionally, the so-called rhizosphere priming effect of deep-rooted perennials like switchgrass may stimulate the subsurface to increase C mineralization and cause elevated CO_2 production from these sites. Therefore, understanding plant-microbe-carbon feedbacks is crucial in understanding the sustainability of switchgrass and other deep-rooted perennial bioenergy cultivation in marginal soils. Our study illustrates the

potential feedback that initial higher C stocks could lead to the depletion of MOC at depth with switchgrass cultivation and the potential for more CO_2 production than at short-rooted annual dominated field sites. This was evident in the higher accumulated soil respiration levels measured at depth for the PDF clay-loam soil, where higher C content and N nutrient availability may have contributed to the microbial communities' preference for increased ^{12}C mineralization after ^{13}C-labeled plant substrate addition. For instance, it has been shown that sandy-loam soils have displayed higher mineralization rates of fresh plant leave inputs than in clay loam soils (Froseth & Bleken, 2015). These differences in soil type mineralization rates may reflect diffusion differences in exoenzymes produced by the microbes, which may depend on other abiotic factors for their diffusion, such as soil texture and the mineral content of the soil. Due to these differing soil type factors, switchgrass C storage may be enhanced for sandy-loam sites as the diffusion of exoenzymes can easily reach 'fresh' organic carbon (*e.g.*, root litter) and therefore have a greater chance of degrading more labile components, thus allowing recalcitrant C sources to remain in the soil for longer periods of time, thereby building up C stocks over time. Our relatively higher C content at the sandy-loam site may also support this idea, but more direct experiments with exoenzymatic diffusion in natural soil settings and detailed C substrate profiles are needed. For the clay soils, although the overall soil C levels may increase under the deep-rooted system, microbial exoenzymes may degrade more of the mineral associated organic matter and change the composition of C stocks.

5.4.2 Microbial efficiency-matrix stabilization under switchgrass

In our study, we used the ratio between delta ^{13}C-Rs and total-Rs to represent how much induced soil respiration is derived from the degradation of the added ^{13}C-labeled plant substrate. In the topsoil layer, no significant differences were observed between Rs ratios for either of the

root types. However, in the subsoil of the sandy-loam site, there was a significantly higher ratio than for the clay-loam site regardless of root type. A higher Rs ratio implies that the microbes have a higher capacity to not only decompose the ^{13}C-labeled plant material but may also have higher assimilation of this material into their biomass. For example, it has been demonstrated in forest soils that rhizosphere priming can increase seasonal microbial biomass (Scott-Denton *et al.,* 2006). Under the framework of microbial efficiency-matrix stabilization (Cotrufo *et al.,* 2013), it is suggested that through microbial degradation of labile plant material, these microbial decomposition products are the primary components of stable SOM. These microbially derived decomposition precursors may then aid in aggregate formation and can form strong chemical bonds to the mineral soil matrix, thus increasing the total soil MOC via a 'microbial filter.' Therefore, with this framework in mind, our results with the sandy-loam site may agree with this 'microbial filter' hypothesis and better explain the projected increases in MOC during our 300-year soil carbon simulation model. It has been suggested that litter quality may also play an important role in MOC formation (Mikutta *et al.,* 2019); thus, switchgrass with its 'fresh' root litter inputs deep down in the soil column may further improve MOC formation.

5.4.3 Carbon sequestration

It is estimated that due to agricultural practices, we have lost ~133 Pg of C in the top 2 m of soil over the past 12,000 years (Sanderman *et al.,* 2017), which has incurred a global carbon debt from anthropogenic activities. States in the Midwest like Iowa have lost ~61% of the SOC in the last 80 years (Donigian *et al.,* 2002). Additionally, the US Corn Belt has lost as much as 1.4 ± 0.5 Pg of carbon (Thaler *et al.,* 2021) from the soil due to conventional agricultural practices. As NOAA reports the highest global average measured concentration of CO_2 at 412.5 ppm (NOAA, 2020) in 2020 (reaching the highest point for CO_2 concentrations in three million years), it is

becoming apparent the need for more C capture and sequestration efforts to try and combat the ever-rising CO_2 levels in the atmosphere. Perennial deep-rooted grasses like switchgrass offer an economically feasible solution for prairie environments to help trap C and act as potential soil C sinks while improving soil fertility. However, the ecological impacts on the below-ground microbial community and understanding the effects deep-rooted systems have on SOC and MOC still need to be assessed for sustainable large-scale cultivation efforts. Our study has highlighted the importance of the microbial community and the edaphic conditions in the soil for regulating and building SOC and MOC in the subsurface layers of soil when under the influence of deep-rooted perennials.

Overall, the deep-root system of switchgrass in marginal lands showed no significant difference in C priming effect, observed higher accumulated $^{13}CO_2$-C respiration in the clay-loam site relative to the sandy-loam site, and was projected to not only increase the overall SOC for both the topsoil and subsoil layers but may also increase the MOC in the subsurface sandy-loam soil which may lead to higher rates of C capture and subsequent sequestration at these sites. Our multifaceted approach provides evidence that sandy-loam soils may confer more C capture potential, and thus are findings are an important step forward in outlining sustainable site selection for large-scale bioenergy perennial cultivation on marginal lands to both improve soil fertility and meet C sequestration goals.

CHAPTER SIX

SUMMARY AND OUTPUT

6.1 SUMMARY AND OUTPUT

This dissertation presents several lines of evidence for the critical role soil microbes have in nutrient and carbon cycling through plant-microbe interactions and their impacts on ecosystem functions in grassland ecosystems. The response of microbes to nitrogen deposition or elevated CO_2 depended on functional group and association with plant community members. Generally, plant-microbe interactions have profound impacts on soil carbon stocks, plant physiology, nutrient cycling, and overall soil health. Findings from this work may be vital in quantifying the impacts and ecosystem functionality of microbes and plant-microbe interactions to climate change, nitrogen deposition concerns, marginal land usage for bioenergy crop production, modeling greenhouse trace gas fluxes and future soil carbon stocks, as well as formulating new hypotheses on microbial temporal and spatial diversity scaling laws.

First, the effect of elevated carbon dioxide and nitrogen deposition was assessed on the free-living diazotrophic community along with the bacterial and fungal communities in a nitrogen-limited grassland ecosystem. Results revealed that individually, nitrogen deposition and elevated CO_2 treatments increased the estimated nitrogen fixation rates. However, the combination of these treatments resulted in a suppression of nitrogen fixation rates back to ambient conditions. Additionally, diazotrophic community alpha diversity was unaffected by the treatments, but beta diversity and greater dispersion in the community were observed, which may explain shifts in specific taxa that changed the overall community functionality. This study provides critical information about the functional response of diazotrophic bacteria to leading anthropogenic climate factors and may help to provide a basis for future work on plant-microbial interactions and nutrient cycling.

Secondly, the impact of switchgrass establishment on soil chemistry, microbial communities, heterotrophic respiration, and GHG trace gas fluxes were measured in two contrasting marginal soils (low in N/P nutrient availability) with a history of high rates of topsoil erosion. The plot with switchgrass at the sandy-loam site significantly increased the total carbon in the soil but not at the clay-loam site, which was marked by higher heterotrophic respiration rates. Plots with switchgrass did show a significant reduction in methane consumption regardless of soil texture/nutrient availability. This study stresses the importance of site selection for marginal land conversion to bioenergy crop cultivation and the ecological consequences of such changes in land usage. This study may also be important for future modeling efforts of the soil carbon flux in grasslands and agro/bioenergy crop sites.

Third, utilizing the temporal and spatial scale afforded from the sampling of the trace gas/switchgrass establishment project, we further investigated the species-time-area relationships within the prokaryotic community of the two marginal land sites both with and without switchgrass. Our results showed that species turnover overtime was higher than with increasing scale (*i.e.,* area) and that the species-area relationship was positively related to the soil heterogeneity of P in the soil. This study may provide more fundamental linkages to how soil heterogeneity dictates soil microbial biodiversity scaling.

Fourth, the subsurface microbial priming response to perennial deep-rooted systems was evaluated against short-rooted annuals in marginal soils to understand the consequences of heterotrophic respiration in deep soil layers and the effect on native soil carbon stocks. This study provided evidence that a switchgrass deep-rooted influenced soil system has a differential response to carbon priming in the subsurface soils and that depending on soil type, nutrient condition, and microbial community structure, there is the potential for switchgrass to alter the deep soil carbon

pool. This study highlights that microbial community composition and soil type may alter the carbon composition in the subsoil layers under deep-rooted systems as a result of the rhizosphere priming effect. This work may be important for outlining more sustainable site selection for large-scale bioenergy cultivation projects on marginal lands that help to build up soil carbon stocks.

In conclusion, the work presented in this dissertation is a small part of a much larger effort to better understand the role microbial ecology will have in addressing the climate change crisis, furthering fundamental science and our understanding of the intricate dynamics of plant-microbial interactions, and hopefully provide insight into future modeling and theoretical ecological frameworks to address the challenges of the future.

Listed below are individual manuscripts, published or in preparation, in relation to or worked on during this dissertation. Chapter 2 in this dissertation is published as article 1 below. The Publishers of the journal granted the author to re-use this published material in this dissertation by copyright policies.

Peer reviewed journal papers published or accepted while working on this dissertation:

1. **Bates, C.**, Escalas, A., Kuang, J., Hale, L., Wang, Y., Herman, D., Nuccio, E., Wan, X., Bhattacharyya, A., Fu, Y., Tian, R., Wang, G., Ning, D., Yang, Y., Wu, L., Pett-Ridge, J., Saha, M., Craven, K., Brodie, E., Firestone, M., and Zhou, J. Conversion of marginal land into switchgrass conditionally accrues soil carbon but reduces methane consumption. **ISME J** (2021). https://doi.org/10.1038/s41396-021-00916-y
2. Tao, X., Feng, J., Yang, Y., Wang, G., Tian, R., Fan, F., Ning, D., **Bates, C.**, Hale, L., Yuan., M., Wu, L., Gao, Q., Lei, J., Schuur, E., Yu, J., Bracho, R., Luo, Y., Konstantinidis, K., Johnston, E., Cole, J., Penton, R., Tiedje, J., and Zhou, J. Winter

warming in Alaska accelerates lignin decomposition contributed by Proteobacteria. **Microbiome** 8, 84 (2020). https://doi.org/10.1186/s40168-020-00838-5

3. Gao, Q., Gao, S., **Bates, C**., Zeng, Y., Lei, J., Su, H., Dong, Q., Qin, Z., Zhao, J., Zhang, Q., Ning, D., Huang, Y., Zhou, J., and Yang, Y. The microbial network property as a bio-indicator of antibiotic transmission in the environment. **Sci. Total Environ** 758 (2020). https://doi.org/10.1016/j.scitotenv.2020.143712
4. Kuang, J., **Bates, C.**, Wan, X., Ning, D., Shu, W., and Zhou, J. High historical variability weakens the effects of current climate differentiation on microbial community dissimilarity and assembly. **Glob Chang Biol** (2021). DOI: 10.1111/gcb.15848. In the press.

Manuscripts under review:

5. Tao, X., Feng, J., Yang, Y., Guo, X., Ning, D., **Bates, C**., Kempher, M., Zang, Y., Zhang, Y., Zhou, X., and Zhou, J. Long-term warming accelerates soil carbon degradation in the temperate grassland by enlarging and restructuring active bacterial communities. Under review.
6. Hale, L., Zhou, X., Guo, X., **Bates, C.**, Curtis, D., Wu, L., Ning, D., Wang, G., and Zhou, J. Warming alters the magnitude of soil microbial biodiversity and ecosystem function relationships. Under review in **PNAS**.
7. Kuang, J., Li, S., Cadotte, M., Chen, Y., Ke, P., **Bates, C.**, Wan, X., Wang, P., Zhou, J., and Shu, W. Root-associated fungal community reflects host spatial co-occurrence patterns in a subtropical forest. In review in **ISME Communications**.

8. Wan, X., Zhen, J., **Bates, C.**, Hao, Y., and Wang, D. Gut microbiome of wild and reserved Yangtze finless porpoise revealed habitat-specificity: clues to conservation management. Under review.
9. Dai, T., Wen, D., Wu, L., **Bates, C.**, Guo, X., Liu, S., Zhou, J., and Yang, Y. Nutrient supply establishes "hunger games" in global marine bacterial communities. Under review in **Nature Communications**.

Manuscripts in preparation:

10. **Bates, C.**, Tao, X., Yu, Z., He, Z., Ning, D., Fan, Y., Wu, L., Hobbie, S., Reich, P., Yang, Y., and Zhou, J. Additive effects of elevated CO_2 and nitrogen deposition suppress nitrogen fixation rates in a diverse grassland. In preparation.
11. **Bates, C.**, Kuang., J., Escalas, A., Hale, L., Wang, Y., Wan, X., Fu, Y., Tian, R., Ning, D., Yang, Y., Wu, L., Pett-Ridge, J., Saha, M., Carven, K., Firestone, M., and Zhou, J. Soil heterogeneity regulates the microbial species-time-area relationship under switchgrass in marginal lands. In preparation.
12. Kuang, J., **Bates, C**., Wang, Y., Nuccio, E., Fu, Y., Tian, R., Wang, G., Ning, D., Yang, Y., Wu, L., Pett-Ridge, J., Malay, S., Craven, K., Brodie, E., Firestone, M., and Zhou, J. Switchgrass alters subsurface microbial communities which influences the deep C priming effect in marginal lands. In preparation.
13. Wang, Y., Navarro, J., Nuccio, E., Baker, N., Ning, D., Simmons, T., Kuang, J., **Bates, C.**, Hale, L., Zhalnina, K., Brodie, E., Scheible, W., Udvardi, M., Pett-Ridge, J., Saha, M., Wu, L., Zhou, J., Firestone, M., and Craven, K. The succession of rhizosphere

microbial community is associated with switchgrass establishment in marginal soils. In preparation.

14. Kuang, J., Ning, D., Yuan, M., Shi, S., Nuccio, E., Shi, J., **Bates, C.**, He, Z., Pett-Ridge, J., Brodie, E., Firestone, M., and Zhou, J. Disentangling filtering and competition in functional trait-based community assembly during succession. In preparation.
15. Gao, Q., Yang, Y., Xue, K., **Bates, C.**, Xi, C., He, Z., Hobbie, S., Reich, P., and Zhou, J. Nitrogen deposition offsets decade-long elevated CO_2 effect on grassland soil microbial communities. In preparation.

APPENDIX A: SUPPLEMENTARY FIGURES

Figure S2.1 to **Figure S2.4** for **Chapter 2**:

S2.1 Dispersion by PCoA and ANOSIM results for free-living diazotrophic microbial community by *nifH* sequencing

S2.2 Alpha diversity indexes for the BioCON site

S2.3 Dispersion by PCoA and ANOSIM results for the 16S bacterial communities

S2.4 Dispersion by PCoA and ANOSIM of the fungal community

Figure S3.1 to **Figure S3.** for **Chapter 3**:

S3.1 Layout for the field sites, collar positions, and soil sampling details

S3.2 Root biomass estimates methods

S3.3 Correlation plot between environmental, microbial, and soil geochemistry variables

S3.4 Dissimilarity between soil chemistry samples through the seasons at each site between SG and FL plots

S3.5 Changes in soil chemistry through the seasons at each site between SG and FL plots

S3.6 Change in microbial alpha diversity measures through the seasons at each site between SG and FL plots

Figure S4.1 to **Figure S4.** for **Chapter 4**:

S4.1 Difference is soil chemistry and heterogeneity between plots

S4.2 Seasonal dynamics of z values with increasing area at each time point

S4.3 Heterogeneity of phosphorus turnover within the largest area in each plot

Figure S5.1 to **Figure S5.14** for **Chapter 5**:

S5.1 Daily respired CO_2-C between controls and ^{13}C-labled plant residue soil incubations by site, root system treatment, depth, and day

S5.2 Effects of added ^{13}C-labeled plant residue on the priming effect between the deep and shallow rooted systems

S5.3 Ratio of primed to substrate-induced respired CO_2-C between PDF and RR sites for deep rooted SG soil at different soil depths

S5.4 Phospholipid fatty acid methyl esters (FAMEs) for microbial biomass estimation and identification

S5.5 Mean activity and carbon substrate usage in the original soils with BioLog Ecoplates

S5.6 Carbon substrate usage after soil incubations with BioLog Ecoplates

S5.7 Carbon substrate richness after soil incubations with BioLog Ecoplates

S5.8 Bacterial species richness for observed number of OTUs by depth and root type

S5.9 Phylogenetic diversity by depth and root type

S5.10 Major bacterial phyla at the PDF site

S5.11 Major bacterial phyla at the RR site

S5.12 Non-metric multidimensional scaling of the bacterial community

S5.13 Lab and field-based model calibration of Rh

S5.14 Effects of added ^{13}C-labeled plant material on Rs

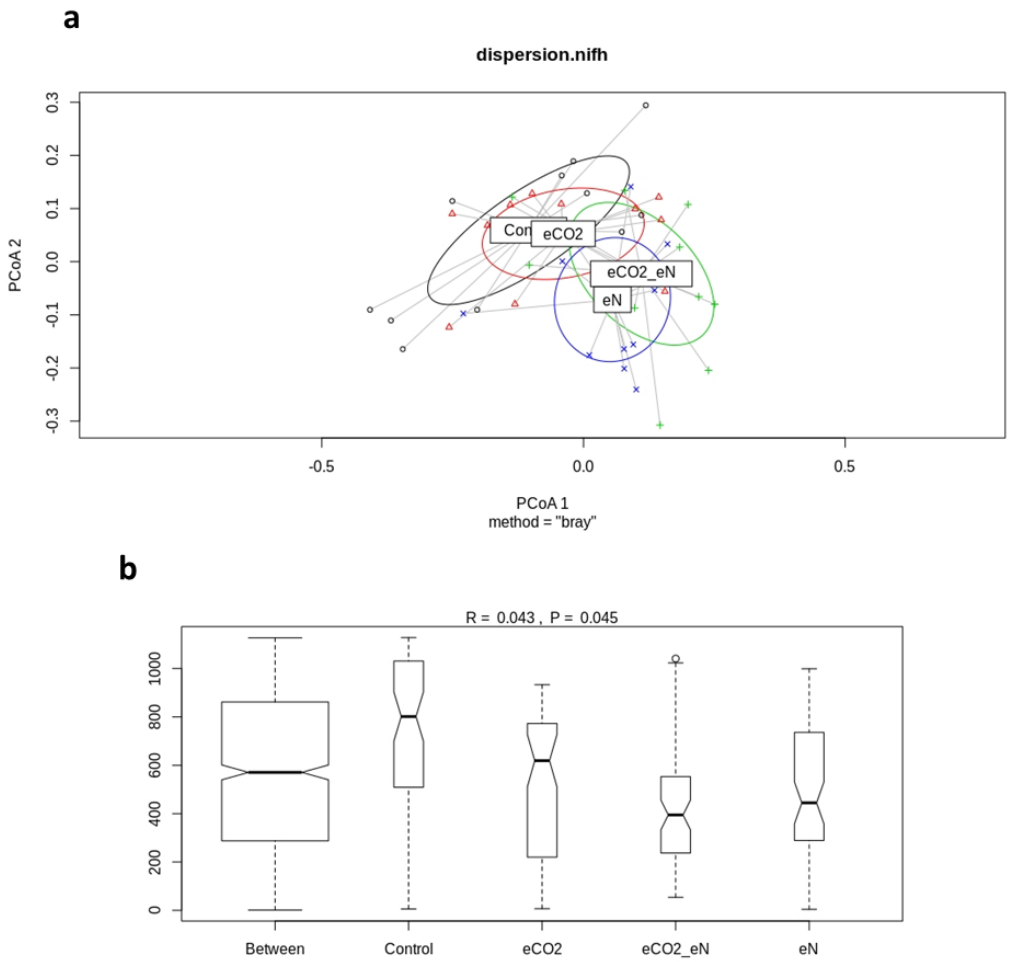

Supplementary Figure 2.1 Dispersion by PCoA and ANOSIM results for free-living diazotrophic microbial community by *nifH* sequencing of: a, *nifH* gene dispersion and **b**, ANOSIM results of the *nifH* community. No significant difference found between the groups for *nifH* gene abundance.

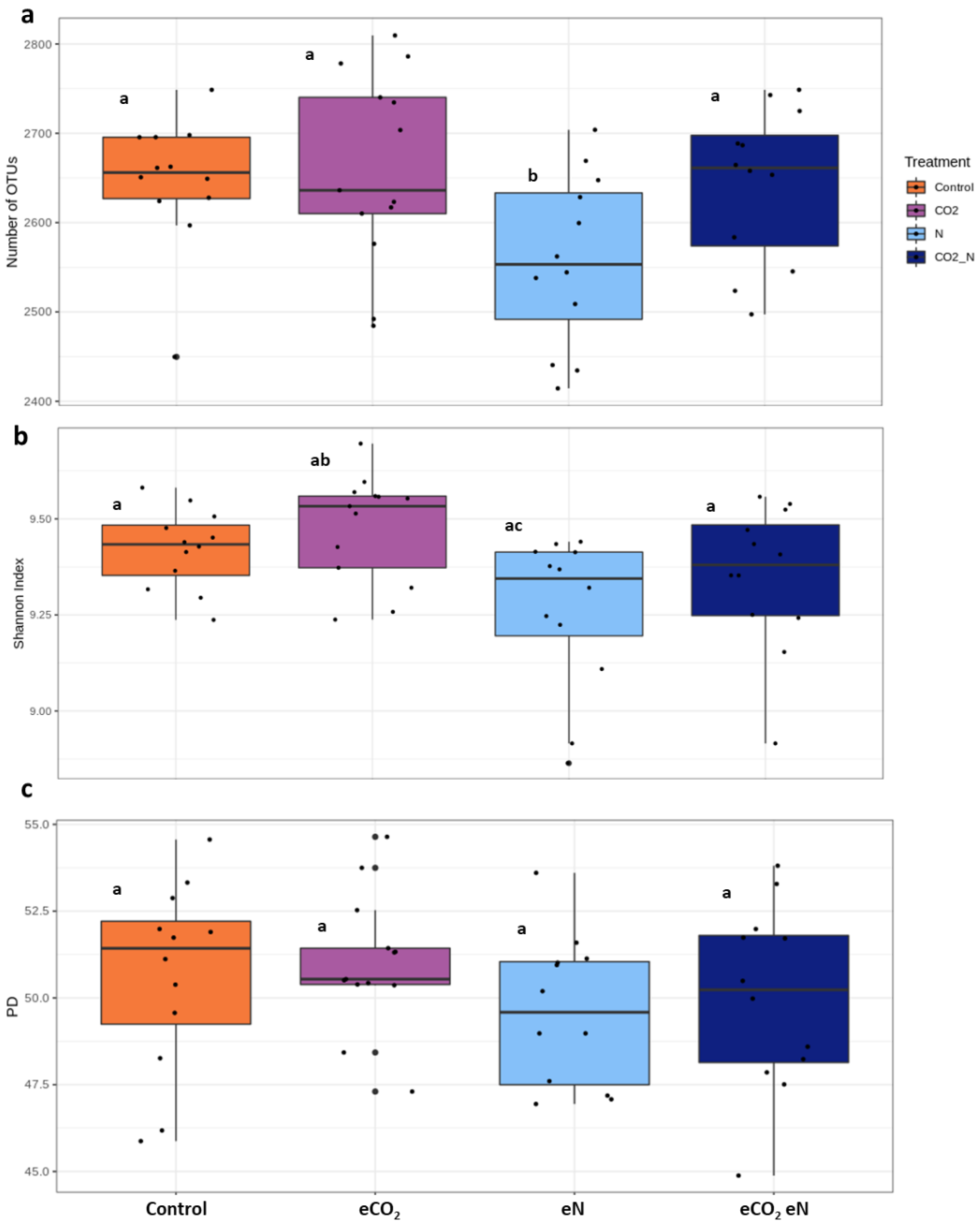

Supplementary Figure 2.2 Alpha diversity indexes for the BioCON site for: a, number of OTUs; **b**, Shannon diversity index; and **c**, phylogenetic diversity between treatments.

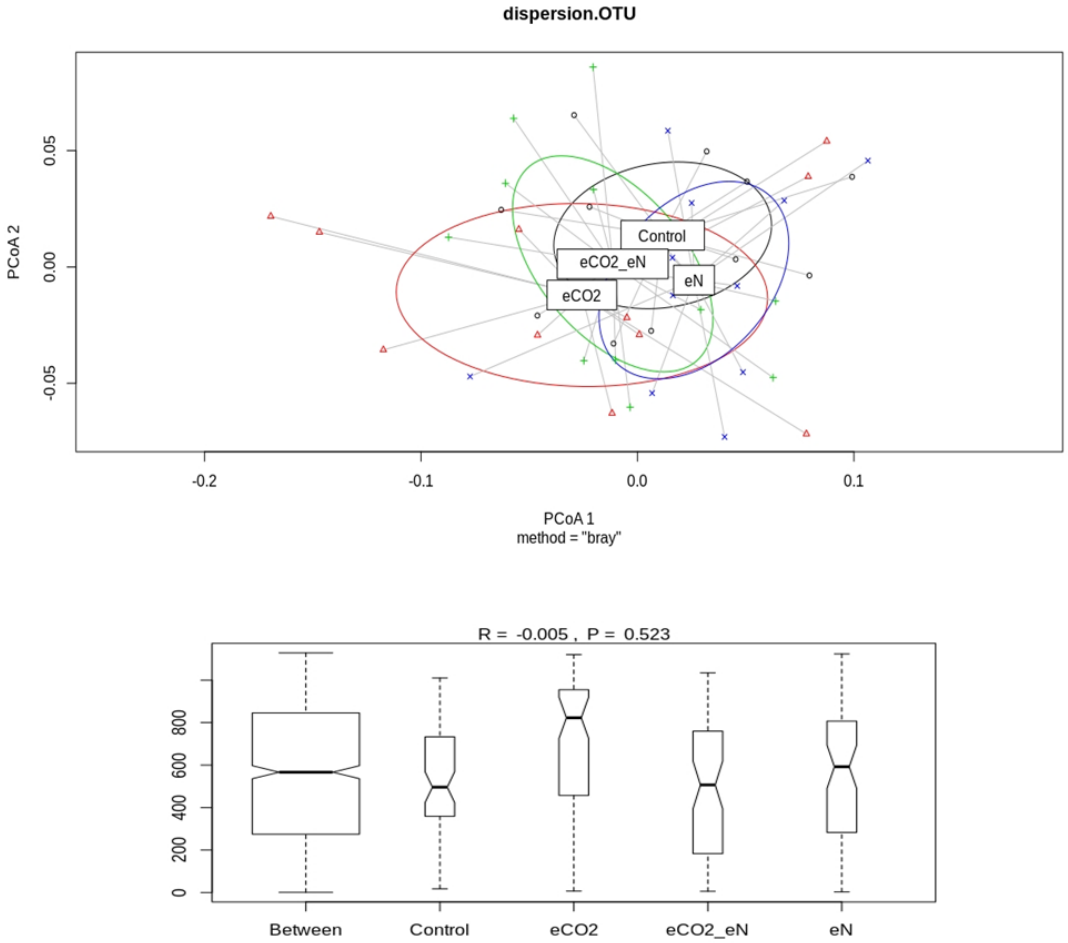

Supplementary Figure 2.3 Dispersion by PCoA and ANOSIM results for: a, the 16S microbial community by treatment and **b**, nonsignificant ANOSIM result.

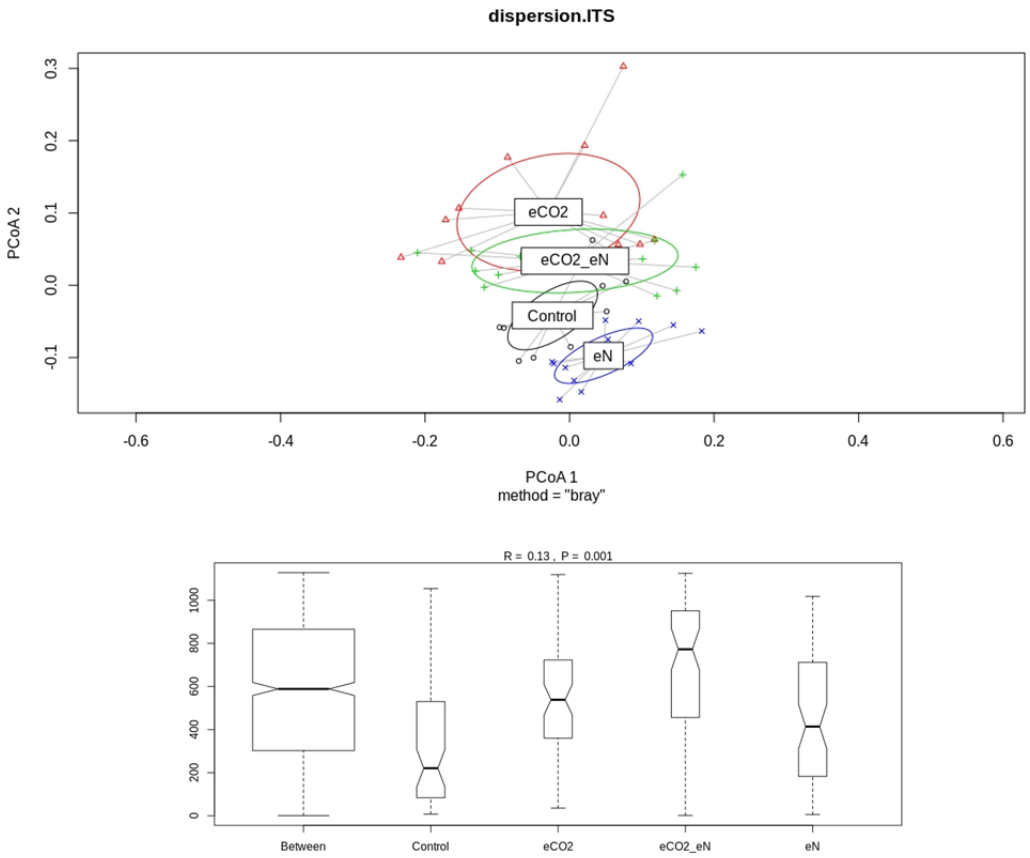

Supplementary Figure 2.4 Dispersion of the ITS fungal community for: a, the PCoA of the community structure and **b**, ANOSIM which resulted in a Signiant ($p < 0.01$) difference in the treatment groups.

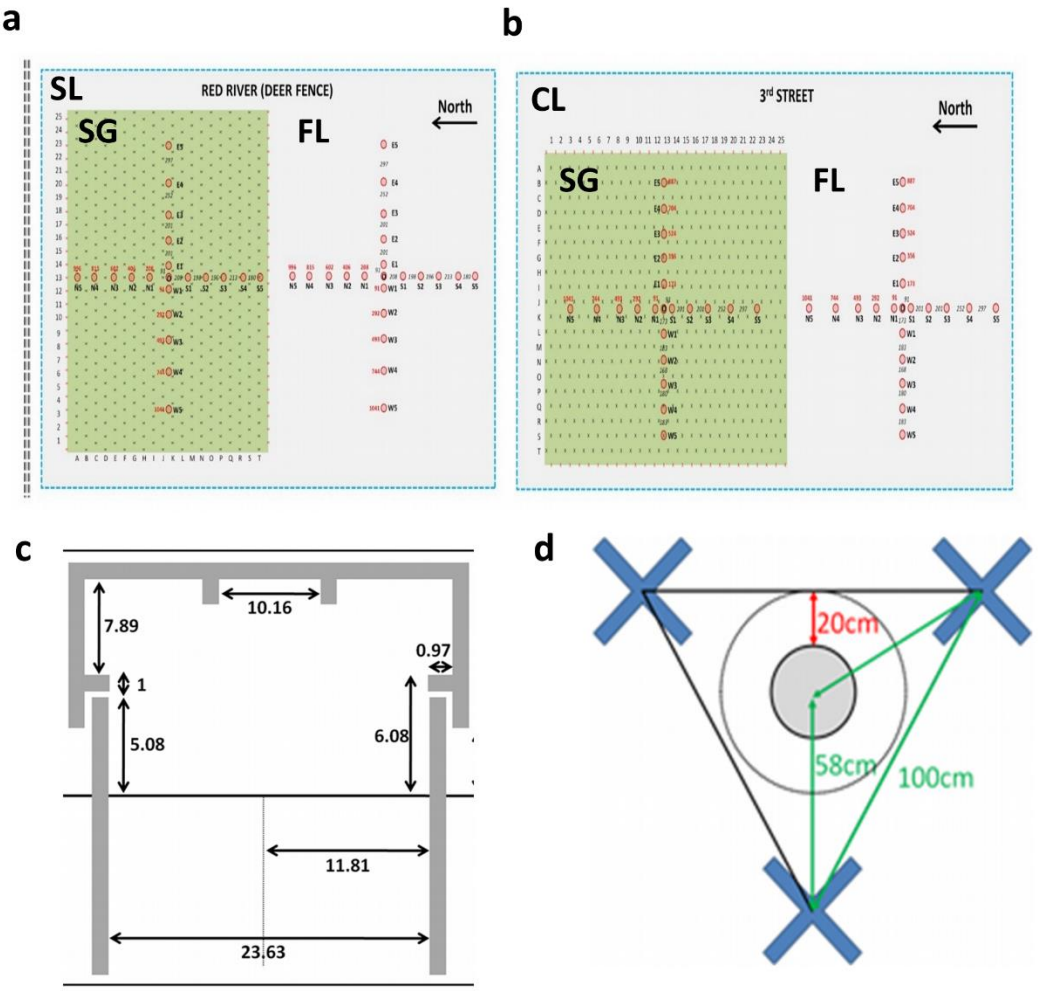

Figure S3.1, Layout for the field sites, collar positions, and soil sampling details: a, layout of the SL field site and location of trace gas collars for each plot; **b**, layout of the CL field site and location of the trace gas collars for each plot; **c**, diagram of trace gas collar and chamber dimensions; **d**, diagram of collar position in relation to switchgrass plants and soil sampling details. Blue X's represent switchgrass plants and the gray circle represents the trace gas collar.

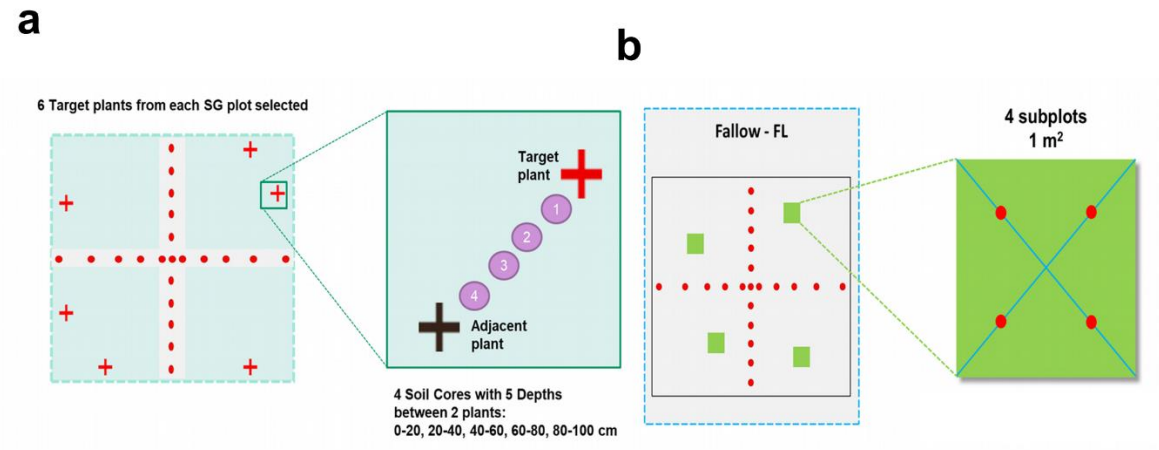

Figure S3.2, Root biomass estimates methods for: a, graphic for how switchgrass plants were selected for root biomass estimation; **b**, graphic for how fallow root biomass estimation was conducted using four 1 m^2 subplots in each quadrant of the plot.

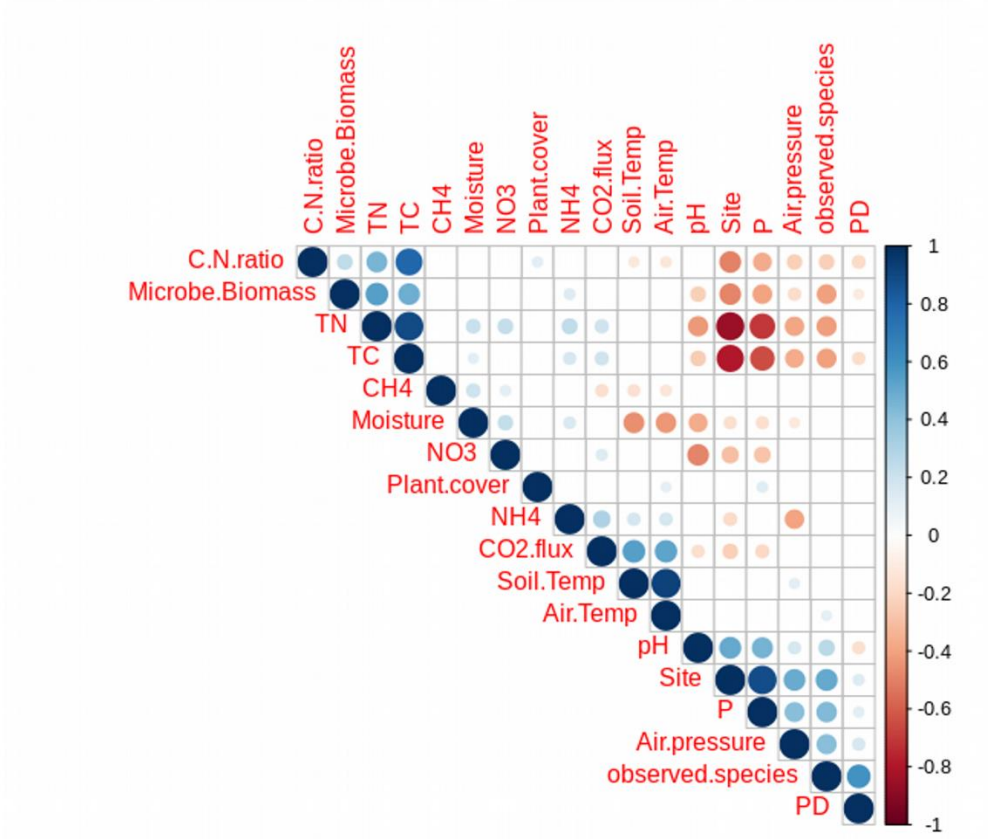

Figure S3.3, Correlation plot between environmental, microbial, and soil geochemistry variables. Blue circles indicate significant positive correlations while red circles indicate negative correlations. Larger darker circles indicate a more significant and stronger correlation between variables. Positive correlations for site represent SL site while negative correspond to the CL site. 'Microbe.Biomass' was estimated using DNA concentrations after soil extractions. 'observed.species' is the total species richness (alpha diversity) of the samples. 'PD' represents the whole tree phylogenetic diversity of the plots. Positive correlations for 'Plant.cover' represent switchgrass plots and negative for fallow plots.

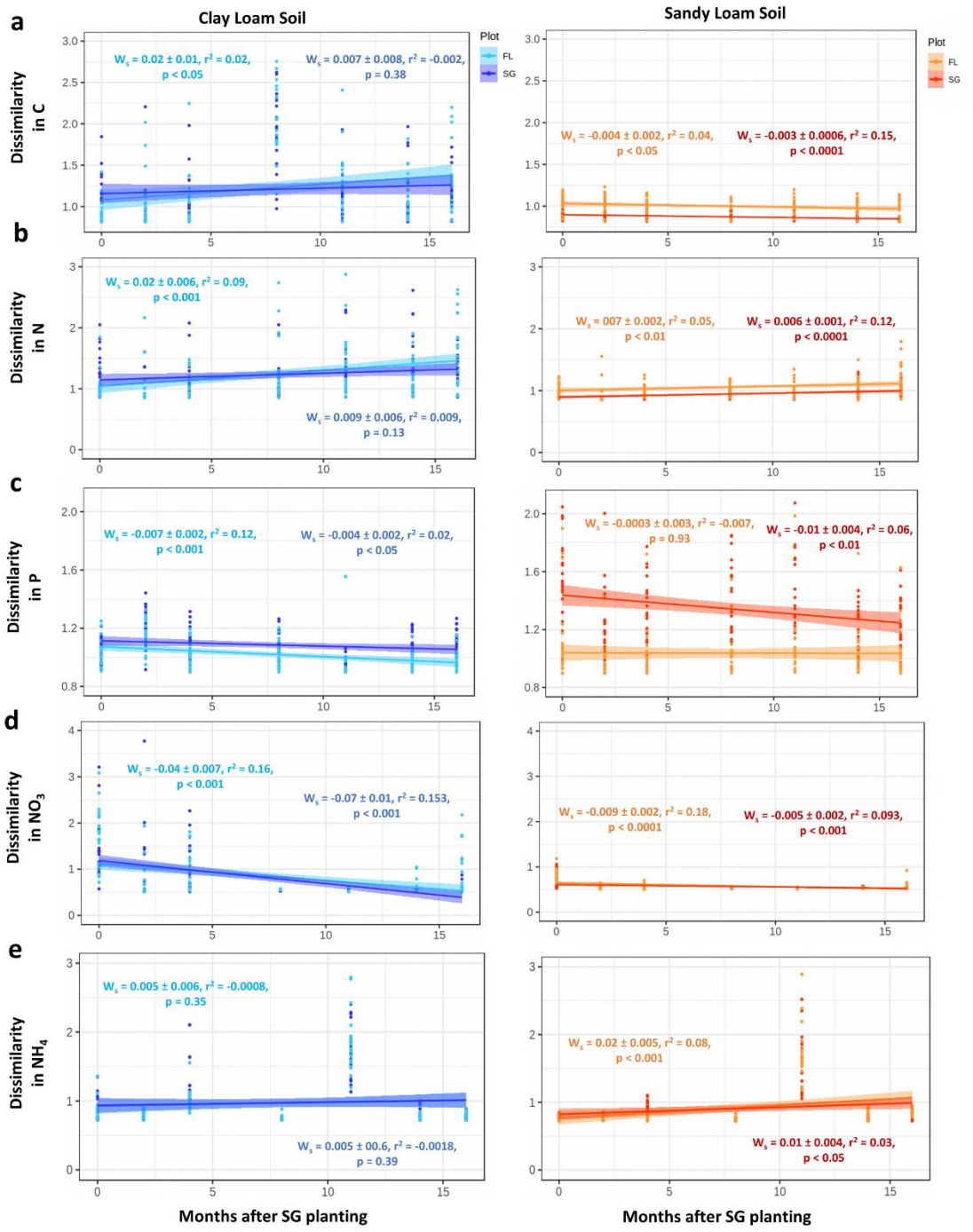

Figure S3.4, Dissimilarity between soil chemistry samples through the seasons at each site between SG and FL plots for: a, dissimilarity in soil carbon samples; **b**, dissimilarity in soil nitrogen content; **c**, dissimilarity in plant available phosphate content; **d**, dissimilarity in nitrate content; **e**, dissimilarity in ammonium. Ws is the slope of each line and the error associated with each slope while p-values represent the significance of each trend line. Each time point is comprised of twenty-one replicates per plot.

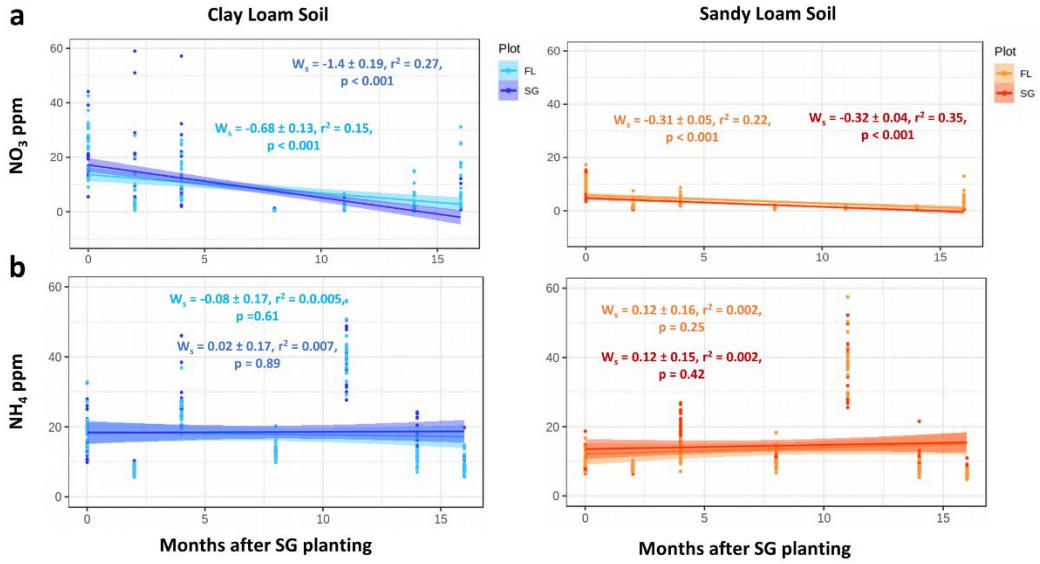

Figure S3.5, Changes in soil chemistry through the seasons at each site between SG and FL plots for: a, concentration of nitrate content; **b**, ammonium content. Ws is the slope of each line and the error associated with each slope while p-values represent the significance of each trend line. Each time point is comprised of twenty-one replicates per plot.

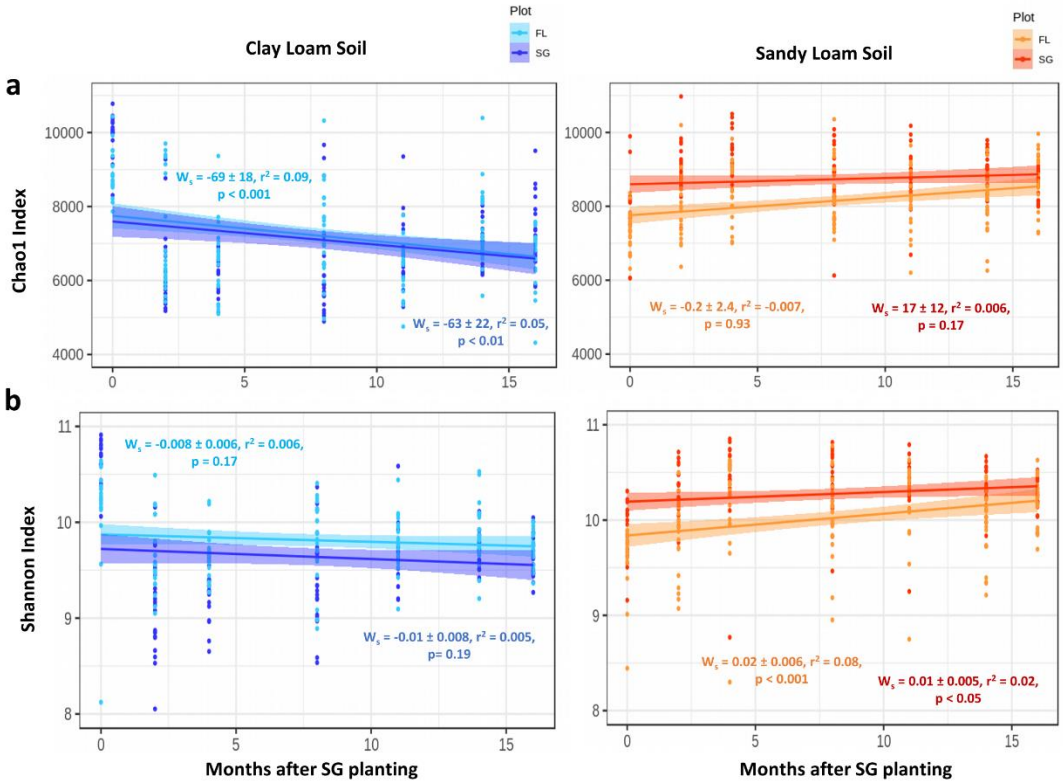

Figure S3.6, Change in microbial alpha diversity measures through the seasons at each site between SG and FL plots for: a, chao1 index; **b,** Shannon index. Ws is the slope of each line and the error associated with each slope while p-values represent the significance of each trend line. Each time point is comprised of twenty-one replicates per plot.

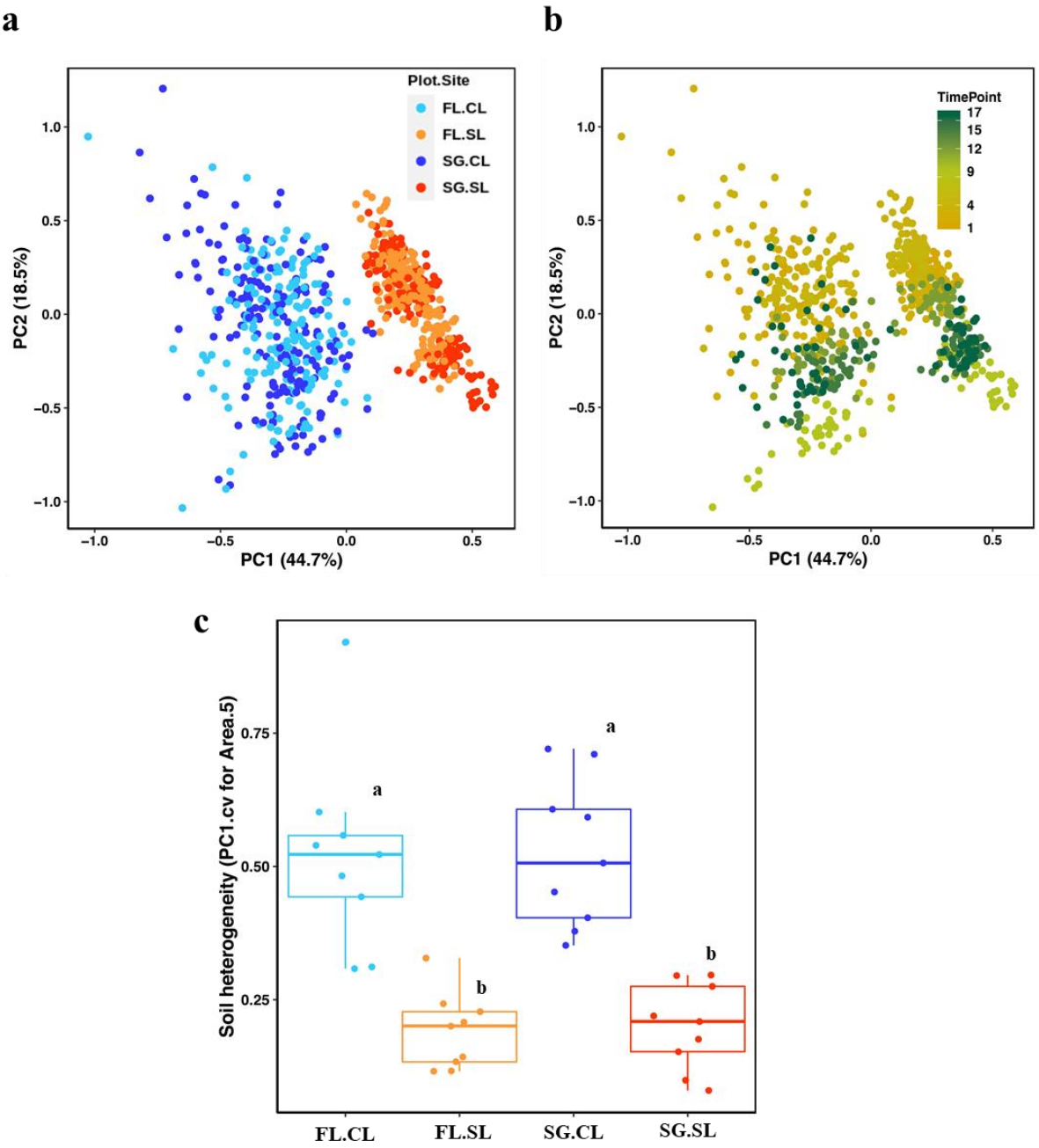

Figure S4.1, Difference is soil chemistry and heterogeneity between plots for: a, a principal component analysis (PCA) for soil chemical variables with the variation explained displayed on the axis; **b**, the PCA displayed by the samples by time point ; **c**, the soil heterogeneity for the turnover of PC1 using the largest area of all plots. Significance established by pairwise Wilcoxon test with $p < 0.05$.

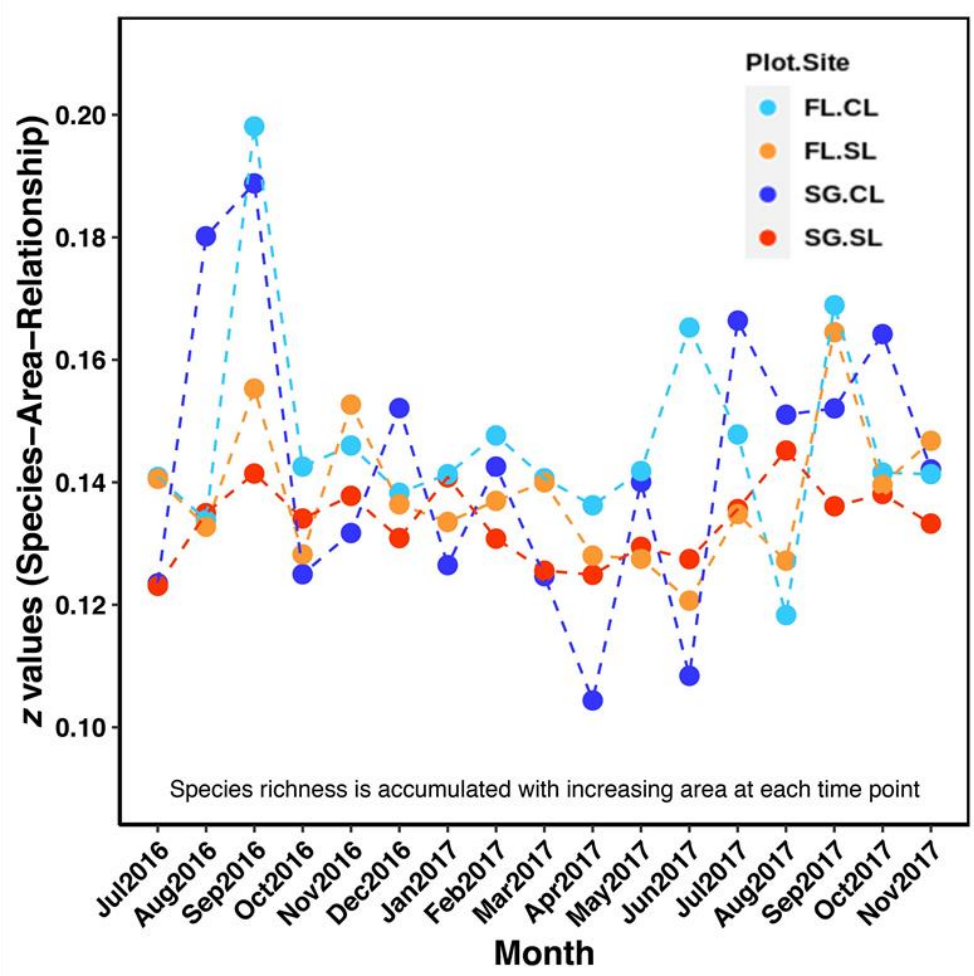

Figure S4.2, Seasonal dynamics of z values with increasing area at each time point. Species richness is accumulated with each point for each plot.

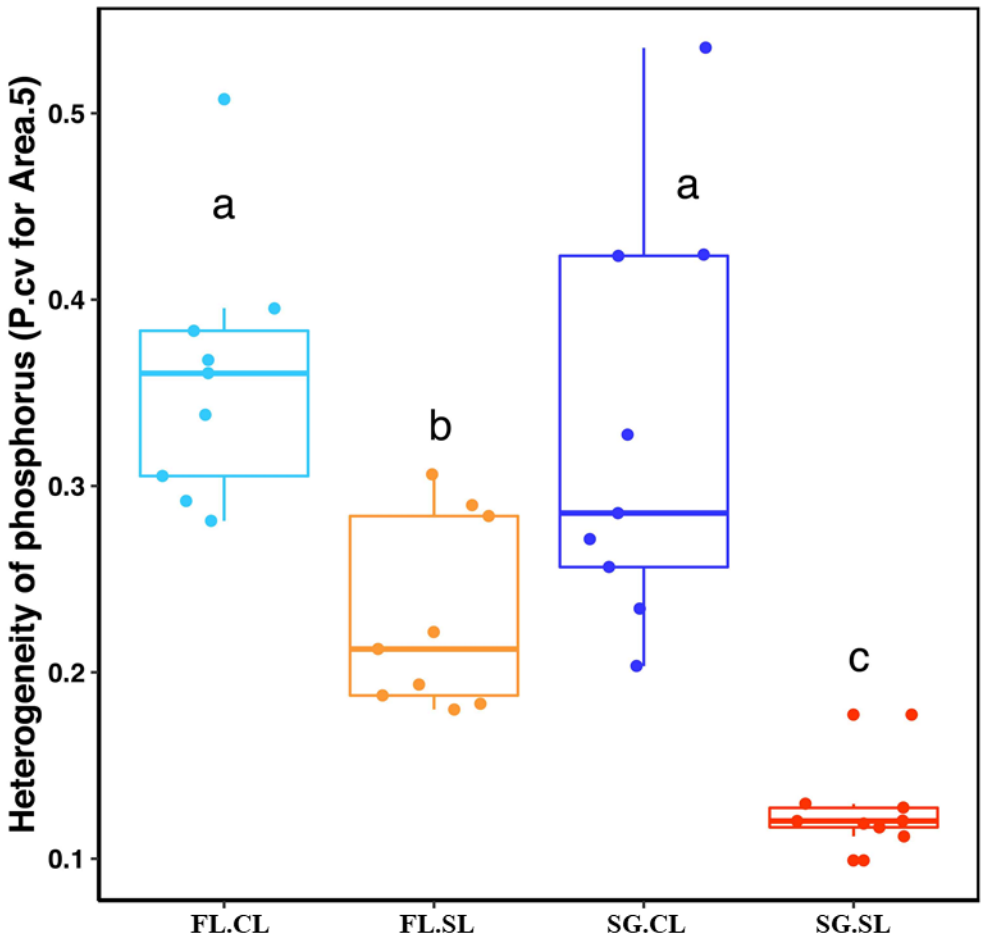

Figure S4.3, Heterogeneity of phosphorus turnover within the largest area in each plot. Significance established by pairwise Wilcoxon test with p values < 0.05.

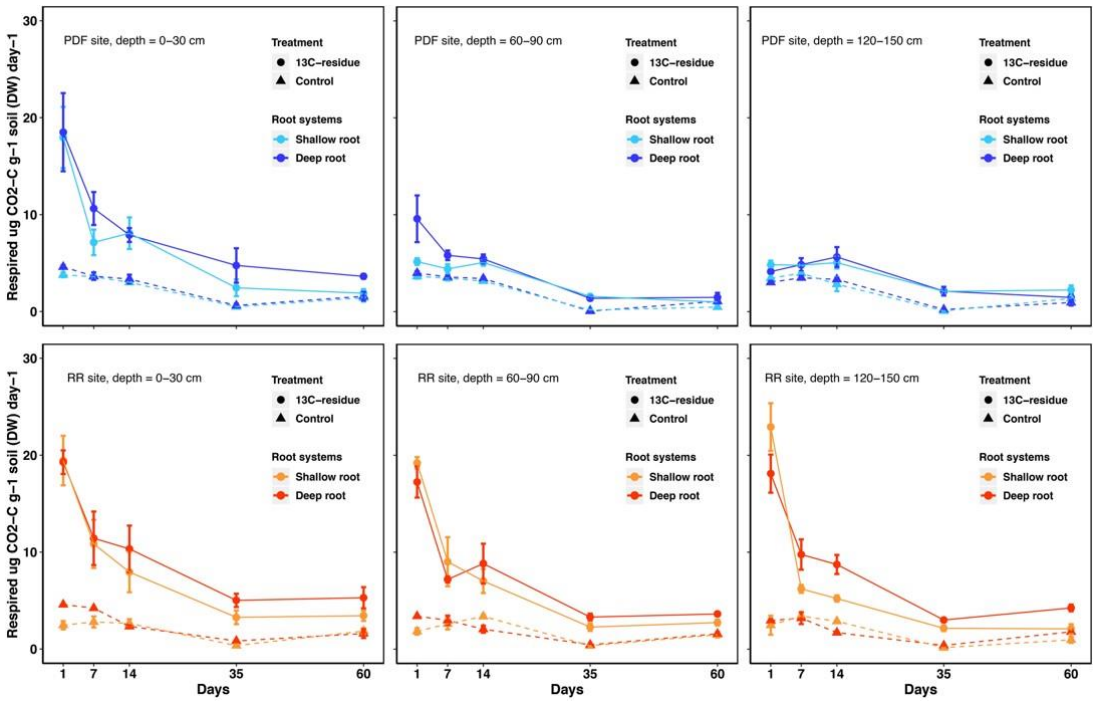

Figure S5.1, Daily respired CO_2-C between controls and ^{13}C-labeled plant residue soil incubations by site, root system treatment, depth, and day. Values are given as mean ± standard error of the mean (n=3).

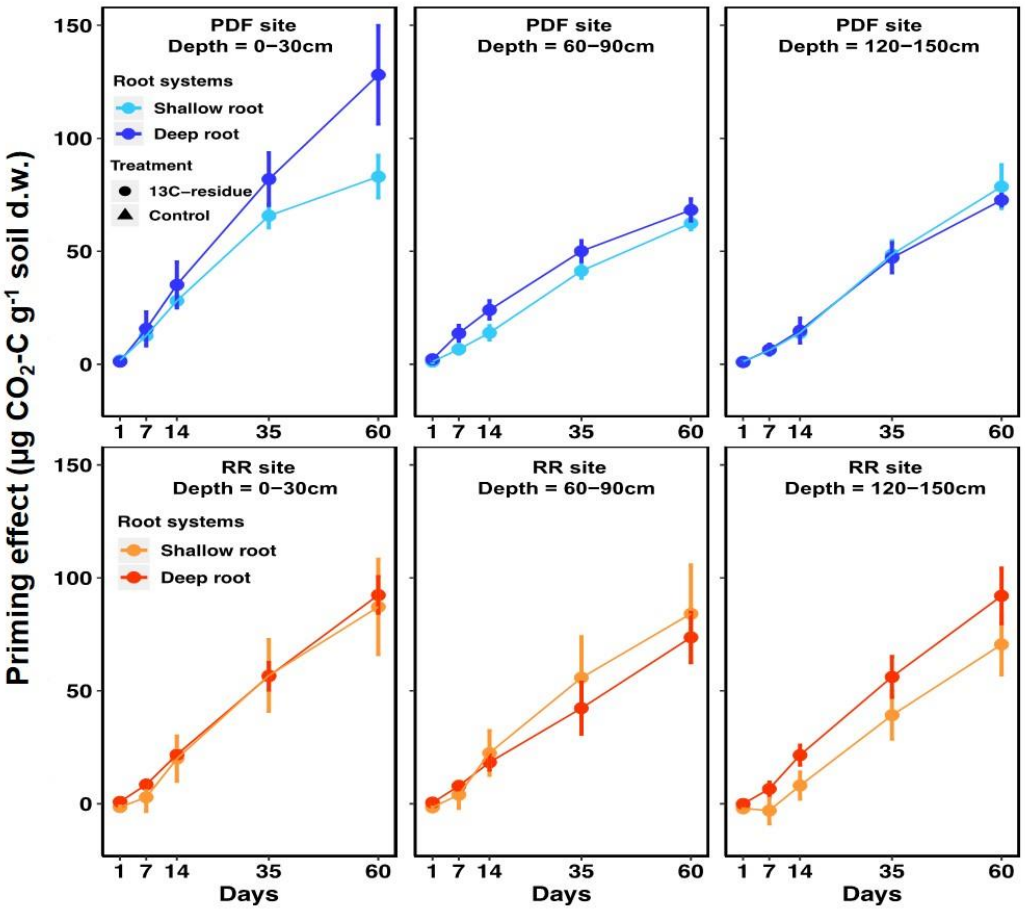

Figure S5.2, Effects of added ^{13}C-labeled plant residue on the priming effect between the deep and shallow rooted systems for: a, the PDF site from 0-30cm soil depth; b, the PDF site from 60-90cm; **c**, the PDF site from 120-150cm**; d,** the RR site from 0-30cm; e, the RR site from 60-30cm; f, the RR site from 120-150cm. Values given as mean ± standard error of the mean (n = 3).

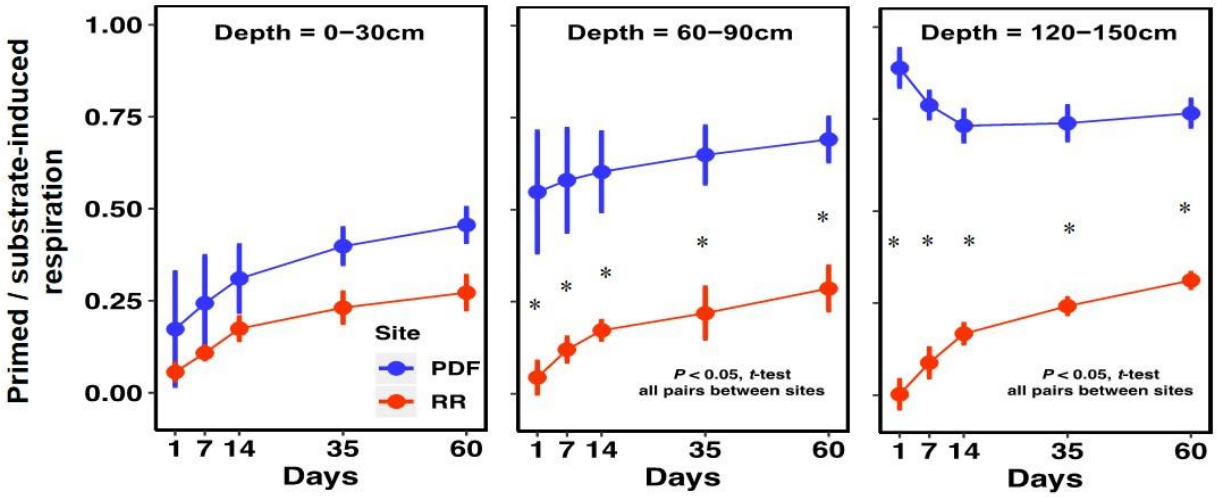

Figure S5.3, Ratio of primed to substrate-induced respired CO_2-C between PDF and RR sites for deep rooted SG soil at different soil depths. Values are given as mean ± standard error of the mean (n=3).

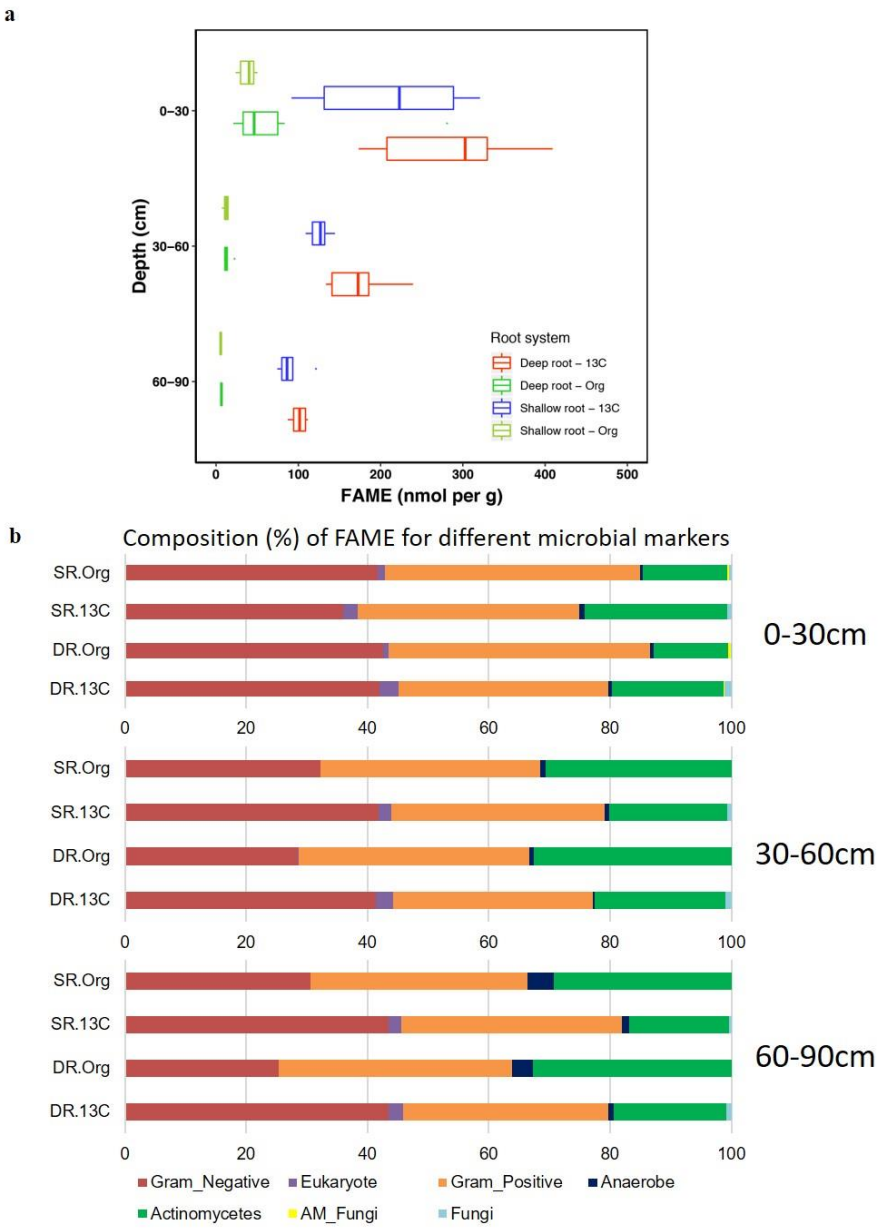

Figure S5.4, Phospholipid fatty acid methyl esters (FAMEs) for microbial biomass estimation and identification for: a, comparison of total microbial biomass between original soils and after ^{13}C priming soil incubations; **b**, compositional breakdown of FAMEs associated with different microbial markers in each sample for the first three depths.

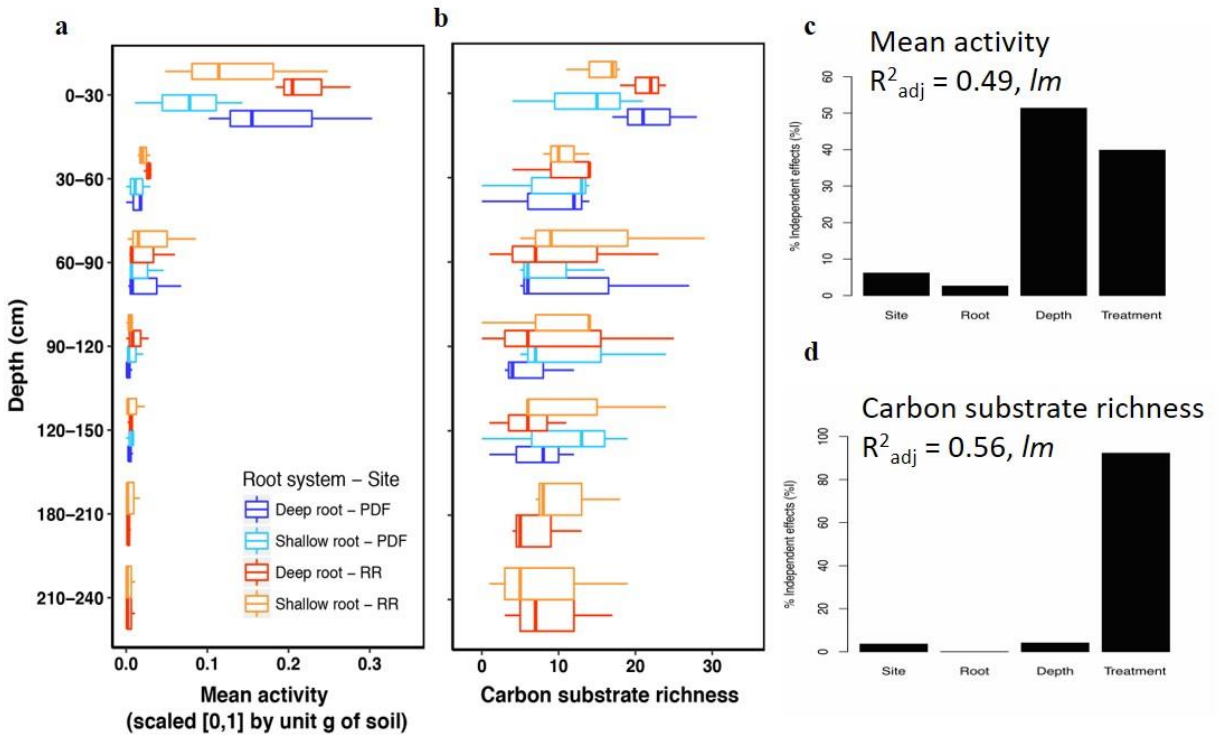

Figure S5.5, Mean activity and carbon substrate usage in the original soils with BioLog Ecoplates for: **a**, mean activity scaled for each treatment by soil depth; **b**, carbon substrate richness by depth, treatment, and site; **c**, hierarchical partitioning using multiple regressions to identify the most likely causal factors determining differences in mean activity levels, and **d**, hierarchical partitioning for most likely casual factors determining differences in carbon substrate richness.

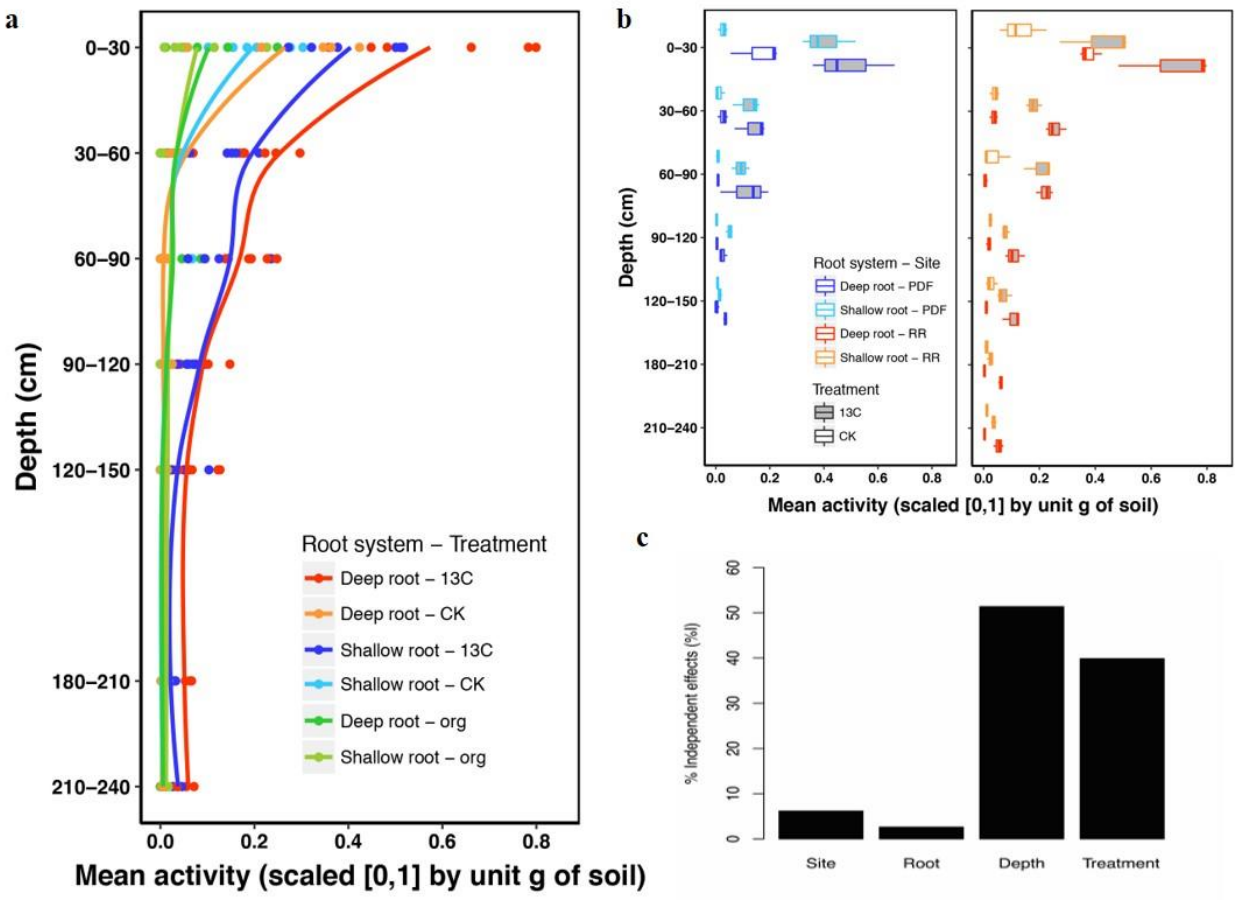

Figure S5.6, Carbon substrate usage after soil incubations with BioLog Ecoplates for: **a**, mean activity scaled for each treatment by soil depth; **b**, comparison of mean activity of carbon substrates between soil types after soil priming incubation; **c**, hierarchical partitioning using multiple regressions to identify the most likely causal factors determining differences in mean activity levels.

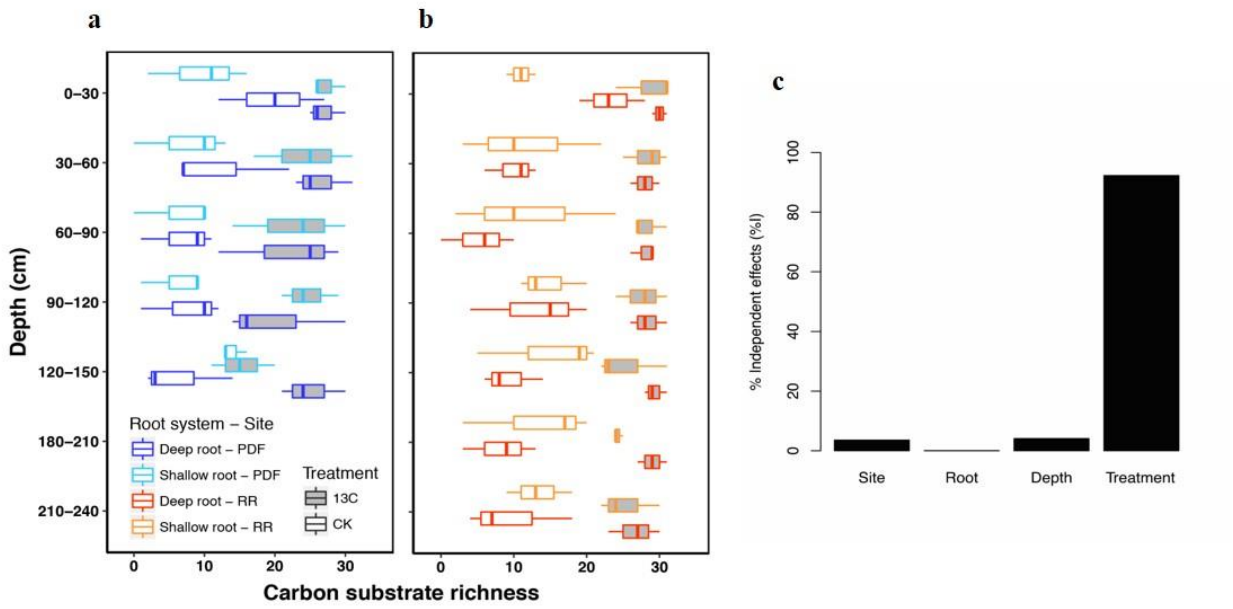

Figure S5.7, Carbon substrate richness after soil incubations with BioLog Ecoplates for: a, at the PDF site between control and ^{13}C groups; **b**, at the RR site between control and ^{13}C groups; **c**, hierarchical partitioning using multiple regressions to identify the most likely causal factors determining differences for carbon substrate richness.

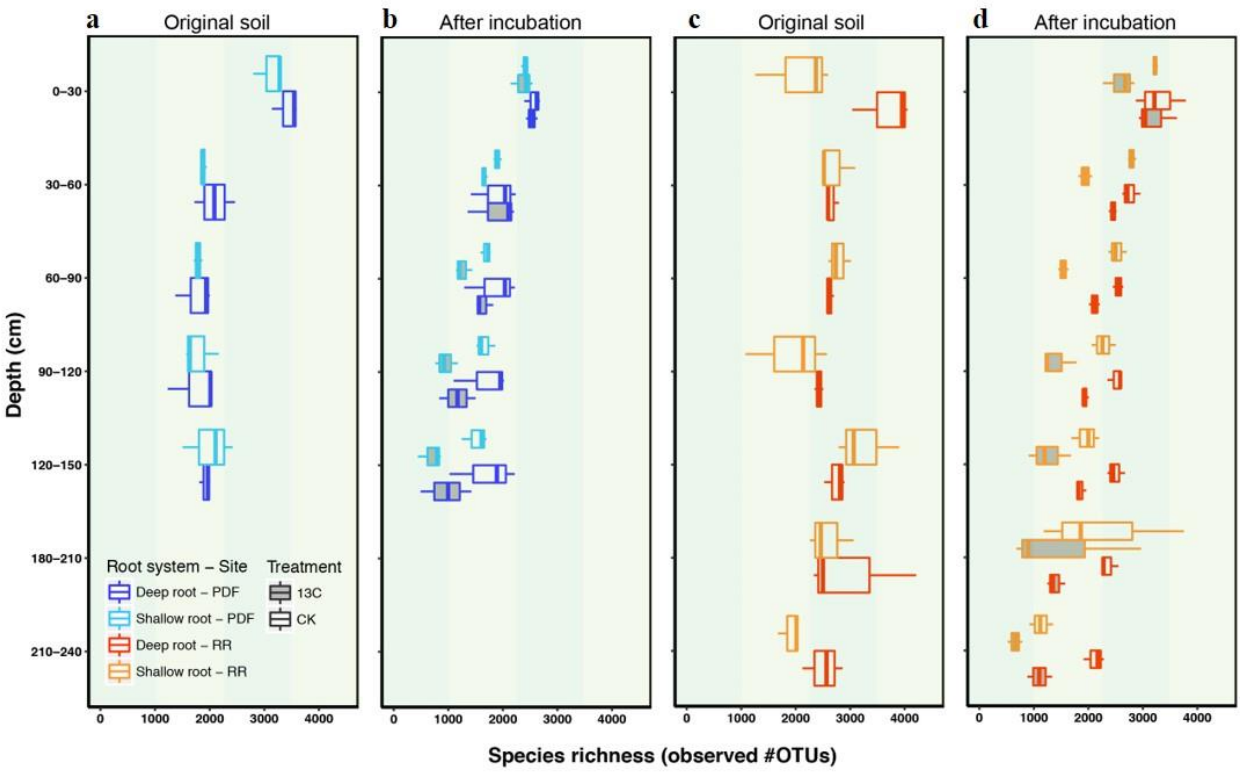

Figure S5.8, Bacterial species richness for observed number of OTUs by depth and root type for: a, the PDF site for the original soils; **b**, the PDF site after ^{13}C-labeled material was added; **c**, the RR site for the original soils; **d**, the RR site after ^{13}C-labeled material was added.

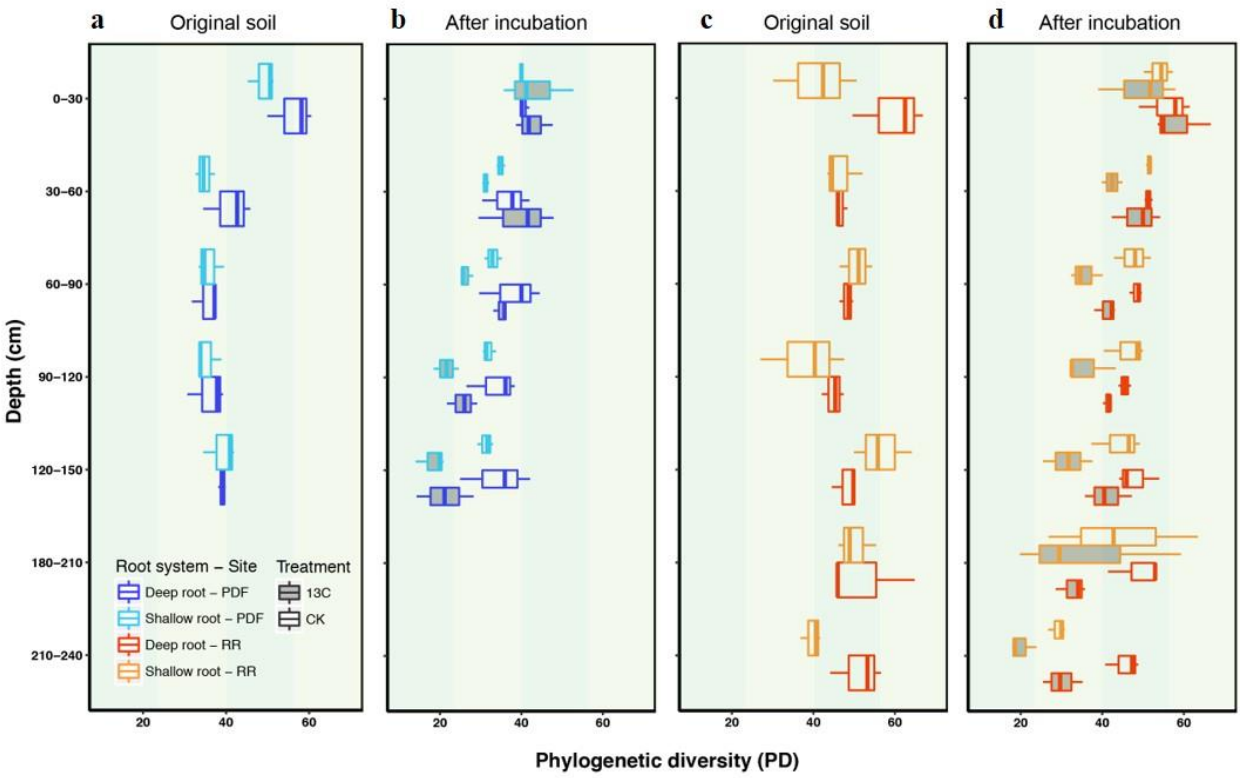

Figure S5.9, Phylogenetic diversity by depth and root type for: a, the PDF site for the original soils; **b**, the PDF site after ^{13}C-labeled material was added; **c**, the RR site for the original soils; **d**, the RR site after ^{13}C-labeled material was added.

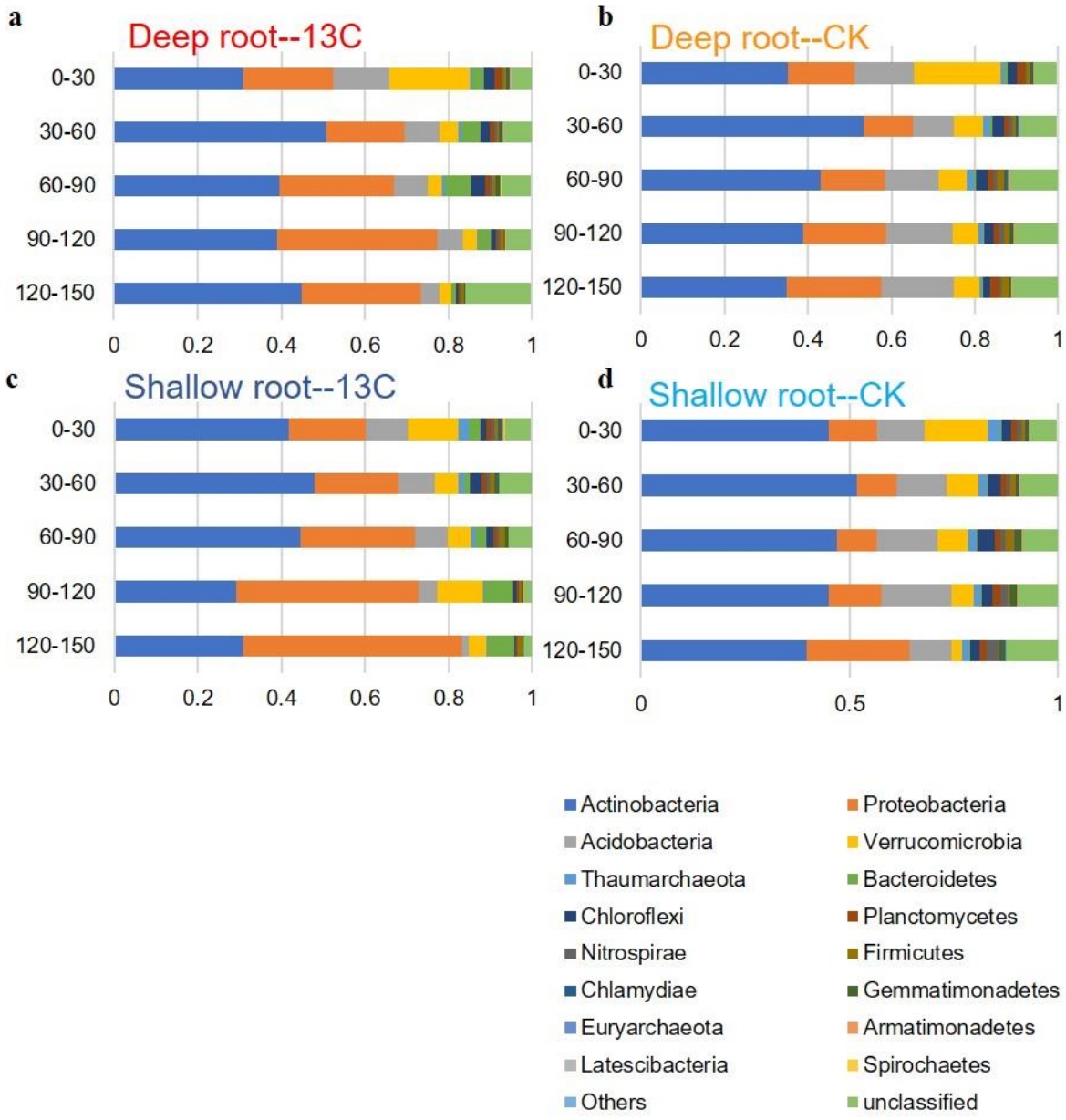

Figure S5.10, Major bacterial phyla at the PDF site for: a, the deep-rooted ^{13}C-labeled plant material added group; **b**, the deep-rooted control group; **c**, the shallow-rooted ^{13}C-labled plant material added group; **d**, the shallow-rooted control group.

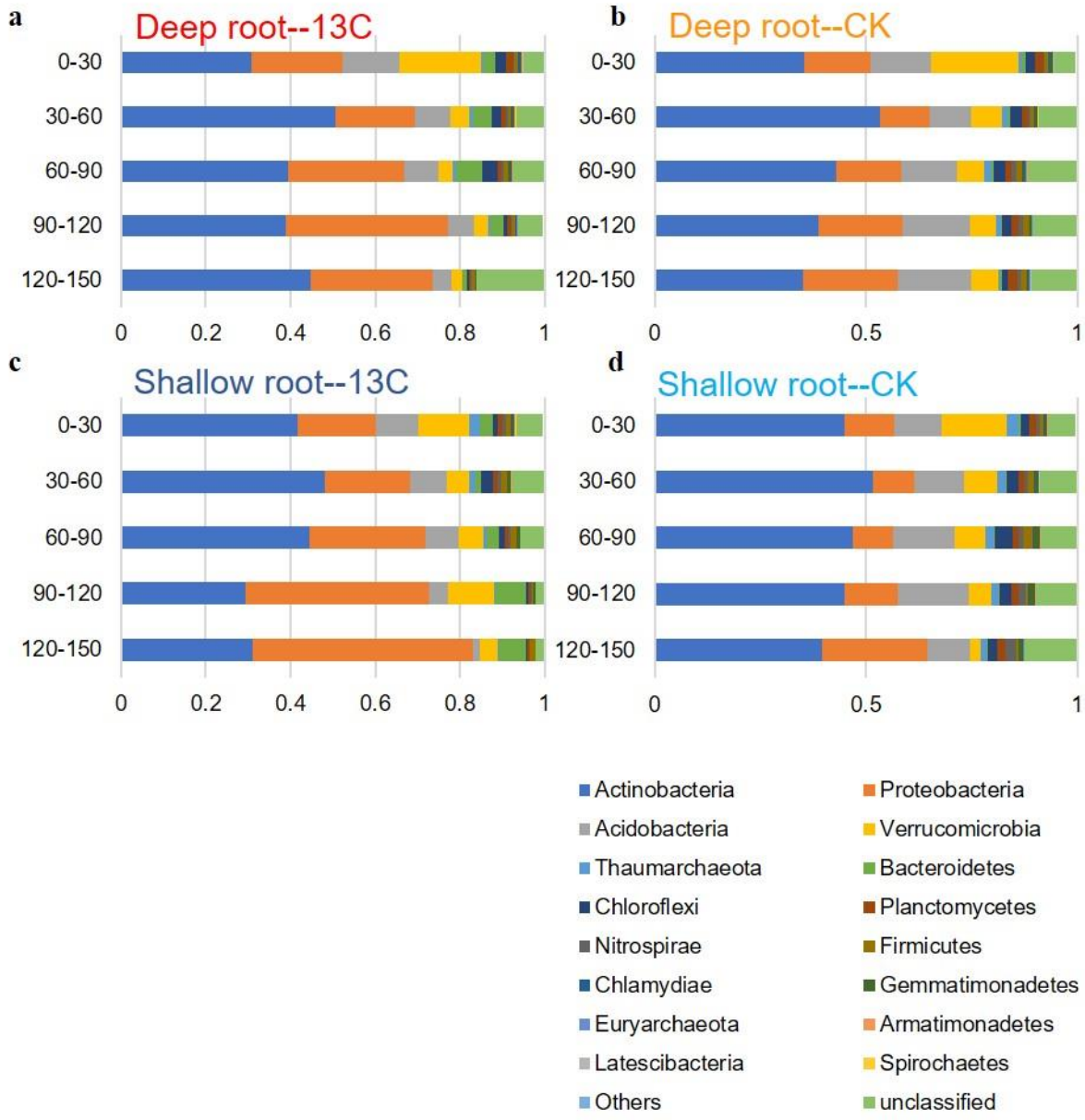

Figure S5.11, Major bacterial phyla at the RR site for: a, the deep-rooted ^{13}C-labeled plant material added group; **b**, the deep-rooted control group; **c**, the shallow-rooted ^{13}C-labled plant material added group; **d**, the shallow-rooted control group.

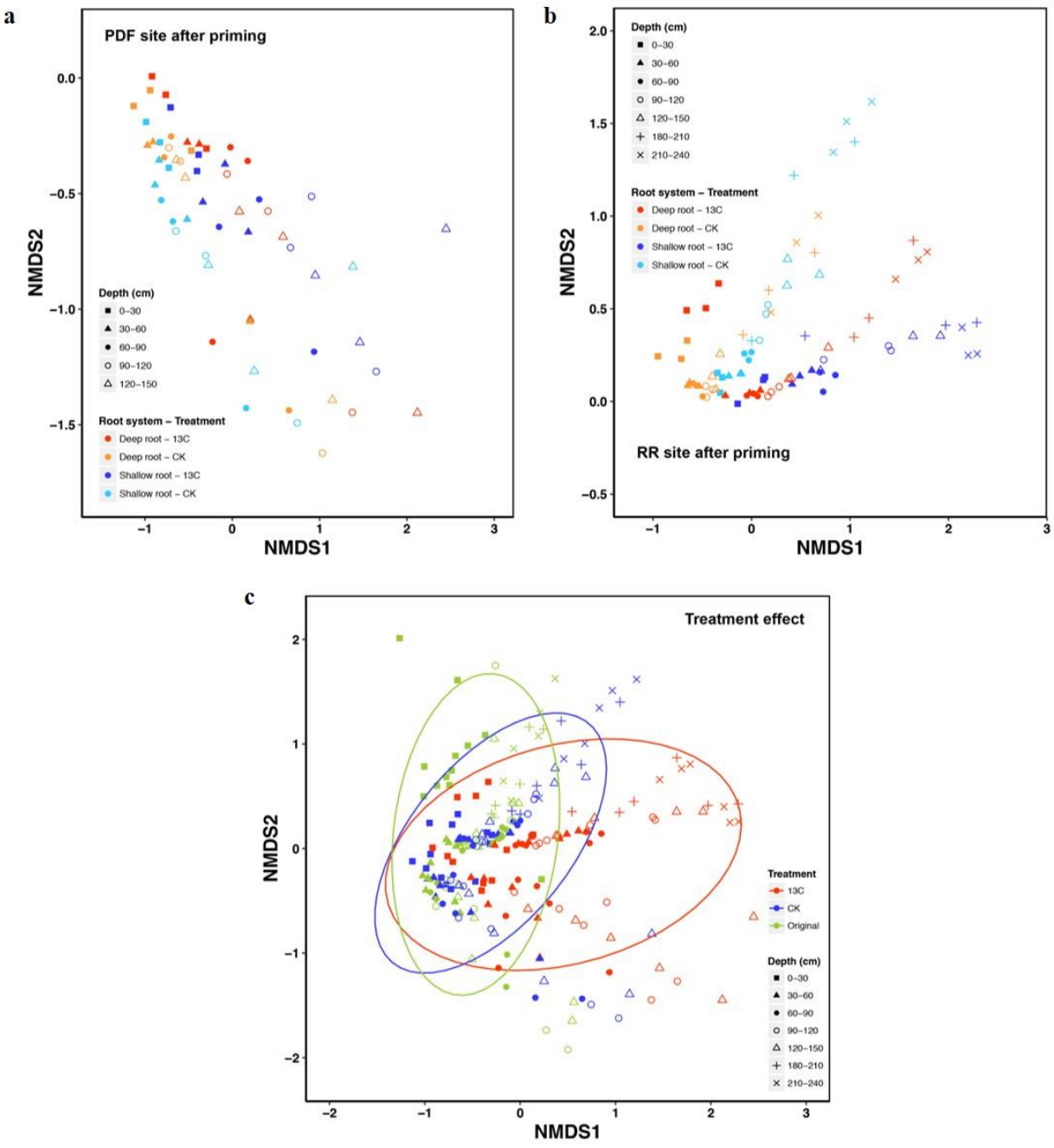

Figure S5.12, Non-metric multidimensional scaling of the bacterial community for: a, the PDF site samples after the soil priming incubation by soil depth; **b**, the RR site samples after the soil priming incubation by soil depth; **c**, the treatment effect between the original soils, control and ^{13}C priming soil incubations.

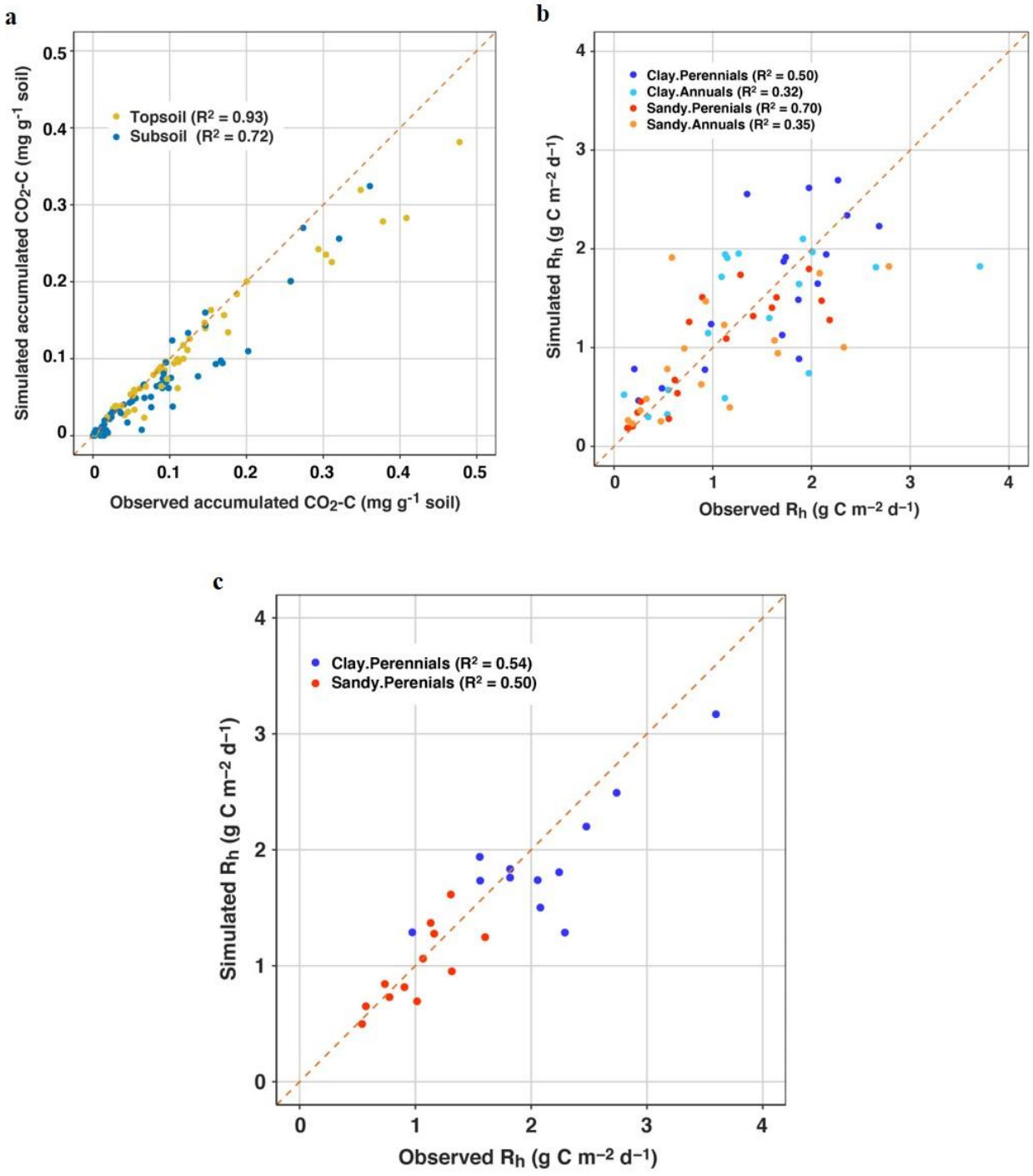

Figure S5.13, Lab and field-based model calibration of Rh for: a, lab-based model performance between simulated accumulated C-CO_2 and observed accumulated C-CO_2; **b**, field-based model performance for simulated Rh and observed Rh; **c**, total field model validation of Rh with switchgrass plots only.

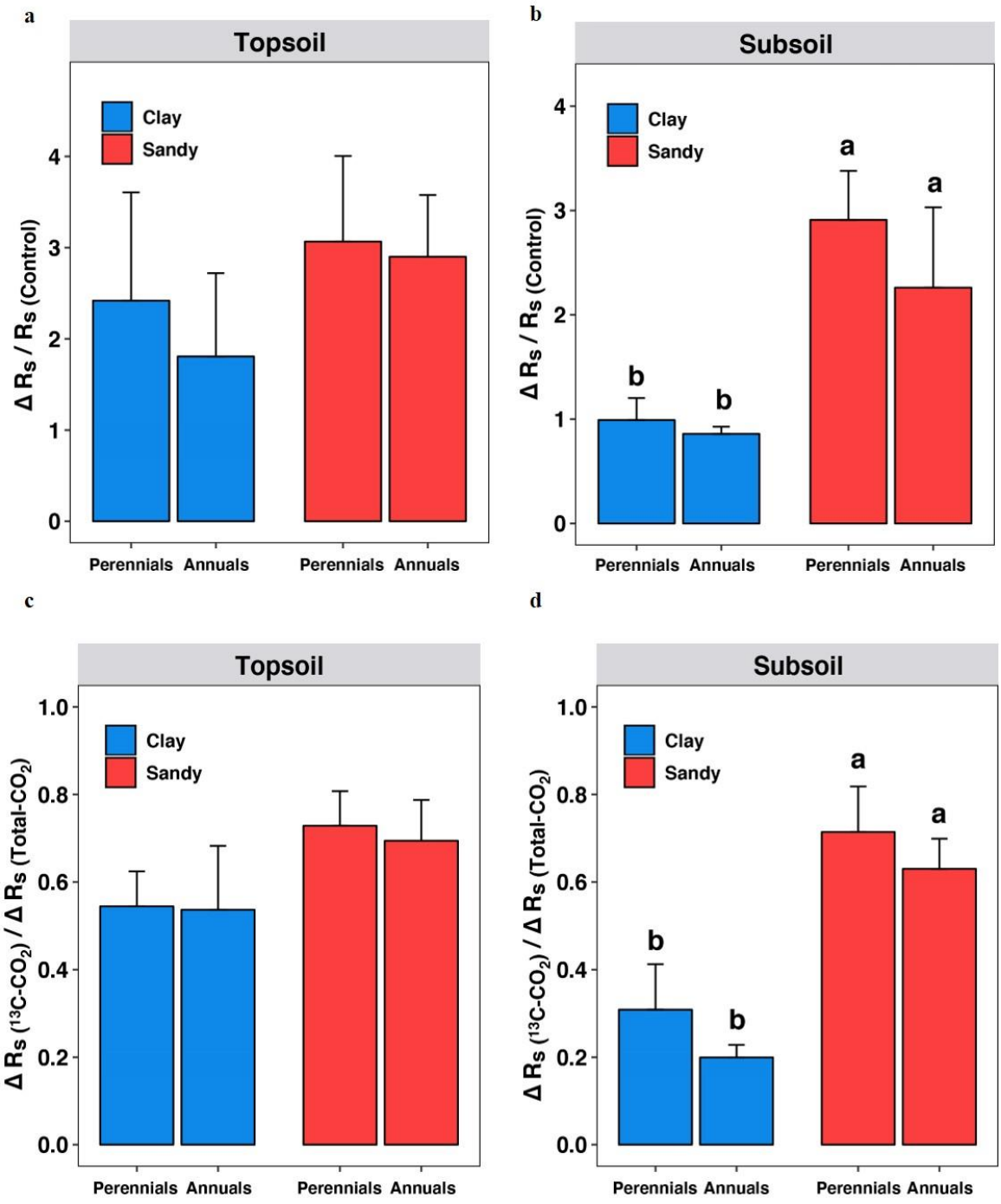

Figure S5.14, Effects of added ^{13}C-labeled plant material on Rs for: a, the difference between Rs / Rs (control) ratio in topsoil for each soil type; **b**, the difference between Rs / Rs (control) ratio in the subsoil for each soil type; **c**, the ratio between delta ^{13}C-Rs and delta total Rs in the topsoil for each soil type; **d**, the ratio between delta ^{13}C-Rs and delta total Rs in the subsoil for each soil type.

APPENDIX B: SUPPLAMENTARY TABLES

Table S2.1 to **Table S2.3** for **Chapter 2**:

S2.1 ANOVA and effect size by Cohen's d for the N fixation rates compared to control plots

S2.2 Estimates of *nifH* richness and alpha diversity for each plot. No significant difference observed between treatments

S2.3 Adonis, ANOSIM, and MRPP for 16S, ITS, and *nifH* community dissimilarity between treatments

Table S3.1 to **Table S3.6** for **Chapter 3**:

S3.1 Soil texture, chemistry, and P fractions by depth for each site averaged from three replicate soil pits taken in 2016 before switchgrass planting

S3.2 Seasonal data set for environmental factors, soil chemistry, and GHG fluxes by sample ID

S3.3 Identification of variable names in found in Table S3.2

S3.4 GHG flux and community metrics differences by Wilcox Sign Ranked Test and Mann-Whitney U test for effect size between switchgrass (SG) and fallow (FL) plots (n = 1,428)

S3.5 PERMANANOVA for 16S beta community structure by different treatment effects based off 999 permutations (n =1,428)

S3.6 p-values from t-test between relative abundances of major phyla for SG vs FL groups of each soil type by time point. p values adjusted by conservative bonferroni correction method (n = 1,428)

Table S5.1 for **Chapter 5**:

S5.1 FAME peak identification and category assignment for each biomarker used

Table S2.1 ANOVA and effect size by Cohen's d for the N fixation rates compared to control plots.

ANOVA N-Fixation Rates			Cohen's d	
eC				
Mean Square	3044	d estimate	2.571196	**Large**
F-value	36.06	lower	1.366411	
P-value	**<0.001**	upper 95%	3.775981	
eN				
Mean Square	1328.4	d estimate	-2.45705	**Large**
F-value	34.65	lower	-3.60646	
P-value	**<0.001**	upper 95%	-1.30763	
eNeC				
Mean Square	54.47	d estimate	0.424928	No Effect
F-Value	1.083	lower	-0.43123	
P-Value	0.309	upper 95%	1.281085	

Table S2.2 Estimates of *nifH* richness and alpha diversity for each plot. No significant difference observed between treatments.

	Control	**eC**	**eN**	**eNeC**
Observed Species Number Total	1077	1184	1145	1229
Observed Species Mean ± SD	239 ± 60	280 ± 39	274 ± 61	274 ± 57
Chao1 Mean ± SD	618 ± 139	700 ± 115	719 ± 144	665 ± 106
Shannon Index Mean ± SD	2.7 ± 0.72	2.8 ± 0.66	2.95 ± 0.69	2.92 ± 0.63
Simpson Index Mean ± SD	0.75 ± 0.16	0.74 ± 0.16	0.76 ± 0.16	0.76 ± 0.12

Table S2.3 Adonis, Anosim, and MRPP for 16S, ITS, and *nifH* community dissimilarity between treatments.

Variable	Adonis p value	ANOISM p value	MRPP p value
16S bacterial community	**0.033***	0.5	**0.018***
ITS fungal commmunity	**0.01***	**0.001****	**0.021***
nifH community	**0.03***	**0.045***	**0.048***

Table S3.1 Soil texture, chemistry, and P fractions by depth for each site averaged from three replicate soil pits taken in 2016 before switchgrass planting.

Site	Soil Depth	% Sand	% Silt	% Clay	% C	% N	% OM	pH	As ppm	B ppm	Ca ppm	Cr ppm	Cu ppm	Fe ppm	K ppm	Mg ppm	Mn ppm	Na ppm	Ni ppm	Pb ppm	Zn ppm
Ardmore Site (CL)	0 cm	60.2	21.9	17.9	0.9	0.1	1.8	5.3	3.0	2.0	729.8	6.9	3.9	4013.2	531.8	634.2	173.3	181.2	3.0	76.8	11.8
	20 cm	50.1	19.9	29.9	0.4	0.0	0.8	5.5	3.0	3.0	884.3	8.9	3.9	6173.5	880.4	970.2	185.6	229.0	4.9	8.9	13.8
	40 cm	56.9	9.2	33.9	0.4	0.0	0.7	6.1	4.0	3.0	1831.2	14.0	8.0	13283.9	1235.5	1597.9	66.1	303.4	8.0	23.0	25.0
	60 cm	40.5	23.8	35.7	0.3	0.0	0.6	6.4	6.0	5.0	2071.4	18.0	8.0	16184.2	1413.3	2027.4	54.0	360.1	9.0	10.0	23.0
	80 cm	50.3	17.9	31.8	0.2	0.0	0.4	6.3	6.9	5.0	1959.6	16.8	7.9	15202.1	1413.7	2046.8	77.3	338.8	8.9	7.9	22.8
	140 cm	64.4	11.0	24.7	0.1	0.0	0.2	5.9	5.9	3.0	1437.1	10.9	5.9	11256.7	1057.5	1363.7	59.5	252.7	5.0	5.0	15.9
	200 cm	67.5	11.8	20.7	0.1	0.0	0.1	6.0	5.0	3.0	1597.9	9.9	6.9	9448.5	1010.7	1342.0	99.2	246.0	5.0	5.0	15.9
Burneyville Site (SL)	10 cm	64.0	26.0	10.0	0.4	0.0	0.9	5.8	3.0	3.9	1074.7	7.9	4.9	6756.1	1057.0	2268.8	202.1	180.4	5.9	3.9	35.5
	20 cm	59.7	27.9	12.4	0.3	0.0	0.6	6.1	2.0	4.0	1396.1	8.0	5.0	7334.2	1072.5	2605.1	225.1	248.0	9.0	3.0	15.9
	40 cm	60.0	24.0	16.0	0.3	0.0	0.5	6.6	3.0	5.0	1497.3	8.9	5.0	7824.6	1054.9	3002.6	208.8	256.5	8.0	2.0	15.9
	60 cm	44.4	37.7	17.9	0.2	0.0	0.5	6.8	2.0	4.0	1500.2	8.0	4.0	6807.2	834.3	2889.8	194.4	241.2	8.0	3.0	15.0
	100 cm	44.3	46.4	9.3	0.2	0.0	0.4	7.1	2.0	4.9	1455.4	8.8	4.9	7882.3	999.4	3267.5	186.7	238.8	7.9	2.0	16.7
	180 cm	54.5	39.5	6.1	0.1	0.0	0.3	7.5	4.0	6.9	1659.1	9.9	4.9	8473.6	1181.0	3577.5	196.0	282.1	7.9	2.0	19.8

Table S3.2 see published manuscript to download the table as the table has over 1,428 samples https://doi.org/10.1038/s41396-021-00916-y

Table S3.3 Identification of variable names in found in Table S2.

ID	Unit	Description
SampleID	NA	Identification Number of Specific Sample in the Dataset
SampleName	NA	Unique string of identification details for each sample
Date	NA	Numeric date of sample taken by year, month and day
Year	NA	Year sample was taken
Season	NA	Season of the year sample was taken
Month	NA	Month sample was taken
Months_After_SG	NA	Numeric expression of the number of months elapsed after the planting of switchgrass at each site
CL	NA	Clay Loam Field Site Near Ardmore, OK
SL	NA	Sandy Loam Field Site Near Buryneville, OK
SG	NA	Switchgrass Plot
FL	NA	Fallow mixed grasses plot
CollarPosition	NA	Trace Gas Collar Position Location
Direction	Cardinal direction	Direction collar was positioned at in the field
Ring	NA	Position of collar from the center with 1 indicated the collar is closest to the origin
Subplot	NA	Site-Plot
pH	0-14	Soil pH taken by mixing 10g of soil with 50ml of ddH20, mixing and measuring in the lab via pH probe
Moisture_Grav	%	Percent soil moisture after drying and calculating the % change
RELH	%	5-minute relative humidity at 1.5m
TAIR	Celsius	5-minute average air temperature at 1.5m
WSPD	Miles per hour	5-minute averaged wind speed at 10m
WDIR	Cardinal direction	5-minute averaged wind direction at 10m
WMAX	Miles per hour	Highest 3-second wind speed measurment each day
RAIN	Inches	Liquid precipitation measured each day
PRES	Milibars	Station atmospheric pressure
TS10	Degrees Celsius	Average temperature at a depth of 10cm for sod covered soil
TB10	Degrees Celsius	Average temperature at a depth of 10cm for bare soil
TR25	Degrees Celsius	The calibrated change in temperature of the soil over time after a heat pulse is interoduced at 25cm depth
TR60	Degrees Celsius	The calibrated change in temperature of the soil over time after a heat pulse is interoduced at 60cm depth
N03_N	ppm	soil Nitrate by KCL soil extraction in parts per million
NH4_N	ppm	Ammonium by KCL soil extrations in parts per million
P	ppm	Plant available phosphate by Melich III soil extraction in parts per million
TN	%	Percent soil Nitrogen
TC	%	Percent soil Carbon
CO2_dry.aic_lin	AIC	AIC score for linear model CO2
CO2_dry.aic_quad	AIC	AIC score for quadradic model CO2
CO2_dry.aic_exp	AIC	AIC score for exponential model CO2
CO2_dry.r2_lin	r^2	R squared value for each model
CO2_dry.r2_quad	r^2	R squared value for each model
CO2_dry.r2_exp	r^2	R squared value for each model
CO2_dry.slope_lin	slope	Slope for each model
CO2_dry.slope_quad	slope	Slope for each model
CO2_dry.slope_exp	slope	Slope for each model
CO2_dry.best_model	Categorical	which model had the best AIC score to fit the data for that sample
CO2_dry.aic_best	AIC	AIC score for the best model
CO2_dry.r2_best	r^2	R squared value for best model
CO2_dry.slope_best	slope	Slope for best model
N20_dry.aic_lin	AIC	AIC score for linear model N20
N20_dry.aic_quad	AIC	AIC score for quadradic model N20
N20_dry.aic_exp	AIC	AIC score for exponential model N20
N20_dry.r2_lin	r^2	R squared value for each model
N20_dry.r2_quad	r^2	R squared value for each model
N20_dry.r2_exp	r^2	R squared value for each model
N20_dry.slope_lin	slope	Slope for each model
N20_dry.slope_quad	slope	Slope for each model
N20_dry.slope_exp	slope	Slope for each model
N20_dry.best_model	Categorical	which model had the best AIC score to fit the data for that sample
N20_dry.aic_best	AIC	AIC score for the best model
N20_dry.r2_best	r^2	R squared value for best model
N20_dry.slope_best	slope	Slope for best model
CH4_dry.aic_lin	AIC	AIC score for linear model CH4
CH4_dry.aic_quad	AIC	AIC score for quadradic model CH4
CH4_dry.aic_exp	AIC	AIC score for exponential model CH4
CH4_dry.r2_lin	r^2	R squared value for each model
CH4_dry.r2_quad	r^2	R squared value for each model
CH4_dry.r2_exp	r^2	R squared value for each model
CH4_dry.slope_lin	slope	Slope for each model
CH4_dry.slope_quad	slope	Slope for each model
CH4_dry.slope_exp	slope	Slope for each model
CH4_dry.best_model	Categorical	which model had the best AIC score to fit the data for that sample
CH4_dry.aic_best	AIC	AIC score for the best model
CH4_dry.r2_best	r^2	R squared value for best model
CH4_dry.slope_best	slope	Slope for best model
Flux_CO2_dry.Christ	$mmol \cdot m^{-2} \cdot h^{-1}$	Flux as calculated from Christiansen et al., 2015
Flux_N2O_dry.Christ	$mmol \cdot m^{-2} \cdot h^{-1}$	Flux as calculated from Christiansen et al., 2015
Flux_CH4_dry.Christ	$mmol \cdot m^{-2} \cdot h^{-1}$	Flux as calculated from Christiansen et al., 2015
DCA1	NA	Axis 1 of the deterented correpsondence analysis for the microbial community structure
DCA2	NA	Axis 2 of the deterented correpsondence analysis for the microbial community structure
observed_species	Species number	The number of observed OTUs found after every sample was rarified to 30k reads per sample
PD_whole_tree	Phylogenetic Distance	The phylogenetic distance using the whole tree
chao1	Index values	Chao1 index
shannon	Index Vaues	Shannon diversity index
simpson	Index Vaues	Simpson index
PC1	NA	PC1 values of the principal component analysis on soil samples containing 43.2% of the variation
PC2	NA	PC2 values of the principal component analysis on soil samples containing 18.95% of the variation

Table S3.4 GHG flux and community metrics differences by Wilcox Sign Ranked Test and Mann-Whitney U test for effect size between switchgrass (SG) and fallow (FL) plots (n = 1,428).

Variable	SL (SG v FL)			Effect Size Category	CL (SG v FL)			Effect Size Category
	z-value	p-value	r-Effect Size		z-value	p-value	r-Effect Size	
CO_2	0.26	0.7932	0.00	-	3.47	**0.000528*** **	0.13	Small
CH_4	9.77	**<2.2e-16*** **	0.37	Medium	4.01	**5.957e-5*** **	0.15	Small
N_2O	-0.36	0.7176	0.00	-	1.55	0.05075	0.00	-
Observed Species	6.60	**4.194e-11*** **	0.38	Medium	-1.33	0.184	0.00	-
Shannon	5.67	**1.446e-08*** **	0.33	Medium	-4.19	**2.76e-05*** **	0.24	Small
Simpson	3.28	**0.001054** **	0.19	Small	-5.89	**3.767e-09*** **	0.34	Medium
Chao1	6.04	**1.587e-09*** **	0.35	Medium	-0.68	0.49	0.00	-
PD whole Tree	2.72	**0.006436** **	0.16	Small	-3.22	**0.001301** **	0.19	Small

Effect size determined by Mann-Whitney U test with small (0.1 - < 0.3), medium (0.3 - < 0.5), and large (> 0.5) ranges.

Table S3.5 PERMANANOVA for 16S beta community structure by different treatment effects based off 999 permutations (n =1,428).

Group	PERMANOVA Table			
	MeanSqs	**F.Model**	**R^2**	**p**
Time	0.0083	9.248	0.00532	**0.002** **
Site Effect (CL or SL)	0.1152	128.3	0.07381	**0.001*** **
Plant Cover (SG or FL)	0.0115	12.78	0.00735	**0.001*** **
Time:Plant Cover	0.0048	5.377	0.00309	0.02
Plant Cover: Site Effect	0.0018	1.987	0.00114	0.15
Time: Site Effect	0.0911	101.5	0.05839	**0.001*** **
Plant Cover: Time : Site Effect	0.0526	58.58	0.03371	**0.001*** **

Table S3.6 p-values from t-test between relative abundances of major phyla for SG vs FL groups of each soil type by time point. p values adjusted by conservative bonferroni correction method (n = 1,428).

Phylum	T0 - July 2016		T2 - September 2016		T4 - November 2016		T8 - March 2017		T11 - June 2017		T14 - September 2017		T16 - November 2017	
	SL	CL	SL	CL	SL	CL	SL	CL	SL	CL	SL	CL	SL	CL
Acidobacteria	0.23	0.19	0.26	0.14	0.73	0.2	0.07	0.61	0.14	0.51	**<0.001*** **	0.052	**<0.001*** **	0.99
Actinobacteria	**<0.001*** **	0.28	0.68	0.095	0.55	0.44	0.58	**<0.001*** **	0.95	0.22	0.5	**<0.001*** **	0.83	0.65
Bacteroidetes	0.14	0.69	0.17	**<0.001*** **	0.62	0.092	0.62	**<0.001*** **	0.27	0.092	**<0.001*** **	0.11	**<0.001*** **	0.93
Chlamydiae	0.14	0.078	0.28	0.18	0.15	**0.045***	0.65	0.85	0.97	**<0.001*** **	0.52	0.7	0.078	0.336
Chloroflexi	0.056	0.84	0.49	0.087	0.13	0.45	0.14	**0.02***	0.23	0.64	0.18	**0.042***	0.2	0.63
Cyanobacteria/Chloroplast	0.56	**<0.001*** **	0.24	0.071	0.53	**<0.001*** **	0.051	0.99	**0.034***	0.064	0.05	**0.032***	0.2	**<0.001*** **
Deinococcus-Thermus	**<0.001*** **	0.35	0.12	0.77	0.92	0.13	0.89	**<0.001*** **	0.087	0.075	0.75	**0.015***	**<0.001*** **	0.55
Firmicutes	0.53	**<0.001*** **	0.34	0.14	0.36	0.09	0.42	**<0.001*** **	0.53	0.76	**<0.001*** **	0.071	0.63	**0.028***
Gemmatimonadetes	0.14	0.18	0.43	0.98	0.6	0.52	0.87	0.068	0.14	0.069	0.63	0.37	0.45	0.064
Parcubacteria	0.49	0.54	0.066	0.24	0.36	0.087	0.094	0.69	0.34	0.29	0.38	0.42	0.36	0.17
Plactomycetes	0.28	0.54	**<0.001*** **	0.42	0.25	0.45	**<0.001*** **	**0.021***	0.27	0.053	0.43	0.48	0.3	0.14
Proteobacteria	0.14	0.8	0.14	0.26	0.19	0.22	**<0.001*** **	0.29	0.16	0.62	0.31	0.71	0.06	0.59
Verrucomicrobia	0.12	0.053	0.06	0.38	0.42	0.25	0.28	**<0.001*** **	**<0.001*** **	0.25	0.34	0.46	**0.042***	0.85

Table S5.1 FAME peak identification and category assignment for each biomarker used.

Category	Peak Name	IUPAC/ Systematic Name	Common Name
AM Fungi	16:1 w5c	(11Z)-11-Hexadecenoic Acid	cis-11-Palmitoleic Acid
Fungi	18:2 w6c	(9Z,12Z)-9,12-Octadecadienoic Acid	Linoleic Acid (LA)
Actinomycetes	16:0 10-methyl	10-Methylhexadecanoic Acid	10-Methylpalmitic Acid
	17:1 w7c 10-methyl	(10Z)-10-Methyl-10-Heptadecenoic Acid	-
	17:0 10-methyl	10-Methylheptadecanoic Acid	-
	18:1 w7c 10-methyl	(11Z)-10-Methyl-11-Octadecenoic Acid	-
	18:0 10-methyl	10-Methyloctadecanoic Acid	Tuberculostearic Acid
	19:1 w7c 10-methyl	(12Z)-10-Methyl-12-Nonadecenoic Acid	-
	20:0 10-methyl	10-Methylicosanoic Acid	-
	22:0 10-methyl	10-Methyldocosanoic Acid	-
Gram Negative	10:0 2OH	2-Hydroxydecanoic Acid	2-Hydroxycapric Acid
	10:0 3OH	3-Hydroxydecanoic Acid	3-Hydroxycapric Acid
	11:0 iso 3OH	3-Hydroxy-9-Methyldecanoic Acid	-
	12:1 w8c	(4Z)-4-Dodecenoic Acid	-
	12:1 w5c	(7Z)-7-Dodecenoic Acid	-
	13:1 w5c	(8Z)-8-Tridecenoic Acid	-
	13:1 w4c	(9Z)-9-Tridecenoic Acid	-
	13:1 w3c	(10Z)-10-Tridecenoic Acid	-
	12:0 2OH	2-Hydroxydodecanoic Acid	2-Hydroxylauric Acid
	14:1 w9c	(5Z)-5-Tetradecenoic Acid	-
	14:1 w8c	(6Z)-6-Tetradecenoic Acid	-
	14:1 w7c	(7Z)-7-Tetradecenoic Acid	-
	14:1 w5c	(9Z)-9-Tetradecenoic Acid	Myristoleic Acid
	14:0 iso 3OH	3-Hydroxy-12-Methyltridecanoic Acid	-
	15:1 w9c	(6Z)-6-Pentadecenoic Acid	-
	15:1 w8c	(7Z)-7-Pentadecenoic Acid	-
	15:1 w7c	(8Z)-8-Pentadecenoic Acid	-
	15:1 w6c	(9Z)-9-Pentadecenoic Acid	-
	15:1 w5c	(10Z)-10-Pentadecenoic Acid	-
	14:0 2OH	2-Hydroxytetradecanoic Acid	2-Hydroxymyristic Acid
	16:1 w9c	(7Z)-7-Hexadecenoic Acid	cis-7-Palmitoleic Acid
	16:1 w7c	(9Z)-9-Hexadecenoic Acid	Palmitoleic Acid
	14:0 3OH	3-Hydroxy-12-Methyltridecanoic Acid	-
	16:1 w6c	(10Z)-10-Hexadecenoic Acid	cis-10-Palmitoleic Acid
	16:1 w4c	(12Z)-12-Hexadecenoic Acid	cis-12-Palmitoleic Acid
	16:1 w3c	(13Z)-13-Hexadecenoic Acid	cis-13-Palmitoleic Acid
	17:1 w9c	(7Z)-15-Methyl-7-Hexadecenoic Acid	-
	17:1 w8c	(9Z)-9-Heptadecenoic Acid	cis-Margaroleic Acid
	17:1 w7c	(10Z)-10-Heptadecenoic Acid	-
	17:1 w6c	(11Z)-11-Heptadecenoic Acid	-
	17:0 cyclo w7c	cis-9,10-Methylene-Hexadecanoic Acid	-
	17:1 w5c	(12Z)-12-Heptadecenoic Acid	-
	17:1 w4c	(13Z)-13-Heptadecenoic Acid	-
	17:1 w3c	(14Z)-14-Heptadecenoic Acid	-
	16:0 2OH	2-Hydroxyhexadecanoic Acid	2-Hydroxypalmitic Acid
	18:0 cyclo w6c	cis-11,12-Methylene-Heptadecanoic Acid	-
	18:1 w8c	(10Z)-10-Octadecenoic Acid	cis-10-Oleic Acid
	18:1 w7c	(11Z)-11-Octadecenoic Acid	cis-Vaccenic Acid
	18:1 w6c	(12Z)-12-Octadecenoic Acid	cis-12-Oleic Acid
	18:1 w5c	(13Z)-13-Octadecenoic Acid	cis-13-Oleic Acid
	18:1 w3c	(15Z)-15-Octadecenoic Acid	cis-15-Oleic Acid
	19:1 w9c	(10Z)-10-Nonadecenoic Acid	-
	19:1 w8c	(11Z)-11-Nonadecenoic Acid	-
	19:1 w7c	(12Z)-12-Nonadecenoic Acid	-
	19:1 w6c	(13Z)-13-Nonadecenoic Acid	-
	19:0 cyclo w7c	cis-9,10-Methylene-Octadecanoic Acid	Dihydrosterculic Acid
	19:0 cyclo w6c	cis-11,12-Methylene-Octadecanoic Acid	Lactobacillic Acid
	20:1 w9c	(11Z)-11-Icosenoic Acid	Gondoic Acid
	20:1 w8c	(12Z)-12-Icosenoic Acid	-
	20:1 w6c	(14Z)-14-Icosenoic Acid	-
	20:1 w4c	(16Z)-16-Icosenoic Acid	-
	20:0 cyclo w6c	cis-13,14-Methylene-Nonadecanoic Acid	-
	21:1 w9c	(12Z)-12-Heneicosenoic Acid	-
	21:1 w8c	(13Z)-13-Heneicosenoic Acid	-
	21:1 w6c	(15Z)-15-Heneicosenoic Acid	-
	21:1 w5c	(16Z)-16-Heneicosenoic Acid	-
	21:1 w4c	(17Z)-17-Heneicosenoic Acid	-
	21:1 w3c	(18Z)-18-Heneicosenoic Acid	-
	22:1 w9c	(13Z)-13-Docosenoic Acid	Erucic Acid
	22:1 w8c	(14Z)-14-Docosenoic Acid	-
	22:1 w6c	(16Z)-16-Docosenoic Acid	-
	22:1 w5c	(17Z)-17-Docosenoic Acid	-
	22:1 w3c	(19Z)-19-Docosenoic Acid	-
	22:0 cyclo w6c	cis-15,16-Methylene-Heneicosanoic Acid	-
	24:1 w9c	(15Z)-15-Tetracosenoic Acid	Nervonic Acid
	24:1 w7c	(17Z)-17-Tetracosenoic Acid	-
Gram Positive	11:0 iso	9-Methyldecanoic Acid	9-Methylcapric Acid
	11:0 anteiso	8-Methyldecanoic Acid	8-Methylcapric Acid
	12:0 iso	10-Methylundecanoic Acid	Isolauric Acid
	12:0 anteiso	9-Methylundecanoic Acid	Anteisolauric Acid
	13:0 iso	11-Methyldodecanoic Acid	Isotridecanoic Acid
	13:0 anteiso	10-Methyldodecanoic Acid	Anteisotridecanoic Acid
	14:1 iso w7c	(6Z)-12-Methyl-6-Tridecenoic Acid	-
	14:0 iso	12-Methyltridecanoic Acid	Isomyristic Acid
	14:0 anteiso	11-Methyltridecanoic Acid	Anteisomyristic Acid
	15:1 iso w9c	(5Z)-13-Methyl-5-Tetradecenoic Acid	-
	15:1 iso w6c	(8Z)-13-Methyl-8-Tetradecenoic Acid	-
	15:1 anteiso w9c	(5Z)-12-Methyl-5-Tetradecenoic Acid	-
	15:0 iso	13-Methyltetradecanoic Acid	13-Methylmyristic Acid
	15:0 anteiso	12-Methyltetradecanoic Acid	12-Methylmyristic Acid
	16:0 iso	14-Methylpentadecanoic Acid	Isopalmitic Acid
	16:0 anteiso	13-Methylpentadecanoic Acid	Anteisopalmitic Acid
	17:1 iso w9c	(7Z)-15-Methyl-7-Hexadecenoic Acid	-
	17:0 iso	15-Methylhexadecanoic Acid	Isomargaric Acid
	17:0 anteiso	14-Methylhexadecanoic Acid	Anteisomargaric Acid
	18:0 iso	16-Methylheptadecanoic Acid	Isostearic Acid
	17:1 anteiso w9c	(7Z)-14-Methyl-7-Hexadecenoic Acid	-
	17:1 iso w10c	(6Z)-15-Methyl-6-Hexadecenoic Acid	-
	17:1 anteiso w7c	(9Z)-14-Methyl-9-Hexadecenoic Acid	-
	18:1 w9c	(9Z)-9-Octadecenoic Acid	Oleic Acid
	19:0 cyclo w9c	cis-9,10-Methylene-Octadecanoic Acid	Dihydrosterculic Acid
	19:0 iso	17-Methyloctadecanoic Acid	17-Methylstearic Acid
	19:0 anteiso	16-Methyloctadecanoic Acid	16-Methylstearic Acid
	20:0 iso	18-Methylnonadecanoic Acid	Isoarachidic Acid
	22:0 iso	20-Methylhenicosanoic Acid	Isobehenic Acid
Eukaryote	15:4 w3c	(3Z,6Z,9Z,12Z)-3,6,9,12-Pentadecatetraenoic Acid	-
	15:3 w3c	(6Z,9Z,12Z)-6,9,12-Pentadecatrienoic Acid	-
	16:4 w3c	(4Z,7Z,10Z,13Z)-4,7,10,13-Hexadecatetraenoic Acid	-
	16:3 w6c	(4Z,7Z,10Z)-4,7,10-Hexadecatrienoic Acid	-
	18:3 w6c	(12Z,15Z,18Z)-12,15,18-Octadecatrienoic Acid	-
	18:4 w3c	(6Z,9Z,12Z,15Z)-6,9,12,15-Octadecatetraenoic Acid	-
	19:4 w6c	(4Z, 7Z,10Z,13Z)-4,7,10,13-Nonadecatetraenoic Acid	-
	19:3 w6c	(7Z,10Z,13Z)-7,10,13-Nonadecatrienoic Acid	-
	19:3 w3c	(10Z,13Z,16Z)-10,13,16-Nonadecatrienoic Acid	-
	20:4 w6c	(5Z,8Z,11Z,14Z)-5,8,11,14-Icosatetraenoic Acid	Arachidonic Acid (AA)
	20:5 w3c	(5Z,8Z,11Z,14Z,17Z)-5,8,11,14,17-Icosapentaenoic Acid	Eicosapentaenoic Acid (EPA)
	20:3 w6c	(8Z,11Z,14Z)-8,11,14-Icosatrienoic Acid	-
	20:2 w6c	(11Z,14Z)-11,14-Icosadienoic Acid	Eicosadienoic Acid
	21:3 w6c	(9Z,12Z,15Z)-9,12,15-Heneicosatrienoic Acid	-
	21:3 w3c	(12Z,15Z,18Z)-12,15,18-Heneicosatrienoic Acid	-
	22:5 w6c	(4Z,7Z,10Z,13Z,16Z)-4,7,10,13,16-Docosapentaenoic Acid	Osbond Acid
	22:6 w3c	(4Z,7Z,10Z,13Z,16Z,19Z)-4,7,10,13,16,19-Docosahexaenoic Acid	Docosahexaenoic Acid (DHA)
	22:4 w6c	(7Z,10Z,13Z,16Z)-7,10,13,16-Docosatetraenoic Acid	Adrenic Acid
	22:5 w3c	(7Z,10Z,13Z,16Z,19Z)-7,10,13,16,19-Docosapentaenoic Acid	Docosapentaenoic (DPA)
	22:2 w6c	(13Z,16Z)-13,16-Docosadienoic Acid	Docosadienoic Acid
	23:4 w6c	(8Z,11Z,14Z,17Z)-8,11,14,17-Tricosatetraenoic Acid	-
	23:3 w6c	(11Z,14Z,17Z)-11,14,17-Tricosatrienoic Acid	-
	23:3 w3c	(14Z,17Z,20Z)-14,17,20-Tricosatrienoic Acid	-
	23:1 w5c	(18Z)-18-Tricosenoic Acid	-
	23:1 w4c	(19Z)-19-Tricosenoic Acid	-
	24:4 w6c	(9Z,12Z,15Z,18Z)-9,12,15,18-Tetracosatetraenoic Acid	Tetracosatetraenoic Acid
	24:3 w6c	(12Z,15Z,18Z)-12,15,18-Tetracosatrienoic Acid	-
	24:3 w3c	(15Z,18Z,21Z)-15,18,21- Tetracosatrienoic Acid	-
	24:1 w3c	(21Z)-21-Tetracosenoic Acid	-

BIBLIOGRAPHY

Abraha M, Gelfand I, Hamilton SK, Chen J, Robertson GP (2019). Carbon debt of field-scale conservation reserve program grasslands converted to annual and perennial bioenergy crops. *Environ Res Lett*., **14**: 1748-9326.

Adler, P. B. & Lauenroth, W. K. (2003) The power of time: spatiotemporal scaling of species diversity. *Ecol. Lett*., **6**: 749–756.

Ainsworth EA, Long SP. (2005). What have we learned from 15 years of free-air CO_2 enrichment (FACE)? A meta-analytic review of the responses of photosynthesis, canopy properties and plant production to rising CO_2. *New Phytologist*, **165**: 351–372.

Anderson MJ. (2006) Distance-based tests for homogeneity of multivariate dispersions. *Biometrics,* **62**(1): 245-53.

Anderson MJ. (2017) Permutational Multivariate Analysis of Variance (PERMANOVA). In Wiley StatsRef: Statistics Reference Online (eds N. Balakrishnan, T. Colton, B. Everitt, W. Piegorsch, F. Ruggeri and J.L. Teugels).

Anderson-teixeira, K., Davis, S., Masters, M., & Delucia, E. (2009). Changes in soil organic carbon under biofuel crops. *GCB Bioenergy*, **1**(1): 75–96.

Anderson-Teixeria et al. (2012) Biofuels on the landscape: Is "land sharing" preferable to "land sparing"? *Ecological Applications*, **22**(8): 2035-48.

Angert A, Biraud S, Bonfils C et al. (2005) Drier summers cancel out the CO_2 uptake enhancement induced by warmer springs. *Proceedings of the National Academy of Sciences of the United States of America,* **102**: 10823–10827.

AOAC Official Method 972.43, (1997) Microchemical Determination of Carbon, Hydrogen, and Nitrogen, Automated Method, in *Official Methods of Analysis of AOAC International*, 16th Edition, Chapter 12, pp. 5-6, AOAC International, Arlington, VA.

Ashiq MW, Bazrgar AB, Fei H, Coleman B, Vessey K, Gordon A, et al. (2017) A nutrient-based sustainability assessment of purpose-grown poplar and switchgrass biomass production systems established on marginal lands in Canada. *Can J Plant Sci.,* **98**(2): 255-266.

Baer, S. G., Adams, T., Scott, D. A., Blair, J. M., and Collins, S. L. (2020). Soil heterogeneity increases plant diversity after 20 years of manipulation during grassland restoration. *Ecological Applications,* **30**(1): e02014. 10.1002/eap.2014.

Bahulikar RA, Torres-Jerez I, Worley E, Craven K, Udvardi MK. (2014) Diversity of nitrogen-fixing bacteria associated with switchgrass in the native tallgrass prairie of Northern Oklahoma. *Appl Environ Microbiol.*, **80**(18): 5636-43.

Baig, S., Medlyn, B. E., Mercado, L. M. & Zaehle, S. (2015) Does the growth response of woody plants to elevated CO2 increase with temperature? A model-oriented meta-analysis. *Glob. Change Biol*., **21**: 4303–4319.

Balesdent, J. et al. (2018) Atmosphere-soil carbon transfer as a function of soil depth. *Nature*, **559**: 599–602.

Bardgett, R.D., Freeman, C. & Ostle, N.J. (2008). Microbial contributions to climate change through carbon-cycle feedbacks. The ISME Journal **2**: 805–814.

Barea, J.-M., Ferrol, N., Azcón-Aguilar, C. & Azcón, R. (Springer, 20018) The ecophysiology of plant-phosphorus interactions, 143-163.

Barney, J. N., Mann, J. J., Kyser, G. B., Blumwald, E., Van Deynze, A., & DiTomaso, J. M. (2009). Tolerance of switchgrass to extreme soil moisture stress: Ecological implications. *Plant Science*, **177**(6): 724–732.

Bartlett KB, Harriss RC. (1993) Review and assessment of methane emissions from wetlands. *Chemosphere*, **26**: 261-320.

Bass-Becking, L.G.M. (1934) Geobiologie of Inleiding to de Milieukunde, W.P van Stockum & Zoon N.V.

Bates D, Mächler M, Bolker BM, Walker SC. (2015) Fitting linear mixed-effects models using lme4. *J Stat Softw*., **67**: Issue 1.

Bates, C.T., Escalas, A., Kuang, J. et al. (2021) Conversion of marginal land into switchgrass conditionally accrues soil carbon but reduces methane consumption. *ISME J.*

Bauer, J. T., Kleczewski, N. M., Bever, J. D., Clay, K., & Reynolds, H. L. (2012). Nitrogen-fixing bacteria, arbuscular mycorrhizal fungi, and the productivity and structure of prairie grassland communities. *Oecologia*, **170**(4): 1089–1098.

Baumhardt LR. Dust Bowl Era. (2003) In: *Encyclopedia of Water Science*.

Bengtsson, J., Bullock, J. M., Egoh, B., Everson, C., Everson, T., O'Connor, T., O'Farrell, P. J., Smith, H. G., and Lindborg, R. (2019). Grasslands—more important for ecosystem services than you might think. *Ecosphere*, **10**(2):e02582.

Blažka, P. and Fischer, Z. (2014) Moisture, Water Holding, Drying and Wetting in Forest Soils. *Open Journal of Soil Science*, **4**, 174-184.

Bononi, L., Chiaramonte, J.B., Pansa, C.C. et al. (2020). Phosphorus-solubilizing Trichoderma spp. from Amazon soils improve soybean plant growth. *Sci Rep*, **10**: 2858.

Bouton JH. Molecular breeding of switchgrass for use as a biofuel crop. (2007). *Current Opinion in Genetics and Development*, **17**(6):553-8.

Bouton, J. in Genetic Improvement of Bioenergy Crops (ed W. Vermerris) 295-308 (Springer Science and Business Media, 2008).

Bowman RA, Moir JO. Basics EDTA as an extractant for soil organic phosphorus. (1993). *Soil Science Society of America Journal*, **57**(6): 1516-1518.

Buyer, Jeffrey S, and Myron Sasser. (2012). High Throughput Phospholipid Fatty Acid Analysis of Soils. *Applied soil ecology*, **61**: 127.

C.W. Bingemann, J.E. Varner, W.P. Martin. (1953). The effect of the addition of organic materials on the decomposition of an organic soil. *Soil Science Society of America Proceedings*, **17**: 34-38.

Cahill, J. F., and B. B. Casper. (1999). Growth consequences of soil nutrient heterogeneity for two old-field herbs, Ambrosia artemisiifolia and Phytolacca americanum grown individually and in combination. *Annals of Botany*, **83**: 471– 478.

Čapek, P., Manzoni, S., Kaštovská, E. et al. (2018). A plant–microbe interaction framework explaining nutrient effects on primary production. *Nat Ecol Evol*, **2**: 1588–1596.

Caporaso JG, Kuczynski J, Stombaugh J, Bittinger K, Bushman FD, Costello EK, et al. (2010). QIIME allows analysis of high-throughput community sequencing data. *Nature Methods*. **7**(5):335-6.

Caporaso, J., Lauber, C., Walters, W. *et al.* (2012) Ultra-high-throughput microbial community analysis on the Illumina HiSeq and MiSeq platforms. *ISME J*, **6**: 1621–1624.

Carol Adair, E., Reich, P.B., Trost, J.J. and Hobbie, S.E. (2011), Elevated CO_2 stimulates grassland soil respiration by increasing carbon inputs rather than by enhancing soil moisture. *Glob Change Biol*, **17**: 3546-3563.

Carrillo, Y., Dijkstra, F. A., LeCain, D. & Pendall, E. (2016). Mediation of soil C decomposition by arbuscular mycorrizhal fungi in grass rhizospheres under elevated CO_2. *Biogeochemistry*, **127**: 45–55.

Castresana J. (2000). Selection of conserved blocks from multiple alignments for their use in phylogenetic analysis. *Mol Biol Evol.*, **17**(4): 540-552.

Changfu Huo, Yiqi Luo, Weixin Cheng. (2017). Rhizosphere priming effect: A meta-analysis, *Soil Biology and Biochemistry*, **111**: Pages 78-84.

Chapin, F. S., Matson, P. A. & Vitousek, P. M. Principles of Terrestrial Ecosystem Ecology. 2nd edn (Springer, New York, 2011).

Chen C, Chen HYH, Chen X, Huang Z. (2019) Meta-analysis shows positive effects of plant diversity on microbial biomass and respiration. *Nat Commun*., **10**: 1332.

Chen, J, Elsgaard, L, van Groenigen, KJ, et al. (2020). Soil carbon loss with warming: New evidence from carbon-degrading enzymes. *Glob Change Biol*., **26**: 1944–1952.

Cheng W, Parton WJ, Gonzalez-Meler MA, Phillips R, Asao S, Mcnickle GG, et al. (2014). Synthesis and modeling perspectives of rhizosphere priming. *New Phytologist*, **201**(1): 31-44.

Christiansen JR, Outhwaite J, Smukler SM. (2015). Comparison of CO_2, CH_4 and N_2O soil-atmosphere exchange measured in static chambers with cavity ring-down spectroscopy and gas chromatography. *Agric For Meteorol.*, **211**: 48-57.

Ciais P, Reichstein M, Viovy N et al. (2005) Europe-wide reduction in primary productivity caused by heat and drought in 2003. *Nature*, **437**: 529–533.

Cisneros-Dozal, L.M., Trumbore, S. & Hanson, P.J. (2006). Partitioning sources of soil-respired CO2 and their seasonal variation using a unique radiocarbon tracer. *Global Change Biology*, **12**: 194–204.

Clark RB, Baligar VC, Zobel RW. (2005). Response of mycorrhizal switchgrass to phosphorus fractions in acidic soil. *Commun Soil Sci Plant Anal.*, **36**: 1337-1359.

Cline LC, Zak DR. (2015). Soil microbial communities are shaped by plant-driven changes in resource availability during secondary succession. *Ecology*, **96**(12): 3374-85.

Collins, H. P., Smith, J. L., Fransen, S., Alva, A. K., Kruger, C. E., & Granatstein, D. M. (2010). Carbon Sequestration under Irrigated Switchgrass (Panicum virgatum L.) Production. *Soil Science Society of America Journal*, **74**(6), 2049–2058.

Cotrufo, M. F., Ranalli, M. G., Haddix, M. L., Six, J. & Lugato, E. (2019). Soil carbon storage informed by particulate and mineral-associated organic matter. *Nat. Geosci*., **12**: 989–994.

Cotrufo, M.F., Wallenstein, M.D., Boot, C.M., Denef, K. and Paul, E. (2013), The Microbial Efficiency-Matrix Stabilization (MEMS) framework integrates plant litter decomposition with soil organic matter stabilization: do labile plant inputs form stable soil organic matter? *Glob Change Biol*, **19**: 988-995.

Craig, M. E. et al. (2018). Tree mycorrhizal type predicts within-site variability in the storage and distribution of soil organic matter. *Glob. Change Biol.*, **24**: 3317–3330.

Craine, J.M., Reich, P.B., David Tilman, G., Ellsworth, D., Fargione, J., Knops, J. and Naeem, S. (2003), The role of plant species in biomass production and response to elevated CO_2. N. *Ecology Letters*, **6**: 623-625.

Crews TE, Peoples MB (2005) Can the synchrony of nitrogen supply and crop demand be improved in legume and fertilizer-based agroecosystems? A review. *Nutr Cycl Agroecosyst*, **72**:101–120.

Csonka LN. (1989). Physiological and genetic responses of bacteria to osmotic stress. *Microbiol. Rev.*, **53**(1):121– 47.

Curd, E. E., Martiny, J. B. H., Li, H., and Smith, T. B. (2018). Bacterial diversity is positively correlated with soil heterogeneity. *Ecosphere*, **9**(1):e02079. 10.1002/ecs2.2079

Dabney SM, Shields FD, Temple DM, Langendoen EJ. (2004). Erosion processes in gullies modified by establishing grass hedges. *Trans Am Soc Agric Eng.*, **47**(5).

Davide Roncarati, Vincenzo Scarlato, (2017). Regulation of heat-shock genes in bacteria: from signal sensing to gene expression output, *FEMS Microbiology Reviews*, **41**(4): 549–574.

Deng, Y., Ning, D., Qin, Y., Xue, K., Wu, L., He, Z., Yin, H., Liang, Y., Buzzard, V., Michaletz, S.T. and Zhou, J. (2018), Spatial scaling of forest soil microbial communities across a temperature gradient. *Environ Microbiol*, **20**: 3504-3513.

Deutsch CA, Tewksbury JJ, Huey RB, Sheldon KS, Ghalambor CK, Haak DC, et al. (2008). Impacts of climate warming on terrestrial ectotherms across latitude. *Proc Natl Acad Sci.*, **105**(18) 6668-6672.

Diamond D. Phosphorus in soil extracts. (1995). QuikChem Method 10-115-01-1-A. *Lachat instruments*, Milwaukee, WI.

Dillon ME, Wang G, Huey RB. (2010). Global metabolic impacts of recent climate warming. *Nature*, **467**: 704-706.

Dise NB. (1993). Methane emission from Minnesota peatlands: Spatial and seasonal variability. *Global Biogeochem Cycles*, **7**(1): 123-142.

Ditomaso JM, Barney JN, Mann JJ, Kyser G. (2013). For switchgrass cultivated as biofuel in California, invasiveness limited by several steps. *California Agriculture*, **67**(2): 96-103.

Donigian, A S, Barnwell, T O, Jackson, R B, Patwardhan, A S, and Weinrich, K B. (1994). Assessment of alternative management practices and policies affecting soil carbon in agroecosystems of the central United States. U.S. Environmental Protection Agency, Washington, D.C., EPA/600/R-94/067.

Drake, J. E. et al. (2011). Increases in the flux of carbon belowground stimulate nitrogen uptake and sustain the long-term enhancement of forest productivity under elevated CO_2. *Ecol. Lett.*, **14**: 349–357.

Edgar RC. (2010). Search and clustering orders of magnitude faster than BLAST. *Bioinformatics*, **26**(19):2460-1.

Edgar RC. (2013). UPARSE: Highly accurate OTU sequences from microbial amplicon reads. *Nat Methods*, **10**: 996-998.

Egerton-Warburton L, Johnson N, Allen E (2007) Mycorrhizal community dynamics following nitrogen fertilization: A cross-site test in five grasslands. *Ecol Monogr*, **77**: 527–544.

Einsmann, J. C., R. H. Jones, M. Pu, and R. J. Mitchell. (1999). Nutrient foraging traits in 10 co-occurring plant species of contrasting life forms. *Journal of Ecology*, **87**: 609– 619.

Elbersen, W., Poppens, R., & Bakker, R. (2013). Switchgrass (Panicum virgatum L.) A perennial biomass grass for efficient production of feedstock for the biobased economy. NL Agency, 28.

Eldor, A. (2015). Soil microbiology, ecology, and biochemistry (4th ed.). Chapter 14 Amsterdam: Elsevier.

Evan A. Thaler, Isaac J. Larsen, Qian Yu. (2021). The extent of soil loss across the US Corn Belt. *Proceedings of the National Academy of Sciences*, **118** (8): e1922375118.

FAO, (2014). Global Land Cover-SHARE of year 2014-Beta Release 1.0 http://www.glcn.org/databases/lc_glcshare_en.jsp

Fenchel, T. and Finlay, B.J. (2004) The ubiquity of small species: patterns of local and global diversity. *BioScience*, **54**: 777–784.

Feng, J., Wang, C., Lei, J. et al. (2020). Warming-induced permafrost thaw exacerbates tundra soil carbon decomposition mediated by microbial community. *Microbiome*, **8**: 3.

Ferchaud, F., Vitte, G. & Mary, B. (2016). Changes in soil carbon stocks under perennial and annual bioenergy crops. *GCB Bioenergy*, **8**: 290-306.

Ferraro, P. J. *et al.* (2015). Estimating the impacts of conservation on ecosystem services and poverty by integrating modeling and evaluation. *Proc. Natl. Acad. Sci. U. S. A.*, **112** (24): 7420-7425.

Filippidou S, Wunderlin T, Junier T, Jeanneret N, Dorador C, et al. (2016). A combination of extreme environmental conditions favor the prevalence of endospore-forming firmicutes. *Front. Microbiol.*, **7**:1707.

Finlay BJ. (2002). Global dispersal of free-living microbial eukaryote species. Science. **296**(5570):1061-3.

Finzi A.C., R.Z. Abramoff, K.S. Spiller, E.R. Brzostek, B.A. Darby, M.A. Kramer, R.P. Phillips (2015). Rhizosphere processes are quantitatively important components of terrestrial carbon and nutrient cycles. *Global Change Biology*, **21**: 2082-2094.

Fiona M. Seaton, Paul B.L. George, Inma Lebron, Davey L. Jones, Simon Creer, David A. Robinson, (2020). Soil textural heterogeneity impacts bacterial but not fungal diversity, *Soil Biology and Biochemistry*, **144**: 107766.

Fontaine, S. *et al.* (2007). Stability of organic carbon in deep soil layers controlled by fresh carbon supply. *Nature*, **450**: 277-280.

Fowler, D. et al. (2013). The global nitrogen cycle in the twenty-first century. *Philos. Trans. R. Soc. B*, **368**: 20130164.

Frank AB, Berdahl JD, Hanson JD, Liebig MA, Johnson HA. (2004). Biomass and carbon partitioning in switchgrass. *Crop Sci.*, **44**(4): 1391-1396.

Frank DA (2007). Drought effects on above- and belowground production of a grazed. temperature grassland ecosystem. *Oecologia*, **152**: 131–139.

Frank, D.A., Pontes, A.W. & McFarlane, K.J. (2012). Controls on Soil Organic Carbon Stocks and Turnover Among North American Ecosystems. *Ecosystems*, **15**: 604–615.

Frasier I, Noellemeyer E, Fernández R, Quiroga A. (2016). Direct field method for root biomass quantification in agroecosystems. *MethodsX.*, **3**: 513-519.

Frasier, R. A. (1925) Statistical methods for research workers. Edinburgh: Oliver and Boyd.

Friedlingstein, P. et al. (2014). Uncertainties in CMIP5 climate projections due to carbon cycle feedbacks. *J. Clim.*, **27**: 511–526.

Friedlingstein, P. et al. (2020). Global carbon budget 2020. *Earth Syst. Sci. Data*, **12**: 3269–3340.

Fritsche UR, Sims REH, Monti A. (2010). Direct and indirect land-use competition issues for energy crops and their sustainable production - an overview. *Biofuels, Bioproducts and Biorefining.*, **4**(6): 692-704.

Froseth RB, Bleken MA, (2015). Effect of low temperature and soil type on the decomposition rate of organic carbon and clover leaves, and related priming effect. *Soil Biology and Biochemistry*, **80**: 156-166.

Galloway, J. N. (2000). Nitrogen mobilization in Asia. *Nutr. Cycl. Agroecosyst.*, **57**: 1–12.

Galloway, J. N. et al. (2004). Nitrogen cycles: past, present, and future. *Biogeochemistry*, **70**: 153–226.

Gelfand I, Sahajpal R, Zhang X, Izaurralde RC, Gross KL, Robertson GP. (2013). Sustainable bioenergy production from marginal lands in the US Midwest. *Nature*, **493**: 514-517.

Ghimire SR, Charlton ND, Craven KD. (2009). The mycorrhizal fungus, *sebacina vermifera*, enhances seed germination and biomass production in switchgrass (*panicum virgatum l*). *Bioenergy Res*., **2**: 51-58.

Ghimire, S. R. & Craven, K. D. (2011). Enhancement of Switchgrass (*Panicum virgatum L*.) Biomass Production under Drought Conditions by the Ectomycorrhizal Fungus *Sebacina vermifera*. *Applied and Environmental Microbiology*, **77**: 7063-7067.

Giardine, et al. (2005). Galaxy: a platform for interactive large-scale genome analysis. *Genome Res.*, **15**: 1451-1455.

Govindasamy, P, Liu, R, Provin, T, et al. (2021). Soil carbon improvement under long-term (36 years) no-till sorghum production in a sub-tropical environment. *Soil Use Manage*, **37**: 37– 48.

Green J, Bohannan BJ. (2006). Spatial scaling of microbial biodiversity. *Trends Ecol Evol*., **21**(9): 501-7.

Guo, L. B. & Gifford, R. M. (2002). Soil carbon stocks and land use change: A meta analysis. *Glob. Chang. Biol.*, **8**(4): 345-360.

Guo, X., Zhou, X., Hale, L. et al. (2019). Climate warming accelerates temporal scaling of grassland soil microbial biodiversity. *Nat Ecol Evol*, **3**: 612–619.

Harper, R. J. & Tibbett, M. (2013). The hidden organic carbon in deep mineral soils. *Plant Soil*, **368**: 641-648.

Hestrin R, Lee MR, Whitaker BK, Pett-Ridge J. (2020). The switchgrass microbiome: A review of structure, function, and taxonomic distribution. *Phytobiomes J*., **5**(1):e 2471-2906.

Hiederer, R & Kochy, M. *Global Soil Organic Carbon Estimates and the Harmonized World soil Database* (Public. Office EU, 2011).

Högberg, P., Nordgren, A., Buchmann, N., Taylor, A.F.S., Ekblad, A., Högberg, M.N. et al. (2001). Large-scale forest girdling shows that current photosynthesis drives soil respiration. *Nature*, **411**: 789–792.

Horner-Devine, M. C., Lage, M., Hughes, J. B. & Bohannan, B. J. (2004). A taxa–area relationship for bacteria. *Nature*, **432**: 750–753.

Hsu, SF., Buckley, D. (2009). Evidence for the functional significance of diazotroph community structure in soil. *ISME J*, **3**: 124–136.

Hu, L., Robert, C.A.M., Cadot, S. et al. (2018). Root exudate metabolites drive plant-soil feedbacks on growth and defense by shaping the rhizosphere microbiota. *Nat Commun*, **9**: 2738.

Hungate, B. A. *et al.* (1997). The fate of carbon in grasslands under carbon dioxide enrichment. *Nature*, **388**: 576-579.

Hutchings, M.J., John, E.A. and Wijesinghe, D.K. (2003). Toward understanding the consequences of soil heterogeneity for plant populations and communities. Ecology, **84**: 2322-2334.

IPCC (2000). Land Use, Land Use Change, and Forestry. Summary for Policymakers. Cambridge University Press, Cambridge.

IPCC (2007). Climate Change 2007: Synthesis Report. Contribution of Working Groups I, II and III to the Fourth Assessment Report of the Intergovernmental Panel on Climate Change (eds Core Writing Team, R.K. Pachaur & A. Reisinger), IPCC, Geneva.

IPCC (2014). Climate Change 2014: Synthesis Report. Contribution of Working Groups I, II and III to the Fifth Assessment Report of the Intergovernmental Panel on Climate Change. Ipcc.

IPCC (2018). Global warming of 1.5°C. Ipcc - Sr15.

IPCC, (2021): Index. In: Climate Change 2021: The Physical Science Basis. Contribution of Working Group I to the Sixth Assessment Report of the Intergovernmental Panel on Climate Change [Masson-Delmotte, V., P. Zhai, A. Pirani, S. L. Connors, C. Péan, S. Berger, N. Caud, Y. Chen, L. Goldfarb, M. I. Gomis, M. Huang, K. Leitzell, E. Lonnoy, J.B.R. Matthews, T. K. Maycock, T. Waterfield, O. Yelekçi, R. Yu and B. Zhou (eds.)]. Cambridge University Press. In Press.

Jackson RB, Saunois M, Bousquet P, Canadell JG, Poulter B, Stavert AR, et al. Increasing anthropogenic methane emissions arise equally from agricultural and fossil fuel sources. Environmental Research Letters. 2020.

Jackson, R. B., and M. M. Caldwell. (1996). "Integrating Resource Heterogeneity and Plant Plasticity: Modelling Nitrate and Phosphate Uptake in a Patchy Soil Environment." *Journal of Ecology*, **84**(6): 891–903.

Jackson, R., Manwaring, J. & Caldwell, M. (1990). Rapid physiological adjustment of roots to localized soil enrichment. *Nature*, **344**: 58–60.

Janssens IA, et al. (2010) Reduction of forest soil respiration in response to nitrogen deposition. *Nat Geosci*, **3**:315–322.

Jastrow, J. D. et al. (2005). Elevated atmospheric carbon dioxide increases soil carbon. *Glob. Change Biol.*, **11**: 2057–2064.

Jessica Green, Brendan J.M. Bohannan, (2006). Spatial scaling of microbial biodiversity, *Trends in Ecology & Evolution*, **21**(9): 501-507.

Jesus E da C, Liang C, Quensen JF, Susilawati E, Jackson RD, Balser TC, et al. (2016). Influence of corn, switchgrass, and prairie cropping systems on soil microbial communities in the upper Midwest of the United States. *GCB Bioenergy*, **8**(2): 481-494.

Jiajie Feng, C. Ryan Penton, Zhili He, Joy D. Van Nostrand, Mengting M. Yuan, Liyou Wu, Cong Wang, Yujia Qin, Zhou J. Shi, Xue Guo, Edward A. G. Schuur, Yiqi Luo, Rosvel Bracho, Konstantinos T. Konstantinidis, James R. Cole, James M. Tiedje, Yunfeng Yang, Jizhong Zhou. Warming-induced permafrost thaw exacerbates tundra soil carbon decomposition mediated by microbial community. *mBio*, **10** (1): e02521-18.

Jobbagy, E. G. & Jackson, R. B. (2000). The vertical distribution of soil organic carbon and its relation to climate and vegetation. *Ecol. Appl.*, **10**: 423-436.

Johnston, A.S.A., Sibly, R.M. (2018). The influence of soil communities on the temperature sensitivity of soil respiration. *Nat Ecol Evol*, **2**: 1597–1602.

Jones SE, Lennon JT. 2010. Dormancy contributes to the maintenance of microbial diversity. *PNAS*, **107**(13):5881–86.

Kang H, Fahey TJ, Bae K, Fisk M, Sherman RE, Yanai RD, et al. (2016). Response of forest soil respiration to nutrient addition depends on site fertility. *Biogeochemistry*, **127**: 113-124.

Kantola, I. B., Masters, M. D. & DeLucia, E. H. (2017). Soil particulate organic matter increases under perennial bioenergy crop agriculture. *Soil Biol. Biochem.*, **113**: 184-191.

Kaschuk G., Hungria M. (2017) Diversity and Importance of Diazotrophic Bacteria to Agricultural Sustainability in the Tropics. In: de Azevedo J., Quecine M. (eds) Diversity and Benefits of Microorganisms from the Tropics. *Springer, Cham*., pp 269-292.

Katoh K. (2002). MAFFT: a novel method for rapid multiple sequence alignment based on fast Fourier transform. *Nucleic Acids Res*., **30**(14): 3059-66.

Keenan, T. et al. (2016). Recent pause in the growth rate of atmospheric CO2 due to enhanced terrestrial carbon uptake. *Nat. Commun*., **7**: 13428.

Kenneth J. Locey, Jay T. Lennon. (2016). Scaling laws predict global microbial diversity. *Proceedings of the National Academy of Sciences*, **113**(21): 5970-5975.

Ker K, Seguin P, Driscoll BT, Fyles JW, Smith DL. (2014). Evidence for enhanced N availability during switchgrass establishment and seeding year production following inoculation with rhizosphere endophytes. *Arch Agron Soil Sci*., **60**(11): 1553-1563.

Killham K, Firestone MK. (1984). Salt stress control of intracellular solutes in Streptomycetes indigenous to saline soils. *Appl. Environ. Microbiol*., **47**(2): 301–6.

Kim S, Lowman S, Hou G, Nowak J, Flinn B, Mei C. (2012). Growth promotion and colonization of switchgrass (*Panicum virgatum*) cv. alamo by bacterial endophyte burkholderia phytofirmans strain PsJN. *Biotechnol Biofuels*, **5**, 37.

Könneke, M., Bernhard, A., de la Torre, J. et al. (2005). Isolation of an autotrophic ammonia-oxidizing marine archaeon. *Nature*, **437**: 543–546.

Koven, C. D., Lawrence, D. M. & Riley, W. J. (2015). Permafrost carbon-climate feedback is sensitive to deep soil carbon decomposability but not deep soil nitrogen dynamics. *Proc. Natl. Acad. Sci. U. S. A.*, **112**(12): 3752-3757.

Kuang, J., Bates, C.T., Wan, X., Ning, D., Deng, D., Shu, W. and Zhou, J. (2021), High historical variability weakens the effects of current climate differentiation on microbial community dissimilarity and assembly. *Glob Change Biol*., In the press.

Kuczynski J, Stombaugh J, Walters WA, González A, Caporaso JG, Knight R. (2012). Using QIIME to analyze 16s rRNA gene sequences from microbial communities. *Curr Protoc Microbiol.*, Chapter 10: Unit 10.7.

Kuzyakov, Y., Horwath, W. R., Dorodnikov, M. & Blagodatskaya, E. (2019). Review and synthesis of the effects of elevated atmospheric CO2 on soil processes: no changes in pools, but increased fluxes and accelerated cycles. *Soil Biol. Biochem*., **128**: 66–78.

Lange M, Eisenhauer N, Sierra CA, Bessler H, Engels C, Griffiths RI, et al. (2015). Plant diversity increases soil microbial activity and soil carbon storage. *Nat Commun*., **6**: 6707.

Lange M, Habekost M, Eisenhauer N, Roscher C, Bessler H, Engels C, et al. (2014). Biotic and abiotic properties mediating plant diversity effects on soil microbial communities in an experimental grassland. *PLoS One*, **9**(5): e96182.

Lee DK, Doolittle JJ, Owens VN. (2007). Soil carbon dioxide fluxes in established switchgrass land managed for biomass production. *Soil Biol Biochem*, **39**(1): 178-186.

Leff Jonathan W., Stuart E. Jones, Suzanne M. Prober, Albert Barberán, Elizabeth T. Borer, Jennifer L. Firn, W. Stanley Harpole, Sarah E. Hobbie, Kirsten S. Hofmockel, Johannes M. H. Knops, Rebecca L. McCulley, Kimberly La Pierre, Anita C. Risch, Eric W. Seabloom, Martin Schütz, Christopher Steenbock, Carly J. Stevens, Noah Fierer. (2015). Soil microbial responses to elevated nutrients. *Proceedings of the National Academy of Sciences*, 112 (35): 10967-10972.

Leff JW, Jones SE, Prober SM, Barberán A, Borer ET, Firn JL, et al. (2015). Consistent responses of soil microbial communities to elevated nutrient inputs in grasslands across the globe. *Proc Natl Acad Sci U S A*, **112**(35): 10967-10972.

Li, E., de Jonge, R., Liu, C. et al. (2021). Rapid evolution of bacterial mutualism in the plant rhizosphere. *Nat Commun*, **12**: 3829.

Li, W., & Ma, Z. S. (2019). Diversity scaling of human vaginal microbial communities. *Zoological research*, **40**(6): 587–594.

Liang T, Yang G, Ma Y, Yao Q, Ma Y, Ma H, et al. (2019). Seasonal dynamics of microbial diversity in the rhizosphere of Ulmus pumila L. var. sabulosa in a steppe desert area of Northern China. *PeerJ*, **7**: e7526.

Liang, JL., Liu, J., Jia, P. et al. (2020). Novel phosphate-solubilizing bacteria enhance soil phosphorus cycling following ecological restoration of land degraded by mining. *ISME J*, **14**: 1600–1613.

Liang, Y., Jiang, Y., Wang, F. et al. (2015). Long-term soil transplant simulating climate change with latitude significantly alters microbial temporal turnover. *ISME J*, **9**: 2561–2572.

Liebig MA, Schmer MR, Vogel KP, Mitchell RB. (2008). Soil Carbon Storage by Switchgrass Grown for Bioenergy. *BioEnergy Res*., **1**: 215-222.

Locey KJ, Lennon JT. (2016). Scaling laws predict global microbial diversity. *Proc Natl Acad Sci U S A*, **113**(21): 5970-5975.

Löhnis F. (1926). Nitrogen availability of green manures. *Soil Science*, **22**: 253-290.

Ma, Z., Wood, C. W., & Bransby, D. I. (2000). Soil management impacts on soil carbon sequestration by switchgrass. *Biomass and Bioenergy*, **18**(6): 469–477.

Mao Y, Yannarell AC, Davis SC, Mackie RI. (2013). Impact of different bioenergy crops on N-cycling bacterial and archaeal communities in soil. Environ Microbiol., **15**(3): 928-942.

Masai, E., Katayama, Y. & Fukuda, M. (2007). Genetic and biochemical investigations on bacterial catabolic pathways for lignin-derived aromatic compounds. *Bioscience Biotechnology & Biochemistry*, **71**: 1–15.

McKeague J, Day J. (1966). Dithionite-and oxalate-extractable Fe and AL as aids in 577 differentiating various classes of soils. *Can. J. Soil Sci*., **46**(1): 13-22.

McLaughlin, S. B., & Kszos, L. A. (2005). Development of switchgrass (Panicum virgatum) as a bioenergy feedstock in the United States. *Biomass and Bioenergy*, **28**(6): 515.

McLean, E. Soil pH and lime requirement. (1982). Methods of soil analysis. Part 2. Chemical and microbiological properties, *American Society of Agronomy, Soil Science Society of America.*

Mehra OP and Jackson ML. (2013). Iron oxide remobal from soils and clays by a dithionite-citrate system buffered with sodium bicarbonate. In Clays and clay materials (pp. 317-327). *Pergamon*.

Meyer, K.M., Memiaghe, H., Korte, L. et al. (2018). Why do microbes exhibit weak biogeographic patterns? *ISME J*, **12**: 1404–1413.

Mikutta, R., Turner, S., Schippers, A. et al. (2019). Microbial and abiotic controls on mineral-associated organic matter in soil profiles along an ecosystem gradient. *Sci Re*p, **9**: 10294.

Milbrandt, A. R., Heimiller, D. M., Perry, A. D., & Field, C. B. (2014). Renewable energy potential on marginal lands in the United States. *Renewable and Sustainable Energy Reviews*, **29**: 473-481.

Monti A, Barbanti L, Zatta A, Zegada-Lizarazu W. (2012). The contribution of switchgrass in reducing GHG emissions. *GCB Bioenergy*, **4**(4): 420-434.

More TT, Yadav JSS, Yan S, Tyagi RD, Surampalli RY. (2014). Extracellular polymeric substances of bacteria and their potential environmental applications. *J. Environ. Manag*., **144**: 1–25.

Mulkey VR, Owens VN, Lee DK. (2006). Management of switchgrass-dominated conservation reserve program lands for biomass production in South Dakota. *Crop Sci*., **46**: 712-720.

Murphy, K.M., Edwards, J., Louie, K.B. et al. (2021). Bioactive diterpenoids impact the composition of the root-associated microbiome in maize (Zea mays). *Sci Rep*, **11**: 333.

Naeth, M. A., Bailey, A. W., Chanasyk, D. S., & Pluth, D. J. (1991). Water holding capacity of litter and soil organic matter in mixed prairie and fescue grassland ecosystems of Alberta. *Journal of Range Management*, **44**(1): 13-17.

Nelson DW, Sommers LE. (1996). Total Carbon, Organic Carbon, and Organic Matter. Chapter 34, p 1001-1006. JM Bigham et al. (ed) *Soil Science Society of America and America Society of Agronomy*. Methods of Soil Analysis. Part 3. Chemical Methods-SSA Book Series no. 5. Madison, WI.

Nie, M., Lu, M., Bell, J., Raut, S. & Pendall, E. (2013). Altered root traits due to elevated CO_2: a meta-analysis. *Glob. Ecol. Biogeogr*., **22**: 1095–1105.

Nielsen, U.N., Ayres, E., Wall, D.H. and Bardgett, R.D. (2011), Soil biodiversity and carbon cycling: a review and synthesis of studies examining diversity–function relationships. *European Journal of Soil Science*, **62**: 105-116.

NOAA National Centers for Environmental Information, State of the Climate: (2021). Global Climate Report for Annual 2020, online January 2021, retrieved on March 15, 2021.

NOAA (2021). Despite pandemic shutdowns, carbon dioxide and methane surged in 2020.

Norby, R. J. et al. (2005). Forest response to elevated CO_2 is conserved across a broad range of productivity. *Proc. Natl Acad. Sci. USA*, **102**: 18052–18056.

Olsen SR, Sommers LE. Phosphorus. In: AL Page, et al. (eds.) (1982). Methods of soil analysis: Part 2. Chemical and microbiological properties p. 403-430. *Agron. Mongr. 9. 2nd ed. ASA and SSA*, Madison, WI.

Olson, J. S. (1963). Energy storage and the balance of producers and decomposers in ecological systems. *Ecology*, **44**: 322–331.

Ormeño-Orrillo E, Hungria M, Martínez-Romero E (2013) Dinitrogen-fixing prokaryotes. In: Rosemberg E, de Long EF, Lory S, Stackebrandt E, Thompson F (eds) The prokaryotes – prokaryotic physiology and biochemistry. *Springer, Berlin Heidelberg*.

Papke, R.T. and Ward, D.M. (2004) The importance of physical isolation to microbial diversification. *FEMS Microbiol. Ecol.*, **48**: 293.

Patzold, S., Mertens, F.M., Bornemann, L. et al. (2008). Soil heterogeneity at the field scale: a challenge for precision crop protection. *Precision Agric*, **9**: 367–390.

Paul, E.A. (2007). Soil Microbiology, Ecology, and Biogeochemistry, 3rd edn. *Academic Press*, Amsterdam.

Pawlowski, K., Ribeiro, A. & Bisseling, T. in Biotechnol. Ann. Rev. Vol. 2 (ed. Raafat El-Gewely, M.) 151–184 (*Elsevier*, 1996).

Peñuelas, J., Sardans, J., Estiarte, M., Ogaya, R., Carnicer, J., Coll, M., Barbeta, A., Rivas-Ubach, A., Llusià, J., Garbulsky, M., Filella, I. and Jump, A.S. (2013), Evidence of current impact of climate change on life: a walk from genes to the biosphere. *Glob Change Biol*, **19**: 2303-2338.

Pilar Andrés, John C. Moore, Rodney T. Simpson, Greg Selby, Francesca Cotrufo, Karolien Denef, Michelle L. Haddix, E. Ashley Shaw, Cecilia Milano de Tomasel, Roberto Molowny-Horas, Diana H. Wall, (2016). Soil food web stability in response to grazing in a semi-arid prairie: The importance of soil textural heterogeneity, *Soil Biology and Biochemistry*, **97**: 131-143.

Poeplau C, Helfrich M, Dechow R, Szoboszlay M, Tebbe CC, Don A, et al. (2019). Increased microbial anabolism contributes to soil carbon sequestration by mineral fertilization in temperate grasslands. *Soil Biol Biochem.*, **130**: 167-176.

Preston, F. W. (1960). Time and space and the variation of species. *Ecology*, **41**: 611–627.

Price MN, Dehal PS, Arkin AP. (2009). Fasttree: Computing large minimum evolution trees with profiles instead of a distance matrix. *Mol Biol Evol*., **26**(7): 1641-1650.

Prober SM, Leff JW, Bates ST, Borer ET, Firn J, Harpole WS, et al. (2015). Plant diversity predicts beta but not alpha diversity of soil microbes across grasslands worldwide. *Ecol Lett.*, **18**(1): 85-95.

Prokopy WR. (1995). Phopshorus in 0.5 M sodium bicarbonate soil extracts. QuikChem Method 12-115-01-1-B. *Lachat Instruments*, Milwaukee, WI.

R Core Team. R Core Team (2014). R: A language and environment for statistical computing. R Found Stat Comput Vienna, Austria URL http//wwwR-project.org/.

Raich, J.W. & Potter, C.S. (1995). Global patterns of carbon-dioxide emissions from soils. *Global Biogeochemical Cycles*, **9**: 23–36.

Ramirez KS, Craine JM, Fierer N (2012) Consistent effects of nitrogen amendments on soil microbial communities and processes across biomes. *Glob Change Biol*, **18**: 1918–1927.

Raymond, J., Siefert, J. L., Staples, C. R. & Blankenship, R. E. (2004). The natural history of nitrogen fixation. *Mol. Biol. Evol.*, **21**: 541–554.

Reche, I. et al. (2005) Does ecosystem size determine aquatic bacterial richness? *Ecology*, **86**: 1715–1722.

Reed, S. C., Cleveland, C. C., & Townsend, A. R. (2007). Controls over leaf litter and soil nitrogen fixation in two lowland tropical rain forests. *Biotropica*, **39**: 585–592.

Reed, S. C., Cleveland, C. C., & Townsend, A. R. (2011). Functional ecology of free-living nitrogen fixation: A contemporary perspective. *Annual Review of Ecology, Evolution, and Systematics*, **42**: 489–512.

Remy, W., Taylor, T. N., Hass, H. & Kerp, H. (1994). Four hundred-million-year-old vesicular arbuscular mycorrhizae. *Proceedings of the National Academy of Sciences*, **91**: 11841-11843.

Richardson, A.E., Barea, JM., McNeill, A.M. et al. (2009). Acquisition of phosphorus and nitrogen in the rhizosphere and plant growth promotion by microorganisms. *Plant Soil*, **321**: 305–339.

Risser, P. G., & Parton, W. J. (1982). Ecosystem Analysis of the Tallgrass Prairie: Nitrogen Cycle. *Ecology*, **63**(5): 1342–1351.

Rivas-Ubach A, Sardans J, Perez-Trujillo M, Estiarte M, Penuelas J (2012) Strong relationship between elemental stoichiometry and metabolome in plants. *Proceedings of the National Academy of Sciences of the United States of America*, **109**: 4181-4186.

Rivett, D.W., Mombrikotb, S.B., Gweon, H.S. et al. (2021). Bacterial communities in larger islands have reduced temporal turnover. *ISME J*, in the press.

Robertson GP, Grace PR. (2004). Greenhouse gas fluxes in tropical and temperate agriculture: The need for a full-cost accounting of global warming potentials. *Environ Dev Sustain*, **6**: 51-63.

Robinson, D. (1994), The responses of plants to non-uniform supplies of nutrients. *New Phytologist*, **127**: 635-674.

Rodríguez, H., & Fraga, R. (1999). Phosphate solubilizing bacteria and their role in plant growth promotion. *Biotechnology Advances*, **17**(4–5): 319–339.

Roley SS, Xue C, Hamilton SK, Tiedje JM, Robertson GP. (2019). Isotopic evidence for episodic nitrogen fixation in switchgrass (*Panicum virgatum L.*). *Soil Biol Biochem*, **129**: 90-98.

Romani, A.M., Fischer, H., Mille-Lindblom, C. & Tranvik, L.J. (2006). Interactions of bacteria and fungi on decomposing litter: differential extracellular enzyme activities. *Ecology*, **10**: 2559–2569.

Rosenzweig, M.L. (1995) Species Diversity in Space and Time, *Cambridge University Press*.

Rosseel Y. (2012). Lavaan: An R package for structural equation modeling. *J Stat Softw*, **48**: 2.

Rousk, K., Jones, D. L., & DeLuca, T. H. (2014). Exposure to nitrogen does not eliminate N2 fixation in the feather moss Pleurozium schreberi (Brid.) Mitt. *Plant and Soil*, **374**: 513–521.

Sah RN, Miller RO. (1996). Spontaneous reaction for acid dissolution of biological tissues in closed vessels. *Anal. Chem*, **64**: 230-233.

Sanderman Jonathan, Tomislav Hengl, Gregory J. Fiske. (2017). Soil carbon debt of human land use. *Proceedings of the National Academy of Sciences*, **114** (36): 9575-9580.

Sanderson, M. A. et al. (1996). Switchgrass as a sustainable bioenergy crop. *Bioresource Technology*, **56**: 83-93.

Saunois M, Stavert AR, Poulter B, Bousquet P, Canadell JG, Jackson RB, et al. (2019). The Global Methane Budget 2000-2017. *Earth Syst Sci Data Discuss*., **12**: 1561-1623.

Schimel, D., Stephens, B. B. & Fisher, J. B. (2015). Effect of increasing CO_2 on the terrestrial carbon cycle. *Proc. Natl Acad. Sci. USA*, **112**: 436–441.

Schimel Joshua. (2018). Life in Dry Soils: Effects of Drought on Soil Microbial Communities and Processes. *Annual Review of Ecology, Evolution, and Systematics*, **49**(1): 409-432.

Schubert SD, Suarez MJ, Pegion PJ, Koster RD, Bacmeister JT. (2004). On the Cause of the 1930s Dust Bowl. *Science*, (**80**-).

Schuur, E. A. G. *et al.* (2015). Climate change and the permafrost carbon feedback. *Nature*, **520**: 171-179.

Scott-Denton, L. E., Rosenstiel, T.N. and Monson, R.K. (2006). Differential controls by climate and substrate over the heterotrophic and rhizospheric components of soil respiration. *Global Change Biology*, **12**: 205-216.

Shade, A., Caporaso, J. G., Handelsman, J., Knight, R. & Fierer, N. (2013). A meta-analysis of changes in bacterial and archaeal communities with time. *ISME J*., **7**: 1493–1506.

Shahzad T, Rashid MI, Maire V, Barot S, Perveen N, Alvarez G, et al. (2018). Root penetration in deep soil layers stimulates mineralization of millennia-old organic carbon. *Soil Biol Biochem*, **124**: 150-160.

Sheldrick BH, Wang C. (1993). Particle-size Distribution. Pp. 499-511. In: Carter, MR (ed), Soil Sampling and Methods of Analysis, *Canadian Society of Soil Science*.

Sher Y, Baker NR, Herman D, Fossum C, Hale L, Zhang X, et al. (2020). Microbial extracellular polysaccharide production and aggregate stability controlled by switchgrass (*Panicum virgatum*) root biomass and soil water potential. *Soil Biol Biochem.*, **143**: 107742.

Slessarev EW, Nuccio EE, McFarlane KJ, Ramon CE, Saha M, Firestone MK, et al. (2020). Quantifying the effects of switchgrass (*Panicum virgatum*) on deep organic C stocks using natural abundance ^{14}C in three marginal soils. *GCB Bioenergy*, **12**(10): 834-847.

Smercia D., Evans S., Friesen M., Tiemann L. (2019). To fix or not to fix: controls on free-living nitrogen fixation in the rhizosphere. *Applied and Environmental microbiology*, **85**: 6.

Soil Sampling and Methods of Analysis. (2007). Soil Sampling and Methods of Analysis.

Sollins, P., Swanston, C. & Kramer, M. (2007). Stabilization and destabilization of soil organic matter—a new focus. *Biogeochemistry*, **85,** 1–7.

Stocker TF, Qin D, Plattner GK, Tignor MMB, Allen SK, Boschung J, et al. (2013). Climate change 2013 the physical science basis: Working Group I contribution to the fifth assessment report of the intergovernmental panel on climate change. Climate Change 2013 the Physical Science Basis: Working Group I Contribution to the Fifth Assessment Report of the Intergovernmental Panel on Climate Change.

Stoof CR, Richards BK, Woodbury PB, Fabio ES, Brumbach AR, Cherney J, et al. (2015). Untapped Potential: Opportunities and Challenges for Sustainable Bioenergy Production from Marginal Lands in the Northeast USA. *Bioenergy Research*, **8**: 482-501.

Subke, J.A., Inglima, I. & Cotrufo, M.F. (2006). Trends and methodological impacts in soil CO_2 efflux partitioning: a metaanalytical review. *Global Change Biology*, **12**: 921–943.

Terrer C, Vicca S, Hungate BA, Phillips RP, Prentice IC. (2016). Mycorrhizal. association as a primary control of the CO_2 fertilization effect. *Science*, **353**: 72–74.

Terrer, C., Vicca, S., Stocker, B.D., Hungate, B.A., Phillips, R.P., Reich, P.B., Finzi, A.C. and Prentice, I.C. (2018), Ecosystem responses to elevated CO_2 governed by plant–soil interactions and the cost of nitrogen acquisition. *New Phytol*, **217**: 507-522.

Terrer, C., Phillips, R.P., Hungate, B.A. et al. (2021). A trade-off between plant and soil carbon storage under elevated CO_2. *Nature*, **591**: 599–603.

Thakur MP, Milcu A, Manning P, Niklaus PA, Roscher C, Power S, et al. (2015). Plant diversity drives soil microbial biomass carbon in grasslands irrespective of global environmental change factors. *Glob Chang Biol*, **21**(11): 4076-4085.

Tiedje J. (1988). Ecology of denitrification and dissimilatory nitrate reduction to ammonium. P 179-244. In A.J.B. Zehnder (ed), Environmental Microbiology of Anaerobes. *John Wiley and Sons*, N.Y.

Tiemann LK, Grandy AS. (2015). Mechanisms of soil carbon accrual and storage in bioenergy cropping systems. *GCB Bioenergy*, **7**(2): 161-174.

Tiessen, H., Cuevas, E. & Chacon, P. (1994). The role of soil organic matter in sustaining soil fertility. *Nature*, **371**: 783–785.

Tilman, D., Hill, J. & Lehman, C. (2006). Carbon-Negative Biofuels from Low-Input High-Diversity Grassland Biomass. *Science*, **314**: 1598-1600.

Todd-Brown, K. E. O. et al. (2014). Changes in soil organic carbon storage predicted by Earth system models during the 21st century. *Biogeosciences*, **11**: 2341–2356.

Torbert, H.A., Prior, S.A., Rogers, H.H. et al. (2000). Review of elevated atmospheric CO_2 effects on agro-ecosystems: residue decomposition processes and soil C storage. *Plant and Soil*, **224**: 59–73.

Torn, M. S., Trumbore, S. E., Chadwick, O. A., Vitousek, P. M. & Hendricks, D. M. (1997). Mineral control of soil organic carbon storage and turnover. *Nature*, **389**: 170-173.

Treseder K (2004) A meta-analysis of mycorrhizal responses to nitrogen, phosphorus, and atmospheric CO_2 in field studies. New Phytol, **164**: 347–355.

Treseder KK (2008) Nitrogen additions and microbial biomass: A meta-analysis of ecosystem studies. *Ecol Lett*, **11**(10): 1111–1120.

Tukey, John (1949) Comparing Individual Means in the Analysis of Variance. *Biometrics*, **5**(2): 99–114.

van der Gast, C. J., Ager, D. & Lilley, A. K. (2008). Temporal scaling of bacterial taxa is influenced by both stochastic and deterministic ecological factors. *Environ. Microbiol*., **10**: 1411–1418.

van Groenigen, K. J., Qi, X., Osenberg, C. W., Luo, Y. & Hungate, B. A. (2014). Faster decomposition under increased atmospheric CO2 limits soil carbon storage. *Science*, **344**: 508.

Van Nostrand, JD, Yin H, Wu L, Yuan T, Zhou J. (2016). Hybridization of Environmental Microbial Community Nucleic Acis by GeoChip. *Methods Mol. Biol.*, **1399**: 183–96.

Wagai R, Brye KR, Gower ST, Norman JM, Bundy LG. (1998). Land use and environmental factors influencing soil surface CO2 flux and microbial biomass in natural and managed ecosystems in southern Wisconsin. *Soil Biol Biochem*., **30**(12): 1501-1509.

Waldrop, M.P., Firestone, M.K. (2004). Microbial community utilization of recalcitrant and simple carbon compounds: impact of oak-woodland plant communities. *Oceologia*, **138**: 275-284.

Waldrop, M. P., Zak, D. K., Sinsabaugh, R. L., Gallo, M. & Lauber, C. (2004). Nitrogen deposition modifies soil carbon storage through changes in microbial enzymatic activity. *Ecol. Appl*., **14**: 1172–1177.

Wang G, Post WM, Mayes MA, Frerichs JT, Sindhu J. (2012). Parameter estimation for models of ligninolytic and cellulolytic enzyme kinetics. *Soil Biol Biochem*., **48**: 28–38.

Wang K, Peng C, Zhu Q, Zhou X, Wang M, Zhang K, et al. (2017). Modeling global soil carbon and soil microbial carbon by integrating microbial processes into the ecosystem process model TRIPLEX-GHG. *J Adv Model Earth Sys.*, **9**(6): 2368–84.

Wang Q, Garrity GM, Tiedje JM, Cole JR. (2007). Naïve Bayesian classifier for rapid assignment of rRNA sequences into the new bacterial taxonomy. *Appl Environ Microbiol.*, **73**(16): 5261-7.

Wang, G., Post, W. M. & Mayes, M. A. (2013). Development of microbial-enzyme-mediated decomposition model parameters through steady-state and dynamic analyses. *Ecol. Appl.*, **23**(1): 255-272.

Wang, G. *et al.* (2015). Microbial dormancy improves development and experimental validation of ecosystem model. *ISME J.*, **9**(1): 226-37.

Ward BB. (1996). Nitrification and ammonification in aquatic systems. *Life Support Biosph Sci.*, **3**(1-2): 25-9.

Welsh, D. T. (2000). Nitrogen fixation in seagrass meadows: regulation, plant–bacteria interactions and significance to primary productivity. *Ecol. Lett.*, **3**: 58–71.

Wessén E, Nyberg K, Jansson JK, Hallin S (2010) Responses of bacterial and archaeal ammonia oxidizers to soil organic and fertilizer amendments under long-term management. *Appl Soil Ecol*, **45**: 193–200.

Whitaker, R.J. et al. (2003) Geographic barriers isolate endemic populations of hyperthermophilic archaea. *Science*, **301**: 976–978.

White, E P. et al. (2006). A comparison of the species–time relationship across ecosystems and taxonomic groups. *Oikos*, **112**: 185–195.

Wickham H. (2009). ggplot2: elegant graphics for data analysis. *Springer New York*.

Wijesinghe, D. K., E. A. John, S. Beurskens, and M. J. Hutchings. (2001). Root system size and precision in nutrient foraging: responses to spatial pattern of nutrient supply in six herbaceous species. *Journal of Ecology*, **89**: 972– 983.

Winogradsky, S. (1890). Recherches sur les organismes de la nitrification. *Ann. Inst. Pasteur* (Paris) **4**: 213–231.

Wood JM. (2015). Bacterial responses to osmotic challenges. *J. Gen. Physiol.*, **145**(5):381–88.

Worster D. (1982). Dust bowl: the Southern Plains in the 1930s (Oklahoma and Kansas). Dust bowl South Plains 1930s (Oklahoma Kansas).

Wu L, Wen C, Qin Y, Yin H, Tu Q, Van Nostrand JD, et al. (2015). Phasing amplicon sequencing on Illumina Miseq for robust environmental microbial community analysis. *BMC Microbiol*., **15**: 125.

Xiaolu Tang, Jie Du, Yuehong Shi, Ningfei Lei, Guo Chen, Longxi Cao, Xiangjun Pei. (2020). Global patterns of soil heterotrophic respiration – A meta-analysis of available dataset, *CATENA*, **191**: 104574.

Yan M., N. Guo, H. Ren, X. Zhang, G. Zhou. (2015). Autotrophic and heterotrophic respiration of a poplar plantation chronosequence in northwest China. *For. Ecol. Manag*., **337**: 119-125.

Ye, H. *et al.* (2015). Equation-free mechanistic ecosystem forecasting using empirical dynamic modeling. *Proc. Natl. Acad. Sci. U. S. A.*, **112**(13): e1569-e1576.

Yuyu Yang, Lei Liu, Feng Zhang, Xiuying Zhang, Wen Xu, Xuejun Liu, Zhen Wang, and Yaowen Xie (2021). Soil nitrous oxide emissions by atmospheric nitrogen deposition over global agricultural systems. *Environmental Science & Technology*, **55** (8): 4420-4429.

Zan CS, Fyles JW, Girouard P, Samson RA. (2001). Carbon sequestration in perennial bioenergy, annual corn and uncultivated systems in southern Quebec. *Agric Ecosyst Environ.*, **86**(2): 135-144.

Zhang J, Kobert K, Flouri T, Stamatakis A. (2014). PEAR: a fast and accurate Illumina Paired-End reAd mergeR. *Bioinformatics*, **30**(5): 614-20.

Zhao MS, Running SW (2010) Drought-induced reduction in global terrestrial net primary production from 2000 through 2009. *Science*, **329**: 940–943.

Zheng, M, Zhou, Z, Luo, Y, Zhao, P, Mo, J. (2019). Global pattern and controls of biological nitrogen fixation under nutrient enrichment: A meta-analysis. *Glob Change Biol*., **25**: 3018– 3030.

Zhou J, Bruns MA, Tiedje JM. (1996). DNA recovery from soils of diverse composition. Appl Environ Microbiol., **62**(2): 316-22.

Zhou L, Zhou X, Shao J, Nie Y, He Y, Jiang L, Wu Z, Bai SH. (2016). Interactive effects of global change factors on soil respiration and its components: a metaanalysis. *Global Change Biology*, **22**: 3157–3169.

Zhou, J., Deng, Y., Shen, L. et al. (2016). Temperature mediates continental-scale diversity of microbes in forest soils. *Nat Commun*, **7**: 12083.

Zhou, J., Kang, S., Schadt, C. W. & Garten, C. T. Jr. (2008). Spatial scaling of functional gene diversity across various microbial taxa. *Proc. Natl Acad. Sci. USA*, **105**: 7768–7773.

Zumft, W. G. (1997). Cell biology and molecular basis of denitrification. *Microbiology and Molecular Biology Reviews*, **61**(4), 533–616.